

TE
662
.A3
no.
FHWA-
RD-
78-
159

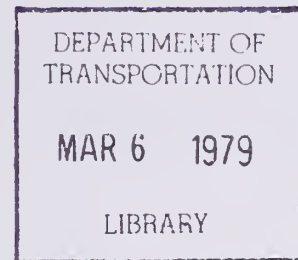
Report No. FHWA-RD-78-159

INTEGRATED APPROACH TO CAVITY SYSTEM SEISMIC EVALUATION



October 1978
Final Report

This document is available to the public
through the National Technical Information
Service, Springfield, Virginia 22161



Prepared for
FEDERAL HIGHWAY ADMINISTRATION
Offices of Research & Development
Washington, D.C. 20590

FOREWORD

This report is the result of research conducted at Purdue University for the Federal Highway Administration (FHWA), Office of Research, under FHWA Purchase Order P.O. 7-3-0065. The report will be of interest to those researchers concerned with earthquake vulnerability and analysis of large underground cavity systems. A methodology is developed to compare the performance of different design alternatives of cavity systems.

Copies of the report are being distributed by FHWA transmittal memorandum. Additional copies may be obtained from the National Technical Information Service, 5285 Port Royal Road, Springfield, Virginia 22161.



Charles F. Scheffey
Director, Office of Research
Federal Highway Administration

Notice

This document is disseminated under the sponsorship of the Department of Transportation in the interest of information exchange. The United States Government assumes no liability for its contents or use thereof.

The contents of this report reflect the view of the authors, who are responsible for the facts and the accuracy of the data presented herein. The contents do not necessarily reflect the official views or policy of the Department of Transportation.

This report does not constitute a standard, specification, or regulation.

78-117
 FHWA
 no. A 32
 662

1. Report No. FHWA-RD-78-159		2. Government Accession No.		3. Recipient's Catalog No.	
4. Title and Subtitle Integrated Approach to Cavity System Seismic Evaluation				5. Report Date October 1978	
				6. Performing Organization Code	
7. Author(s) Basile Dendrou				8. Performing Organization Report No.	
9. Performing Organization Name and Address Purdue University West Lafayette, Indiana 47907				10. Work Unit No. (TRAIS) 35B3-411 <i>FCP</i>	
				11. Contract or Grant No. P.O. 7-3-0065	
12. Sponsoring Agency Name and Address Offices of Research and Development Federal Highway Administration U.S. Department of Transportation Washington, D.C. 20590				13. Type of Report and Period Covered Final Report	
				14. Sponsoring Agency Code S0810	
15. Supplementary Notes FHWA Contract Manager: James D. Cooper, HRS-11.					
16. Abstract A methodology is developed to compare different design alternatives of a cavity system. The performance of each alternative is evaluated according to six independent criteria representing the behavioral mode of the cavity system under a seisme. The computational part of the study is based on a two-dimensional Finite Elements uncertainty analysis and provides the quantification of the above-mentioned criteria. An inference model links together the statistical data of the important physical parameters obtained from a site investigation and the main analytical model which possesses four computational steps; namely the evaluation of the effects of: (1) an underground waterflow on the rock media; (2) the excavation on the rock media; (3) a seismic perturbation on the rock media; (4) the displacement of the rock media on the liner. The rock media is assumed to be isotropic both in the physical and statistical sense. Computations are performed for each design alternative, in a two-dimensional geometric framework using triangular and beam type Finite Elements.					
17. Key Words Earthquake, Tunnels, Cavities, Finite Element, Underground Openings, Tunnel Response			18. Distribution Statement No restrictions. This document is available through the National Technical Information Service, Springfield, Virginia 22161.		
19. Security Classif. (of this report) Unclassified		20. Security Classif. (of this page) Unclassified		21. No. of Pages 320	22. Price

Finite Elements.
 DEPARTMENT OF
 TRANSPORTATION

 MAR 6 1979

 LIBRARY

ACKNOWLEDGMENTS

The author is indebted to Professor W. R. Judd, his major professor, for his advice, encouragement and assistance during the preparation of the thesis.

Appreciation is also expressed to Professors E. C. Ting, J. Yao, J. J. Talavage and A. G. Altschaeffl for serving on the Advisory Committee and for their constructive criticisms.

Appreciation is also expressed to the faculty of the Geotechnical Department, and Professor M. E. Harr.

Financial support for the research was provided by the School of Civil Engineering of Purdue University and the Federal Highway Administration.

Careful typing of the manuscript by Mrs. Ramona Hill and Mrs. Sherry Miller is gratefully acknowledged.

Finally the author wishes to thank his friends Elias Houstis and Stergios Dendrou for their infallible moral support during his graduate work at Purdue University.

TABLE OF CONTENTS

	<u>Page</u>
LIST OF TABLES	vi
LIST OF FIGURES.	viii
LIST OF SYMBOLS.	xii
CHAPTER 1 - INTRODUCTION	1
1.1 Motivation	1
1.2 Problem Components	4
1.3 Objectives and Procedures.	5
1.4 Relevance of the Study	7
CHAPTER 2 - REVIEW OF THEORETICAL AND EXPERIMENTAL BACKGROUND. .	9
2.1 Introduction	9
2.2 Earthquake Ground Motion	10
2.2.1 Earthquake Signal on the Earth Surface.	12
2.2.2 Seismic Response of Underground Structures.	13
2.3 Fundamentals of the Theory of Motion	16
2.4 Simulation Models and Their Conceptual Basis	19
2.4.1 Conceptual Models	19
2.4.2 Methods of Resolution of the Mathematical Formulation	21
2.4.3 Adopted Mathematical Resolution	23
2.5 Quantifying the Uncertainty.	24
2.6 Comparing Different Alternatives	26
CHAPTER 3 - DEVELOPMENT OF THE MODEL SIMULATING THE CAVITY SYSTEM	29
3.1 Introduction	29
3.2 Geometric Framework and Boundary Conditions of the Model.	32
3.2.1 Geometric Framework	32
3.2.2 Boundary Conditions	33
3.3 Evaluation of the Physical Properties Governing the Behavior of the Media.	41
3.4 Analytical Model Handling the Uncertainty of the Transfer Mechanism	42
3.5 Input Seismic Load	46
3.6 Model Implementation	48

	<u>Page</u>
CHAPTER 4 - PHYSICAL PARAMETERS DESCRIBING THE CAVITY SYSTEM . . .	53
4.1 Introduction	53
4.2 Nature of the Geologic Environment	53
4.3 Quantifying the Physical Parameter of the Rock Media . . .	55
4.4 Mechanical Properties of Rock with Respect to Dis-	
continuityes and Their Spatial Distribution.	58
4.4.1 Intrinsic Parameters.	58
4.4.2 Extrinsic Parameters.	64
4.4.3 Dynamic Parameters.	67
4.4.4 Rock Quality Designation (RQD).	70
4.5 Spatial Distribution of the Mechanical Parameters.	72
4.6 Mechanical Properties of Liner Materials	75
4.7 Hypothetical Case Study.	75
CHAPTER 5 - INFERENCE MODEL AND ITS INTERFACE WITH THE ANALYTICAL	
UNCERTAINTY MODEL.	83
5.1 Introduction	83
5.2 Justification of the Moving Average Technique.	84
5.3 Implementation of the Inference Model in a Two-	
Dimensional Geometric Space.	86
5.3.1 Statistical Model and Corresponding Assumptions . .	86
5.3.2 Identification of the Best Estimator.	90
5.4 Interfacing the Inference Model with the Analytical Model. . .	93
5.4.1 Uncertainty Analysis in the Analytical Model. . . .	93
5.4.2 Coupling of the Inference Model with the	
Analytical Uncertainty Model.	94
5.5 Description of the Algorithm	94
5.6 Example of Application and Discussion.	97
5.7 Remarks on the Applicability of the Method	106
CHAPTER 6 - UNCERTAINTY ANALYSIS IN THE ANALYTICAL MODEL	119
6.1 Introduction	119
6.2 General Assumptions Concerning the Analysis in	
Conjunction with the F.E.M.	120
6.2.1 Discretization Criteria	120
6.2.2 Constitutive Relationships.	124
6.3 Finite Elements Used to Discretize the Cavity System . . .	125
6.3.1 Triangular Element with Six d.o.f.	127
6.3.2 Beam Element with Six d.o.f.	128
6.4 Uncertainty Analysis Related to the Underground Flow	
Problem.	133
6.5 Uncertainty Analysis of Initial Stress Conditions	
Created by the Excavation.	137
6.6 Uncertainty Analysis Related to the Modal Dynamic	
Analysis	142
6.7 Uncertainty Related to the Stability of the Liner.	151
6.8 Remarks Concerning the Given Computational Scheme.	158

	<u>Page</u>
CHAPTER 7 - MODEL PROVIDING THE INPUT SEISMIC DISTURBANCE	159
7.1 Introduction.	159
7.2 Analytical Treatment of the Model	161
7.3 Aposteriori Component	165
7.4 Apriori Component and Parametric Study.	167
7.5 Generation of Pseudo Earthquakes.	168
CHAPTER 8 - EVALUATION OF DESIGN ALTERNATIVES	175
8.1 Introduction.	175
8.2 Classes of Alternatives for Cavity Systems.	176
8.3 Classes of Criteria of Selection.	177
8.4 Formalization of Sorting Algorithm.	179
8.4.1 Problem Components and Nomenclature.	180
8.4.2 Outranking Relation and Basic Assumptions.	181
8.5 Example of Application.	185
CHAPTER 9 - EXAMPLES OF APPLICATION OF THE MODEL.	192
9.1 Geologic Structure of the Site.	192
9.2 Input Data for the Analytical Treatment	193
9.3 Intermediate Results of the Uncertainty Analysis.	196
9.4 Comparison of Different Alternatives.	215
CHAPTER 10 - CONCLUSIONS AND RECOMMENDATIONS.	227
10.1 Conclusions	227
10.2 Perspective for Future Work	229
BIBLIOGRAPHY.	231
APPENDICES.	239
Appendix A - Expression Allowing the Evaluation of the Dynamic Modulus of Elasticity.	239
Appendix B - Computations Related to the Inference Model.	241
Appendix C - Computations Related to the Finite Element Uncertainty Analysis	245
Appendix D - Computations Related to the Earthquake Generation Model	257
Appendix E - Computations Related to the Evaluation of the Entropy of Information	259
Appendix F - Computer Programs and Subroutines in Relation with the Different Computational Units of the Study	261

LIST OF TABLES

	<u>Page</u>
TABLE 2.1 EARTHQUAKE SIGNALS AT DEPTH	15
TABLE 3.1 EXAMPLE OF EXISTING UNDERGROUND OPENINGS.	37
TABLE 4.1 MECHANICAL CLASSIFICATION OF ROCKS.	57
TABLE 4.2 RESULTS OF A HYPOTHETICAL SITE INVESTIGATION.	79
TABLE 5.1 RESULTS OF STATISTICAL CHARACTERISTICS FOR PROBLEM ONE	101
TABLE 5.2 RESULTS OF STATISTICAL CHARACTERISTICS FOR PROBLEM TWO	101
TABLE 5.3 DEVIATIONS AND COEFFICIENTS OF MULTIPLE CORRELATION OF THE ESTIMATIONS OBTAINED BY REGRESSION AND COR- RELATIVE SCHEME FOR TWO DIFFERENT SETS OF β POINTS.	114
TABLE 5.4 DEVIATIONS AND COEFFICIENTS OF MULTIPLE CORRELATION FOR THE ESTIMATIONS OBTAINED BY CORRELATIVE SCHEME 2 USING LINEAR AND COMPUTED VARIOGRAM FOR TWO SETS OF β POINTS.	115
TABLE 5.5 THE MEAN, COEFFICIENT OF VARIATION AND ABSOLUTE RELATIVE ERROR OF THE ESTIMATES OBTAINED BY CORRELATIVE SCHEME 1 AND 2 WITH A LINEAR VARIOGRAM AT POINTS $A=(90,10)$, $B=(90,40)$ FOR TWO SETS OF β POINTS	116
TABLE 5.6 THE ABSOLUTE RELATIVE ERROR IN PERCENT OF THE COM- PUTED HEAD USING THE REGRESSION-FINITE ELEMENT AND CORRELATIVE FINITE ELEMENT MODELS AT THE POINTS $A=(90,10)$, $B=(90,40)$	117
TABLE 5.7 THE COEFFICIENT OF VARIATION OF THE HEAD AT POINTS A, B FOR THREE DIFFERENT BOUNDARY CONDITIONS OBTAINED BY THE INFERENCE FINITE ELEMENT.	118
TABLE 6.1 LINEAR AND NONLINEAR COMPONENTS OF THE STRAIN ENERGY OF A BEAM ELEMENT	130

	<u>Page</u>
TABLE 9.1 INPUT DATA OBTAINED FROM A SITE INVESTIGATION AND LABORATORY TESTS.	198
TABLE 9.2 RESULTS OF THE INFERENCE MODEL.	199
TABLE 9.3 ORGANIZATIONAL SCHEME OF THE INPUT DATA RELATED TO THE F.E. ANALYSIS	201
TABLE 9.4 RESULTS OF THE UNDERGROUND FLOW ANALYSIS.	204
TABLE 9.5 DISPLACEMENTS DUE TO THE EXCAVATION	205
TABLE 9.6 NATURAL FREQUENCIES OBTAINED FROM THE MODAL ANALYSIS. .	208
TABLE 9.7 DISPLACEMENTS DUE TO THE SEISME	210
TABLE 9.8 EVOLUTION OF MAXIMUM COMPRESSIVE STRESSES IN THE ROCK MEDIA.	214
TABLE 9.9 MAXIMUM DEFORMATIONS OF THE LINER	216
TABLE 9.10 SHEAR STRENGTH IN THE ROCK MEDIA.	218
TABLE 9.11 INPUT DATA FOR ALGORITHM ELECTRE (WITH COEFFICIENT OF VARIATION)	219
TABLE 9.12 INPUT DATA FOR ALGORITHM ELECTRE (WITH ENTROPY)	220

LIST OF FIGURES

		<u>Page</u>
FIGURE 1.1	CONCEPTUALIZATION OF AN UNDERGROUND OPENING.	3
FIGURE 2.1	SCALES IN WHICH THE EARTHQUAKE PHENOMENON TAKES PLACE.	11
FIGURE 3.1	TYPICAL CAVITY SYSTEM	31
FIGURE 3.2	EFFECT OF DIFFERENT WAVELENGTH SEISMIC LOADS (MACROSCALE)	34
FIGURE 3.3	TYPICAL SEISMIC ACCELEROGRAM	35
FIGURE 3.4	TYPICAL GEOLOGY OF A SITE.	38
FIGURE 3.5	THREE-SCALE GEOMETRY OF THE UNDERGROUND OPENING SYSTEM	40
FIGURE 3.6	EXAMPLE OF SEISMIC ACCELERATION SPECTRA AT DIFFERENT SITE LOCATIONS	49
FIGURE 3.7	CONCEPTUALIZATION OF A SEISMIC RESPONSE MECHANISM.	50
FIGURE 3.8	LOGICAL FLOW-CHART OF THE DIFFERENT PHASES OF THE STUDY.	51
FIGURE 4.1	TYPICAL GEOLOGICAL ENVIRONMENTS.	54
FIGURE 4.2	POSSIBLE STATES OF FISSURATION IN A ROCK MASS.	59
FIGURE 4.3	MOHR-COULOMB CRITERION	63
FIGURE 4.4	PERMEABILITY COEFFICIENT VS. CONFINING PRESSURE.	65
FIGURE 4.5	MAXIMUM AND MINIMUM IN SITU STRESSES VS. DEPTH	65
FIGURE 4.6	POSSIBLE RESPONSE CURVES OF THE DISPLACEMENTS OBTAINED IN THE FIELD.	69
FIGURE 4.7	R.Q.D. VALUES VS. MEAN DISCONTINUITY SPACING	71
FIGURE 4.8	ROCK VOLUME, BORINGS AND SAMPLES	73

	<u>Page</u>
FIGURE 4.9 COVARIANCE VS. DISTANCE	71
FIGURE 4.10 LINER'S MATERIAL.	76
FIGURE 4.11 SOME MEASURE PHYSICAL PARAMETERS FROM A SITE INVESTIGATION	81
FIGURE 4.12 LOCATION OF THE WATER TABLE	82
FIGURE 5.1 VARIABILITY OF PHYSICAL PARAMETERS.	85
FIGURE 5.2 VARIOGRAM VS. DISTANCE.	85
FIGURE 5.3 LOCAL APPROXIMATIONS OF GENERAL TRENDS.	89
FIGURE 5.4 APPROXIMATE VARIOGRAM FUNCTION FROM ACTUAL DATA . . .	91
FIGURE 5.5 FLOW CHART OF PROGRAM INFMOD (INFERENCE MODEL). . . .	95
FIGURE 5.6 ILLUSTRATION OF PROBLEM 1 (SPHERICAL TREND)	98
FIGURE 5.7 ESTIMATED STATISTICAL CHARACTERISTICS OF PROBLEM 1. .	99
FIGURE 5.8 GENERAL TREND FUNCTION OF THE PERMEABILITY.	103
FIGURE 5.9 TOPOLOGICAL CONSIDERATIONS FOR THE ESTIMATION NODE. .	103
FIGURE 5.10 ESTIMATED VARIANCES VS. NUMBER OF KNOWN POINTS. . . .	104
FIGURE 5.11 ESTIMATED STATISTICAL CHARACTERISTICS OF PROBLEM 2. .	105
FIGURE 5.12 EFFECT OF BOUNDARY CONDITIONS ON ESTIMATED VARIANCES	104
FIGURE 5.13 RESULTS OF THE INFERENCE MODEL COUPLED WITH THE F.E.M.	107
FIGURE 5.14 ILLUSTRATION OF THE ESTIMATION PROCEDURES	109
FIGURE 5.15 ASSUMED FUNCTIONS FOR THE COMPARISON OF TREND SURFACE ESTIMATES VS. MOVING AVERAGE ESTIMATES (INFERENCE MODEL).	112
FIGURE 5.16 MEASURED AND APPROXIMATED VARIOGRAM OF THE EXAMINED FUNCTIONS	113
FIGURE 6.1 F.E.M. DISCRETIZATION OF SCALE 1.	121
FIGURE 6.2 A MESH SIZING VARIATION SCHEME.	123

	<u>Page</u>
FIGURE 6.3 RANGE OF STRESSES AND STRAINS AT DIFFERENT STAGES OF THE ANALYSIS.	126
FIGURE 6.4 ILLUSTRATION OF THE BEAM FINITE ELEMENT	132
FIGURE 6.5 HERMITE POLYNOMIALS APPROXIMATING $v(x)$	132
FIGURE 6.6 FLOW CHART OF PROGRAM STFLOW.	136
FIGURE 6.7 STRESS FIELD AROUND THE EXCAVATION.	139
FIGURE 6.8 POISSON'S RATIO VS. STRESSES IN ROCKS	140
FIGURE 6.9 FLOW CHART OF PROGRAM EXCAV	143
FIGURE 6.10 EXISTING PHASE DIFFERENCES IN THE MOTION AT THE BOUNDARIES.	144
FIGURE 6.11 TYPES OF FINITE ELEMENTS.	146
FIGURE 6.12 FLOW CHART OF PROGRAM DYNMODE	152
FIGURE 6.13 PARAMETERS DESCRIBING THE LINER'S BEHAVIOR.	154
FIGURE 6.14 FLOW CHART OF PROGRAM STLINER	157
FIGURE 7.1 ILLUSTRATION OF DIFFERENT GEOLOGICAL ENVIRONMENT. . .	160
FIGURE 7.2 COMPUTATIONAL SCHEME OF THE EARTHQUAKE GENERATION MODEL	164
FIGURE 7.3 TRANSFER FUNCTION $(H(j\omega))^2$	160
FIGURE 7.4 MAXIMUM VALUES OF THE TRANSFER FUNCTION $(H(j\omega))^2$. . .	169
FIGURE 7.5 TRANSFER FUNCTION FOR DIFFERENT VALUES OF THE FREQUENCY RATIO F	170
FIGURE 7.6 DECOMPOSITION OF THE GENERATED ACCELERATION	172
FIGURE 7.7 OBSERVED SIMILARITY BETWEEN PROPOSED GENERATED SIGNALS AND OBSERVED EARTHQUAKES.	174
FIGURE 8.1 ILLUSTRATIVE EXAMPLE.	186
FIGURE 8.2 FLOW CHART OF PROGRAM DELECTRE.	187
FIGURE 8.3 EXAMPLE OF APPLICATION OF DELECTRE.	190
FIGURE 8.4 INTERPRETATION OF THE OUTPUT OBTAINED FROM DELECTRE .	191

	<u>Page</u>
FIGURE 9.1 GENERAL GEOMETRIC CONFIGURATION OF THE DIFFERENT CONSTRUCTION ALTERNATIVES FOR THE PROPOSED CAVITY SYSTEM.	194
FIGURE 9.2 SEQUENCE OF COMPUTATIONAL STEPS	195
FIGURE 9.3 ORGANIZATIONAL SCHEME OF A SITE INVESTIGATION	197
FIGURE 9.4 RESULTS OF (INFM D) SPATIAL DISTRIBUTION OF THE COEFFICIENT OF VARIATION OF PARAMETER R.Q.D	200
FIGURE 9.5 RESULTS OF UNDERGROUND FLOW FOR DIFFERENT CASES	203
FIGURE 9.6 RESULTS OF THE EXCAVATION	206
FIGURE 9.7 ACCELERATION SIGNALS.	209
FIGURE 9.8 GROUND MOTION RESPONSE SPECTRA.	211
FIGURE 9.9 PROPAGATION OF THE SEISMIC PERTURBATION	212
FIGURE 9.10 VARIATION OF STRESSES	213
FIGURE 9.11 DEFORMATION OF THE LINER	217
FIGURE 9.12 DISTRIBUTION OF THE ENTROPY OF INFORMATION OF THE STATIC AND DYNAMIC DISPLACEMENTS (CASE OF DEEP CAVITY)	221
FIGURE 9.13 ILLUSTRATION OF THE RESULTS OBTAINED BY DELECTRE (STATIC CASE)	224
FIGURE 9.14 ILLUSTRATION OF THE RESULTS OBTAINED BY DELECTRE (DYNAMIC CASE).	225

LIST OF SYMBOLS

CHAPTER 3

c	= damping matrix
$\{F\}$	= load vector
K	= stiffness matrix
L	= wavelength
R	= radius of cavity
T	= predominant period
$\{u\}$	= displacement vector
v_s	= shear wave velocity
σ_z^2	= variance of variable z

CHAPTER 4

E	= Modulus of Elasticity
E_c	= Modulus of Elasticity of concrete liner
E_s	= Modulus of Elasticity of steel liner
G	= shear modulus
I	= intensity of jointing
k_x	= permeability coefficient in x-direction
P_c	= confining pressure
RQD	= rock quality designation

u	= interstitial water pressure
V_p	= velocity of the compression wave
V_s	= velocity of the shear wave
\bar{z}	= mean value of rock physical parameter z
ν	= Poisson's ratio
ξ_i	= damping ratio
ρ	= mass density
τ_{\max}	= shear strength
τ_c	= apparent cohesion
ϕ	= angle of internal friction

CHAPTER 5

a_β	= unknown weight coefficients
$c(d)$	= covariance function
$f^i(x,y)$	= a priori known function approximating $\bar{z}(x,y)$
FZ	= fluctuating term of physical parameter Z
k	= stiffness matrix
\hat{z}	= estimation of physical property z
\bar{z}	= mean value of physical property z
\bar{z}_β	= mean values of known data points
$\gamma(d)$	= variogram function
σ_z^2	= variance of physical parameter Z

CHAPTER 6

$\{d\}$	= displacement at nodes
d_F	= displacement of free node

E_i = Initial Modulus of Elasticity
 $[k]$ = stiffness matrix
 k_x = permeability coefficient in x-direction
 $[m_F]$ = mass matrix
 $[Nk]$ = nonlinear stiffness matrix of liner
 $\{u\}$ = general displacements
 V_x = velocity of flow in x-direction
 \bar{v} = mean velocity of propagated wave
 $\text{VAR}(\omega_i)$ = variance of natural frequency ω_i

$\{\epsilon\}$ = strain vector
 Λ_j = eigenvalue
 ξ_i = damping ratio
 $\{\sigma\}$ = stress vector
 ϕ_j = approximate linear function
 ω_i = natural frequency

CHAPTER 7

F = frequency ratio
 H = transfer function
 k = stiffness of a posteriori component
 K = stiffness of a priori component
 m = mass of a posteriori component
 M = mass of a priori component
 M = mass ratio

- S_0 = power spectral density function
- ξ = damping ratio of a posteriori component
- Ξ = damping ratio of a priori component
- $\phi(t)$ = intensity variance function of a shot noise process
- ω_n = natural frequency of a posteriori component
- Ω_n = natural frequency of a priori component

CHAPTER 8

- c_{ij} = concord index
- d_{ij} = discord index
- E = Entropy
- $CVR(p)$ = deterministic component
- $G(P,Q,S)$ = graph
- $H(p)$ = heuristic component of weight coefficient
- S = number of criteria considered simultaneously in the sorting procedure
- $W(p)$ = weight coefficient of attribute p
- γ_p = mapping of among alternatives according to criterion p

CHAPTER 1

INTRODUCTION

1.1 Motivation

Large permanent underground openings in rock have been constructed throughout the world. They are used for housing hydroelectric plants, nuclear powerplants, aircraft hangars, ship docks, storage of petroleum products and as part of ore mining operations. In all of these uses there appears to be only nominal, if any consideration given to the vulnerability of such openings to earthquake effects. Moreover, research of the world literature has located only scanty data from actual measurements of earthquake effects underground (43).

Although all of the data up to this point show that the intensity of vibration is considerably reduced at a depth, as compared to that at the surface, Staunton (87) states that the generalization that earthquake vibrations are not very perceptible underground does not always hold.

Several approaches exist to analyze the response of underground openings to earthquake shaking (25). They confirm to some extent the general trend of the empirical data. The usual procedure consists of simulating the physical world with an analytical model and predicting the behavior of the opening under earthquake conditions. However, the presently existing models do not provide a good answer to the problem

partly due to the introduction of over simplifying assumptions in the analysis. Figure 1.1 is an illustration of such an approach.

A seismic disturbance is assumed to hit the vicinity of the cavern. The safety of the cavern should be assessed. It is usually evaluated knowing the response of the cavity to the above disturbance. The response is obtained by making a number of simplifying assumptions concerning the physical parameters of the rock structure: the medium is considered to be continuous and the boundary conditions simplified to the point of considering the initial ambient stresses to be uniformly distributed - a case which is rarely actually encountered in reality. Finally the statistical characteristics of the surrounding rock medium should be considered and their causes evaluated, an aspect that is not often taken into consideration. Moreover, a scheme should be developed to make a qualitative evaluation of the data resulting from the analytical model. It is necessary to develop a means of comparing different design alternatives that exist for projects of such importance. It is believed that a dynamic analysis of the cavity system will affect the choice of the best design alternative.

The term "cavity system" is introduced to define the underground opening, its geometry, the surrounding geologic characteristics and the bolting system or liner required for the stability of the opening.

The present work is a more systematic study of the dynamic effects on cavity systems, including development of evaluative criteria to judge the performance of various design solutions with respect to the depth, shape of the opening, and the cavity wall reinforcement (rock bolting and lining). This study focuses on the development and implementation of a general methodology towards this goal.

PROTOTYPE

ANALYTICAL MODEL

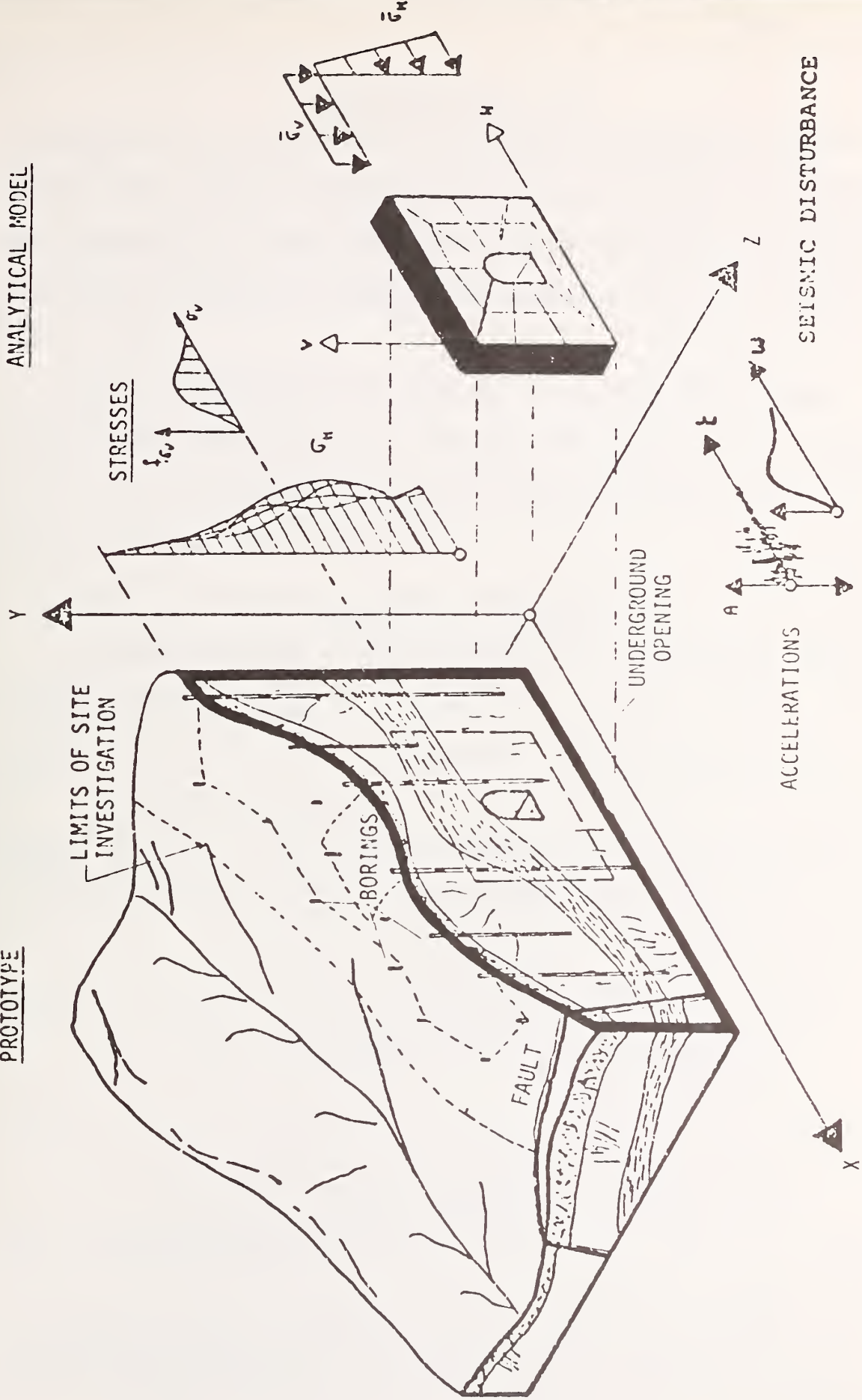


FIGURE 1.1 CONCEPTUALIZATION OF AN UNDERGROUND OPENING

1.2 Problem Components

The cavity system is a physical system and as such it is usually approximated by models with idealized components that permit a precise mathematical definition of the system. The choice of an adequate model having all the critical features of the physical system is a difficult, if not an impossible task.

Two alternatives exist in modeling the performance of a cavity system. They represent the extremes of the spectrum of possibilities. If on the one hand an oversimplified model is used, the results will loosely or not at all approximate the behavior of the system. On the other hand if a complicated model is used, it may be difficult and costly, or very often impossible to use with existing mathematical tools. However, the main concern here is to define an adequate model, i.e. flexible with respect to the entire spectrum of possible inputs. Therefore, it is essential to define the relationship between the inputs to the system and the outputs representing the response of the system. For this purpose, the need is to identify the different elements of the problem.

The basic analytical components are:

- The geologic and rock property analysis
- The seismic analysis
- The rock mechanics analysis
- The evaluation of performance criteria.

A detailed review of the existing theoretical background concerning the above components is given in Chapter 2.

In the present analysis the to be simulated geologic environment will be a cavity lying between two faulting systems or major

discontinuities: the latter will constitute the geometric boundaries of the model. This is a realistic assumption since extensive dislocation and fragmentation of portions of the earth's crust have occurred in the past throughout all areas of the globe and are active at the present time.

Concerning the geometric framework of the study, the range of width for the rock cavity will be between 20-40 meters. The analytical model will be designed to handle a maximum distance between main rock discontinuities of 300 to 500 meters.

1.3 Objectives and Procedures

Following the general ideas displayed in the introduction, the objectives of the present study are:

FIRST To develop a model of the behavior of a cavity system under an earthquake disturbance.

SECOND To define a realistic design procedure for a cavity system, taking into account all possible information from site investigation, including the geologic features of a particular site.

THIRD To develop a systematic procedure comparing the different possible design alternatives for such underground openings.

FOURTH To achieve these objectives within the framework of a numerical procedure simple and easy to use, based on the physical data obtainable from a field investigation, and results easy to interpret physically.

The analysis will be based (1) on a deterministic concept as far as the transfer mechanism is concerned; (2) on a statistical tool for

the description of the physical parameters involved including the input seismic disturbance.

The study of an underground opening is understood to require the following phases:

Phase 1 Find the physical parameters that most accurately describe the rock media. Take into consideration their variability as observed from a site investigation.

Phase 2 Find the analytical model for a realistic representation of the media according to the physical data inferred from the site investigation.

Phase 3 Define the input seismic disturbance signal, adequately taking into consideration the random nature of the rock media.

Phase 4 Combine the output from the previous phases to produce a numerically-based evaluation of the seismic vulnerability of the cavity system.

Phase 5 Compare several design alternatives according to criteria produced by the analysis.

The analysis of the geologic and rock properties is necessary since it provides the parameters describing the physical behavior of the cavity system. These parameters are inferred from a field investigation and used as an input to the analytical model along with the seismic signal from the seismic analysis. The outcome of the dynamic analysis is used to establish evaluative criteria for a given structure. Finally several alternatives will be compared for the given site. This will permit determination of the most adequate design for a given site, based upon the assumptions made during the study.

1.4 Relevance of the Study

In every project dealing with the construction of an underground cavity, the concern is to evaluate the technical feasibility of constructing and maintaining such a structure. To realize this goal, improvements in the related design procedures are needed and can be achieved only by an increased awareness of the mechanisms and modes of behavior of the cavity system. Deere and Peck (16) recognized that this awareness can be reached best by a combination of theoretical considerations and studies of the observed behavior of cavities in the field. Moreover, because of the complexity encountered in the design procedures, it will be useful to perform parametric and sensitivity analyses of the different components of the model, in a framework borrowed from Systems Analysis Concepts.

It is believed that the outcome of the proposed study outlined in the previous paragraph, could be used to increase the awareness of the mechanisms to predict the behavior of the structure under consideration and to facilitate the design of such cavity systems. More specifically the aforementioned results could be helpful in the following manner:

1. In a preliminary design to assesses
 - (a) The acceptable range of structural (rock) response to seismic effects on large openings.
 - (b) The efficiency in the selection and location of ground motion instruments for permanent installation and monitoring of the opening.
2. In a preliminary design to compare
 - (a) Different construction procedures.
 - (b) Different site locations.

3. In a final design to permit

- (a) The best estimation of the distribution of dynamically - induced stresses and displacements around large openings in rock media.
- (b) The evaluation of the safety level reached in each sequence of input signals.

CHAPTER 2

REVIEW OF THEORETICAL AND EXPERIMENTAL BACKGROUND

2.1 Introduction

The objective of the present chapter is to justify the conceptual basis of the study rather than to produce an exhaustive list of references. Thus I will present the basic assumptions and logical thought sequences necessary to an effective simulation of cavity systems and the development of physical criteria for the comparison of different design alternatives, will be presented in a rational and orderly manner.

In evaluating the effects of earthquakes on a cavity system one has to assess the relationship between the characteristics of the earthquake ground motions, the local rock and geologic conditions at the site, and the response of the structural system to the ground motions.

These intermediate phases are synthesized by determining:

- (1) The nature of the ground motion generated by an earthquake,
and
- (2) Its effects on the cavity system.

Therefore, a brief introduction of the earthquake phenomenon is given with respect to the natural environment.

A review of the theory of motion is necessary to a realization of the relative place occupied by the different solid mechanic approaches

in the framework of the analysis, and to identify the basic physical parameters. These parameters enable the abstract model of the simulation, adopted for simplicity, to be fitted to the real world. Therefore, a close examination of the existing simulation models is required to put the different components of this study into perspective.

Next, the treatment of uncertainty is discussed and related to the variability of the previously mentioned physical parameters. Such uncertainty analysis can actually be considered as the link between prototype and the analytical model.

Finally, methodologies for making sound decisions are presented; these are based on the performance of alternate cavity systems as evaluated by the above analytical models.

Throughout the review of the theoretical and experimental background, reference will be made to the most representative of the published literature.

2.2 Earthquake Ground Motion

The evolution of the seismic phenomenon takes place sequentially as follows. At first a tectonic movement takes place. Then the resulting disturbance propagates through the earth media at a megascale configuration (hundreds of kilometers). Finally the interaction between the resulting signal and the underground opening takes place at a macroscale configuration (a few kilometers), (Figure 2.1).

The present work will be restricted to the cavity system which is defined within the macroscale configuration. The stress waves reaching the boundaries of the macroscale configuration will be of random nature. It is believed that they are similar to the random fluctuations

TYPICAL GEOLOGICAL SECTION		
	<p>EPICENTER</p> <p>ACCELEROGRAM</p> <p>ACCELEROGRAM</p> <p>'ZONE OF INTEREST</p> <p>underground structure</p> <p>FAULTS</p>	<p>MACROSCALE CONFIG.</p> <p>INTERACTION BETWEEN E. Q. SIGNAL AND OPENING</p> <p>- Case histories existing in real E.Q. phenomenon</p> <p>- More data exist from nuclear explosions</p>
TYPES OF MODELLING	<p>INITIATION OF THE PHENOMENON</p>	<p>MEGASCALE CONFIGURATION</p> <p>'PROPAGATION OF THE DISTURBANCE</p>
	<p>APSTERIORI</p> <p>Exact solutions</p>	<p>APRIORI</p> <p>Approx. - FINITE DIFFERENCES</p> <p>- FINITE ELEMENTS</p> <p>STOCHASTIC APPROACH</p> <p>- Inference of seismic ground motion by autocovariance function</p>
	<p>DETERMINISTIC APPROACH</p> <p>- Exact methods</p> <p>- Approximate methods (FINITE ELEMENT)</p> <p>STOCHASTIC APPROACH</p> <p>- Governing equation determ. but forcing function is random</p>	

FIGURE 2.1 SCALES IN WHICH THE EARTHQUAKE PHENOMENON TAKES PLACE

observed in records of strong-motion earthquakes on the surface of the earth. The controversy concerning the relations between surface motion and corresponding underground motions is discussed later. In the following the factors which govern the earthquake motion at the surface are presented.

2.2.1 Earthquake Signals on the Earth Surface

Hofman (32) suggests three sequential studies to define the "design earthquake":

A. A Geological and Seismological Investigation - It requires a listing of all recorded earthquakes in the general area of the site, and the geological faults exceeding 2 km in length that lie within 350 km of the proposed site.

B. A Prediction of Earthquake Strength and Magnitude - It has traditionally been a qualitative study in which correlations between the earthquake signal and the important geologic features are established. The earthquake signal is characterized by its intensity (a purely subjective factor based on the observed damage) and its strength, measured as a peak horizontal-ground acceleration (a fraction of the gravity acceleration g). Many interesting results of such a study are provided by Housner (35) and Seed et al. (83).

C. A Quantitative Evaluation of Earthquake Motions - This is the most interesting part from the engineering point of view because its results can be used directly in an analytical model. The quantitative characteristics of an earthquake are provided either by a response spectrum or by a time-motion record. The latter is preferred for dynamic analyses of complex structures. Therefore, our attention is

focused on the acceleration record whose most important characteristics (35) are: (1) the duration of the record, (2) the predominant period, (3) the peak acceleration, and (4) the root-mean-square (rms) of the record.

From many studies related to seismicity, it can be concluded that real earthquake records in a sense constitute individual events related through a multitude of random parameters to a specific environment. Therefore, they can be considered as a single realization of the above mentioned set of parameters, a unique realization that will never again occur. Moreover, if a parametric study is to be done that considers all possible values that the different random parameters can take, then a simulation capability is needed. References (52) and (63) give a brief history of the simulation techniques proposed in the literature.

The problem of scaling the artificially generated (or design) earthquake signals from actually recorded earthquake signals is treated extensively by Seed et al. (84). However, as a general observation it must be said that the information needed to relate the earthquake magnitude and strength to a specific site is quite limited at the present time. Consequently, predictions of earthquake magnitude are subjective and frequently overestimated.

2.2.2 Seismic Response of Underground Structures

Several studies suggest that the earthquake motion is less pronounced at a certain depth underground than on the surface of the earth. The main investigations supporting this contention are provided by Crowley (12) and a group of Japanese researchers including, in chronological order, Nasu (61), Kanai (46), Shima (86) and recently Okamoto (65).

Crowley gives earthquake characteristics in 20 different locations in the United States and abroad and concludes that the reduction factor between the surface motion and the motion at depth is period dependent (see Table 2.1). The same conclusions come Nasu and Kanai in 1950. Their results are obtained respectively from measurements in the Tana tunnel (Table 2.1) and the Hitachi copper mine. Some contrary observations come from Okamoto who found no significant difference in the displacements at the surface as compared to the displacements underground, at the Kingawa Underground Electric Power plant.

In general the results although sparse in a statistical sense indicate a reduction of the seismic response with depth. These motions are found to be dependent both on the natural frequency of the media and the frequency content of the seismic excitation. Shima's results of the frequency analyses confirm the above statement. He found that a similar periodicity existed in both spectra of the surface and underground at frequencies between 0.7-0.9, 1.1-1.8 and 9.0-9.2 Hertz. He concluded that this result was due to a periodicity contained in the earthquake signal. However, there was another periodicity which appeared at the surface signal alone, at frequencies of 2.4-2.7, 4.3-4.7 and 5.4 Hertz. He believed that this result was a consequence of seismic excitation in the natural periods of the soil layers.

In general the following conclusions can be drawn:

- (1) The similarity between the motions on the surface and at depth increases with the increase of the epicentral distance.
- (2) The similarity between the two motions increases with the increase of the period of the wave.

TABLE 2.1 EARTHQUAKE SIGNAL AT DEPTH

LOCATION	EPICENTRAL DISTANCE d [km]	DEPTH OF MEASUREMENTS D [m]	NATURAL PERIOD OF ROCK MEDIA sec	PERIOD OF SEISMIC SIGNAL sec	DISPLACEMENTS RATIO A_0/A_D
TANA TUNNEL	$d < 100$ km	160.	2.4 4.0	0.3 1.0 2.0 5.0	4.0 2.0 1.5 1.2
HITACHI COPPER MINE		300.			2.-6.
SHIMA'S WORK	$d < 100$ km		2.7 4.3 5.4	0.7 1.1 3.2-5.7	5.0 3.0
KINGAWA und. E.P.P.		67.			

(3) Periodicities reflecting the natural frequencies of the rock media are apparent in a frequency analysis.

(4) The rock media is acting as a filter since the recorded seismograms underground are much simpler than those recorded on the surface.

2.3 Fundamentals of the Theory of Motion

The roots of the study of motion are found in the 17th century in the theories of Newton, Leibniz, Euler, Lagrange and others. A simple presentation of their basic assumptions will show, to some extent, the elegance in these scientists thoughts and at the same time expose the limitations of the existing theory of motion.

Newton's second law of motion was the fundamental basis on which the "vectorial mechanics" was founded. It aims to recognize all the possible forces acting on a given idealized particle, its motion being determined in a unique fashion by the known forces acting on it at every given time. The basic quantity in Newton's formulation is the action of a force measured by the produced momentum. The motion of a particle in space is described by three equations.

On the other hand, Leibniz's concept of vis viva (living force, working force) was the basis of the "analytical mechanics" which bases the study of motion on kinetic and potential energy, two scalar quantities. The energy theorem so stated considers the sum of the kinetic and potential energies to remain unchanged during the motion. Therefore, the motion of a particle is described by one equation. The question then arises of how to relate these two opposing theories. Using Euler's and Lagrange's principle of least action the two different

formulations can be linked together. Moreover Hamilton's procedure enables us to consider the work function with respect not only to the position of the geometric space, but also to the time. This principle of "least action" asserts that the actual motion realized in nature is that particular motion for which this action assumes its smallest value.

Newton's approach can be characterized as a causal description of things while Leibniz's considerations give a purpose rather than a cause to the flow of natural events. Indeed vectorial mechanics isolates the particle and considers it as an individual while analytical mechanics considers the system as a whole. In that respect vectorial mechanics produces a differential equation of motion and the dynamic problem is reduced to the integration of that equation; in analytical mechanics it is sufficient to know one single function which contains implicitly all the forces acting on the particles of the system.

Geometry constitutes the basis of the formulation of the motion in both mechanics. It is present in the acceleration term of Newton's mechanics as well as in the kinetic energy in Leibniz's mechanics.

The above mentioned principles imply a determinism in predicting a future state of the system. It is based on the knowledge of a previous state, or otherwise stated, there is a need to know the initial conditions.

The physical parameters describing the motion are the force, the mass and the acceleration. However, in many cases the initial conditions and physical parameters are difficultly or not at all defined. In presence of such diversity a new approach was developed to handle this uncertainty: the statistical mechanics.

The various branches of mechanics are considered to be imperfect tools in the attempt to reconstruct in our mind the work of empirical facts. As a consequence of this people started investigating the reasonableness of the behavior of some physical parameters under uncertainty. It was the beginning of the Probabilistic reasoning which gave birth to the Probability theory with all the related theories of Statistics, Decision Theory and Operations Research. However probability should be viewed as a subjective concept rather than an objective one which tends to be built on firmer philosophical or logical foundations. This does not by any means reject the existing probability theory because as de Finetti (23) pointed out the definitions of "Objective" probability although useless in an absolute sense, turn out to be of great help when included as such in the subjectivistic theory.

The latter approach is adopted in the present study in which statistical means are used to measure our lack of knowledge of the causes. In that respect, the previously mentioned principle of motion constitutes the causality law and is the vehicle with which to a statistical set of causes, a statistical set of effects is obtained.

2.4 Simulation Models and Their Conceptual Basis

2.4.1 Conceptual Models

The previously mentioned theoretical background constitutes the basis for the development of simulation models. Such models are necessary to reproduce to a certain degree of closeness the behavior of the rock material and the behavior of the structural environment. Clearly for each one of these two cases a different model is needed. In both cases the simulation model provides us with the transfer function between an input and an output quantity, based on experimental evidence. This experimental evidence is obtained either in the field, at the real scale or at a laboratory, at a reduced scale.

Three types of modeling techniques exist. They are:

- A. The "A Priori Model"
- B. The "A Posteriori Model"
- C. The "Pseudo-priori Model"

In what follows a brief description of each technique is given as summarized from Boyer and Cannon.

A. The "A Priori" Model. It can be defined as a pure analytical model. The input of interest is considered to be completely known, as well as all the possibly available necessary physical parameters characterizing the real world. Predictions are made on the basis of the above required information.

The theoretical basis of the model is derived from the concept of continuum which is a mathematical abstraction introduced for convenience of the analysis. The application of the equations of motion, produces the governing equations. Moreover, the validity of the physical

parameters of the model is controlled by the failure criteria developed in concordance with field and laboratory experimental tests.

The mathematical formulation provides us with the following:

- a. A way to predict the change in the relative position of particles in the rock mass due to imposed dynamic loads.
- b. A way to determine the interrelationship between applied loadings and the degree of potential failure.

Stresses can be considered as providing a standard by which the transmission of forces can be measured.

B. The "A Posteriori" Model. This is a technique which involves the use of the desired real-world system, whose response to an input of interest, at the real scale, is actually measured. The two quantities then, input and output are related using a mathematical formulation. Consequently the only way to obtain the transfer mechanism is to perform real scale experimental tests.

There are different methods used to obtain the mathematical form of the transfer mechanism. Among them the following:

1. The Frequency Spectrum Method. A known disturbance is introduced in the media whose transfer mechanism is sought. The magnitude of the steady-state peak input and the steady-state peak output as well as the phase angle between the two, are measured. Then the ratio of the magnitude of the peak output to that of the input are plotted for the range of frequencies of interest. The so obtained plot is called the frequency spectrum. Finally the mathematical form of the transfer mechanism is obtained directly from the frequency spectrum. However, the solution is only approximate since the frequency spectrum is approximated by a piece-wise linear curve.

2. The Convolution Method. The working space is the time domain, and it makes use of the inverse Laplace transform technique. The idea is that an arbitrary input can be considered as the sum of a sequence of impulses and that the global response, assuming the system to be linear, can be found by superposition of the individual impulses.

An "a posteriori" model is used to generate the earthquake loads, which in our case constitute the input of the overall study.

C. The "Pseudo A Priori" Model. This technique is similar to the previous one with the difference that the real-world system is replaced by an equivalent experimental system. Different types of analogies, geometric, dynamic etc. can be adroitly used to that end. However this particular model is beyond the scope of the present study.

2.4.2 Methods of Resolution of the Mathematical Formulation

The modeling techniques built in an abstract framework, have simplified the real situation and have provided the designer with a mathematical formulation. Therefore, at this point the task will be to obtain a solution taking into consideration the physical nature of the parameters and the input quantities. They can either be deterministic or of a random nature. Therefore two cases are to be considered in the analysis.

A. The Deterministic Case. The equation of motion has the form of a hyperbolic partial differential equation.

1. An Exact Solution. An exact solution for our particular case with the complexity of the boundary conditions and the need to reflect complex variations in the rock media is for all practical purposes considered impossible. Indeed all the existing attempts to solve the

problem use oversimplifying assumptions, without however succeeding in simplifying the sequence of numerical operations. Gregory's approach (26) is an example of such a complexity. His paper is concerned with the two-dimensional time harmonic vibrations of an elastic, homogeneous and isotropic half-space, containing a submerged cavity in the form of an infinite circular cylinder.

Another possibility can be the use of the method of characteristics, which is concerned primarily with the determination of the particular directions along which integration with respect to only one of the coordinate directions can be performed. Again the complexity of the boundary conditions can be overwhelming. More flexibility should then be sought in an approximate solution.

2. The Approximate Solution. The approximate solution is derived from the discretization of the geometric space and the accuracy is directly related to the fineness of the discretization. The problem specification then is to find the vector of unknown variables which satisfies the system of hyperbolic partial differential equations in a given domain and for a certain set of boundary conditions. Moreover, the above system is usually transformed to a linear system of equations by one of the several methods belonging to the following categories:

- a. Variational Methods - The differential equation is replaced by a function which satisfies at the same time the differential equation also (Ritz's Method).
- b. Direct Methods - A processor generates a set of algebraic equations from the operator equations (least square, collocation, Gallerkin).

- c. Integral Methods - Consists of the transformation of the differential equation to an integral equation, relating the unknown function and possibly certain of its derivatives to the given value on the boundary. This transformation is obtained either by the Green's function method or by the Distribution Theory. The difference in this procedure is that only the boundaries are discretized and approximated while the medium is considered as a continuum.
- d. Finite Difference Equations - The method is based on the replacement of the differential equations by the corresponding finite-difference equations.

B. The Statistical Case. To our knowledge the only attempt to estimate the response of structures with a large number of degrees of freedom, to a weakly stationary random excitation was made by Kayser (47). In this approach the matrix of complex transfer functions of the system is estimated using an approximate inverse of the transformed system matrix in such a way as to minimize the mean square constraint forces over a finite frequency interval.

2.4.3 Adopted Mathematical Resolution

The approximate procedures a and b of section 2.4.2 are key to the Finite Element approach which according to Houstis et al. (36) is almost uniformly superior to the classical Finite Difference methods. Moreover it is the most commonly used technique. However we should be aware that in using a Finite Element Method, (F.E.M.) nothing can be said about the absolute error committed in the evaluation of the solution. Instead some bounds of the a priori error can be specified

according to the numerical procedure used in each case. The feeling that one has in dealing with F.E.M. is that it is based mainly on prejudice, experience and last but not least on intuition.

On the other hand the previously mentioned statistical resolution technique is attractive but it requires that the system mass damping and stiffness coefficients be constant. Moreover it can potentially handle a much smaller number of degrees of freedom than the F.E.M.

From the above considerations it seems that the best solution approach would be a combination of a F.E.M. technique coupled with an uncertainty analysis characterizing the randomness of the different physical parameters.

2.5 Quantifying the Uncertainty

The previous considerations clearly indicate that in order to perform as accurately as possible the analysis, the uncertainty involved in each physical parameter must be explicitly taken into consideration. Moreover the quantification of this uncertainty must be based at least in part on inferences drawn from measurements obtained either in the real field or from laboratory tests. Uncertainty is encountered in the following elements:

1. Uncertainty in the seismic load
2. Uncertainty in material properties
3. Uncertainty in structural geometry
4. Uncertainty in the construction process
5. Uncertainty arising from the simulation model.

Uncertainties in the process of construction and structural geometry are almost beyond estimation. Consequently, our attention will be focused on the estimation of the statistical properties of the applied seismic loads and the material properties.

The quantification of the uncertainty is obtained using statistical or probabilistic tests. The appropriate method is intrinsically related to the nature of the physical parameter under consideration. Indeed the uncertainty in seismic loading parameters is evaluated by using a frequentist approach, while the uncertainty of the rock material is usually treated by a bayesian approach.

The frequentist concept is based on the assumption that the probability distribution describing statistically a physical parameter is undefined, as suggested by Rosenblueth (77). On the other hand the bayesian concept is formulated within the framework of a complex deterministic universe that our lack of knowledge and technology has failed to define exhaustively by deterministic means.

In engineering, Rosenblueth (77) suggests to use a bayesian concept of probabilities and this is the case of the present study, in which a second-moment technique is adopted. This is justified by the fact that the most accurately defined statistical parameters are the first and second moments of a distribution rather than the probability distribution itself. Moreover the statistical moments are obtained easier from an experimental research in earthquake engineering, with the current equipment and techniques. Rea (73) gives an exhaustive list of such equipment.

2.6 Comparing Different Engineering Alternatives

The ultimate goal in any engineering study is the actual realization of the study, so that the abstract ideas and forms of the analysis take real form and use in real life. It might well be that the final step towards this realization lies outside the world of technology, in the more subtle and elusive domain of Decision Making. Everyday life is made of a sequence of decisions. The problem arises though when a 'best' decision is sought whose consequences are felt over a long period of time and over a large segment of the society. Appropriately then, global or trend decisions impinge on the collectivity. The role of engineers and scientists on the other hand, becomes increasingly important in a world technologically more complex, in providing the necessary and relevant information.

One way of interpreting the contribution of engineers towards "Best Decisions" is by means of Optimization. Given general goals, objectives and criteria, the engineer is called to produce optimal designs. A number of Optimization methodologies and techniques exist, traditionally grouped in the multidisciplinary field of Operations Research, (24). A number of attempts to apply these techniques to the field of Structural Engineering is reported in the literature. Linear Programming, Dynamic Programming, and Non-Linear Programming are the techniques most commonly used, the current trend of development being towards Multiobjective and Stochastic Programming. The most successful among these attempts were edited in a book on structural optimization by R. H. Gallagher et al., (24). To our knowledge no such attempt has been made to date in the particular field of Rock Mechanics. The

complexity displayed in relatively simple structural examples, (82), may well explain this lack of interest in Rock Mechanics.

An alternate approach towards achieving 'Best Decisions' is offered by the so-called Game and Decision theory, (54), traditionally applied to societal systems. The recent recognition of the importance of the evaluation of the uncertainty in engineering calculations, as related to the randomness and probabilistic behavior of physical quantities has stirred the interest in applying Decision Theoretic approaches. An example of such an application is provided in (51), where a preposterior probability analysis (Bayesian Approach) is used to determine the level of required information as related to a Rock Tunnel Exploration study. Resolving the complexity of technical decision problems, augmented by the uncertainty involved in the evaluation, by comparing only a discrete number of technologically sound alternatives, as determined by a Decision Tree technique for example, seems to be a promising avenue. Strong criticism though can result from the use of one single economic criterion (cost minimization objective), and from the strong weight given to subjective probability factors.

An approach giving due importance to the existence of numerous and often conflicting criteria in the selection of a best alternative exists in ELECTRE, (79). In that respect it might be characterized as taking the best out of two worlds, the exact world of Optimization techniques, and the fuzzy world of Game and Decision Theory. Making use of the elegance of a Graph Theoretic approach, it might well prove to be a valuable tool in trying to rationalize the traditional engineering judgement, based on knowledge, experience and intuition. This

approach is adopted in the present study, in an attempt to implement such a "Decision under Conflicitng Criteria" scheme for the case of cavity systems, in Chapter 8.

CHAPTER 3

DEVELOPMENT OF THE MODEL SIMULATING THE CAVITY SYSTEM

3.1 Introduction

The propagation of a disturbance through a medium is defined as a mechanical wave. It is characterized by the transport of energy in the forms of kinetic and potential energy, through motions of particles about an equilibrium position.

The two essential properties of a medium that describe the retransmission of a mechanical disturbance are the Deformability and the Inertia. In effect, if the medium is not deformable, any part of it would immediately experience a disturbance in the form of an acceleration. Likewise, if a medium had no inertia there would be no delay in the displacement of particles and the transmission of the disturbance would be propagated instantaneously to the most distant particle. Therefore, a realistic model simulating the cavity system should be based on:

First - The essential physical properties representing accurately the rock media, which can only be obtained from a field investigation and which are: the mass (inertial component) of the system, the stiffness and damping characteristics of the system and their statistical characteristics, and the water effect properties.

Second - The essential features for an accurate analysis, which are: an adequate description of the randomness of the rock media, inferred from the field investigation, a realistic consideration of the input seismic disturbance, and an accurate mathematical tool for the transfer mechanism taking into account the uncertainty of the physical input data.

The link between the two sets of features and properties is provided by an inference model which take into account the spatial distribution of the field information.

A typical cavity system as shown in Figure 3.1 needs a three-dimensional model for a realistic simulation. The complexity of the numerical formulation required by such an analysis would create computational problems difficult to solve under the actually available computers.. Moreover, a simple mathematical model would provide more flexibility to introduce the statistical characteristics of the physical parameters. Therefore, a two-dimensional analysis seems more adequate. Any vertical section across the opening containing the direction in which the plane wave is propagated can be taken into consideration.

In the following sections a brief introduction is given on the fundamental ideas used to model the real phenomenon as well as the sequence of the numerical procedures used to perform the analysis. The details and results on each computational step are provided in the subsequent chapters.

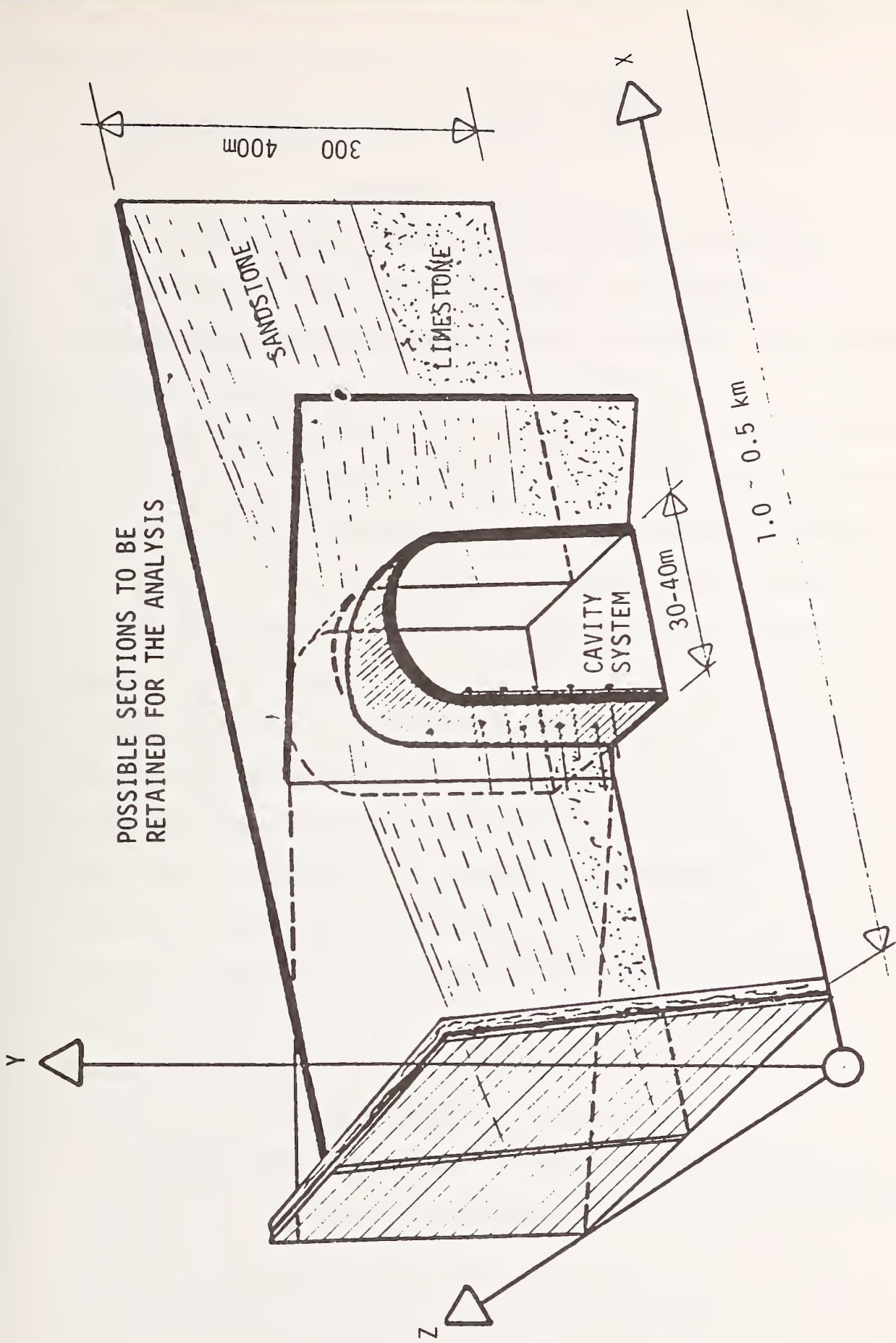


FIGURE 3.1 TYPICAL CAVITY SYSTEM

3.2 Geometric Framework and Boundary Conditions of the Model

3.2.1 Geometric Framework

It must be realized at this point that while the input seismic disturbance propagates in a megascale configuration, the analysis of our model for computational simplicity and efficiency is restrained to the macroscale configuration. The limits between the two configurations can be provided by the wavelength of the traveling seismic wave. Consequently something must be said about the predominant period of the earthquake and the velocity of the wave propagation. One way of estimating the seismic wave length is as follows:

From experimental data we know the range of the velocity with which the waves travel in a particular rock media. ex. the shear wave velocity in the rock is in the range $300 < V_s < 650$ meters per second. From accelerograms of earthquakes that have occurred in the past, the predominant period T causing maximum accelerations was observed to be in the range of $0.2 < T < 0.8$ sec. Consequently, the wavelength $L = V_s \cdot T$ is evaluated in the range of 60 to 300 meters. This information will enable us to determine the extent of the rock media surrounding the opening, that should be taken into consideration for a realistic macroscale simulation.

It must be noticed at this point that small earthquakes as opposed to large earthquakes have predominant periods which are different. Okamoto (66) gives the following data:

	Earthquake scale		
	Large	Medium	Small
Predominant Period (sec)	0.77	0.77-0.46	0.17
Magnitude (Richter scale)	7.5	6.7	< 4.0

He also concludes after studying a small number of underground acceleration records taken at a relatively shallow depth that in the initial stages of the main motions, the underground and surface records are similar, with however an expected slight lag in time.

Another important feature to our problem is the ratio between the radius of the cavity and the wavelength of the traveling wave. In Figure 3.2 two cases are presented. First the situation for which $R/L \leq 1$ (the structure is hit by low frequency seismic load) and secondly the situation where $R/L \geq 1$ (the structure is hit by a high frequency seismic load).

Both cases can occur during an earthquake since we are dealing with different frequencies. They necessitate a further subdivision of the macroscale into a scale 1 region and into a scale 2 region, Figure 3.2. Furthermore, a distinction is made between the low frequencies and the higher frequencies of the input seismic acceleration as shown in Figure 3.3. The problem then consists of defining the relative size of scale 1 and scale 2 as well as the corresponding boundary conditions.

3.2.2 Boundary Conditions

As said earlier, the analysis will be confined to the macroscale configuration. The overall dimensions then of the computational model will have to be defined accordingly. More specifically the location of the boundaries of the rock volume are to be defined. As it was

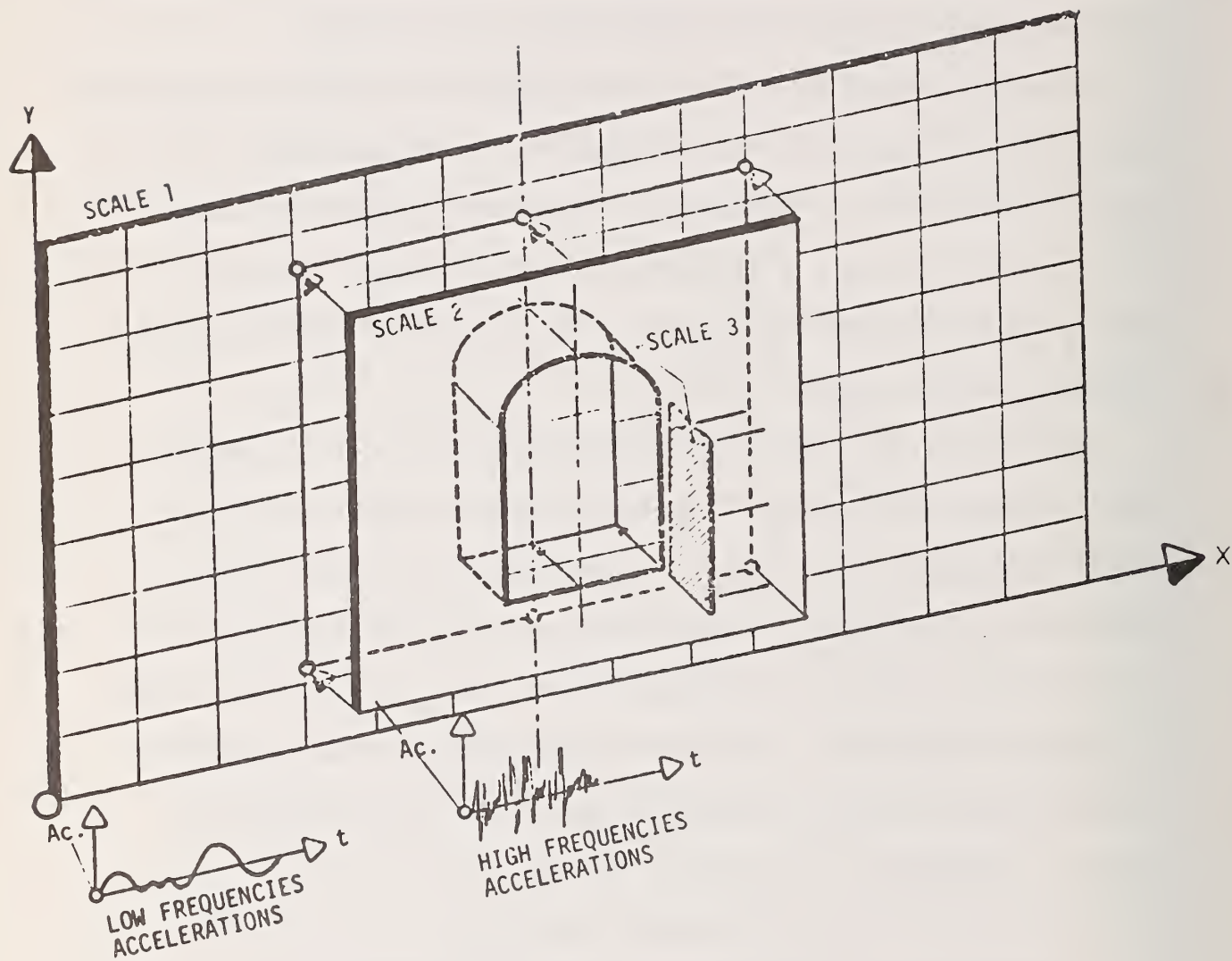


FIGURE 3.2 EFFECT OF DIFFERENT WAVELENGTH SEISMIC LOADS

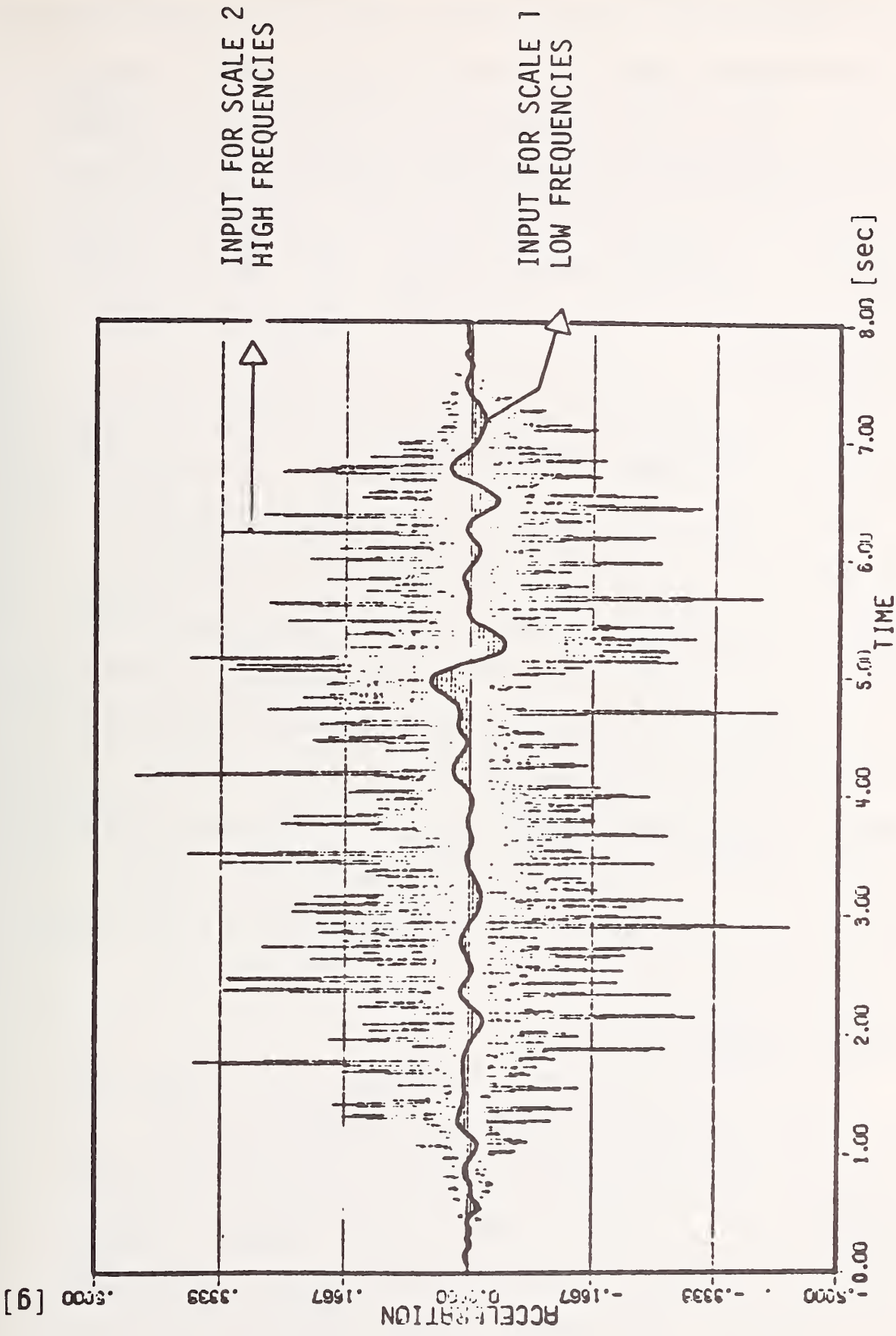


FIGURE 3.3 TYPICAL SEISMIC ACCELEROGRAM

suggested previously, it can be expected that only the higher frequencies of the earthquake signal will directly affect the opening. However, on the other hand the lower frequencies will affect the type of initial conditions to be used on the boundaries, Figure 3.2. In the current practice the location of boundaries is usually determined only from experience, by a trial and error procedure. Two types of boundaries are encountered:

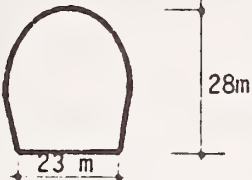
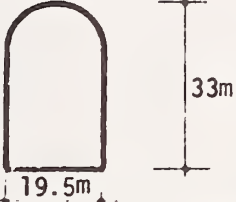
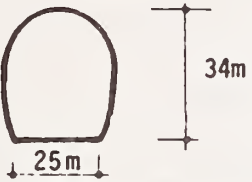
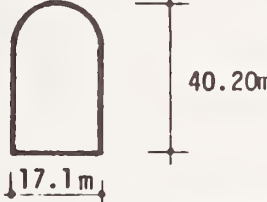

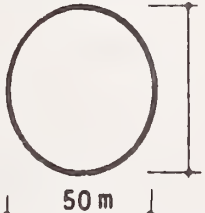
Base Boundaries

In actual practice many designers consider a uniform base motion, provided that the length of the base boundaries is less than one-fourth of the wave length, i.e. less than 15 to 60 meters. However, the size of the cavity systems of interest here does not permit such a simplification. Indeed from the existing underground caverns (see Table 3-1) we can deduce that on the average the diameter of the opening is in the range of 20 to 40 meters, which implies that the expected length of the base boundaries to be used in a model will be in the range of 300 to 400 meters. This clearly shows that, because of the presence of space variations we are concerned with time phase differences which exist from one point to another over the base dimensions of the boundaries.

Lateral Boundaries

Their location is dictated by the presence of a faulting system or of a major discontinuity encountered in any given geologic section, detected by a field investigation. An illustration of the above is given in Figure 3.4, in which several possible locations for the construction of the cavity system are indicated towards a realistic and efficient design. Such a geologic section is most commonly encountered.

TABLE 3.1 EXAMPLES OF EXISTING UNDERGROUND OPENINGS

PROJECT OVERBURDEN (D)	CROSS SECTION DIMENSIONS	TYPE OF ROCK	FINITE ELEMENT MESH	TYPE OF LINING
CAVERN TURLOUGH HILL IRELAND D = 100m		GRANITE	316 NODES 252 ELEMENTS	SHOTCRETE 15 cm ANCHORS 5m LENGTH (38 KN/m ²)
CAVERN WEHR D = 350m		GNEISS	356 NODES 339 ELEMENTS	SHOTCRETE 15 cm ANCHORS 4m LENGTH (24.5 KN/m ²)
CAVERN TAIWAN planned		SANDSTONE	400 NODES 397 ELEMENTS	SHOTCRETE 20 cm ANCHORS 6m LENGTH (24.5 KN/m ²)
MORROW POINT D = 120m		Precambrian METAMORPHIC ROCK (Mica Schist)	554 NODES 561 ELEMENTS	BOLTING SYSTEM
E. HYATT Power-plant D = 91.5m		GRANITE	744 NODES 704 ELEMENTS	BOLTING SYSTEM
PROJECT OF NUCLEAR PLANT IN SWEDEN planned D = 100m				Concrete and steel in a rib like structure

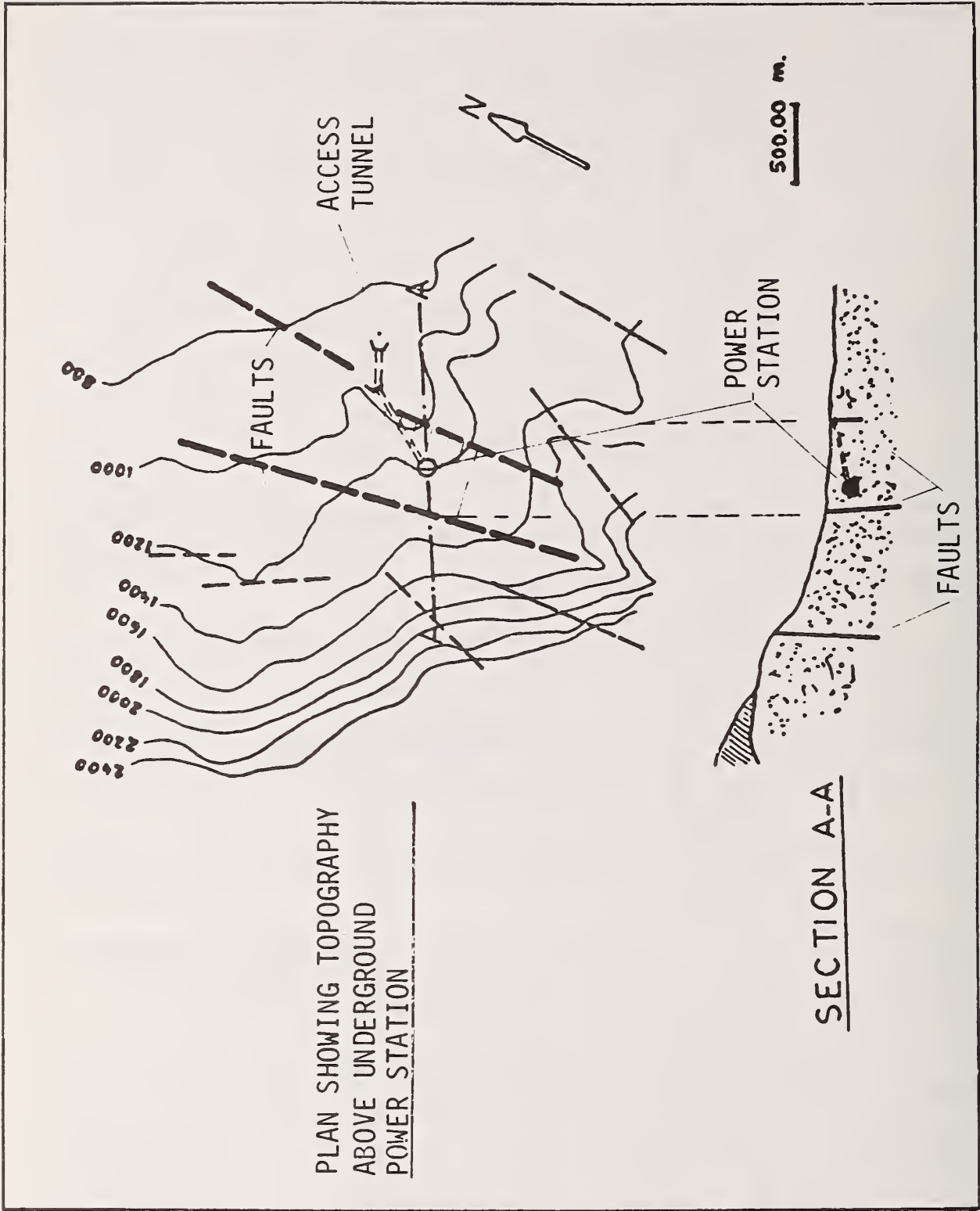


FIGURE 3.4 TYPICAL GEOLOGY OF A SITE

Clearly the rock medium surrounding the opening is the main element supporting the compressive stresses developed by the opening. However, structural elements are usually added, namely anchor bolts and a liner. They merely contribute to make uniform the behavior of the rock material near the opening causing it to behave like a monolithical beam. An interface between these two regions of different scale behavior should be considered in the analysis. A scale 3 is distinguished for the previously defined scale 2, as that region prestressed by the bolts system and the liner, Figure 3.2.

Both, slip and separation can exist between scale 2 and scale 3. However, due to the oscillatory nature of an earthquake we can assume that they will be of short duration and of an intermittent nature. Consequently, as a first approximation, complete fixity between scale 2 and scale 3 is assumed with however compatibility in the inertial forces acting between the two regions.

Summarizing, the geometry of the cavity system is characterized by the following scales, Figure 3.5.

Scale 1: defines the limits of the macroscale configuration.

The media is perturbed by the low frequency seismic wave.

Scale 2: defines the media perturbed by the high frequency seismic wave.

Scale 3: defines the rock-bolts system and liner perturbed region.

The above considerations are based on the behavioral aspect of the rock media but as it is shown later, they are in complete concordance with the requirements of the analytical model.

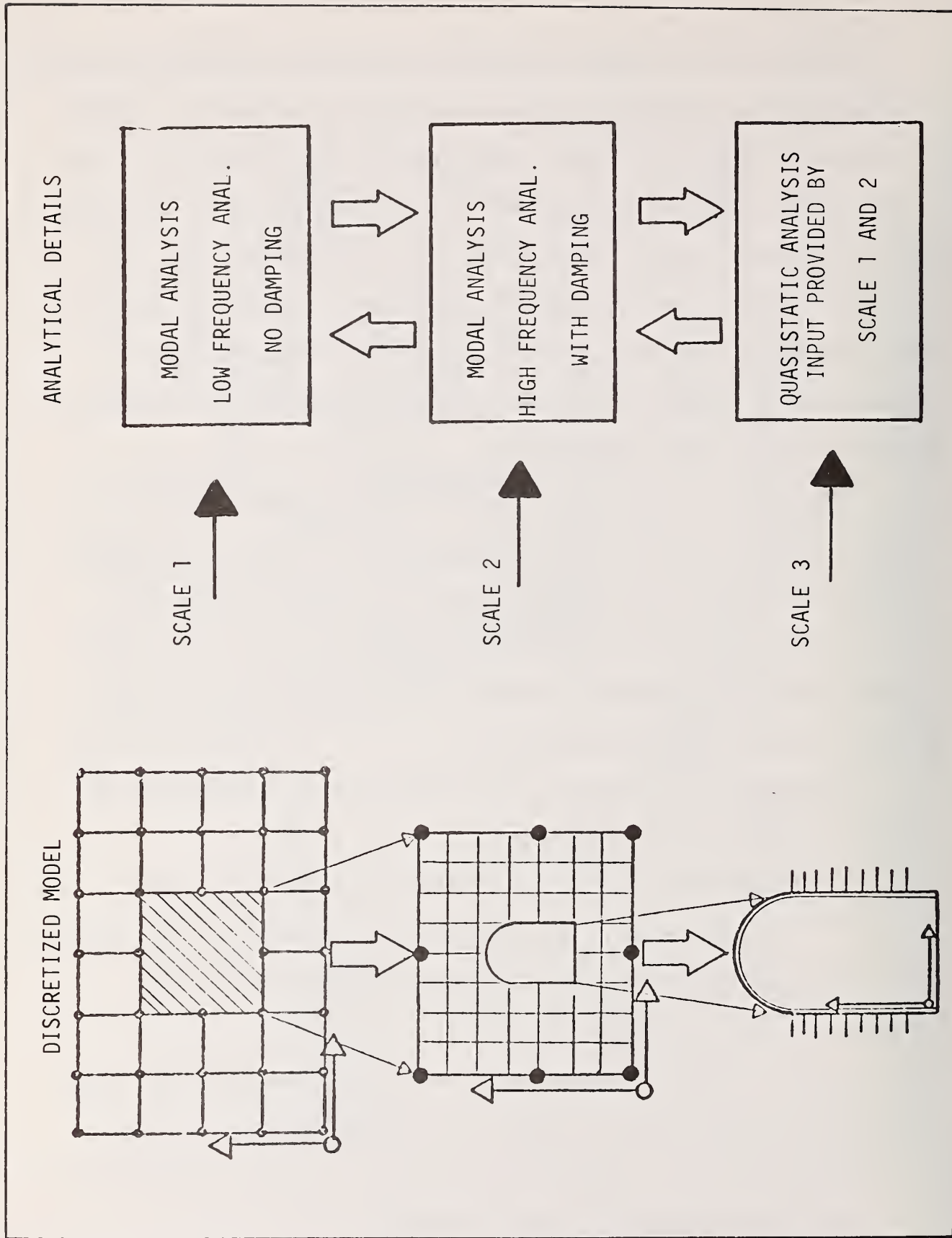


FIGURE 3.5 THREE-SCALE GEOMETRY OF THE UNDERGROUND OPENING SYSTEM

3.3 Evaluation of the Physical Properties Governing the Behavior of the Media

Two material components are considered in this study, namely the rock mass and the reinforced concrete constituting the liner. Their physical properties affecting the dynamic study are the mass, stiffness and damping. In turn these properties depend on some physical parameters determined through site exploration and laboratory tests. A thorough study of these parameters is given in the following chapter. These properties characterize the behavior of the media in every point in the space enclosed by the above specified boundaries. They constitute the fundamental link between the real environment and the analytical model adopted for simulation purposes.

It is generally recognized that within any homogeneous rock mass the physical properties exhibit a variability which must be considered in a design project. This variability is due to different causes during the geologic formation of the strata, and can be estimated from a site investigation. This will in turn provide the designer with the desired physical properties of the rock media at particular locations where the drillings are performed. To handle the variability of the rock media, an uncertainty factor is introduced in the simplified analytical model.

Two interrelated problems are then encountered:

- A. How the above mentioned uncertainty of the physical properties will be inferred from the field information.
- B. How to introduce the uncertainty of these properties in the already existing analytical model simulating the real world.

Both problems can be treated by assuming that the rock properties, say $Z_j(x,y,z)$ are spatial stochastic processes, as suggested by Cornell (3). Thus to a point in space (x,y,z) corresponds merely a probable value of Z_j , whose statistical uncertainty can be decreased at the expense of additional field information.

The above two problems are in common practice solved independently and not coupled together to provide a consistent picture of the real world phenomenon. A usual way to deal with the first problem is by making the assumption that the statistical properties of the rock media are the same throughout the region of interest or in other words, that the process reflecting the randomness of the physical property is stationary. In that case there is no need of an inference model and one can proceed to solve the second problem by applying a first-order uncertainty analysis in connection with the already existing analytical model. This approach was adopted by several investigators in the field of continuum mechanics, B. Cambou (7), L. Esteva (22), and J. Padilla (67).

However, in rock mechanics the above procedure cannot be adopted and the first problem has to be solved exhaustively merely because of the nonstationarity of the physical properties. Following these order of ideas an inference model coupling the field investigation with the analytical procedures is developed in Chapter five, offering the necessary flexibility for a more detailed statistical treatment.

3.4 Analytical Model Handling the Uncertainty of the Transfer Mechanism

A factor of uncertainty was seen to be introduced by the previously mentioned physical properties and parameters. Consequently, this

uncertainty measured by means of the variability of these parameters needs to be introduced in the transfer mechanism, basically described by the equation of motion:

$$[M] \frac{\partial^2 \{u\}}{\partial t^2} + [C] \frac{\partial \{u\}}{\partial t} + [K] \cdot \{u\} = - [M] \frac{\partial^2 \{u_b\}}{\partial t^2} \quad (3-1)$$

in which gravity forces and other external forces are neglected where:

M = is the mass

K = is the stiffness matrix

C = is the damping coefficient

{u} = displacement vector

$\frac{\partial^2 \{u_b\}}{\partial t^2}$ = is the given acceleration at the boundaries.

Randomness in Eq. 3-1, is introduced through the parameters M, C and K. This randomness is expressed by means of estimating their first and second moments. However, nothing can be said about general properties of their probability distribution due to the non-stationarity at the scale of the study.

The first and second moments of the displacements (unknown variables) are then computed using a multivariate technique according to the so called first-order uncertainty analysis by Cornell (3) and Papoulis (68).

Of the various numerical procedures used in practice to solve the above partial differential equation, the finite element method offers the most realistic and simple formulation. The equivalent continuum describing the cavity system is considered as being discretized into small regions or elements with different physical properties.

However, due to the wave nature of the dynamic problem three important discretization criteria are required according to Chopra and Vaish (92). These criteria are discussed in a subsequent chapter. They are fulfilled only if the domain of interest is analyzed in three different scales, in accordance with the dynamic behavior of the rock media, as discussed previously.

The general solution of the governing equation then is of the form:

$$\{u\} = L^{-1} \{F\} \quad (3-2)$$

where $\{u\}$ = the displacement vector

$\{F\}$ = the load vector.

The inverse hyperbolic operator L^{-1} is evaluated through the finite element procedure and is a function of the random variables z_1, z_2, \dots, z_n . Applying now the first order uncertainty analysis as described in Papoulis (68) and applied by Cambou (7) the following moments are obtained:

First Moment

$$E[u(z_1, z_2, \dots, z_n)] \approx \{\bar{u}(z_1, z_2, \dots, z_n)\} + \frac{1}{2} [\sigma_{z_1}^2 \frac{\partial^2 u(\bar{z}_1, \bar{z}_2)}{\partial z_1^2} + \dots] \quad (3-3)$$

The second part of the second member can be neglected being a very small quantity.

Second Moment

$$E[u(z_1, z_2, \dots, z_n)]^2 = \sigma_{z_1}^2 \frac{\partial u(\bar{z}_1, \bar{z}_2, \dots)^2}{\partial z_1} + \sigma_{z_2}^2 \frac{\partial u(\bar{z}_1, \bar{z}_2, \dots)^2}{\partial z_2} + \dots \quad (3-4)$$

The interesting point here is that the evaluation of the partial derivatives can be treated by the finite element approach without any extra computational cost. The numerical details are given in Chapter five. The above equation can be solved according to one of the following numerical techniques:

1. Direct Integration (Working space = time domain or frequency domain).
2. Modal Analysis (Working space = time domain).

These methods differ in the way they handle the damping of the system, as well as the high frequency component of strong earthquake motions. The selection of the adequate technique will be made based on the accuracy of the results and the simplicity in the use of the existing input data.

Consequently, the procedure adopted for the three different scales specified previously is as follows:

A. Scale 1 - It is the largest scale of the model and it is perturbed by the relatively low frequencies of the earthquake signal. Therefore, the damping effect can be neglected. On the other hand, the input perturbation strongly depends on the modes of vibration of scale 1. Therefore, a modal analysis technique seems appropriate for this scale.

B. Scale 2 - It is the intermediate scale in which the rock media must be described as accurately as possible. The finite element mesh will be more dense and the damping of the material should enter into consideration since the higher frequencies will be present.

C. Scale 3 - It is the smallest scale and it requires the more sensitive model. Therefore, the geometric nonlinearities should be taken into consideration.

The overall procedure will make use of plane strain elements which will be triangular or rectangular in the scales one and two and one dimensional elements for scale three. It is to be noticed that only the two or three circular frequencies are needed in this approach and, therefore, the modal analysis is considerably facilitated. Particular attention is given in considering the interaction between these three different scales.

3.5 Input Seismic Load

In the previous chapter the brief introductory remarks concerning the seismic load suggested the use of artificially generated earthquake signals. Indeed the existing building code load classifications have shortcomings concerning the prescription and the characteristics of the dynamic loads. R. Levy gives a detailed account of the existing techniques related to the simulation of earthquakes signals. He concludes that the models based on filtering a white noise input are more adequate in providing a background for earthquake simulation, since they are simple in concept and execution. They are all based on an "A posteriori" modeling approach in which a single degree of freedom oscillator is used to filter the white noise according to some criteria

of the simulation processes. Most of the researchers agree that the significant criteria are:

1. The Maximum Ground Acceleration

The simulated seismic signal should provide similar values for the maximum ground acceleration as measured from actual earthquake.

2. The Response Spectra

The response spectra of the simulated signal when normalized to a common intensity spectrum should be similar to the standard spectra.

3. The Autocovariance

The normalized autocovariance functions for the simulated ground acceleration should exhibit the same characteristics and should tend to fit the envelopes provided from real earthquakes. The underlying assumption here is the stationarity of the process during the period of strongest motion.

4. The Nonstationarity

The simulated seismic signal should exhibit the same nonstationary trend as past observations, i.e., the simulated ground velocity and acceleration should ascend to a maximum value and then decay to zero over the duration of the earthquake.

The lack of strong underground earthquake records, makes the task of calibrating the simulated earthquake signal difficult. In effect, only few investigations are available to date with often contradicting conclusions as seen in Chapter 2. Most of these measurements provide a direct empirical evidence for a reduction in seismic response with depth. However, it is clear in these investigations that the motions are dependent on the natural frequency of the media and the frequency content of the seismic excitation.

The above considerations along with the recorded ground motions at different sites provided by Seed (84) suggest that the geologic media approximately behave like a cluster of discrete masses connected by springs and dashpots. This is particularly evident in site locations 3 and 5 of Figure 3.6. For this reason, a two degree of freedom filter is developed taking into account the natural frequency of the cavity system as well as the damping factors obtained from the existing data as illustrated in Figure 3.7.

The equations of motion for the second degree system are:

$$M\ddot{u}_1 + K(u_1 - y) + C(\dot{u}_1 - \dot{y}) - c(\dot{u}_2 - \dot{u}_1) - k(u_2 - u_1) = 0 \quad (3-5)$$

$$m\ddot{u}_2 + c(\dot{u}_2 - \dot{u}_1) + k(u_2 - u_1) = 0 \quad (3-6)$$

It must be reminded that only a general inference can be assessed of whether or not a simulation process is consistent with the statistics of past earthquakes, since only a small number of earthquake records exists to date.

3.6 Model Implementation

An integrated view of the tasks undertaken in the present study is displayed in Figure 3.8. In particular, Figure 3.8 shows the structure of interaction of the different phases of the analysis. In what follows the flow-diagram is examined in some detail.

The physical parameters which characterize the geological environment and their spatial distribution are estimated in phase one through the use of the Inference model. Phase two is concerned with the implementation of the analytical tool that permits the simulation of the transfer mechanism. Phase three provides the key information concerning the dynamic input for the final computational step of phase two.

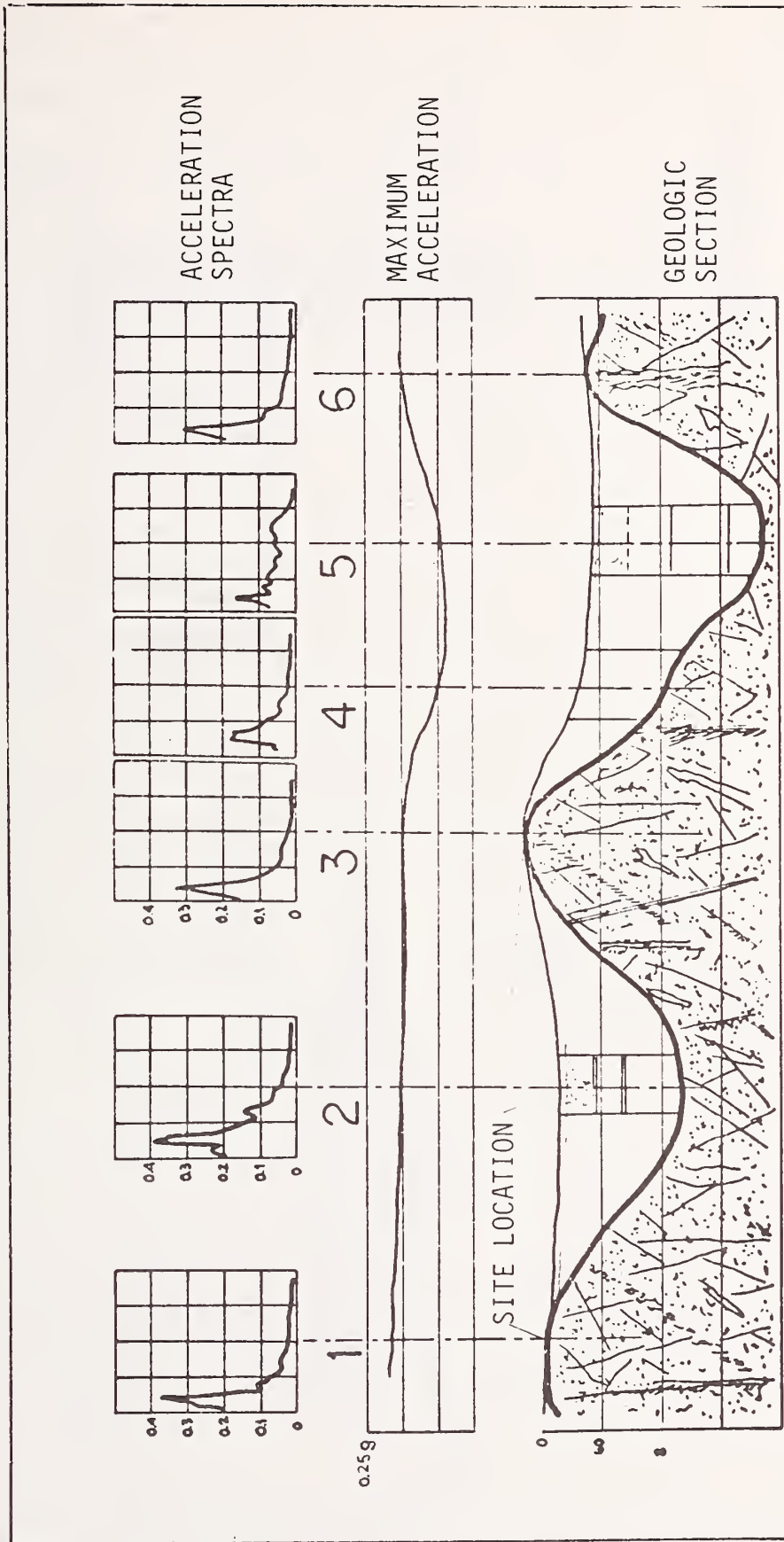
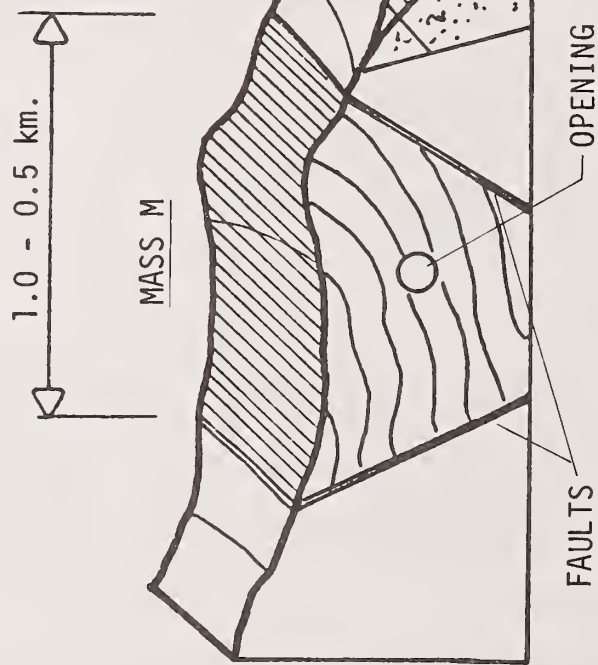


FIGURE 3.6 EXAMPLE OF SEISMIC ACCELERATION SPECTRA AT DIFFERENT SITE LOCATIONS (after Seed, (84))

REAL SITUATION



SIMULATING MODEL

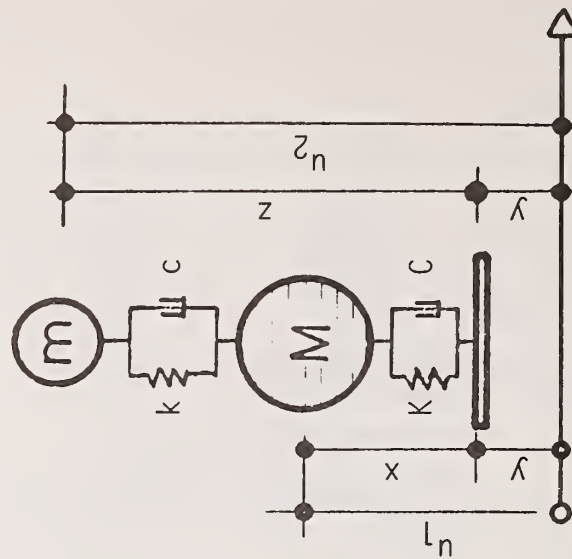


FIGURE 3.7 CONCEPTUALIZATION OF A SEISMIC RESPONSE MECHANISM

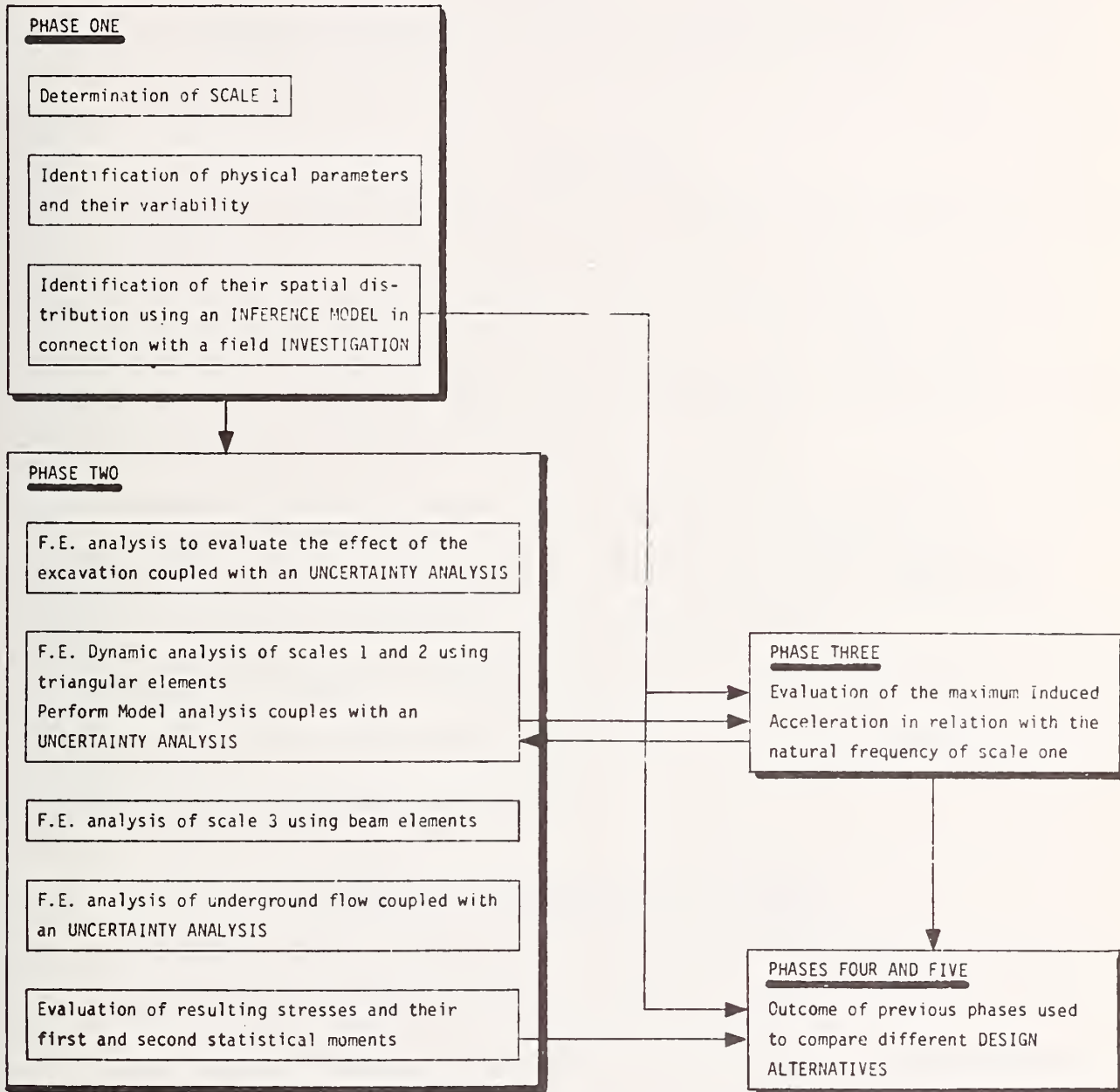


FIGURE 3.8 LOGICAL FLOW-CHART OF THE DIFFERENT PHASES OF THE STUDY

Finally the outcome of phases two and three is combined to provide the evaluation of possible design alternatives, according to a set of performance criteria.

CHAPTER 4

PHYSICAL PARAMETERS DESCRIBING THE CAVITY SYSTEM

4.1 Introduction

The cavity system can be separated into the rock structure and the liner system. The rock structure consists of the rock mass surrounding the opening as defined in section 3.4. The liner system consists of a liner fabricated from any combination of structural materials such as steel and concrete.

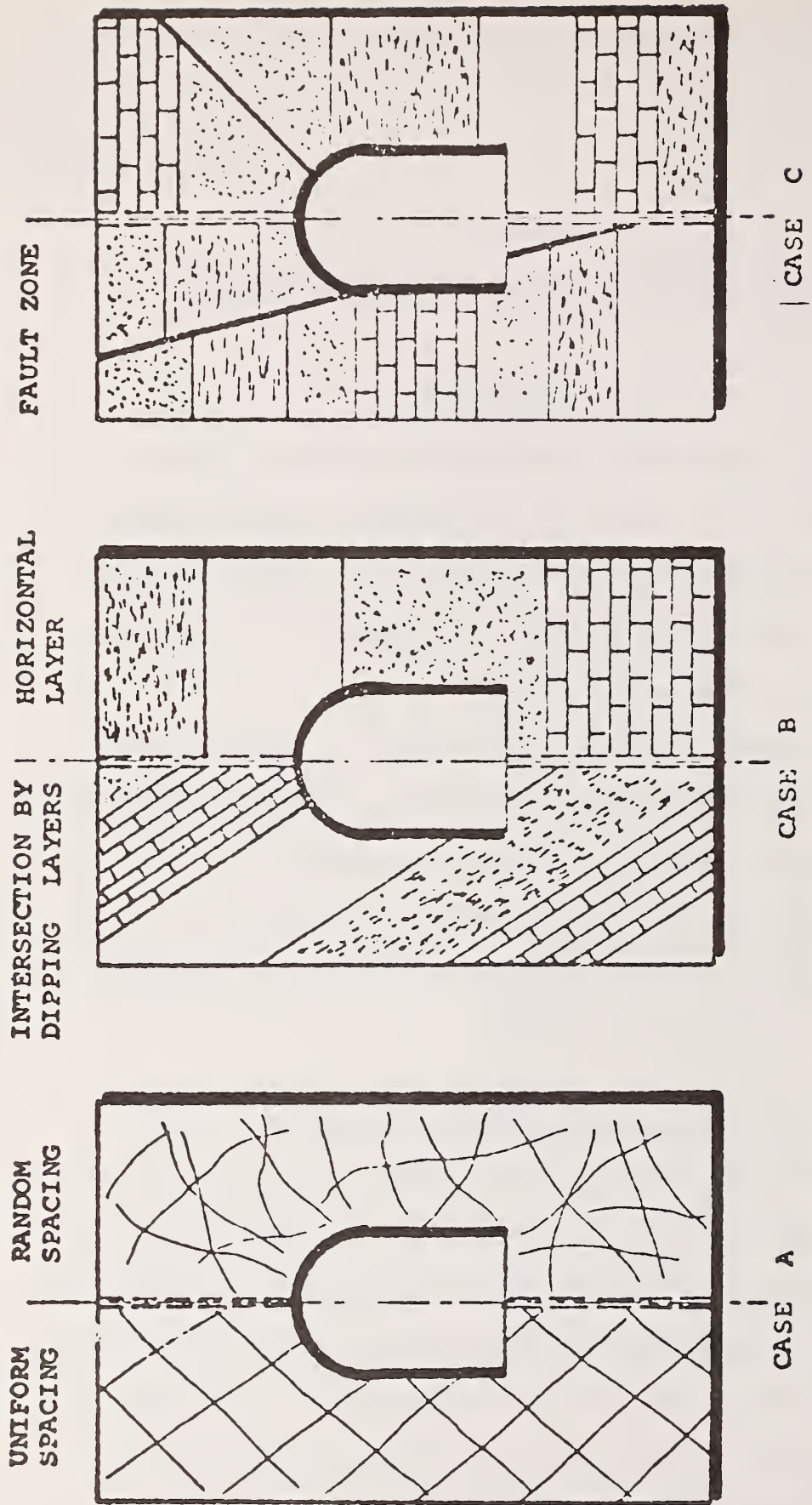
However, the main concern in this chapter is the mechanical properties of the rock mass which are highly variable in comparison with the mechanical properties of the liner materials.

In the following an extensive study of the rock properties is presented while for the liner materials properties the fundamental relationships are taken from Lew (53).

4.2 Nature of the Geologic Environment

Experience shows that any possibly encountered geological environment belongs to one of the three following cases, Figure 4.1:

CASE A: Nonstratified rock mass broken by fractures. In these cases it is assumed that the maximum dimension of any individual rock block is smaller than the widest span of the opening analyzed. The fractures can have a uniform spacing, or a non-uniform or random spacing.



TREATED CASES

FIGURE 4.1 TYPICAL GEOLOGICAL ENVIRONMENTS

CASE B: A layered rock mass having two or more layers, each one with different elastic properties. The opening can be intersected by two or more steeply dipping or horizontal layers.

CASE C: Intersection of any of the preceding environments by a steep-dipping fault.

However, from the design point of view Case C should be avoided because of the high risk of hazard. In the following the focus will be on the geological environments A and B.

The first two cases are treated by a unique analytical model provided that the discrete parts forming the real rock bodies are physically described. This is accomplished through a set of parameters that take into account nature's randomness.

4.3 Quantifying the Physical Parameter of the Rock Media

The design code in structural engineering normally requires the specification of both the configuration and the properties of the material forming the structure. The properties of the construction material as is the case for the liner, are usually known with good accuracy from laboratory investigations. However, this is hardly the case in a geological environment where the designer is faced with a material whose properties far deviate from the ones of idealized materials. Indeed the properties of the existing materials are seldom accurately known. Moreover, they may change significantly within short distances.

These properties are defined in terms of some physical parameters which are quantified from:

- A) In site experiments including 1) seismic and dynamic tests; 2) measurements of the permeability coefficients; 3) measurements of the degree of fracturing in drill cores; 4) measurements of the oscillations of the groundwater level in bore holes, and 5) measurements of the state of stresses in the rock media.
- B) Laboratory experiments including static and dynamic tests on samples obtained from the drill cores.

The combination of the above two experimental works is necessary to obtain as much knowledge as possible while recognizing their biases and imperfections.

Three predominant types of rocks are shown to exist according to a geologic classification. They are the sedimentary, igneous and metamorphic rocks. However, in the present study a classification based on the mechanical behavior of the rock would be more appropriate for the analysis. Table 4.1 provides one such mechanical classification based on Isenberg's work, (38).

In each of the three groups of factors that control the mechanical behavior of rocks, the parameters considered to efficiently represent the behavior of a rock mass, are the following:

First group: Intrinsic parameters -

The modulus of elasticity, and shear modulus, rock porosity and rock permeability, and the strength parameter.

Second group: Extrinsic parameters (Environmental parameters) -

The confining pressure and the pore pressure within the rock. The rate of deformation of the rock.

Third group: Dynamic parameters -

Mass density and internal damping.

TABLE 4.1 MECHANICAL CLASSIFICATION OF ROCKS

CLASS	ADHESION [BARS]	GRAIN STRENGTH [BARS]	GRAIN SIZE MEAN DIAMETER	POROSITY % PERM	PERMEABILITY	ANISOTROPY	
CLASTIC ROCKS	Altered Tuffs	$A \leq 1,000$	$S < 1,000$	$D < 0.1 \text{ mm}$	$10\% < P$	Low	Isotropic
	Shale, Mudstone	$1,000 < A < 10,000$	$S < 1,000$	$D < 0.1 \text{ mm}$	$10\% < P$	Low	Anisotropic
	Unconsolidated Sands	-	$1,000 < S < 10,000$	$5 \text{ mm} < D$	$10\% < P$	High	Isotropic
	Weakly Cemented Sandstones	$1,000 < A < 10,000$	$10,000 < S$	$0.1 < D < 5 \text{ mm}$	$10\% < P$	High	Isotropic
	Strongly Cemented Sandstones	$10,000 < A$	$10,000 < S$	$0.1 < D < 5 \text{ mm}$	$1\% < P < 10\%$	Medium	Isotropic
	Quartzite	$\sim 10,000$	$10,000 < S$	$0.1 < D < 5 \text{ mm}$	$1\% < P < 10\%$	Medium	Isotropic
	'Weathered' Igneous and Metamorphic Rocks	$1,000 < A < 10,000$	$10,000 < S$	$D > 5 \text{ mm}$ $D < .1 \text{ mm}$	$1\% < P < 10\%$	High	Isotropic
	Salt, Gypsum Anhydrite	$A < 1,000$	$1,000 < S$	$0.1 < D < 5 \text{ mm}$	$1\% \approx P$	Medium	Isotropic or Anisotropic
	Coarse, Porous Limestones and Marbles	$1,000 < A < 10,000$	$1,000 < S$	$0.1 < D < 5 \text{ mm}$	$10\% \approx P$	High	Isotropic
	Fine Compact Limestones and Marbles	$1,000 < A < 10,000$	$1,000 < S$	$D < 0.1 \text{ mm}$	$1\% \approx P$	Low	Isotropic or Anisotropic
CRYSTALLINE ROCKS	Phyllite, Slate	$1,000 < A < 10,000$	$1,000 < S < 10,000$	$D < 0.1 \text{ mm}$	$P < 1\%$	Low	Anisotropic
	Schist, Gneiss	$10,000 < A$	$10,000 < S$	$D > 5 \text{ mm}$ $D < .1 \text{ mm}$	$P < 1\%$	Low	Anisotropic
	Basalt, Rhyolite Welded Tuff	$10,000 < A$	$10,000 < S$	$D < 0.1 \text{ mm}$	$P < 1\%$	Low	Isotropic
	Granite, Diorite	$10,000 < A$	$10,000 < S$	$0.1 < D < 5 \text{ mm}$	$P < 1\%$	Low	Isotropic

Figure 4.2 shows the informations that site investigation provides concerning the above mentioned parameters. A considerable discrepancy appears to exist between the values obtained in situ and the laboratory, Judd (44).

Intuitively it can be realized that the laboratory samples are not representative of the larger rock mass system. Indeed there is experimental evidence that the strength of the rock decreases as the sample volume increases (69). This is believed to be the consequence of discontinuities within the rock mass. Their spatial distribution is, therefore, essential if one wants to correlate the laboratory test results for small specimens and the large scale field tests.

In the following an emphasis is put on how to consider the discontinuities in conjunction with the determination of the above mentioned mechanical properties of the rock and on how to define the statistical characteristics of these properties from field investigation.

4.4 Mechanical Properties of Rock with Respect to Discontinuities and Their Spatial Distribution

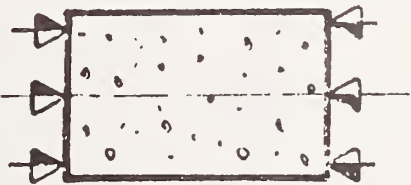
4.4.1 Intrinsic Parameters

As such one can distinguish the modulus of Elasticity (E), shear modulus (G), Poisson's ration (ν), strength parameters and the permeability coefficients k_x and k_y in the x and y direction respectively.

The Modulus of Elasticity E

Rodriguez (69) recently determined the mean value and the dispersion of the modulus of elasticity taking into account the dimensions of the rock mass and the probability of occurrence of the joints existing within the mass. He has shown by means of thousands of simple

NO
DISCONTINUITIES

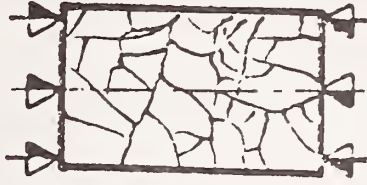


ROCK SAMPLE

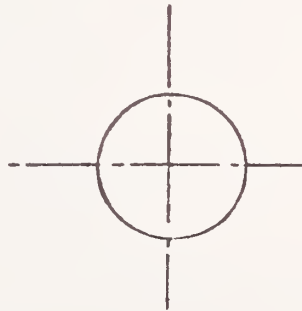
UNIFORM
DISCONTINUITIES



RANDOM
DISCONTINUITIES



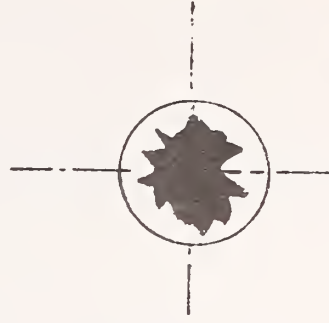
1



2



3



PLOT OF DISCONTINUITIES

FIGURE 4.2 POSSIBLE STATES OF FISSURATION IN A ROCK MASS

comparison tests that the mean value of the modulus of Elasticity is independent of the test area, but rather is influenced by the intensity of jointing. More specifically:

$$\bar{E} = \frac{\bar{E}_I}{1 + m \cdot I} \quad (4.1)$$

where: \bar{E} = the mean modulus of elasticity

\bar{E}_I = the mean modulus of elasticity for the intact mass

m = a fitting parameter depending on the type of rock

I = the intensity of jointing per meter.

On the other hand the mean modulus of elasticity for the intact mass can be evaluated from laboratory dynamic tests from the following expression, Appendix A:

$$\bar{E}_I = \rho \cdot \frac{V_S^2 [3(V_P/V_S)^2 - 4]}{[(V_P/V_S)^2 - 1]} \quad (4.2)$$

where: V_P - the velocity of the compression wave

V_S = the velocity of the shear wave

ρ = the mass density.

The parameter 'm' is obtained through laboratory tests. Rodriguez (69) suggests the following values:

for	LIMESTONE	$m = 0.084$
	GNEISS	$m = 0.015$
	GRANITE	$m = 0.041$

The intensity of jointing is specified according to some norms given in a subsequent paragraph 4.4.4.

The Shear Modulus G

It can be defined from the following relation

$$\bar{G} = \frac{\bar{E}}{2(1 + \bar{\nu})} \quad (4.3)$$

provided that the mean modulus of elasticity and the mean Poisson's ratio are known.

Poisson's Ration $\bar{\nu}$

Kulhawy (50) found that the value of $\bar{\nu}$ tended to decrease with increasing confining pressure. He proposed the following relationship:

$$\bar{\nu} = \bar{\nu}_I - n \log \frac{\sigma_3}{p_a} \quad (4.4)$$

where: $\bar{\nu}_I$ = the Poisson's ratio at a confining pressure of one atmosphere.

It can be obtained from a dynamic test as for the case of the Modulus of Elasticity from the relation

$$\bar{\nu}_I = \frac{1}{2} \left[\frac{(V_p/V_s) - 2}{(V_p/V_s)^2 - 1} \right] \quad (4.5)$$

where: n = a fitting parameter usually between 0.05 - 0.01

σ_3 = the confining pressure

p_a = the atmospheric pressure.

The Strength Parameters

They are directly dependent on the failure criterion that is used. Indeed, recently many models of the strength of the rock have been developed to describe more accurately the behavior of the media. Lundborg (55) used the statistical theory to elaborate a model making

the assumption that the statistically distributed strength follows a Weibull distribution.

On the other hand Sandler (81) developed the so called CAP model for static and dynamic conditions for the computational studies of ground shock. This model is in fact an elaborated version of a plasticity model defined by a yield surface and a strain rate vector.

However, in our case it seems more appropriate to use the Mohr-Coulomb failure criterion which is simple to use and which in addition can be applied to any type of rock and its corresponding state of fissuration as suggested by Talobre (89) and illustrated in Figure 4.2.

Then

$$\tau_{\max} = \tau_c + (S_n - u)\tan \phi \quad (4.6)$$

where: τ_{\max} = shear strength in the failure plane

τ_c = apparent cohesion

ϕ = angle of internal friction

S_n = normal stress to the failure plane (Principal stress)

u = interstitial water pressure

The statistical characteristics of the shear strength can now be evaluated using a multivariate approximation provided that the first and second moments of the independent parameters ϕ , τ_c , and S_n are given.

To our knowledge there is no experimental work done in trying to correlate the parameters ϕ and τ_c with the mean discontinuity spacing. However the range in which the parameters ϕ and τ_c can vary is given in Figure 4.3 along with an illustration of the different strength theories in the domain of principal stresses.

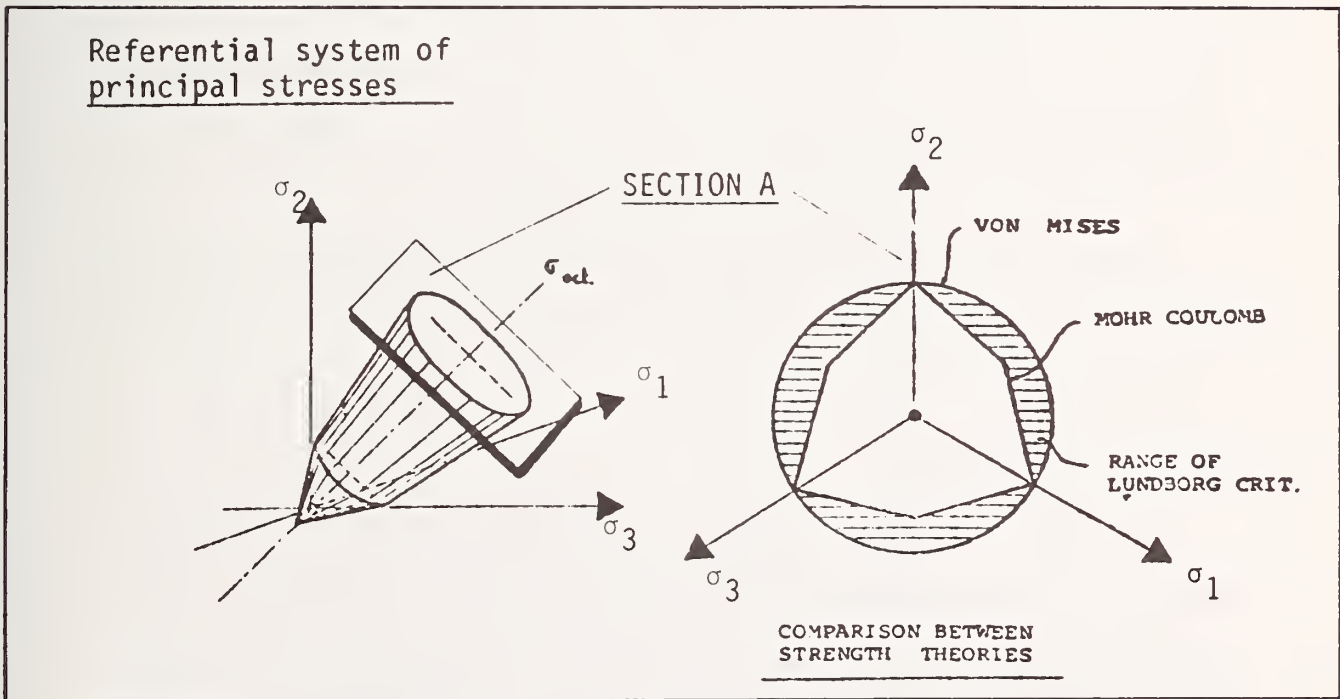
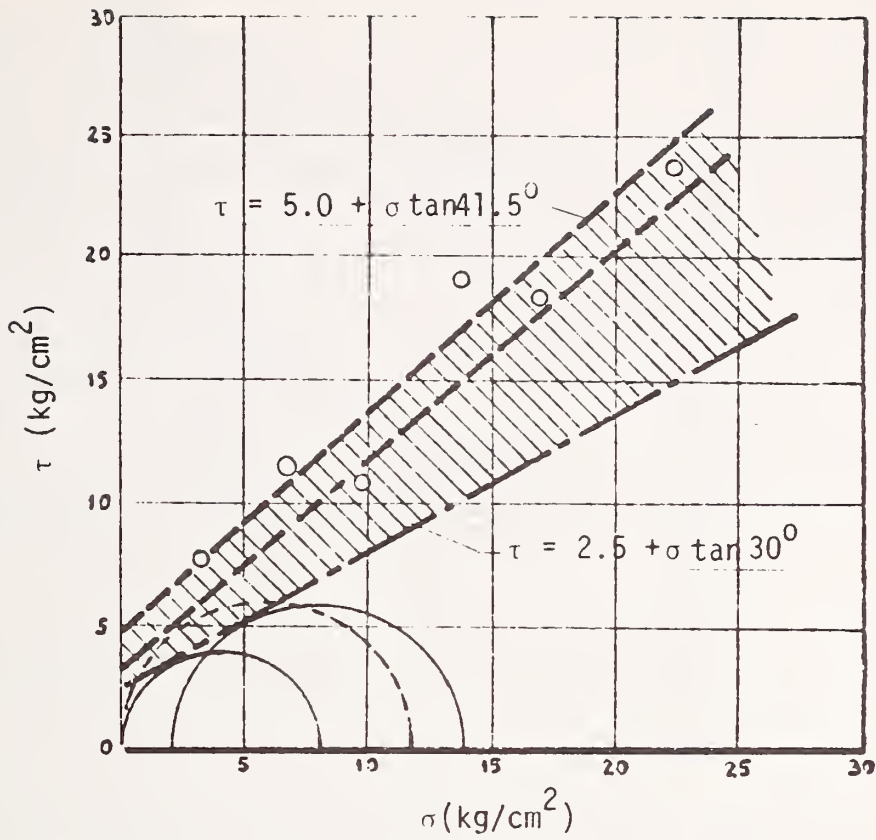


FIGURE 4.3 MOHR-COULOMB CRITERION

The Permeability Coefficient k_x and k_y

Morgenstern (59) studied experimentally the effect of simple systems of parallel cracks on the equivalent permeability of the mass. Clearly the amount of cracks per meter is the governing parameter for the permeability coefficient. However, different results can be obtained depending on whether the flow is increasing or decreasing. Another possibility could be that if high pressures are used flows may also increase due to the so called hydraulic fracturing of the rock.

Nelson (52), suggests the following relation for the permeability:

$$k_{fr} = A + B (P_c)^{-n} \quad (4.7)$$

where: k_{fr} = permeability of the rock matrix plus fractures

P_c = the confining pressure, and

A,B,n = some fitting parameters determined experimentally.

Nelson's results are illustrated in Figure 4.4 and are obtained for a given fracture aperture, which in turn can be evaluated from the known number of cracks per meter of rock.

4.4.2 Extrinsic Parameters

They are the confining pressure and the pore pressure of fluids within the rock mass. They represent somehow the initial conditions of the analysis.

CONFINING PRESSURE

The natural state of stress is needed in defining the initial conditions that need to be introduced in the analytical model. It exists at a point within the rock mass and is dependent of all the previous geologic processes that have acted on the mass. To know with

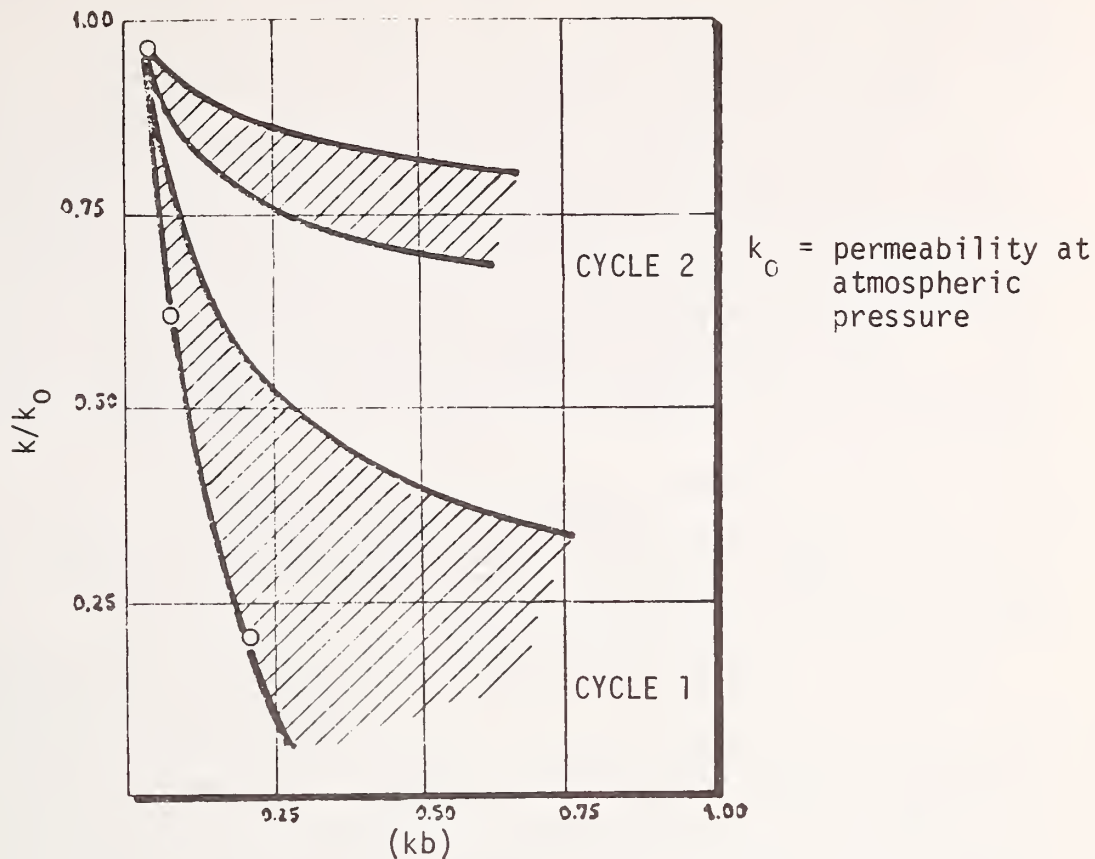


FIGURE 4.4 PERMEABILITY COEFFICIENT VS. CONFINING PRESSURE (AFTER-NELSON)

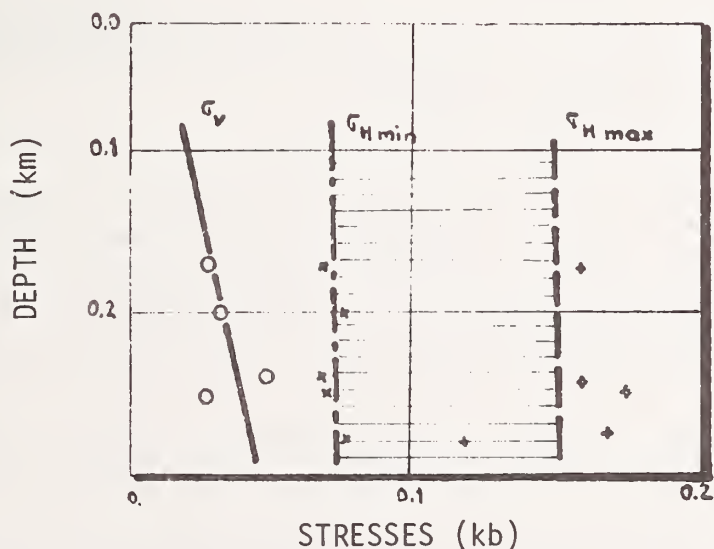


FIGURE 4.5 MAXIMUM AND MINIMUM IN SITU STRESSES VS. DEPTH RESULTS OF HYDROFRACTURING STRESS MEASUREMENTS

any degree of accuracy what all these events have been is an impossible task. Deere (15) gives an emphasis to the fact that there is no justification for the so commonly used assumption that the horizontal stress at a given depth below a horizontal surface is related to the overburden pressure in accordance with the elastic theory by a factor $\nu/1-\nu$. Indeed any one of a number of geologic events could cause the horizontal stress to differ significantly from this value. Major deep-seated tectonic movements and thrust faulting would also lead to certain stress states and boundary conditions which differ greatly from those considered by the elastic theory.

Therefore, a field investigation is a necessity. In the field of tectonophysics two techniques exist for the determination of the in site stresses, the 'stress relief' technique and the 'hydrofracturing' technique. The latter is better suited for our case in which an investigation as deep as 300 meters is required. Haimson (28) recently verified the method experimentally both in the laboratory and in the field. Indeed the magnitudes of the two in site principal stresses may be evaluated as illustrated in Figure 4.5.

WATER PRESSURE

The pore pressure of fluids is commonly obtained from boreholes and could exhibit a pronounced variability. Indeed the observed groundwater level oscillations in boreholes can exceed several meters causing some important differences in the effective stresses of the rock media.

On the other hand, the dynamic action of the earthquakes on the change of the pore pressure is relatively unknown. Indeed there is no

experimental evidence to assess a general theory, with the exception, however, of Biot's theory concerning the dilatational waves in an ideal fluid-saturated solid. Biot's procedure was applied by Hardin (30). He found that a variation in confining pressure produce little change on the wave-propagation velocity in the water. This allows us not to consider the effect of the water table on the wave propagation and to uncouple the flow problem and the dynamic problem concerning the rock media.

4.4.3 Dynamic Parameters

The important parameters to perform any kind of dynamic analysis are the apparent specific gravity and the damping.

The Apparent Specific Gravity

The apparent specific gravity is in fact providing the inertial term in the analytical treatment. Its evaluation does not represent any particular problem and its statistical characteristics are easily obtained from laboratory tests.

Damping Parameter

In the present analysis the term damping defines the energy dissipation properties of the media under cyclic load, and in most cases a conversion of mechanical energy to heat is involved. Moreover, damping is subdivided for convenience into two major headings which shall be identified as 1) the internal damping, and 2) the structural damping.

The internal damping, sometimes called hysteretic damping, is related to the energy dissipation within a volume of rock and it excludes the damping in a configuration originating at interfaces between recognizable parts. It concerns a volume of $100 - 1000 \text{ cm}^3$.

As for the structural damping it is the damping in which energy is dissipated in various configurations of joints or interfaces.

In the case of the cavity system a structural damping would be more appropriate to retain since a modal technique is adopted for the analysis.

The modal damping factors at least for the first few modes can be estimated from the outcome of a forced vibration test performed in situ, in the vicinity of the cavity system, similar to the tests done by Martin (56) at Bon Tempe dam, in which it was assumed that the energy delivered to the dam by the vibration generators was consumed by viscous damping.

Assuming that the damping is small, it is shown that the viscous damping factor or fraction of critical damping can be evaluated from the equation

$$\xi_i = \frac{\Delta f_i}{2f_{ni}} \quad i = 1, \text{ modes} \quad (4.8)$$

where: Δf_i = the width of the resonant peak for the corresponding i^{th} mode of vibration at an amplitude of 0.7 times that of the corresponding resonant amplitude

f_{ni} = the resonant frequency of the i^{th} vibration mode.

Consequently, the damping constants are estimated from the widths of the first 6 to 10 resonance peaks since these are more clearly defined than those of higher modes. This is seen in Figure 4.6 which represents the response curves obtained from the analysis of observed resonance frequencies at different locations.

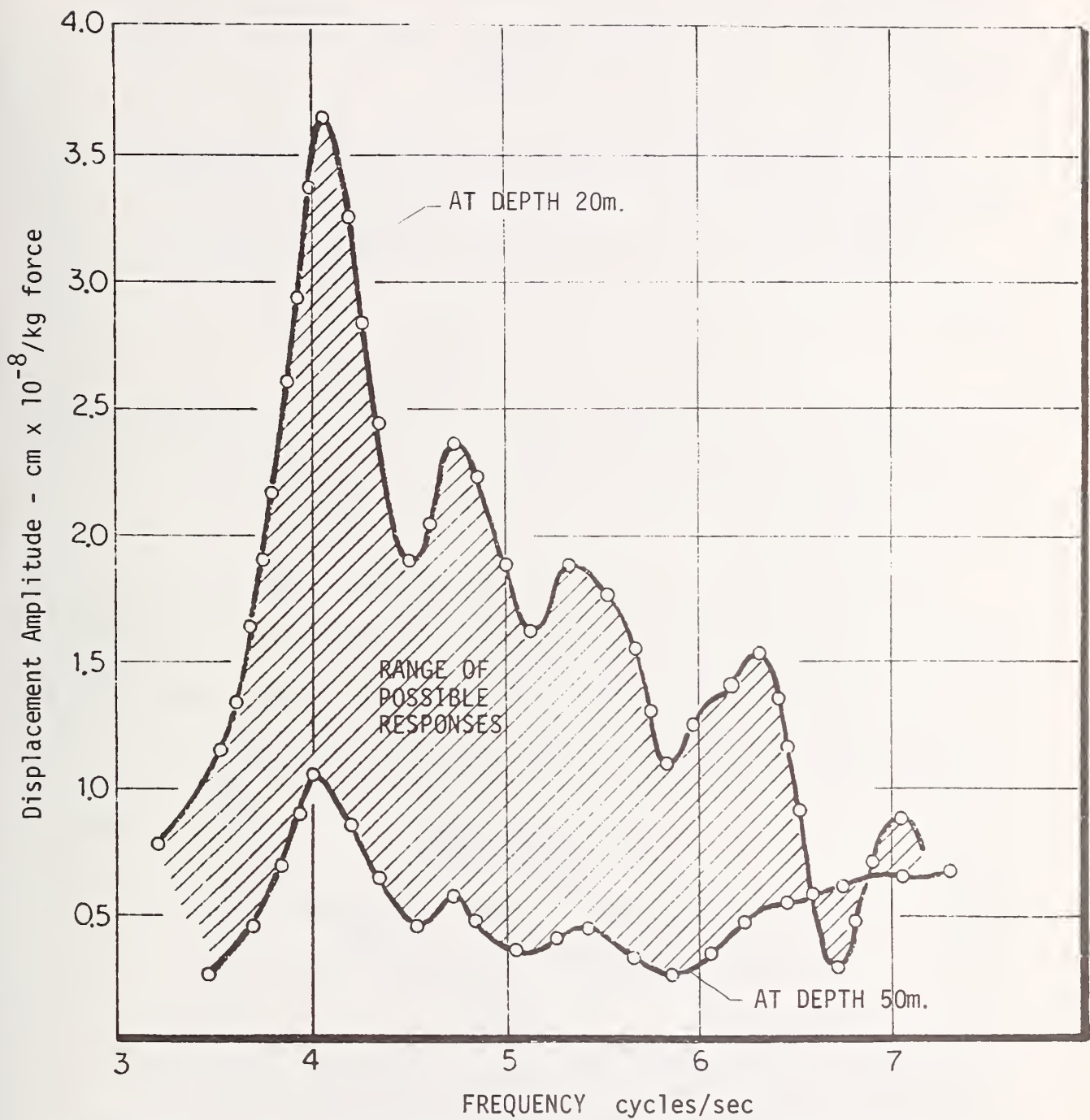


FIGURE 4.6 POSSIBLE RESPONSE CURVES OF THE DISPLACEMENTS MEASURED IN THE FIELD

However, the above test never reaches the pure modes of the cavity structure. The above values then must only be viewed as estimates of the true values of the modal damping factors.

Another alternative would be to perform laboratory tests. Richart (74) indicates that they provide a damping factor which does not correspond to the range of frequencies encountered in a seismic analysis.

Moreover to our knowledge the effect of discontinuities on the damping factor has not been investigated yet.

It seems that most of the designers in practice are adopting a damping factor in the range of 0.05 - 0.25.

4.4.4 Rock Quality Designation (RQD)

From the previous considerations it is obvious that discontinuity characteristics play a major role in controlling the mechanical behavior of a rock mass.

The index universally adopted to describe the discontinuity intensity is the Rock Quality Designation. It reflects the proportion of intact borehole core lengths that are 0.1m or longer, Deere (14). More specifically the RQD is given by the following equation:

$$RQD = 100 \sum_{i=1}^n \frac{x_i}{L} \quad (4.9)$$

where: x_i = the length of the i^{th} length greater than 0.1m

n = the number of intact lengths greater than 0.1m

L = core length

The RQD value is usually evaluated on the rock cores recovered from a site investigation. However the results must be used with extreme caution since natural discontinuities can be confused with the drill induced discontinuities.

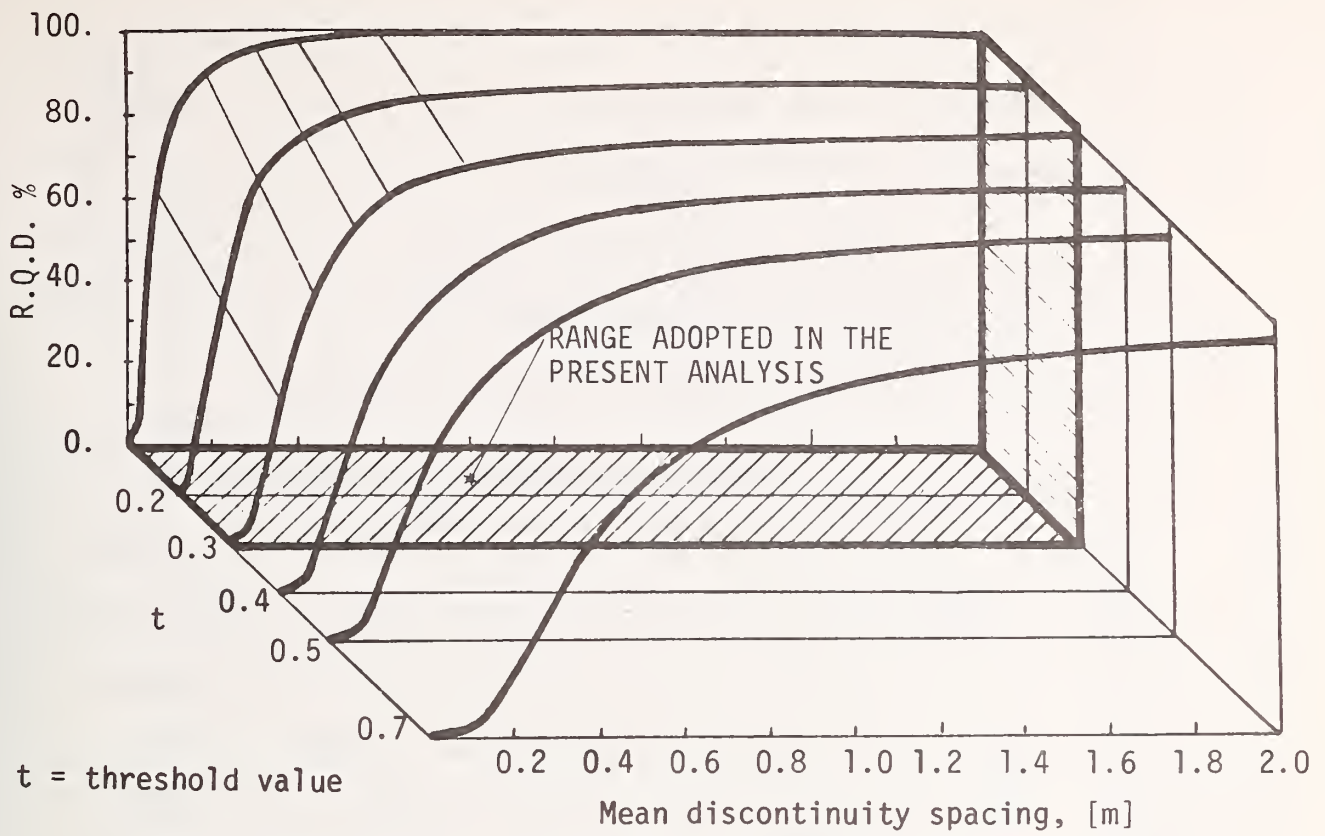


FIGURE 4.7 R.Q.D VALUES VS. MEAN DISCONTINUITY

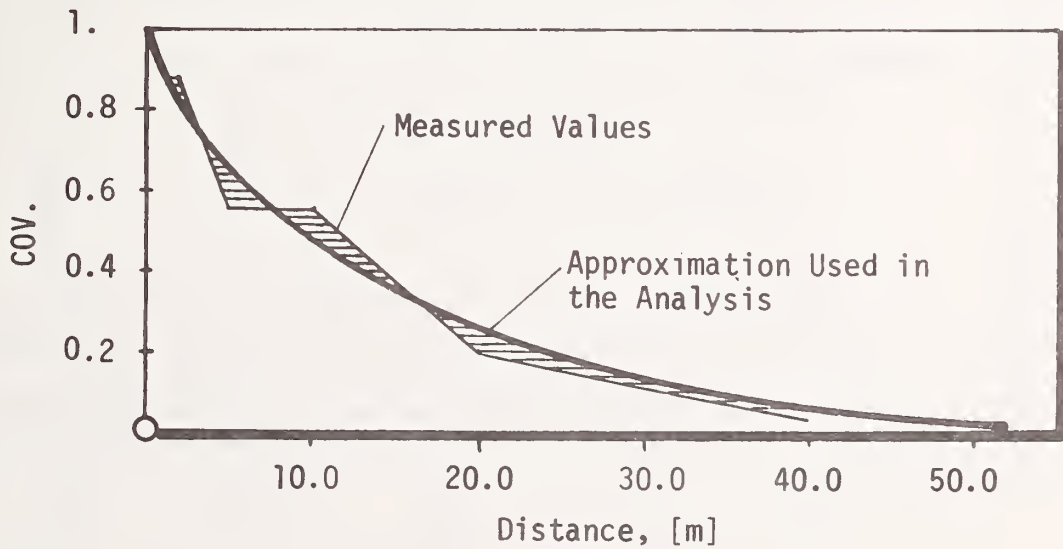


FIGURE 4.9 COVARIANCE OF R.Q.D VS. DISTANCE

Another alternative is to assume the relation established by Priest (72) between the mean discontinuity frequency per metre and the RQD. This relation estimating the RQD is:

$$RQD = 100 e^{-0.1\lambda} (0.1\lambda + 1) \quad (4.10)$$

where: λ = mean discontinuity frequency per metre.

An illustration of the above equation is given in Figure 4.7.

4.5 Spatial Distribution of the Mechanical Parameters

To measure a rock property Z as indicated in section 4.4, a number of samples are taken from borings as shown in Fig. 4.8. The values of the rock property Z (e.g. Modulus of Elasticity) can be interpreted as spatial averages of point properties over finite volumes within the rock mass. These finite volumes can also be characterized as sample volumes, defined by the diameter of the drill and an approximate length of one meter. The choice of one meter of length is suggested by the previously mentioned techniques used to estimate the physical parameters of the rock as a function of its discontinuities.

For the bidimensional analysis the spatial average \bar{Z} of a rock property is defined as:

$$\bar{Z}(X,Y) = \frac{\int Z(x,y) \cdot t \cdot dx \cdot dy}{\text{volume}} \quad (4.11)$$

where: t = the third dimension.

If the sample volume is divided into six cores, (the length to diameter ratio L/D of the core must be in the range from 2.0 to 2.5) the above relation becomes:

$$Z(x,y) = 1/6 \cdot \sum_{i=1}^6 Z_i \quad (4.12)$$

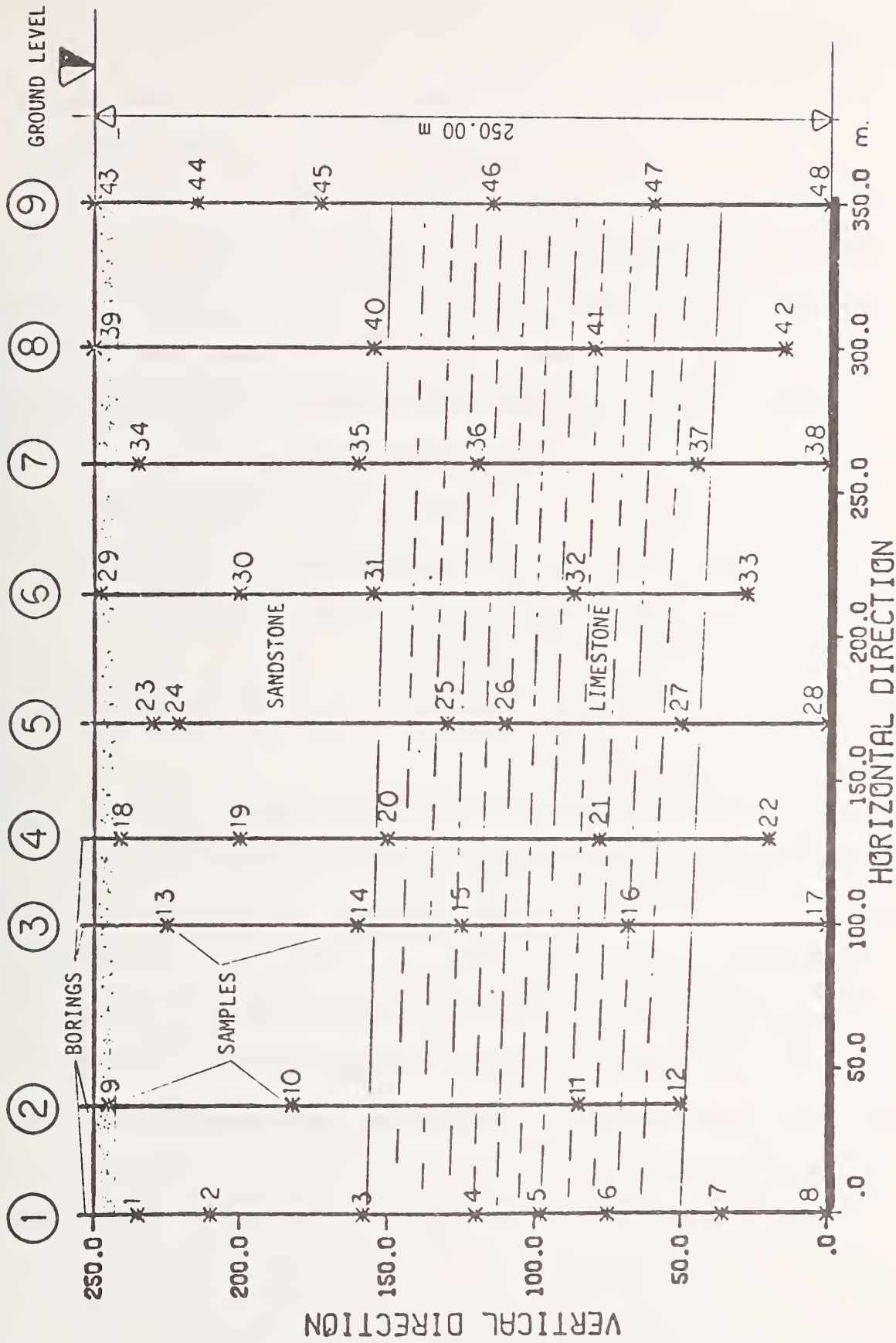


FIGURE 4.8 ROCK VOLUME, BORINGS AND SAMPLES

Furthermore we can assume that the regionalized variable Z is stationary. We then can compute a statistic $C(0)$ by squaring all values of Z_i , taking their sum and dividing by the number of observations:

$$C(0) = \frac{\sum_{i=1}^n Z_i^2}{n} \quad (4.13)$$

where: $n = 6$ for our case, and

$C(0)$ = the variance of Z

To relate the value $\bar{Z}(x_0, y_0)$ at a given point (x_0, y_0) in some manner to the value at points some distance away there is a need of a covariance measure. This is done in the following way.

A vector of distances ' d ' is specified with a specific orientation. Then a plot of the covariance between pairs of points various distances apart is evaluated, using the following relation:

$$C(d \cdot j) = \frac{1}{k} \sum_{i=1}^k Z_i \cdot Z_{(i+j)} \quad (4.14)$$

where: $j =$ an integer taking values from 0 to m .

The covariance defined in that manner expresses the degree of relationship between points a specified distance apart, as shown in Figure 4.9.

Davis (13) suggests a drilling grid to perform such an analysis. However in the present work, results obtained by other investigators are used after adequate transformations. Sample values of the covariances of different mechanical parameters are given in section 4.7 where a case study is presented.

It must be emphasized that the covariance, defined as function of distances, is an essential statistical characteristic of the inference model developed in the following chapter.

4.6 Mechanical Properties of Liner Materials

Two alternate designs are considered here, namely a reinforced concrete liner, and a bolting system plus a concrete liner. Figure .10 gives the spatial configuration of the liner system.

The material properties required for both cases are the Modulus of Elasticity of the concrete, the Poisson ratio of the concrete and the Modulus of Elasticity of the steel. The computational scheme suggested by Lew (53) and Bello (2) is adopted unchanged here also, since the properties of the concrete and steel both in a deterministic and statistical sense are well known.

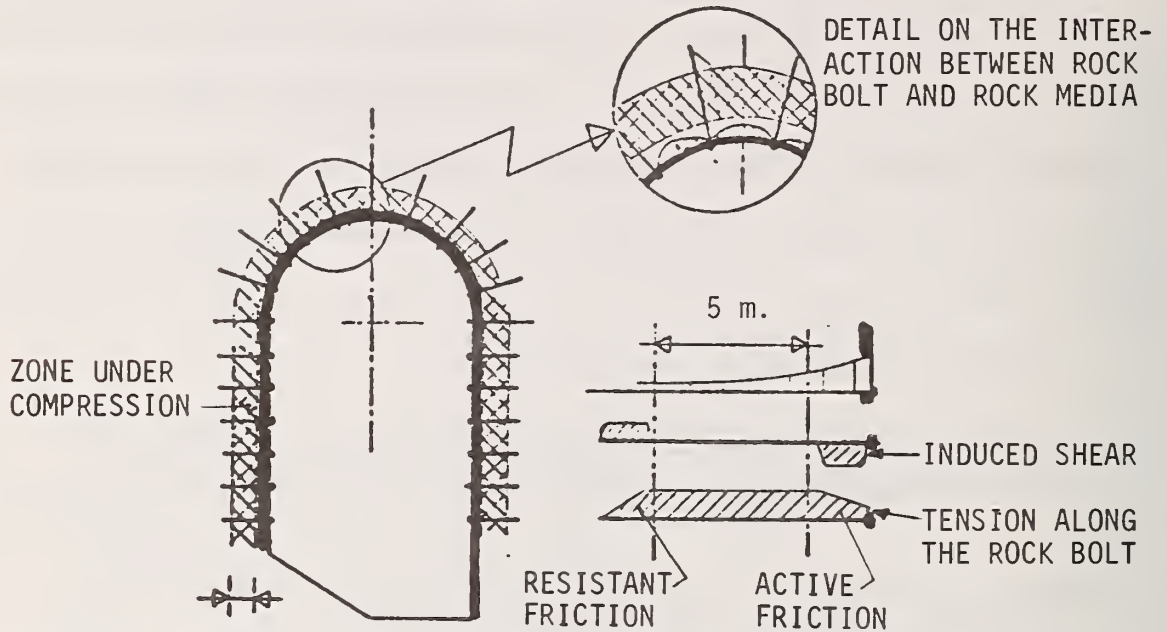
The values retained in our study are:

MODULUS OF ELASTICITY	CONCRETE	$E_c = 2. \times 10^5 \text{ kg/cm}^2$
	STEEL	$E_s = 2. \times 10^6 \text{ kg/cm}^2$
POISSON'S RATIO	CONCRETE	$\nu_c = .2$

4.7 Hypothetical Case Study

A real case would certainly constitute the best choice to test the proposed model. However, the great expenses involved in a site investigation render a real case study prohibitive. The only alternative left is to consider an existing case of underground power plant and simulate the mechanical properties of the rock media, according to the general scheme introduced in section 4.4. This is certainly sufficient for testing the performance of the models developed in the following chapters.

LINER SYSTEM WITH ROCK BOLTS



The rock bolt acts as reinforcement of the rock. The rock displacements develop an active and resistant friction zone at both ends of the bolt. The central part of the bolt has no action of friction stresses, so the tension force is constant.

LINER SYSTEM WITH REINFORCED CONCRETE

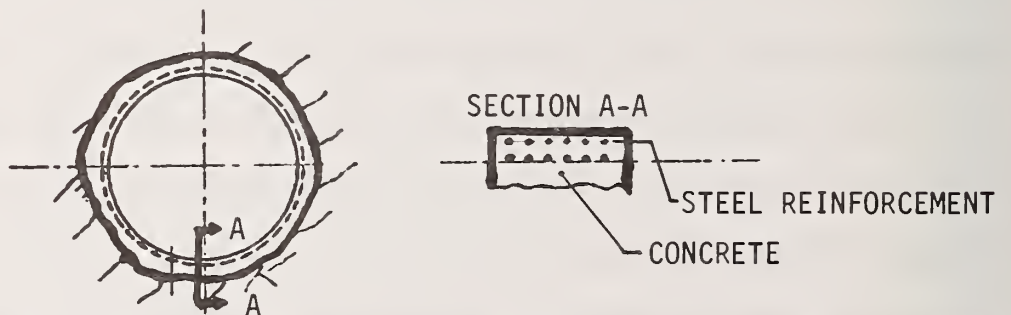


FIGURE 4.10 LINER'S MATERIAL

A geologic vertical section is shown in Figure 4.8 with some hypothetical drillings. The geologic structure of the site is inspired from Poatina's underground power station (21) as presented in Chapter 9. Figure 4.11 shows a hypothetical site exploration, consisting of twenty borings among which nine are in the geological section under consideration. From these nine borings 48 samples of one meter length are assumed extracted and tested in a laboratory. As an example the results of sample no. 24 (Sandstone) and sample no. 27 (Limestone) are presented. The following measurements and tests are assumed performed on the real specimen.

1. Measurements of the dry density and apparent specific gravity
2. Unconfined compressive strength
3. Wave velocities, P-wave and S-wave
4. Evaluation of the elastic constants
5. Effect of loading on elastic constants using cyclic loading to 25, 50, 75 percent of ultimate strength.

SANDSTONE Sample No. 24

Six specimens were considered, characterized as homogeneous, light brown quartzose, elastic (fine-grained) sandstones. They also were moderately cemented and weakly friable to hand pressure. A few small (3-4mm) iron stain inclusions were observed without however any apparent bedding structures or fissures.

LIMESTONE Sample No. 27

Three specimens were considered, characterized as light grey, fine grained, homogeneous. Bedding planes were evident dipping 20-25⁰ with respect to the specimen's direction.

The above tests provide the Intrinsic parameters used in the analysis as summarized in Table 4.2. As far as the Extrinsic and Dynamic parameters are concerned evidently field tests for their determination would require a great deal of effort and expenses. Therefore the appropriate values considered are borrowed from the literature. This is also the case for the determination of the covariances of the mechanical parameters. They are assumed to fit exponential distributions, as suggested by Padilla's work (67), based on a field exploration. The values of the parameters used in the present study are grouped in Figures 4.11 to 4.12 and are similar to the results obtained from a site investigation by the core logging committee of the South Africa Section of the Association of Engineering Geologists (27).

TABLE 4.2 RESULTS OF AN HYPOTHETICAL SITE INVESTIGATION

SAMPLE NO.		24		BORING NO.		SEC 5				
TYPE OF ROCK		SANDSTONE		ELASTIC (FINED GRAINED)						
MEAN DISCONTINUITY SPACING		0.072 m								
ESTIMATED ROD AFTER PRIEST		72%								
LABORATORY MEASUREMENTS										
SPECIM. NUMBER	LENGTH	1 SD	2 SD	3 SD	4 SD	5 SD	6 SD	MEAN VALUE	STANDARD DEVIATION	COEF. OF VARIATION
DIAMETER										
DRY DENSITY	gr/cm ³	2.09	2.1	2.16	2.14	2.08	2.16	2.125	0.036	1.7 %
SPECIFIC GRAVITY		2.42	2.43	2.49	2.46	2.44	2.45	2.448	0.024	1.0 %
UNCONF. COMP. STRENGTH	kg/cm ²	468.00	516.75	494.36				433.55	23.90	4.9 %
TEHILE STRENGTH (BRAZ.)										
LOADING AT PER CENT OF ULTIMATE STRENGTH								CYCLE NO. 1		
P - WAVE VELOCITY	cm/secx10 ³				206.83	219.83	278.02	234.89	37.89	16.1 %
S - WAVE VELOCITY	cm/secx10 ³				137.03	143.63	183.15	154.60	24.91	16.1 %
DYNAMIC ELAST. CONSTANTS										
MODULUS OF ELASTICITY	kg/cm ² x10 ⁶				0.089	0.0991	0.165	0.118	0.024	20.8 %
POISSON'S RATIO					0.11	.128	.117	.118	0.0098	8.3 %
SHEAR MODULUS	kg/cm ² x10 ⁶				0.0358	0.0438	0.0738	0.0525	0.0184	35.2 %
LAME'S CONSTANT	kg/cm ² x10 ⁶				0.0111	0.0149	0.0225	0.0162	0.0058	35.7 %
BULK MODULUS	kg/cm ² x10 ⁶				0.0379	0.0442	0.0717	0.0513	0.0179	35.1 %
STATIC ELASTIC CONSTANTS										
MODULUS OF ELASTICITY	kg/cm ² x10 ⁶				0.0759	0.0759	0.0843	0.0787	0.00035	.4 %
POISSON'S RATIO					.16	.18	.18	0.18	0.0004	.22 %
SHEAR MODULUS										
ADOPTED ELASTIC CONSTANTS	CONSIDERING A MEAN DISCONTINUITY SPACING 0.07 m									
MODULUS OF ELASTICITY								0.100 x 10 ⁶ kg/cm ²		
POISSON'S RATIO								0.11		
SHEAR MODULUS										

TABLE 4.2 cont.

SAMPLE NO.		27		BORING NO.		SEC 5	
TYPE OF ROCK		LIMESTONE					
MEAN DISCONTINUITY SPACING		0.04 m					
ESTIMATED ROD AFTER PRIEST		83%					
LABORATORY MEASUREMENTS							
SPECIM NUMBER	1	2	3	4	5	6	COEF. OF VARIATION
LENGTH							
DIAMETER							
DRY DENSITY	2.70	2.67	2.67	2.67			2.68
SPECIFIC GRAVITY	2.69	2.69	2.63	2.63			2.69
UNCONF. COMP. STRENGTH				586.	779.	710.	691.
TENSILE STRENGTH (BRAZ.)							
LOADING AT PER CENT OF ULTIMATE STRENGTH							
P - WAVE VELOCITY	551.18	539.29	539.64				543.38
S - WAVE VELOCITY	241.90	263.06	266.52				257.17
DYNAMIC ELAST. CONSTANTS							
MODULUS OF ELASTICITY	0.444	0.506	0.517				0.489
POISSON'S RATIO	.38	.34	.39				.35
SHEAR MODULUS	0.161	0.188	0.193				0.180
LAME'S CONSTANT	0.527	0.414	0.405				0.444
BULK MODULUS	0.621	0.539	0.534				0.565
STATIC ELASTIC CONSTANTS							
MODULUS OF ELASTICITY							0.039
POISSON'S RATIO							0.023
SHEAR MODULUS							0.017
ADOPTED ELASTIC CONSTANTS							
CONSIDERING A MEAN DISCONTINUITY SPACING 0.04 m							
MODULUS OF ELASTICITY							0.47 x 10 ⁶ kg/cm ²
POISSON'S RATIO							0.30
SHEAR MODULUS							

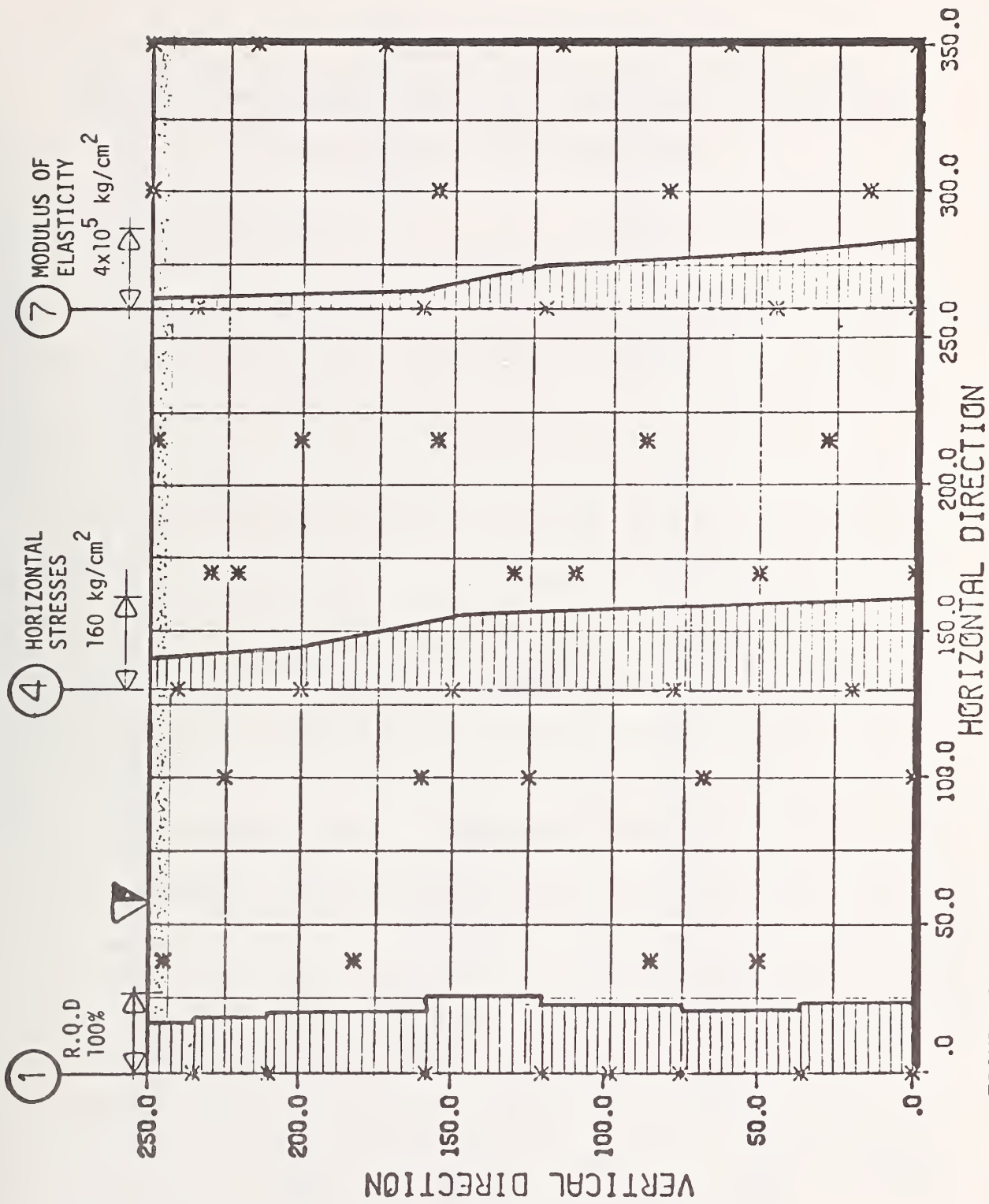


FIGURE 4.11 SOME MEASURED PHYSICAL PARAMETERS FROM A SITE INVESTIGATION

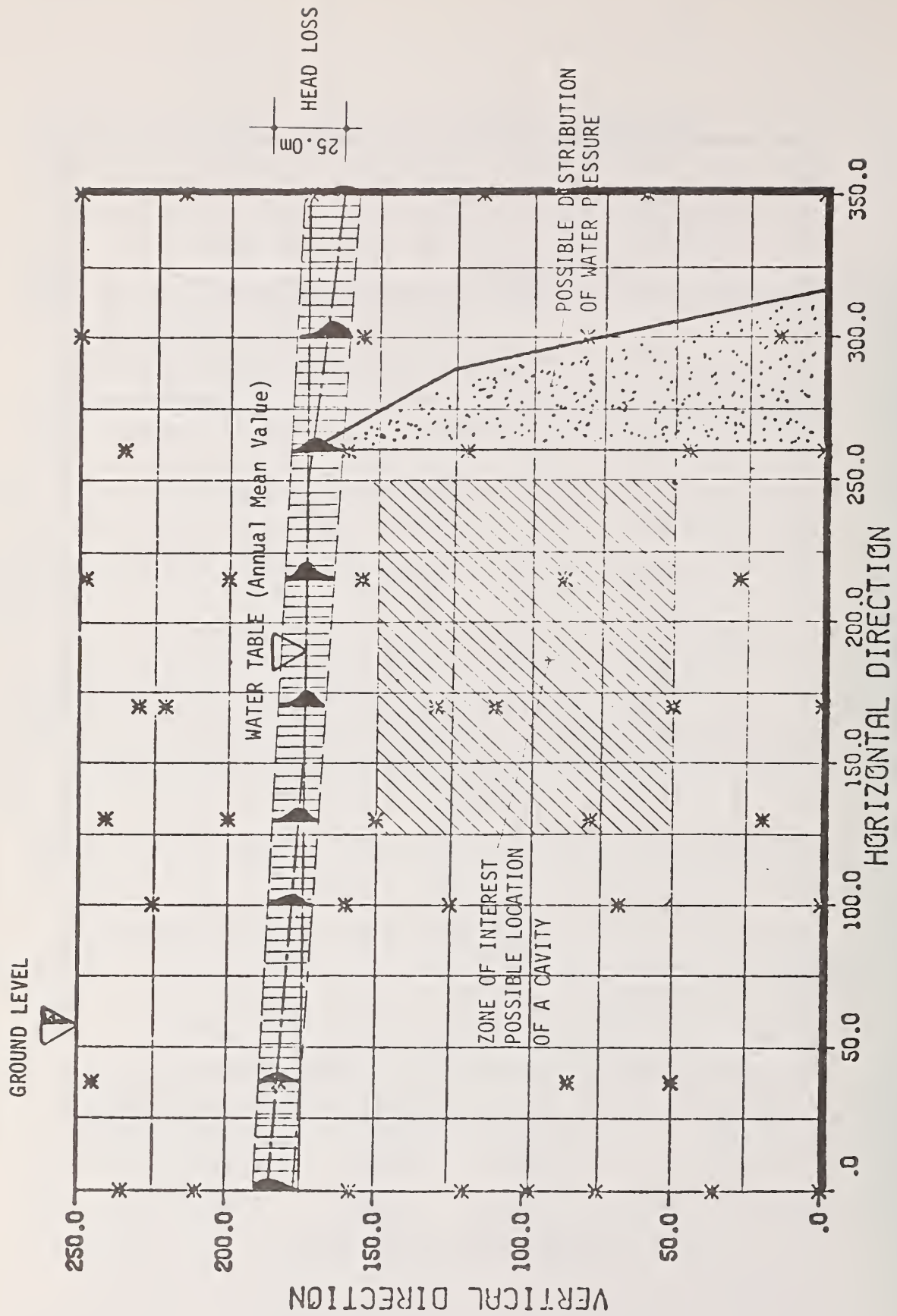


FIGURE 4.12 LOCATION OF THE WATER TABLE

CHAPTER 5
INFERENCE MODEL AND ITS INTERFACE
WITH THE ANALYTICAL UNCERTAINTY MODEL

5.1 Introduction

In Chapter 3 the need of an inference model producing the input data to the main analytical scheme on the basis of field information was demonstrated. Indeed a rock volume is assumed to be made up of a number of elementary volumes within which the physical properties of the rock are treated as stationary. However, the properties assigned to every particular point in a two-dimensional space must be inferred from a limited number of rock samples. Clearly then there is a need of an inference model to generate a complete set of input data from the small amount of information produced by field investigations.

Krumbein (49), describes the fundamental techniques used in defining linear inference models. Such techniques are for example the method of least squares, fitting a polynomial of two variables, etc. However, all these techniques fail to provide an evaluation of how good the estimation is. They also exhibit operational difficulties for the nonstationary case. A different inference scheme is proposed by Matheron (58). It is based on a model originally suggested by Krige (48), and is particularly well suited to treat nonstationary cases. A similar moving average technique is presented hereafter, that generates the spatial

distribution of the physical properties of the rock media, defined in the previous chapter. Also the interfacing of the Inference model with the analytical Finite Element model is shown below.

5.2 Justification of the Moving Average Technique

Drill hole samples most often produce extreme values which are erratic in their spatial distribution. Figure 5.1 gives an illustration of the variability of some commonly investigated physical parameters. Therefore there is a need for models generating smooth spatial distributions of these parameters. Two such models most commonly used are based on trend surface estimates and moving average estimates.

It is generally observed that moving average estimates are superior to trend surface estimates. In the former case the estimation is exclusively based on adjacent informational sets, the more distant sets exerting no influence at all. In the case of the trend surface estimates, the estimation is based on all known data. Moving average estimates tend to be more stable than corresponding polynomial trend estimates obtained from the same number of data points, especially if the sample points are sparse, Whitten (94). Davis (13), observed that moving average schemes in two dimensions have not been significantly tested yet. Indeed the time series analysis from which this method is derived is not as well developed at the present time, as the regression analysis, for example, on which the trend-surface method is based.

Among the moving average methods, the Kriging (names by French geomathematicians in honor of Krige) seems to be the most advantageous. More specifically the Kriging technique makes optimal use of the given data and provides a measure of the variance of the estimation made at

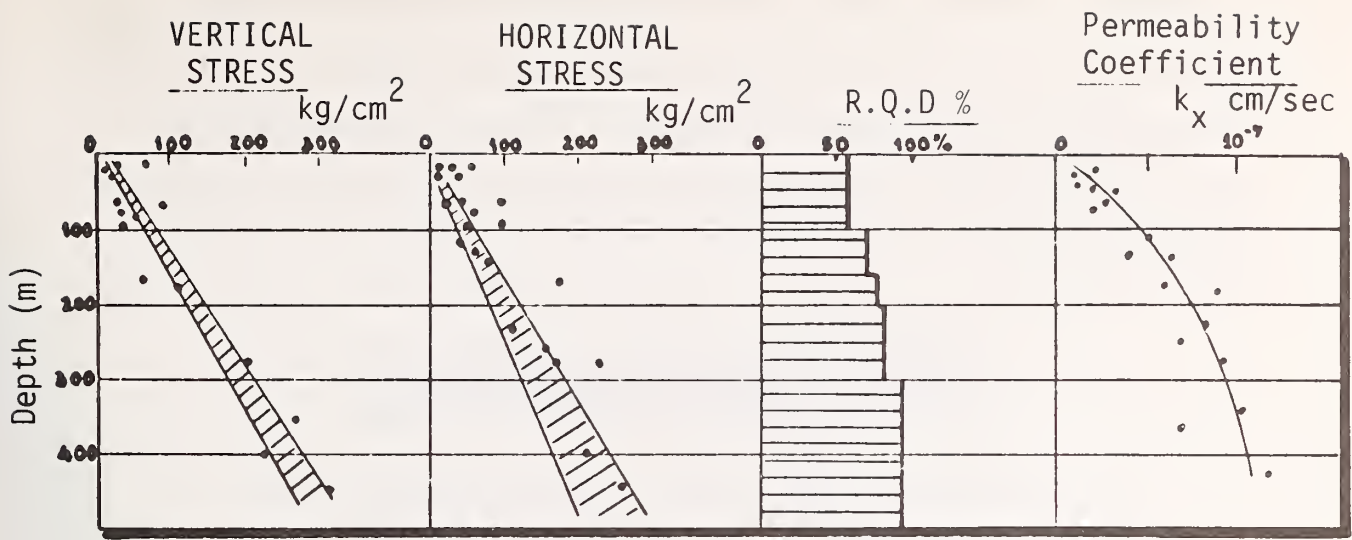


FIGURE 5.1 VARIABILITY OF PHYSICAL PARAMETERS

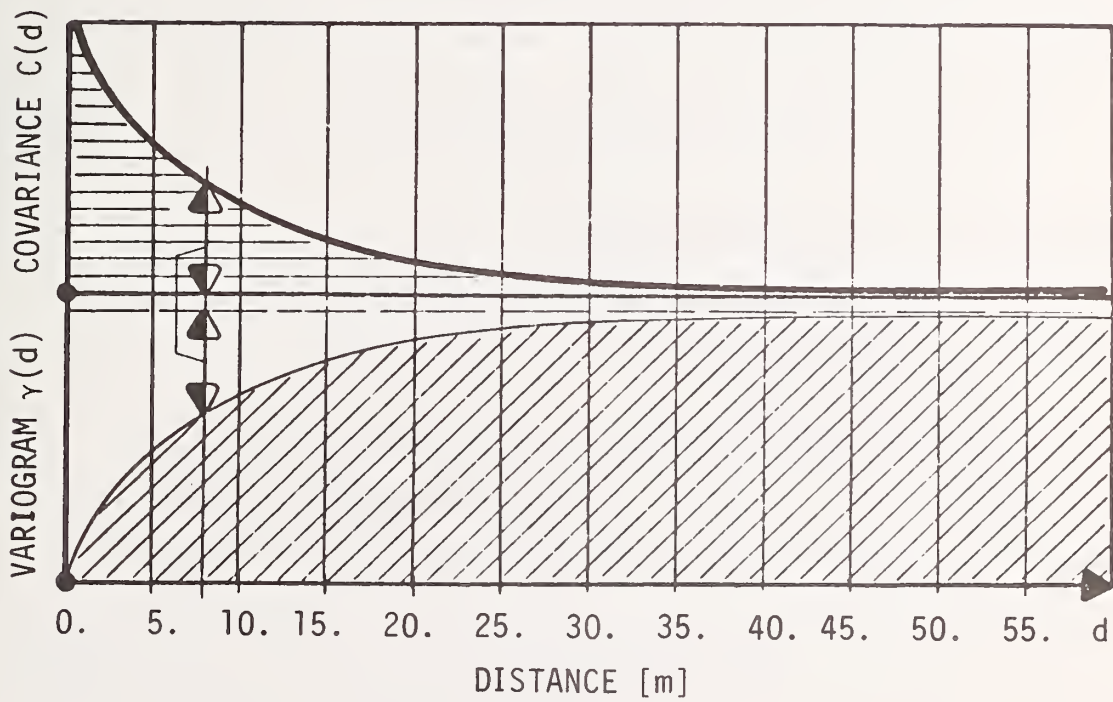


FIGURE 5.2 VARIOGRAM AND COVARIANCE VS. DISTANCE

any specific location. Both these features are essential if the results from the Inference model are to provide the input for an uncertainty analysis as proposed in Chapter 3. However it is believed that a general method incorporating parts of both techniques may give superior results.

5.3 Implementation of the Inference Model in a Two-Dimensional Geometric Space

5.3.1 Statistical Model and Corresponding Assumptions

To determine the values of a rock property $Z(x,y)$ a number of measurements are made on rock samples from bore holes. The set of points where observations are made is indexed by β and Z_β represents the measured value of the random rock property at point β . $\hat{Z}(x_0,y_0)$ is the estimation of property Z at a particular point (x_0,y_0) in the media, evaluated from the measured Z_β values.

One simple way to obtain this estimation is to define \hat{Z} in terms of the known values Z_β according to a linear combination as follows:

$$\hat{Z}(x_0,y_0) = \sum_{\beta=1}^n b_\beta Z_\beta \quad (5.1)$$

where: Z_β are the known data points,

b_β are unknown weight coefficients to be determined by the Inference model.

An alternate approach would be to estimate the mean value of $Z(x,y)$, namely $\bar{Z}(x,y)$ at point (x_0,y_0) , according to a linear combination:

$$\bar{Z}(x_0,y_0) = \sum_{\beta=1}^n a_\beta \bar{Z}_\beta \quad (5.2)$$

where: \bar{z}_β is the mean-value at the known data points,
 a_β are the unknown weight coefficients.

The random variable $Z(x,y)$ in turn can be expressed as follows:

$$Z(x,y) = \bar{Z}(x,y) + FZ(x,y) \quad (5.3)$$

where: $\bar{Z}(x,y)$ is the mean value, and

$FZ(x,y)$ is the fluctuating term around the mean.

This model leads to two possible groups of assumptions. They concern the first and second moments of the random variable $Z(x,y)$. The first group is:

$$E[Z(x,y)] = \bar{Z}(x,y) \quad (5.4)$$

$$E[Z(x_1,y_1), Z(x_2,y_2)] = \bar{Z}(x_1,y_1) \cdot \bar{Z}(x_2,y_2) + C((x_1,y_1), (x_2,y_2)) \quad (5.5)$$

where: $\bar{Z}(x,y)$ is the mean value, and

$C(x_1, \dots)$ is the covariance of the variable $Z(x,y)$.

These assumptions are in many cases too restrictive and need to be replaced by more flexible ones. This can be realized by focusing on the rate of change of the random variable $Z(x,y)$, as follows:

$$E[Z(x_1,y_1) - Z(x_2,y_2)] = \bar{Z}(x_1,y_1) - \bar{Z}(x_2,y_2) \quad (5.6)$$

$$E[(Z(x_1,y_1) - Z(x_2,y_2))^2] = 2 \gamma((x_1,y_1), (x_2,y_2)) \quad (5.7)$$

where: $\gamma(x_1, \dots)$ is the variogram or semivariance of the difference

$$Z(x_1,y_1) - Z(x_2,y_2)$$

Interestingly the variogram $\gamma(d)$ and the covariance $C(d)$ are both defined as functions of the distance between two locations and can be related by Eq. 5.8, as shown in Appendix B:

$$\gamma(d) = C(0) - C(d). \quad (5.8)$$

As shown in Figure 5.2, $\gamma(d)$ and $C(d)$ are complementary.

Both above sets of assumptions concern the stochastic model. An additional set of assumptions is needed to specify the nature of the randomness of the variable $Z(x,y)$, in particular its mean and its variance.

Locally at a point (x,y) the mean $\bar{Z}(x,y)$ is approximated as a linear combination of known functions:

$$\bar{Z}(x,y) = \sum_{i=1}^k a_i f^i(x,y) \quad (5.9)$$

where: a_i are unknown weight coefficients,
 $f^i(x,y)$ are a priori known functions locally approximating $\bar{Z}(x,y)$.

The global trend analysis of most real cases, Davis (13), can be represented by a polynomial equation of the first, second or third order. Therefore it can be intuitively seen that locally the trend can be best approximated by quadratic functions as shown in Figure 5.3. A corresponding norm can be defined for a best approximation with respect to the encountered trend.

The covariance $C(x_1, x_2)$ can be computed from field measurements, and can be represented by the following expression:

$$C(x_1, x_2) = k e^{-\alpha d} \quad (5.10)$$

where: d is the distance between x_1 and x_2 ,
 α, k are fitting parameters.

In many cases the variogram $\gamma(d)$ is more suitable than the covariance $C(d)$ to define the distances over which, realizations of the

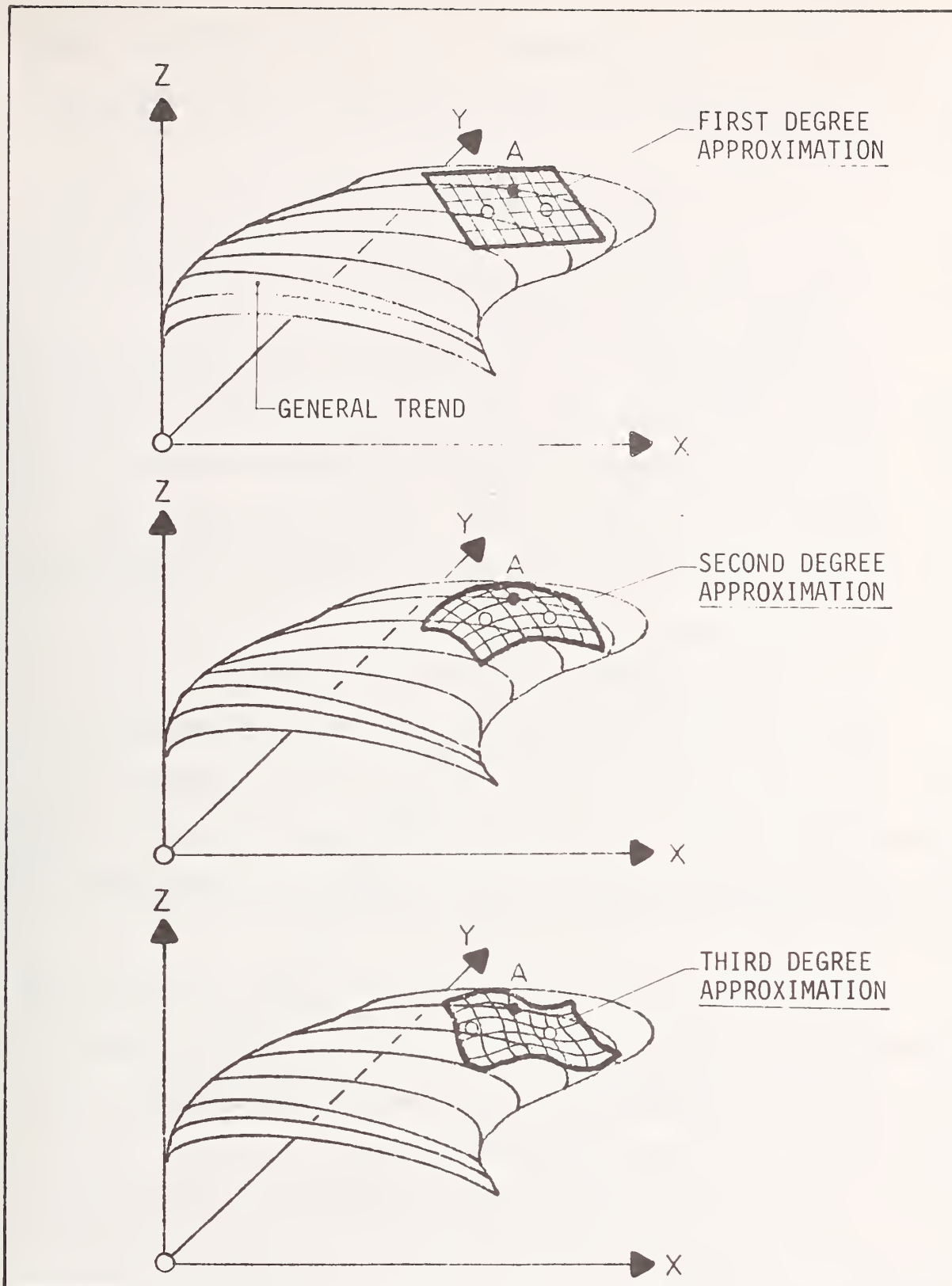


FIGURE 5.3 LOCAL APPROXIMATIONS OF GENERAL TRENDS

random variable Z are interdependent. Thus a range of maximum allowable sampling interval can be evaluated. The expressions most commonly used for $\gamma(d)$ are:

$$\gamma(d) = \beta + 3\alpha \log(d) \quad (5.11)$$

or
$$\gamma(d) = \alpha(d) \quad (5.12)$$

where: α and β are fitting parameters.

The first expression is often referred to as DeWij's model, while the second as Linear model. The selection of the adequate expression for $\gamma(d)$ is difficult since it requires a very careful treatment of the data obtained from field investigation. Matheron (58) gives a case study of such a treatment as illustrated in Figure 5.4. In the present study both expressions were tested.

5.3.2 Identification of the Best Estimator

Summarizing, up to this point two sets of model assumptions are given, Eqs. (5.4) and (5.5) and Eqs. (5.6) and (5.7), concerning the random variables $Z(x,y)$. Both these sets of assumptions can be used to identify estimators of both the random variable $\hat{Z}(x,y)$ and its mean $\bar{Z}(x,y)$.

The first model, (Eqs. (5.4) and (5.5)) is used to obtain the best estimator for the random variable $\hat{Z}(x,y)$ itself. Both models identify the best estimators among all possible functions satisfying the hypothesis concerning the randomness of the rock media, Eq. (5.9). This is done by minimizing the variance of the estimation, Eqs. (5.5), respectively (5.7), subject to the first moment constraints, Eqs. (5.4), respectively (5.6). The Lagrange Multipliers approach is used for this constrained optimization problem. The computations carried out in Appendix B, lead to the following results:

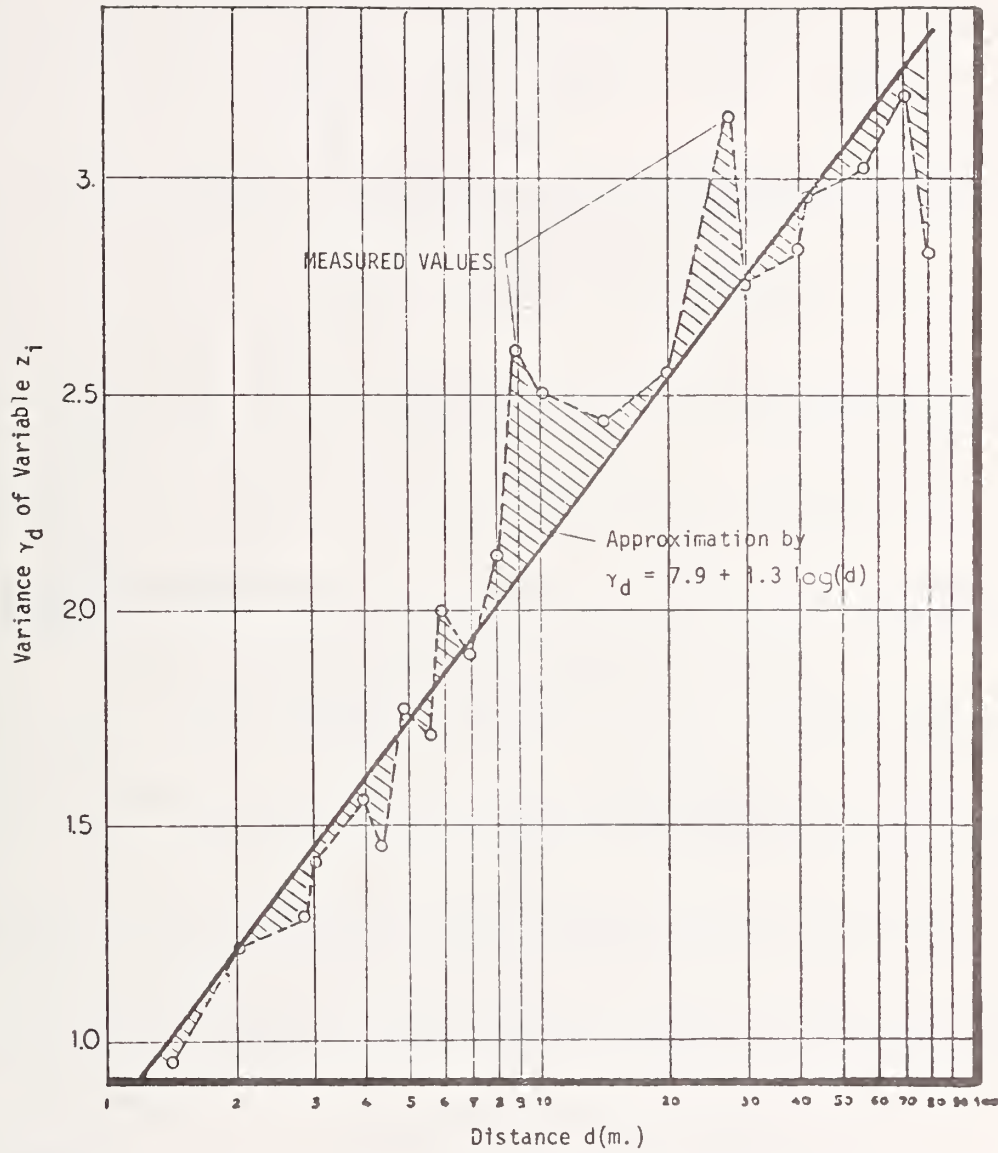


FIGURE 5.4 APPROXIMATE VARIOGRAM FUNCTION FROM ACTUAL DATA

FOR MODEL 1 concerning the estimation of the mean $\bar{Z}(x,y)$ (from Eqs. (5.4) and (5.5)).

The method of Lagrange Multipliers leads to a set of $n + k$ equations with $n + k$ unknowns, namely the weight coefficients:

$$\begin{aligned} \sum_{\beta} a_{\alpha\beta}^{\beta} C_{\alpha\beta} - \sum_{\ell} \mu_{\ell} f_{\alpha}^{\ell} &= 0 ; \alpha, \beta = 1, \dots, n \\ \sum_{\alpha} a_{\alpha}^{\ell} f_{\alpha}^{\ell} - \delta_{\ell}^{\alpha} &= 0 ; \ell = 1, \dots, k \end{aligned} \quad (5.13)$$

where: a_{α}^{β} are the unknown weight coefficients,
 μ_{ℓ} are the Lagrange Multipliers,
 δ_{ℓ}^{α} is the Kronecker delta.

The variance of the estimation is given by:

$$E[\hat{\bar{Z}}(x,y)]^2 = \sum_{\ell} \mu_{\ell} f^{\ell}(x,y) ; \ell = 1, \dots, k \quad (5.14)$$

FOR MODEL 2 concerning the estimation of the random variable $Z(x,y)$ (from Eqs. (5.6) and (5.7)).

Similarly the following system is obtained (Appendix B).

$$\begin{aligned} \sum_{\beta} b^{\beta} \gamma_{\alpha\beta} + \sum_{\ell} \mu_{\ell} f_{\alpha}^{\ell} &= \gamma(x_{\alpha}, x) ; \alpha, \beta = 1, \dots, n \\ \sum_{\alpha} b^{\alpha} f_{\alpha}^{\ell} &= f^{\ell}(x) ; \ell = 1, \dots, k \end{aligned} \quad (5.15)$$

with $\sum_{\alpha} b^{\alpha} = 1$

where: b^{β} are the unknown weight coefficients,
 μ_{ℓ} are the Lagrange Multipliers.

The variance of the estimation is given by:

$$E[Z - \hat{Z}]^2 = \sum_{\alpha} b^{\alpha} \gamma(x_{\alpha}, x) + \sum_{\ell} \mu_{\ell} f_{\alpha}^{\ell} ; \alpha = 1, \dots, n \quad (5.16)$$

$\ell = 1, \dots, k$

5.4 Interfacing the Inference Model with the Analytical Model

5.4.1 Uncertainty Analysis in the Analytical Model

As mentioned previously the analytical model is treated using the finite element technique which provides us with the transfer mechanism between a set of inputs $\{F\}$ and a set of generally unknown outputs $\{u\}$. The general solution is given by the following relation in matrix form:

$$\{u\} = [K]^{-1} \{F\} \quad (5.17)$$

where: $\{K\}$ is generally known as stiffness matrix and is defined as a function of the random variables Z_1, Z_2, \dots, Z_n ,

$\{F\}$ is the loading term.

Applying now the first order uncertainty analysis as described by Papoulis (68), the first and second moments of the unknown vector $\{u\}$ are obtained as follows:

FIRST MOMENT

$$E[\{u(Z_1, Z_2)\}] \approx \{u(\bar{Z}_1, \bar{Z}_2)\} + \frac{1}{2} \left[\sigma_{Z_1}^2 \frac{\partial^2 \{u(\bar{Z}_1, \bar{Z}_2)\}}{\partial Z_1^2} + \dots \right] \quad (5.18)$$

where: $\sigma_{Z_1}^2$ is the variance of the physical parameter Z_1 .

The second part of the right hand side can be neglected being a very small quantity.

SECOND MOMENT

$$E[\{u(Z_1, Z_2)\}^2] \approx \sigma_{Z_1}^2 \left(\frac{\partial \{u(\bar{Z}_1, \bar{Z}_2)\}}{\partial Z_1} \right)^2 + \sigma_{Z_2}^2 \left(\frac{\partial \{u(\bar{Z}_1, \bar{Z}_2)\}}{\partial Z_2} \right)^2 + 2 \frac{\partial \{u(\bar{Z}_1, \bar{Z}_2)\}}{\partial Z_1} \frac{\partial \{u(\bar{Z}_1, \bar{Z}_2)\}}{\partial Z_2} \text{cov}(Z_1, Z_2). \quad (5.19)$$

The partial derivatives in Eq. (5.19) are obtained from the following system:

$$[K(Z_1, Z_2)] \frac{\partial \{u(Z_1, Z_2)\}}{\partial Z_i} = \frac{\partial \{F\}}{\partial Z_i} - \frac{\partial [K(Z_1, Z_2)]}{\partial Z_i} \{u\};$$

$$i = 1, 2 \quad (5.20)$$

The solution is obtained by the classical finite element methodology, (97).

5.4.2 Coupling of the Inference Model with the Analytical Uncertainty Model

The estimates of the spatial mean $\hat{Z}_1(x, y)$, $\hat{Z}_2(x, y)$ and the variances $\sigma_{Z_1}(x, y)$, $\sigma_{Z_2}(x, y)$ provided by the inference model are substituted in the statistical relations of the dependent random variable $\{u\}$, Eqs. (5.18) and (5.19). Thus the first and second moments, as well as the coefficient of variation of $\{u\}$ can be evaluated. The coefficient of variation in particular being an essential statistical property, can be used to evaluate the performance of the analytical model.

For testing purposes, an example was treated borrowed from the field of underground confined flow, as shown in section 5.6. The output of the analysis provides the first and second moments of the unknown hydraulic head $\{u\}$, at any specified location of the domain under consideration.

5.5 Description of the Algorithm

The above described procedure is summarized by the computation steps of the flow chart of Fig. 5.5. The geometric domain under investigation is divided using a rectangular mesh common for the Inference

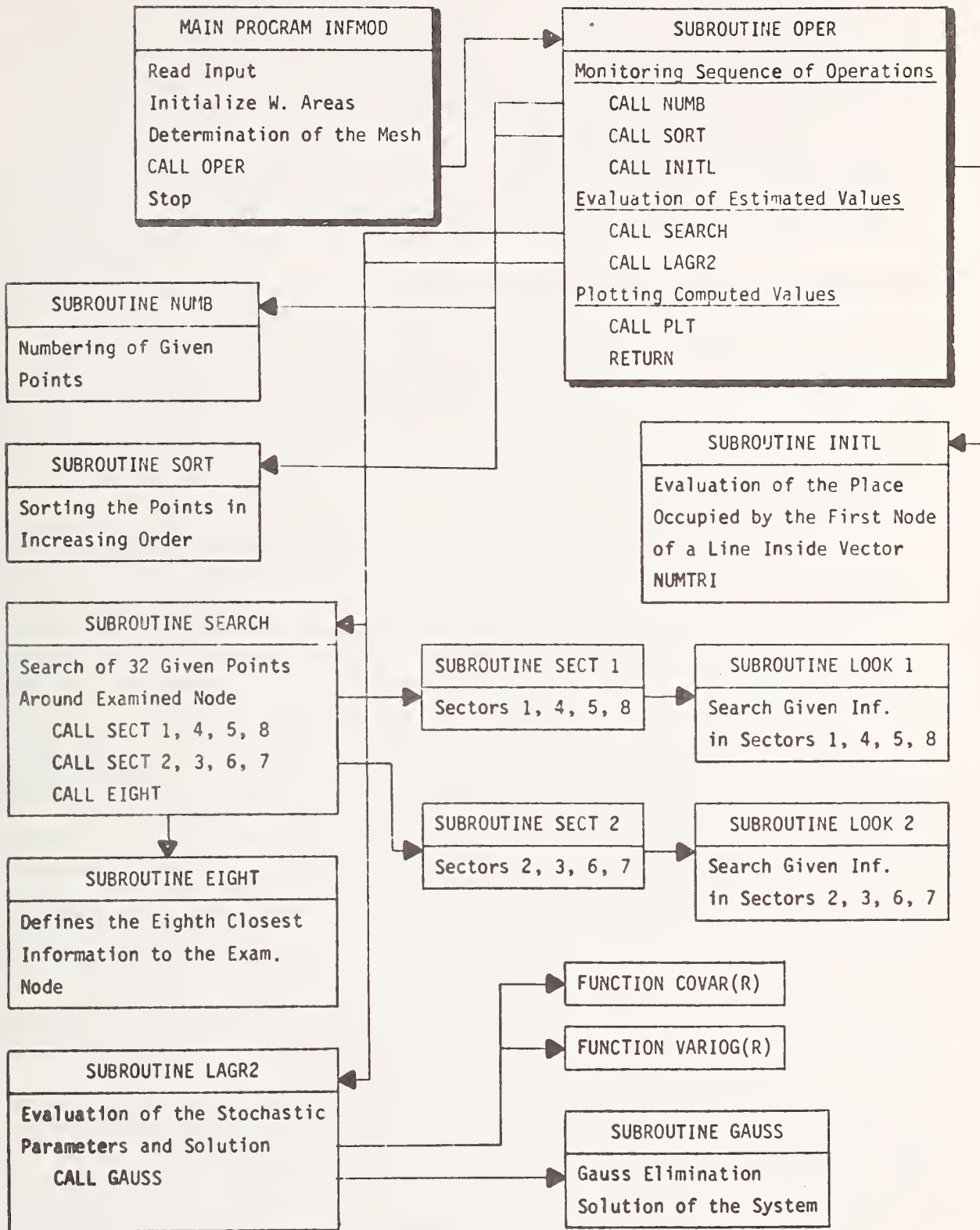


FIGURE 5.5 FLOW CHART OF PROGRAM INFMOD (INFERENCE MODEL)

Model and the analytical model (Finite element mesh). The computations are carried out at each node using a number among the known realizations $Z_{\beta}(x,y)$. Therefore a zone of influence, characteristic of the media are depending on the covariance $C(x_1, x_2)$ and/or the variogram $\gamma(d)$ is defined at each node of the mesh. For computational efficiency, 'n' known points are selected within this zone, to determine the estimation of the random variable $Z(x,y)$ at that particular node. A polynomial comprising k terms, approximates the trend of $Z(x,y)$ in the neighborhood of the node at hand. Thus, at every node (x,y) , a system of $n + k$ equations permits to determine the estimator $\hat{Z}(x,y)$. The outcome of the procedure depends on the number of known points and the density of the provided information $Z_{\beta}(x,y)$.

In case of insufficient information in the domain of interest, the original assumptions are violated. However, in this case the values of variance of the estimation indicate the poor performance of the inference and give the exact location where more information is needed.

The flow chart of Figure 5.5 gives the sequence in which the computations are performed by program INFMOD. The mean values of the physical parameters evaluated by the inference model INFMOD are introduced at each node of the finite element mesh. Thereafter, the computations are performed in a conventional way taking into account the prescribed boundary conditions. The mean values of the unknown vector $\{u\}$ are determined, as well as the vectors $\frac{\partial\{u\}}{\partial Z_i}$, $i = 1,2$. Finally the variance of the unknown vector $\{u\}$ is computed at each node of the mesh. A more detailed description of the finite element programs, developed to be coupled with the Inference model, is given in Chapter 6.

5.6 Example of Application and Discussion

As said in section 5.4 the example of application is borrowed from the field of underground confined flow. Two groups of tests are conducted to explore the limitations and the applicability of the general algorithm. One group concerns the inference model alone, while the other deals with the performance of the finite element model.

FIRST GROUP

The three different tests related to the Inference model, in connection with two different problems, produced the following results:

1. Tests of the statistical convergence

This test was conducted under the assumption of statistical isotropy and for a uniform spatial distribution of the given information points. More specifically in Problem 1 a domain defined by a square mesh of 400 x 400m was examined and the random variable $Z(x,y)$ was assumed to possess a realization lying on a portion of a sphere over this domain, as shown in Figure 5.6. The domain was divided into squares of 25 x 25m having 289 nodes where the computations were performed. The given information was located first on nine points as shown in Figure 5.6, then on twenty-five points and finally on eighty-one points.

The estimation at the 288 nodes of the mesh was performed by both Inference models defined previously (Sect. 5.3). Interestingly enough in the region of great variability of the random variable $Z(x,y)$ the two models show a good agreement in their estimation, as illustrated in Figure 5.7.

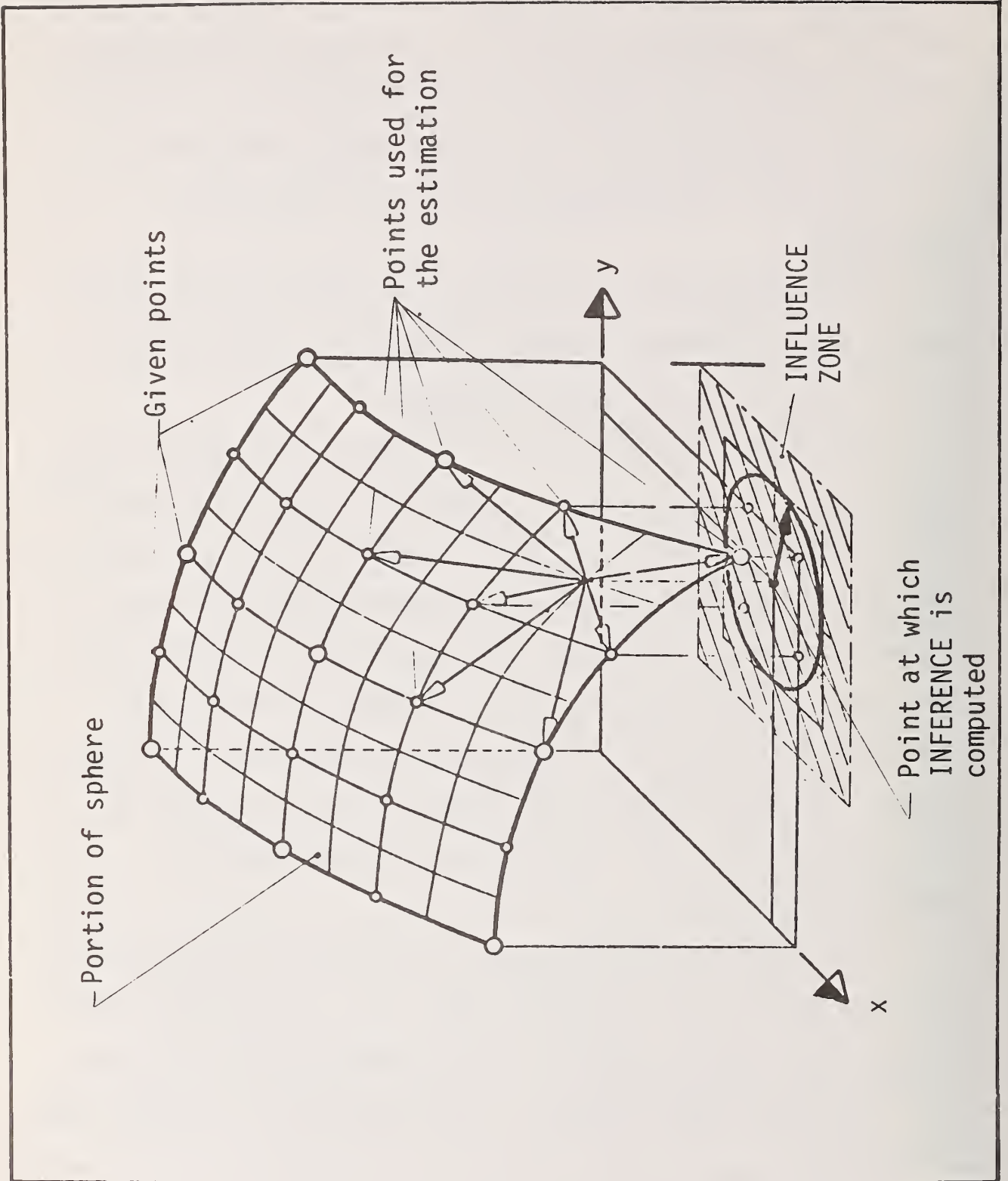


FIGURE 5.6 ILLUSTRATION OF PROBLEM 1 (SPHERICAL TREND)

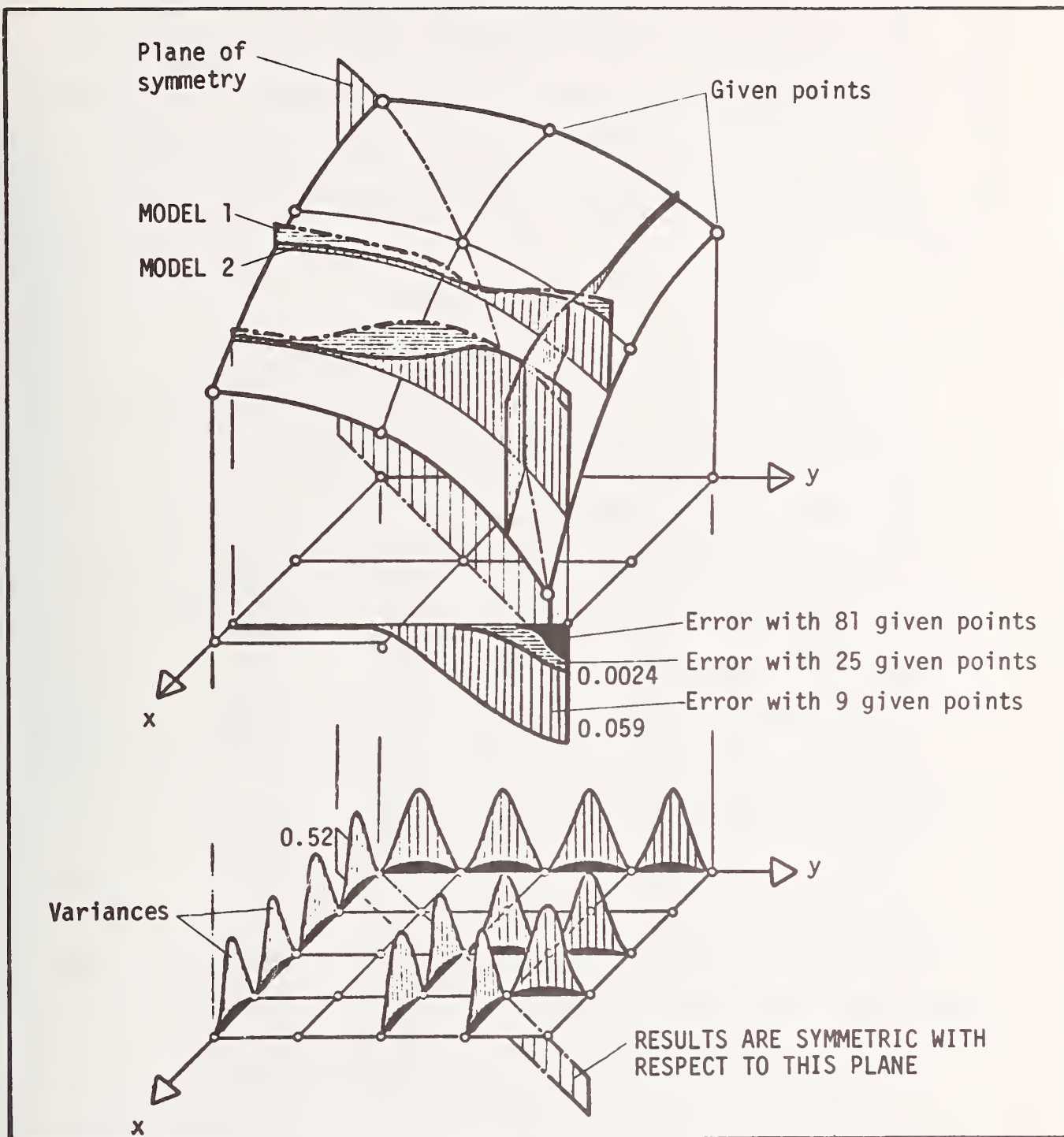


FIGURE 5.7 ESTIMATED STATISTICAL CHARACTERISTICS OF PROBLEM 1

As expected, increasing amount of information, produces a smaller variance of the estimates. The case of largest variance is reported in Table 5.1.

It is to be mentioned that the maximum error obtained is less than 0.1 percent and that the estimated first and second moments are symmetrically distributed with respect to the existing plane of symmetry.

Another interesting feature is that the spatial distribution of the error is similar to that of the variance, justifying the use of the estimated variance as an indicator of the error.

2. Tests of the statistical assumptions

These tests concerned (a) the assumptions on the a priori known function $f(y)$ characterizing the behavior of the mean $\bar{Z}(x,y)$, and (b) the assumption on the general form of the variogram obtained either from site investigation or considered a priori. The tests were performed on the square 400 x 400m of Problem 1 and over a region 50 x 20m of the flow problem (Problem 2).

Several functions $f(x,y)$ were tested in the above mentioned regions and the most satisfactory results from the point of view of both accuracy and efficiency were obtained for the following quadratic function:

$$f(x,y) = a_0 + a_1x + a_2y + a_3x^2 + a_4y^2 + a_5xy \quad (5.21)$$

This form was also suggested from a trend analysis (sect. 5.2), applied to the data of the flow problem as illustrated in Figure 5.8.

The following expressions for the variogram were studied:

$$\gamma(d) = \alpha \log |d| \quad (5.22)$$

$$\gamma(d) = \alpha |d| \quad (5.23)$$

TABLE 5.1 RESULTS OF INFERENCE MODEL FOR PROBLEM 1

NUMBER OF GIVEN INFORMATION	TYPE OF MODEL	MAX ERROR	EXPECTED VALUE	MAX VARIANCE	MAX COEFFICIENT OF VARIATION
9 points	MODEL 1	0.056	3.18	.81	0.28
	MODEL 2	0.049	3.45	1.08	0.30
25 points	MODEL 1	0.011	3.33	.35	0.17
	MODEL 2	0.0047	3.61	0.569	0.21
81 points	MODEL 1	0.002	3.40	0.21	0.135
	MODEL 2	0.0007	3.62	0.249	0.14

TABLE 5.2 RESULTS OF INFERENCE MODEL FOR PROBLEM 2

COORDINATES		ESTIMATED MEAN	ESTIMATED VARIANCE	COEFFICIENT OF VARIATION
x	y	10^{-3} cm/sec	10^{-5} cm/sec	10^{-2}
5.000	5.000	.013	.002	3.651
10.000	5.000	.008	.002	6.137
15.000	5.000	.002	.003	32.673
20.000	5.000	.015	.001	2.167
25.000	5.000	.027	.002	1.813
30.000	5.000	.008	.001	4.449
35.000	5.000	.030	.004	2.041
40.000	5.000	.026	.000	.805
45.000	5.000	.018	.001	1.698
50.000	5.000	.171	.071	1.559
0	10.000	.097	.029	1.736
5.000	10.000	.026	.001	.905
10.000	10.000	.012	.002	3.290
15.000	10.000	.080	.000	.000
20.000	10.000	.053	.004	1.198
25.000	10.000	.061	.001	.603
30.000	10.000	.065	.010	1.534
35.000	10.000	.003	.002	13.735
40.000	10.000	.025	.004	2.696
45.000	10.000	.091	.003	.590
50.000	10.000	.121	.262	4.229
0	15.000	.503	.026	.323
5.000	15.000	.335	.002	.119
10.000	15.000	.254	.004	.262
15.000	15.000	.331	.001	.069
20.000	15.000	.460	.003	.121
25.000	15.000	.454	.001	.053
30.000	15.000	.418	.003	.120
35.000	15.000	.502	.001	.066
40.000	15.000	.315	.002	.133
45.000	15.000	.542	.002	.079
50.000	15.000	.599	.082	.479

where: $d = \sqrt{(x_1 - x_2)^2 + (y_1 - y_2)^2}$ = distance between points (x_1, y_1) and (x_2, y_2) .

For both expressions the results were similar. However, the logarithmic expression offers the advantage of defining an influence zone for its estimation as seen in sect. 5.3.1

3. Tests of the parameters affecting the quality of the estimation

The most important parameter is the distance 'd' between the location of the point of estimation and the location of the points of known data. It was observed that the estimation becomes better as the distance 'd' decreases. This was apparent in both above examples. However, the spatial distribution of the sample points plays a very important role also. Indeed if the estimated point is outside the closed space formed by the set of known points we have an extrapolation scheme while otherwise we have an interpolation scheme as shown in Figure 5.9.

On the other hand if the number of sample points is increased without changing their respective distances, the estimation as expected is not improved, since there is no drastic change in the values of the weight coefficients, Figure 5.10.

As a conclusion of this group of tests one can say that the model is sensitive and provides a message through the values of the variances whenever the basic assumptions are violated. In general the inclusion of new information in the region where the violation is observed is improving the final results considerably as it can be seen in Figure 5.11.

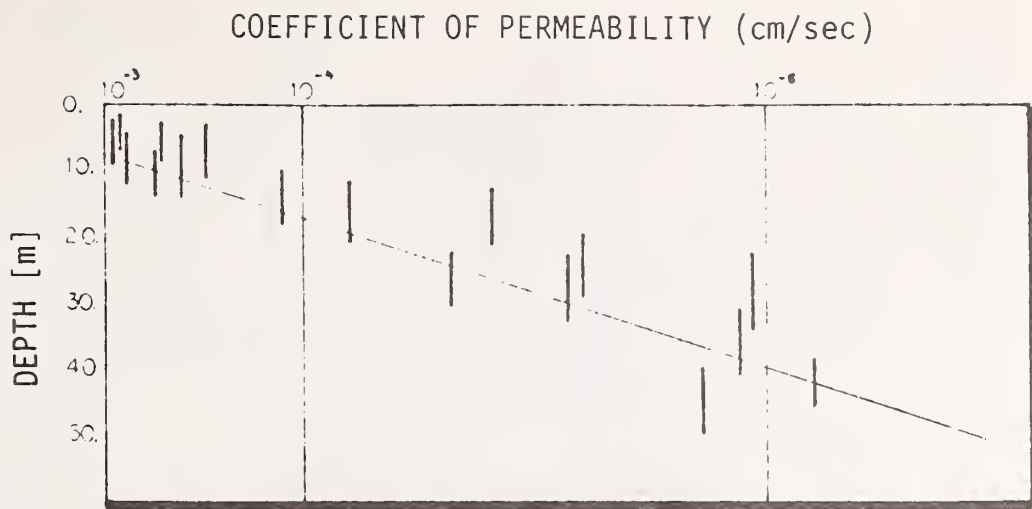


FIGURE 5.8 GENERAL TREND FUNCTION OF THE PERMEABILITY

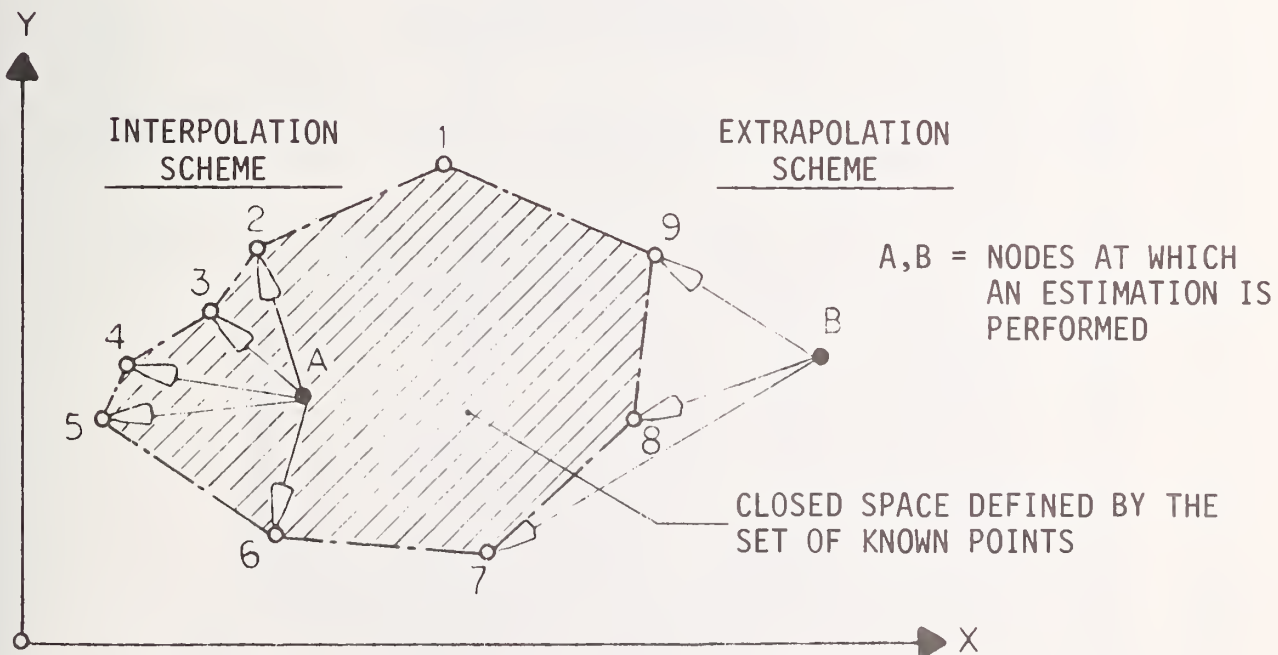


FIGURE 5.9 TOPOLOGICAL CONSIDERATIONS FOR THE ESTIMATION NODE

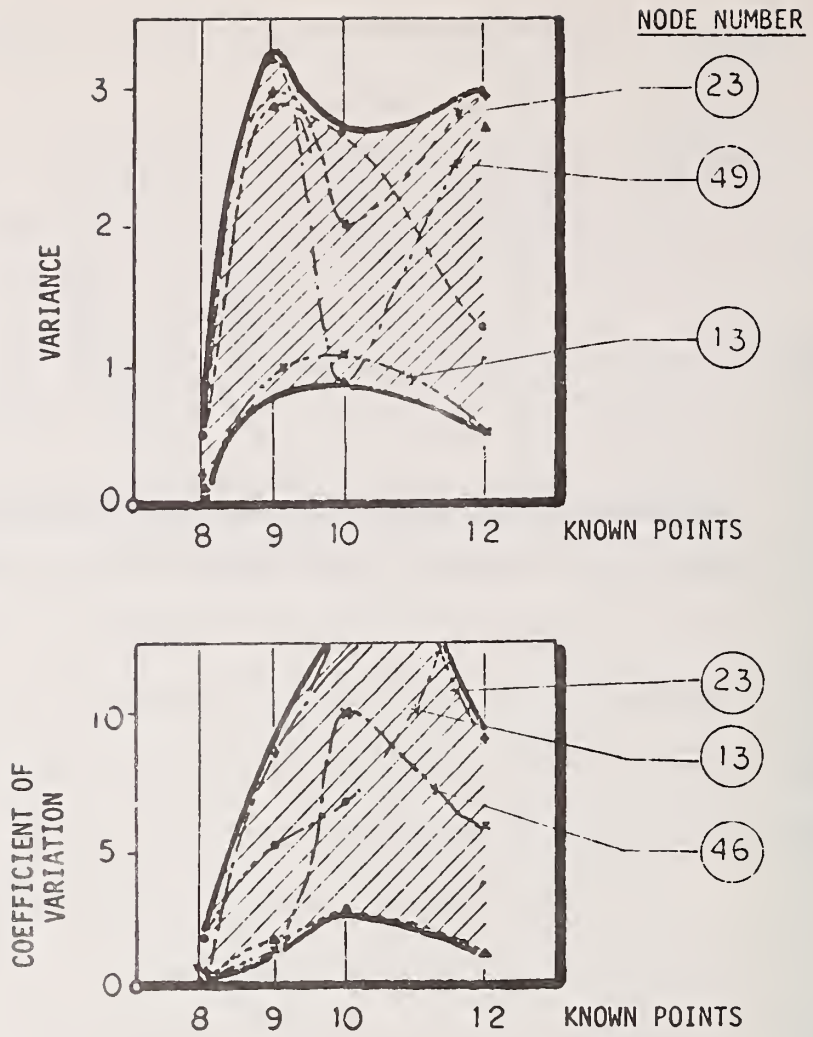


FIGURE 5.10 ESTIMATED VARIANCES VS. THE NUMBER OF KNOWN POINTS

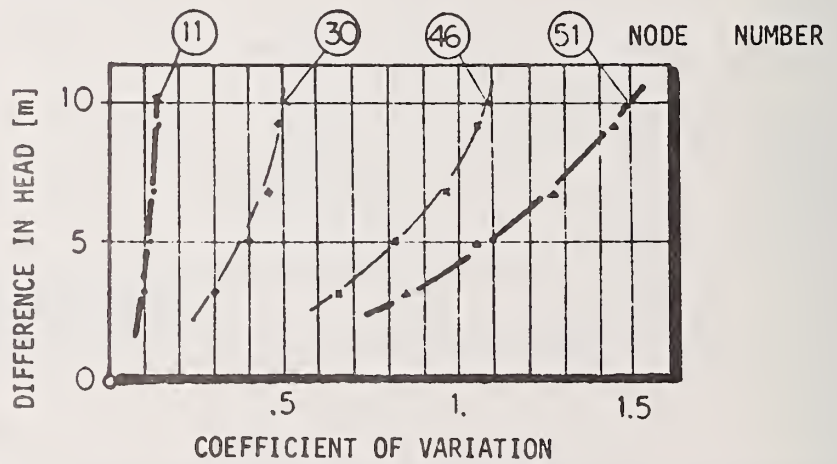


FIGURE 5.12 EFFECT OF BOUNDARY CONDITIONS ON ESTIMATED VARIANCES

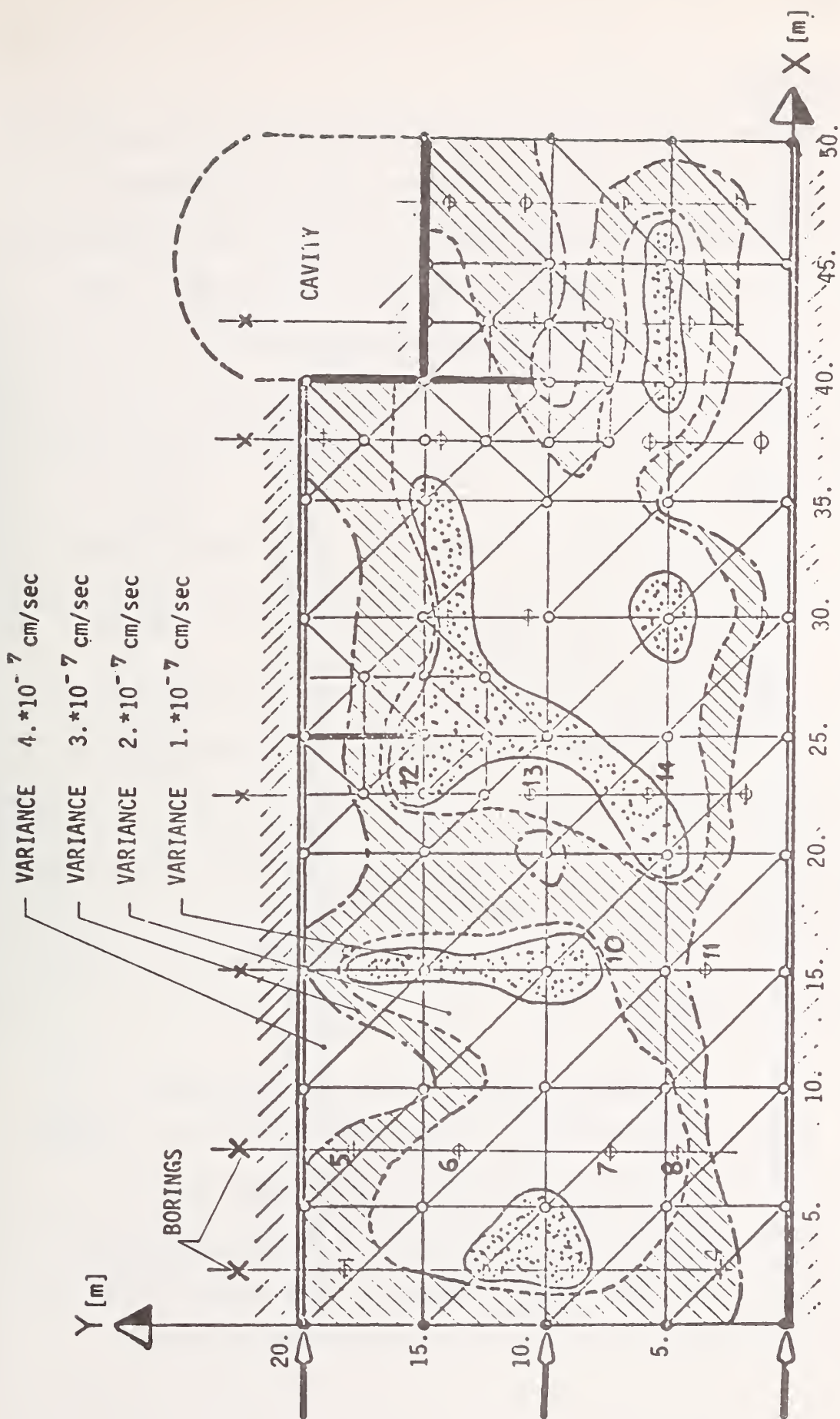


FIGURE 5.11 ESTIMATED STATISTICAL CHARACTERISTICS OF PROBLEM 2 (HORIZONTAL FLOW)

SECOND GROUP

The following tests, related to the coupling of the uncertainty analysis using F.E.M. and the inference model were performed:

1. Tests for the convergence of the statistical characteristics of $\{u\}$ as a function of the size of the element's mesh.

For the First Moment this was done automatically through a mesh generation subroutine. For the Second Moment, a denser mesh was considered only around the flow barriers, where the hydraulic gradient was important.

A satisfactory convergence was observed, as shown in Table 5.2.

2. Tests of the effect of the boundary conditions on the statistical characteristics of $\{u\}$.

Several differential hydraulic heads were considered and their results plotted in Figure 5.12. They display expected responses, namely as the differential head increases, the variance of the unknown quantity $\{u\}$ increases also, showing that the flow becomes more variable reaching eventually a state of nonlaminar flow. Interestingly enough the variances seem to be directly related to the hydraulic gradient, Figure 5.13.

5.7 Remarks on the Applicability of the Method

Becker, Hazen and Scott (1) have produced statistical evidence that data selected from random samples produce more realistic information. Attention then should be given to the randomness of the sample points, as well as the uniformity of the sample volume. The Inference model could be used to advantage here as follows:

DIFFERENCE OF HEADS AT THE BOUNDARIES = 7.00 m.

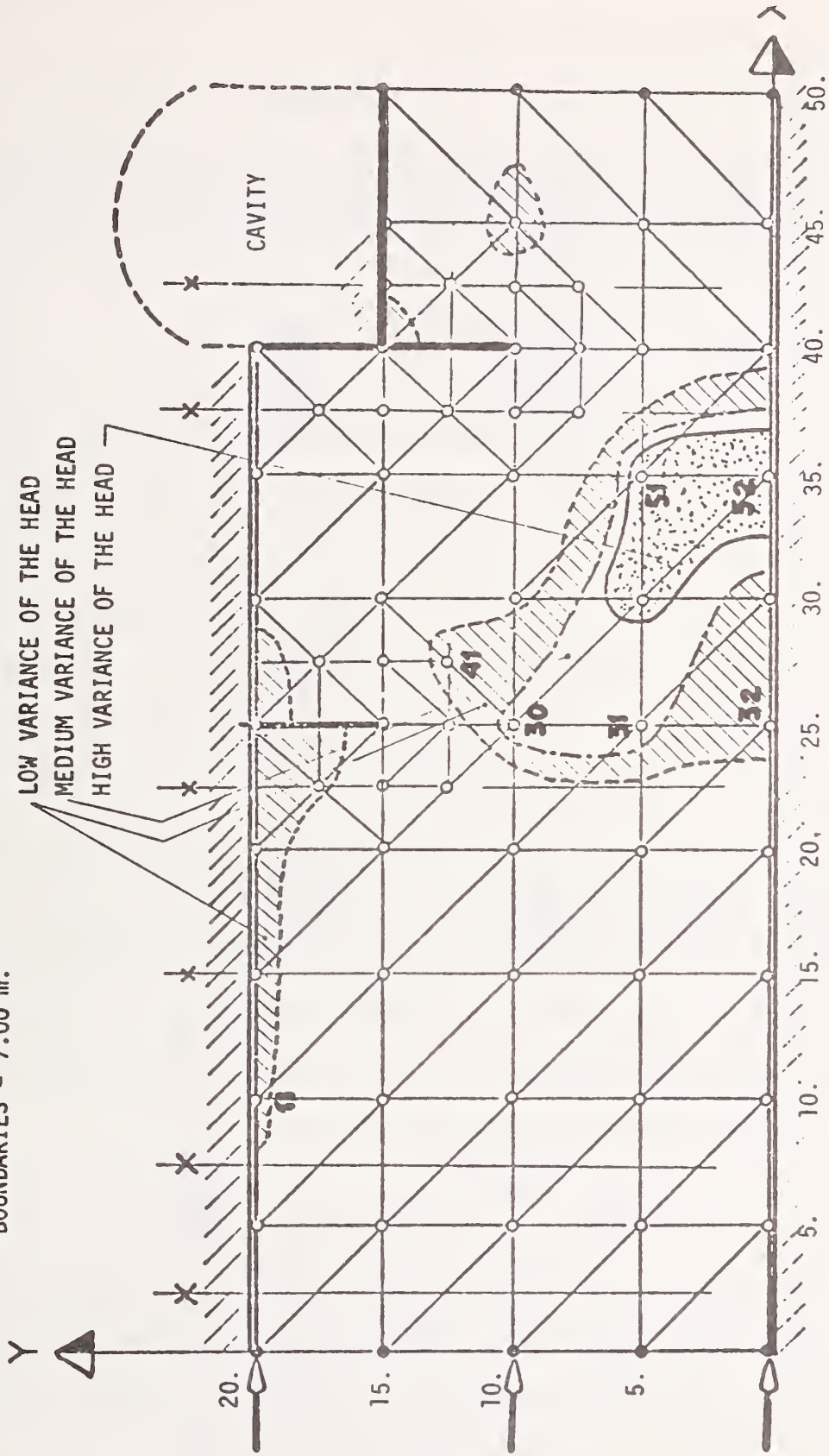


FIGURE 5.13 RESULTS OF THE INFERENCE MODEL COUPLED WITH THE F.E.M. (HORIZONTAL FLOW)

A. Randomness of data points

In the Inference model, the data randomness is automatically tested through the use of the functions describing the statistical constraints, Eqs. 5.13 and 5.15. Indeed, if the provided information does not follow a random pattern, numerical instability is induced which shows that complementary information is needed.

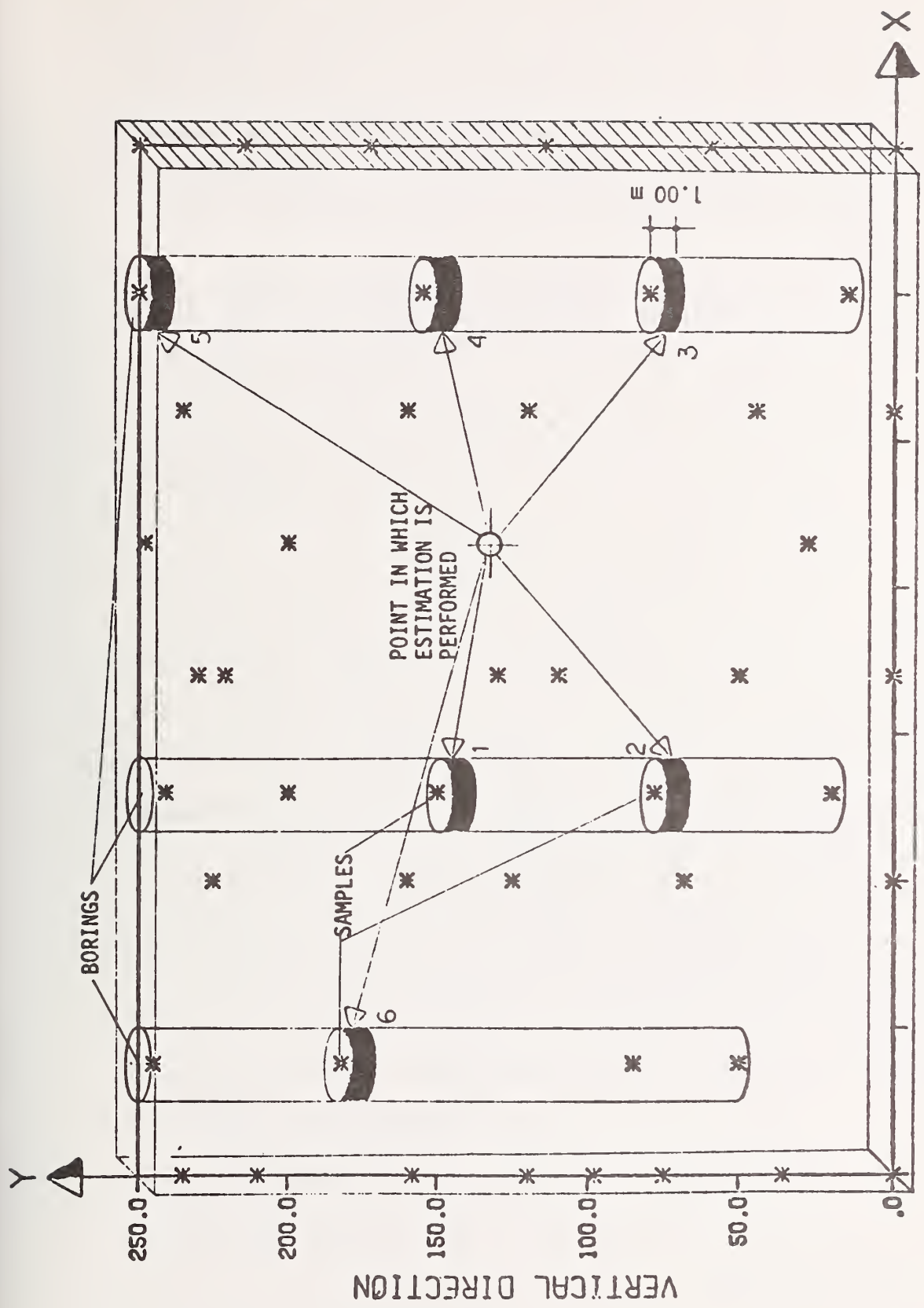
B. Uniform sample volume

It is recognized that a basic requirement for the successful use of statistics in sampling is the uniformity of the sample volume. The Inference model accounts for this size effect through the use of the notion of variogram, (sect. 5.2). The variogram permits to determine the range of significant statistical inference around a given point. On the other hand in Chapter 4 was seen that a one meter boring was sufficient to produce a good statistical description of the physical characteristics of the rock. Therefore, it is proposed here, to use the average values obtained from one meter of borings as the input information to the Inference model, as illustrated in Figure 5.14.

The above consideration are finally checked in a flow problem treated in the square domain $\Omega = (50 < x < 100, y < 50)$ with its solution u (head) subject to boundary conditions

$$u_A \Big|_{x=50} = 100, \quad u_B \Big|_{x=100} = 50 \text{ for } y > 25.$$

A detailed comparison is also performed between the proposed inference correlative model (scheme) and a conventional regression scheme, on a set of five functions representing the permeabilities as illustrated in Figure 5.15.



HORIZONTAL DIRECTION

FIGURE 5.14 ILLUSTRATION OF THE ESTIMATION PROCEDURES

The main conceptual differences of these two schemes are mentioned in section 5.2 and their computational details presented in Appendix B.

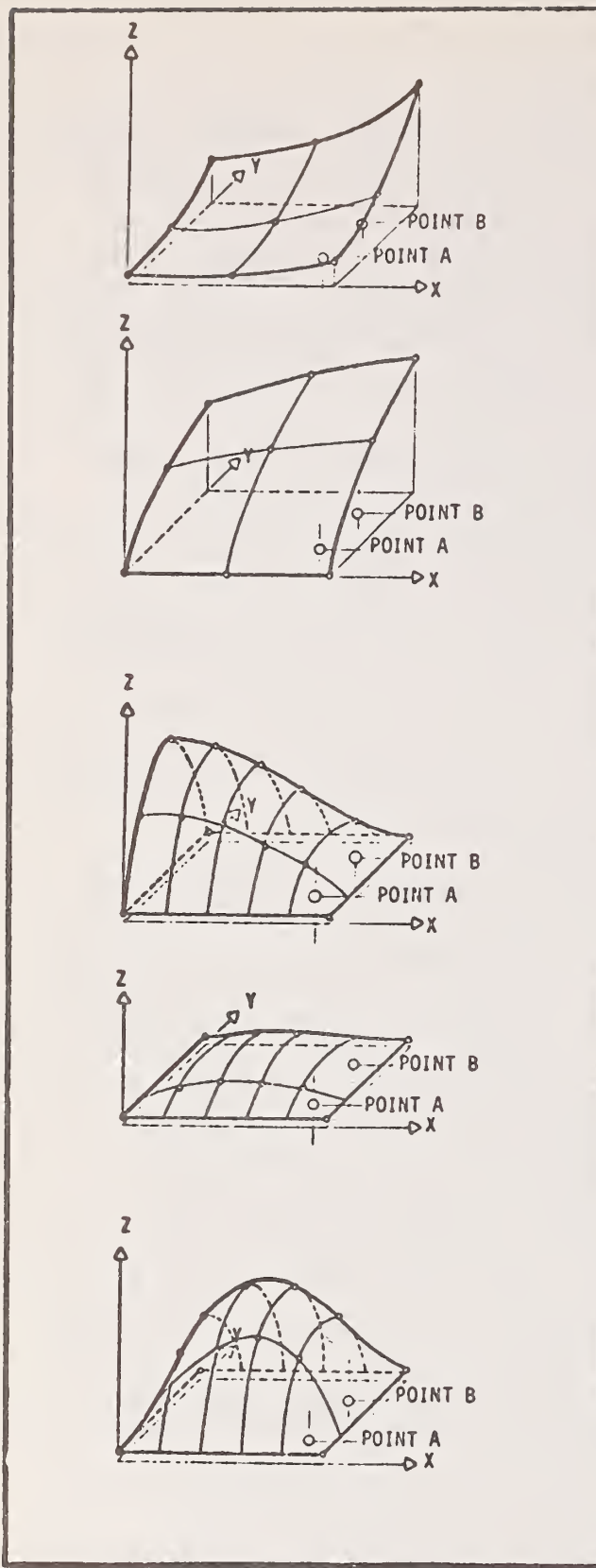
In both estimation schemes, the values of $z(x,y)$ are inferred at the nodes of a 6 x 6 and 11 x 11 mesh of region Ω from a set of measured values of 15 and 25 given β points which lie on the previously mentioned functions.

The regression scheme is implemented by assuming a quadratic polynomial trend while the inference correlative scheme 2 is treated respectively with an assumed linear and a computed discrete variogram. A Monte Carlo technique is used to compute the discrete variogram for each of the z_i functions which in turn is approximated by a least squares cubic spline function (see Figure 5.16).

The results of this investigation are given in Tables 5.3 to 5.7. In Table 5.3 are given the deviations and coefficients of multiple correlation (as defined in Appendix B) of the estimation obtained by the regression and inference schemes. In Table 5.4 the deviations and coefficients of multiple correlation are given for the estimations obtained by an inference model 2 using an assumed linear and a computed variogram. Table 5.5 gives the mean, coefficient of variation and absolute relative error of the estimates $\hat{Z}(x,y)$ obtained by the inference correlative schemes 1 and 2 at points A = (90,10), B(90,40). In Table 5.6 the absolute relative error of the computed head is given using the regression finite element and the inference finite element model of points A(90,10) and B(90,40). Finally in Table 5.7 the coefficient of variation of the head of points A and B are presented for three different boundary conditions.

A number of observations can be made on the above results. On the basis of the computed statistics the inference model has proven to be superior to the regression scheme, in particular for functions 3, 4, and 5 which exhibit rapid slope changes. The coefficient of multiple correlation improves by increasing the number of given points for all functions $Z(x,y)$. The assumed linear variogram performs equally well as the cubic spline least squares approximation of the computed discrete variogram particularly for a dense set of given β points. The inference model 2 with the measured variograms gives better estimates near the boundaries of the flow. The coefficient of variation and absolute relative error computed by the inference model indicate convergence as the number of points of information increases.

In general the absolute relative error indicates the superiority of the inference model 2 in all cases. From Table 5.6 it is seen that the finite-element uncertainty model converges both when the mesh is refined for the same number of given β points or when the number of given β points is increased for the same above mesh. Finally the finite-element inference model proved to be superior to the finite-element regression model in all cases. Also the increase of the difference in head at the boundaries, results in the increase of the coefficient of variation of the head within the flow region, in agreement with the physical expectations.



FUNCTION 1

$$Z(x,y) = \text{EXP}((x+y)/30)$$

FUNCTION 2

$$Z(x,y) = (x \cdot y)^{0.6}$$

FUNCTION 3

$$k = -((x-25)^2 + (y-25)^2)/10^8$$

$$Z(x,y) = \text{EXP}(k) \cdot (x-100) \cdot x(y-50) \cdot y/k$$

FUNCTION 4

$$Z(x,y) = \text{EXP}(k) \cdot (x-100) \cdot (x-50) \cdot y \cdot (y-50)/k$$

FUNCTION 5

$$k = -((x-25)^2 + (y-25)^2)/(100)^3$$

$$Z(x,y) = \text{EXP}(k) \cdot (x-100) \cdot (x-50) \cdot y \cdot (y-50)/k$$

FIGURE 5.15 ASSUMED FUNCTIONS FOR THE COMPARISON OF TREND SURFACE ESTIMATES VS. MOVING AVERAGE ESTIMATES (INFERENCE MODEL)

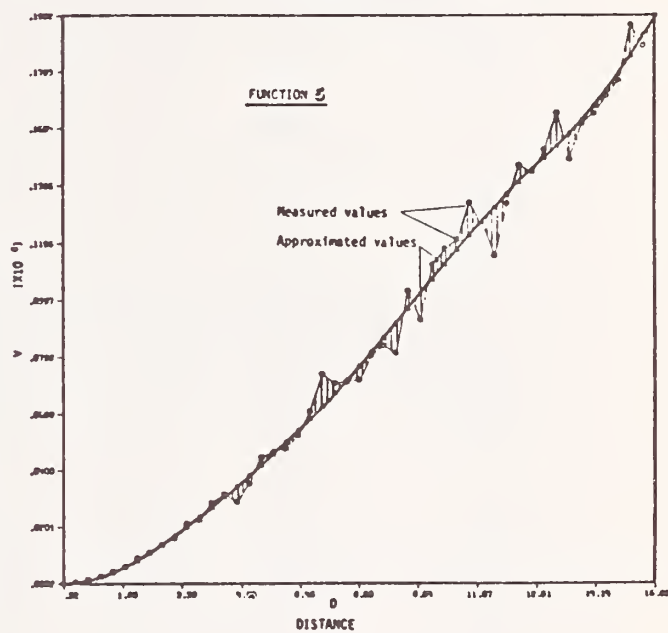
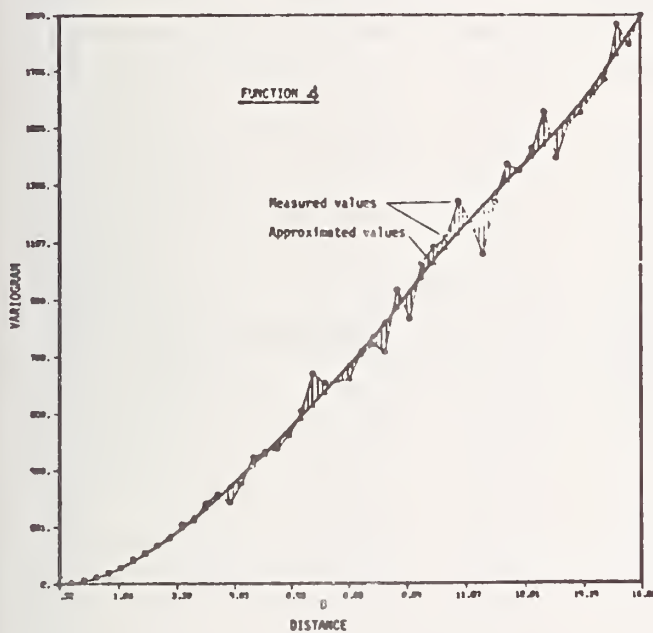
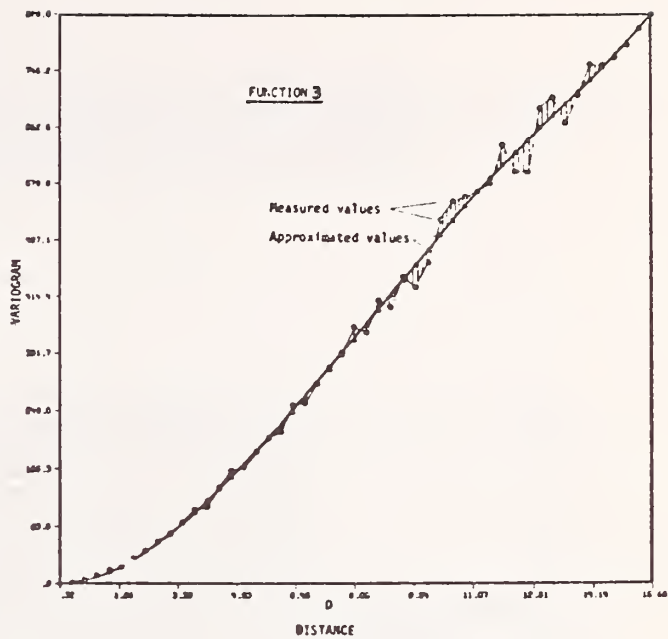
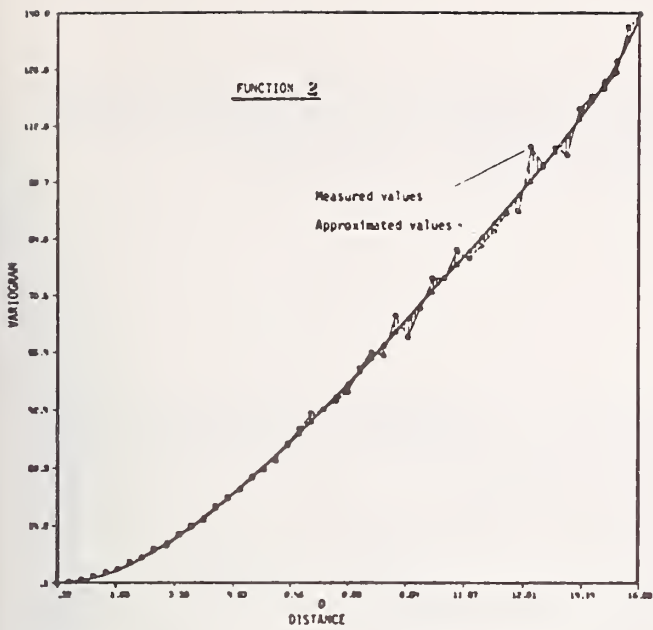


FIGURE 5.16 MEASURED AND APPROXIMATED VARIOGRAM OF THE EXAMINED FUNCTIONS

TABLE 5.3 DEVIATIONS AND COEFFICIENTS OF MULTIPLE CORRELATION OF THE ESTIMATIONS OBTAINED BY REGRESSION AND CORRELATIVE SCHEME FOR TWO DIFFERENT SETS OF β POINTS

		REGRESSION SCHEME		CORRELATIVE SCHEME 2	
		DEVIATION (10^4)	COEFFICIENT OF MULTIPLE CORRELATION	DEVIATION (10^4)	COEFFICIENT OF MULTIPLE CORRELATION
15 GIVEN β POINTS	Function 1	.29	0.97	.14	0.98
	Function 2	.10	0.98	.09	0.99
	Function 3	5.0	0.72	1.46	0.92
	Function 4	0.22	0.69	.14	0.88
	Function 5	32.61	0.69	16.69	0.85
25 GIVEN β POINTS	Function 1	.10	0.98	.12	0.986
	Function 2	.15	0.99	.05	0.996
	Function 3	4.18	0.77	.75	0.96
	Function 4	.28	0.74	.12	0.89
	Function 5	28.22	0.74	12.47	0.89

TABLE 5.4 DEVIATIONS AND COEFFICIENTS OF MULTIPLE CORRELATION FOR THE ESTIMATIONS OBTAINED BY CORRELATIVE SCHEME 2 USING LINEAR AND COMPUTED VARIOGRAM FOR TWO SETS OF β POINTS

		CORRELATIVE SCHEME 2 LINEAR VARIOGRAM		CORRELATIVE SCHEME 2 MEASURED VARIOGRAM	
		DEVIATION (10^4)	COEFFICIENT OF MULTIPLE CORRELATION	DEVIATION (10^4)	COEFFICIENT OF MULTIPLE CORRELATION
15 GIVEN β POINTS	Function 1	.14	0.98	.14	0.982
	Function 2	.09	0.99	0.08	0.99
	Function 3	1.46	0.92	1.73	0.91
	Function 4	.14	0.88	0.12	0.89
	Function 5	16.69	0.85	15.65	0.86
25 GIVEN β POINTS	Function 1	.12	0.986	.12	0.984
	Function 2	.05	0.99	.04	0.995
	Function 3	.75	0.96	.80	0.96
	Function 4	.12	0.89	.15	0.86
	Function 5	12.47	0.89	15.63	0.86

TABLE 5.5 THE MEAN, COEFFICIENT OF VARIATION AND ABSOLUTE RELATIVE ERROR OF THE ESTIMATES OBTAINED BY CORRELATIVE SCHEME 1 AND 2 WITH A LINEAR VARIOGRAM AT POINTS A = (90, 10), B = (90, 40) FOR TWO SETS OF β POINTS

		CORRELATIVE SCHEME 1						CORRELATIVE SCHEME 2					
		POINT A			POINT B			POINT A			POINT B		
		MEAN ESTIMATES	COEFF. OF VARIATION	ABS. RELATIVE ERROR	MEAN ESTIMATES	COEFF. OF VARIATION	ABS. RELATIVE ERROR	MEAN ESTIMATES	COEFF. OF VARIATION	ABS. RELATIVE ERROR	MEAN ESTIMATES	COEFF. OF VARIATION	ABS. RELATIVE ERROR
15 GIVEN β POINTS	FUNC. 1	27.44	0.28	2.	80.65	0.1	6.	27.85	0.11	1.	78.00	0.03	2.
	FUNC. 2	52.07	0.15	12.	130.26	0.06	4.	59.40	0.05	0.28	136.26	0.18	0.13
	FUNC. 3	54.32	0.14	18.	57.20	0.15	24.	48.12	0.07	5.	47.63	0.05	4.
	FUNC. 4	29.54	0.26	14.	31.10	0.27	20.	26.72	0.12	3.	27.05	0.10	4.
	FUNC. 5	205.59	0.04	20.	220.67	0.04	23.	178.43	0.02	5.	180.25	0.01	5.
25 GIVEN β POINTS	FUNC. 1	27.94	0.22	3.7	80.05	0.04	5.	28.13	0.10	0.34	79.69	0.13	4.
	FUNC. 2	58.03	0.11	2.	134.18	0.03	1.	59.46	0.05	0.38	136.11	0.08	0.24
	FUNC. 3	47.13	0.13	2.	51.10	0.06	11.	47.04	0.06	2.	47.52	0.17	3.
	FUNC. 4	26.24	0.23	1.	27.58	0.11	6.	25.89	0.11	0.4	27.06	0.30	4.
	FUNC. 5	172.77	0.04	1.	180.04	0.02	5.4	169.13	0.02	1.	179.68	0.05	5.1

TABLE 5.6 THE ABSOLUTE RELATIVE ERROR IN PERCENT OF THE COMPUTED HEAD USING THE REGRESSION-FINITE ELEMENT AND CORRELATIVE FINITE ELEMENT MODELS AT THE POINTS A = (90, 10), B = (90, 40)

		FUNCTION 1		FUNCTION 2		FUNCTION 3		FUNCTION 4		FUNCTION 5	
		POINT A	POINT B	POINT A	POINT B	POINT A	POINT B	POINT A	POINT B	POINT A	POINT B
15 GIVEN β POINTS	MESH 6x6	1.0	1.2	0.8	0.15	13.	8.6	1.9	2.2	2.1	2.8
		CORREL.	REGRES.								
		0.2	0.3	1.	0.12	3.3	2.2	0.6	1.5	1.9	1.6
		CORREL.	REGRES.								
25 GIVEN β POINTS	MESH 11x11	0.9	0.3	0.2	0.07	8.3	7.8	1.6	2.3	4.0	4.5
		CORREL.	REGRES.								
		0.01	0.07	0.15	0.03	1.4	3.1	0.4	1.1	0.1	1.6
		CORREL.	REGRES.								
25 GIVEN β POINTS	MESH 6x6	1.0	1.1	0.4	0.2	4.6	9.5	0.8	3.0	3.9	4.5
		CORREL.	REGRES.								
		0.2	0.2	0.1	0.06	1.8	3.3	0.5	1.5	1.1	1.6
		CORREL.	REGRES.								
25 GIVEN β POINTS	MESH 11x11	0.9	0.3	0.3	0.01	10.	9.0	2.8	3.0	6.2	4.4
		CORREL.	REGRES.								
		0.011	0.05	0.16	0.0	0.4	3.	0.1	.9	0.1	1.5
		CORREL.	REGRES.								

TABLE 5.7 THE COEFFICIENT OF VARIATION OF THE HEAD AT POINTS A, B, FOR THREE DIFFERENT BOUNDARY CONDITIONS OBTAINED BY THE INFERENCE FINITE ELEMENT

			DIFFERENCE OF HEAD AT THE BOUNDARIES x=50 and x=100					
			$\Delta H = 50$		$\Delta H = 100$		$\Delta H = 150$	
			POINT A	POINT B	POINT A	POINT B	POINT A	POINT B
15 GIVEN β POINTS	FUNCTION 1	MESH 6x6	0.08	.0015	0.10	0.007	0.12	0.01
		MESH 11x11	0.008	0.002	0.013	0.007	0.018	0.01
	FUNCTION 3	MESH 6x6	0.020	0.006	0.024	0.004	0.026	0.0057
		MESH 11x11	0.012	0.009	0.015	0.027	0.018	0.035
25 GIVEN β POINTS	FUNCTION 1	MESH 6x6	0.15	0.015	0.18	0.017	0.23	0.023
		MESH 11x11	0.01	0.008	0.016	0.01	0.02	0.012
	FUNCTION 3	MESH 6x6	0.040	0.010	0.049	0.009	0.058	0.012
		MESH 11x11	0.007	0.007	0.012	0.019	0.016	0.025

CHAPTER 6

UNCERTAINTY ANALYSIS IN THE ANALYTICAL MODEL

6.1 Introduction

In the elaboration of models simulating the cavity system the use of the finite element technique was clearly justified, (section 3.4). Also, the coupling of the inference model with the uncertainty analysis was shown (section 3.4) to provide us with a tool capable of describing the spatial variability of the constitutive relations of the rock.

The objective of the present chapter is to introduce the uncertainty concept within the finite element procedure. The components of this analysis are directly related to the different output quantities needed to evaluate the performance of a given design alternative. These quantities are:

1. The water pressure affecting the effective stress field.
2. The stress field after excavation.
3. The natural frequency of the structure.
4. The maximum level of stress reached during the seismic load.
5. The maximum moments reached in the liner.

The division of the geometric space under consideration into three different scales was developed in Chapter 3 for purposes of simplification of the analysis. It was based on the superposition principle. The details and the use of the selected type of elements is presented hereafter.

Finally the uncertainty analysis is performed for the underground flow problem, the initial stress conditions due to the excavation, the modal analysis adopted for the dynamic phenomenon, and the stability of the liner.

6.2 General Assumptions Concerning the Analysis in Conjunction with the F.E.M.

Two topics will be discussed here, the discretization criteria and the constitutive relationships.

5.2.1 Discretization Criteria

In our particular problem, the governing factor in the discretization, is the dynamic aspect of the phenomenon. It is characterized by energy transmission through wave propagation. The wavelength is known to decrease as the frequency increases. Vaish (92), established three criteria of discretization according to the dynamic characteristics of the phenomenon, namely the size of the system, the variation in mesh sizing, and the size of the elements.

A. The Size of the System:

When modelling very large or infinite systems, the system has to be necessarily truncated by introducing artificial boundaries. However, these boundaries partially reflect energy back into the region of interest causing large errors.

Attempts have been made to devise boundary conditions which would absorb, rather than reflect all the incident energy. For the general two-dimensional plane stress problem no satisfactory boundary conditions have been devised yet to absorb the incident energy. In the present case, Figure 6.1, it can be assumed that the boundaries are far enough

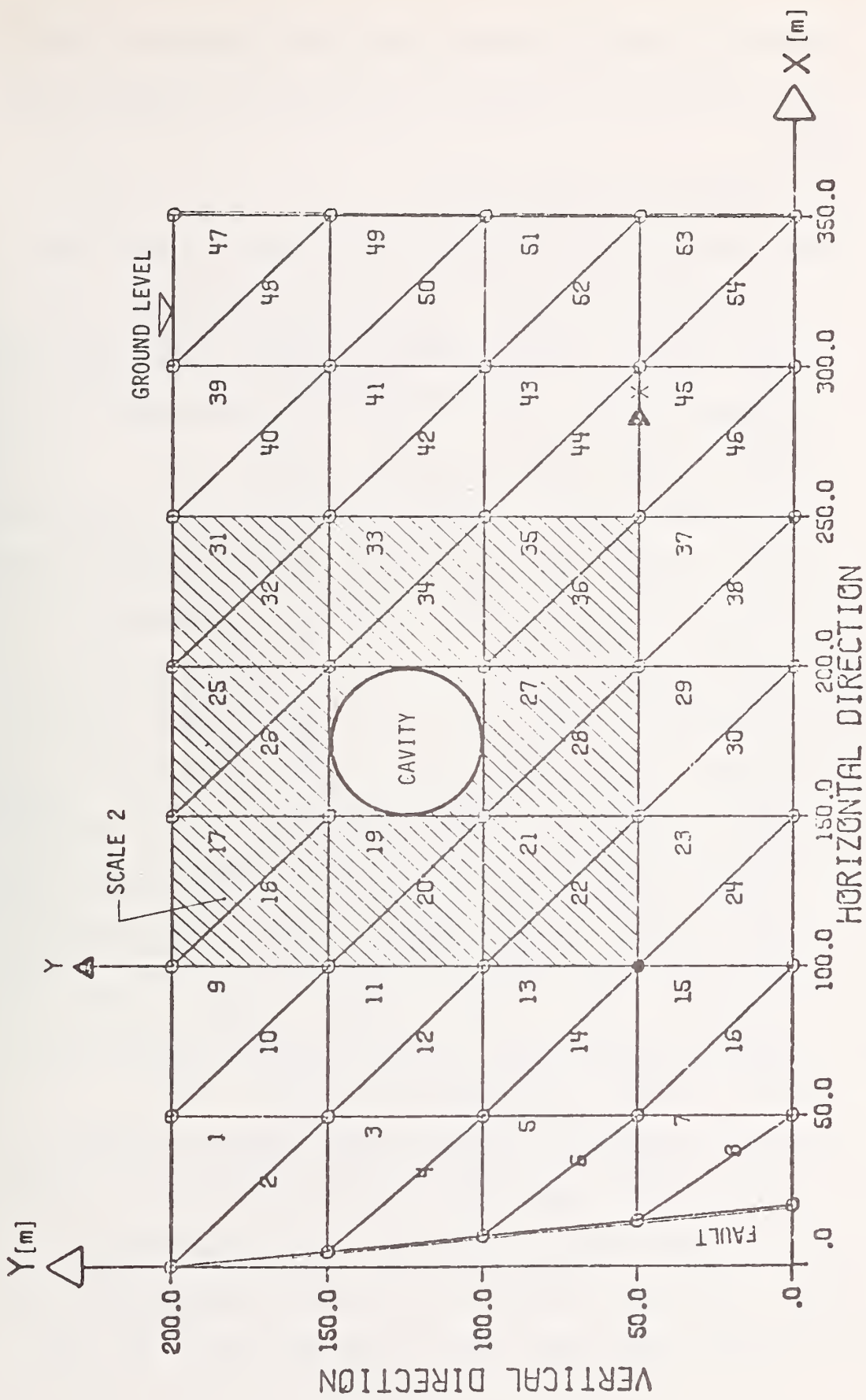


FIGURE 6.1 F.E.M. DISCRETIZATION OF SCALE 1

from the opening so that the reflected waves either dampen out before returning to the region of interest, or arrive after the response time of interest.

B. The Variation in Mesh Sizing:

Sudden changes in finite element size will cause a sudden change of the stiffness at the interface. This can result in energy reflection from such interfaces causing substantial errors. Hence mesh size variation should be gradual. An alternate scheme is proposed hereafter as illustrated by Figure 6.2.

Clearly a seismic signal is composed of several natural frequencies each requiring a different mesh size. A Fourier series technique permits the decomposition of the seismic signal into its components. Applying then the superposition principle, we can imagine a set of different mesh sizes over the same region, each one carrying a portion of the seismic signal, of different frequency content. This is precisely done with scales 1 and 2 as defined in section 3.2.2. Scale 1 carries the low frequencies, while scale 2 carries the high frequencies. Moreover, since the dimension of scale two is a multiple of the seismic wavelength, no significant reflection is expected to take place at the interface.

C. Size of Elements:

Since the deformation of any given finite element is assumed to follow a prescribed form, about eight to ten elements of scales 1 and 2 are required to model a complete wave form. Thus if the wavelength of the largest significant frequency in the analysis is denoted by L_V , the largest dimension of the element should be smaller than $L_V/8 - L_V/10$.

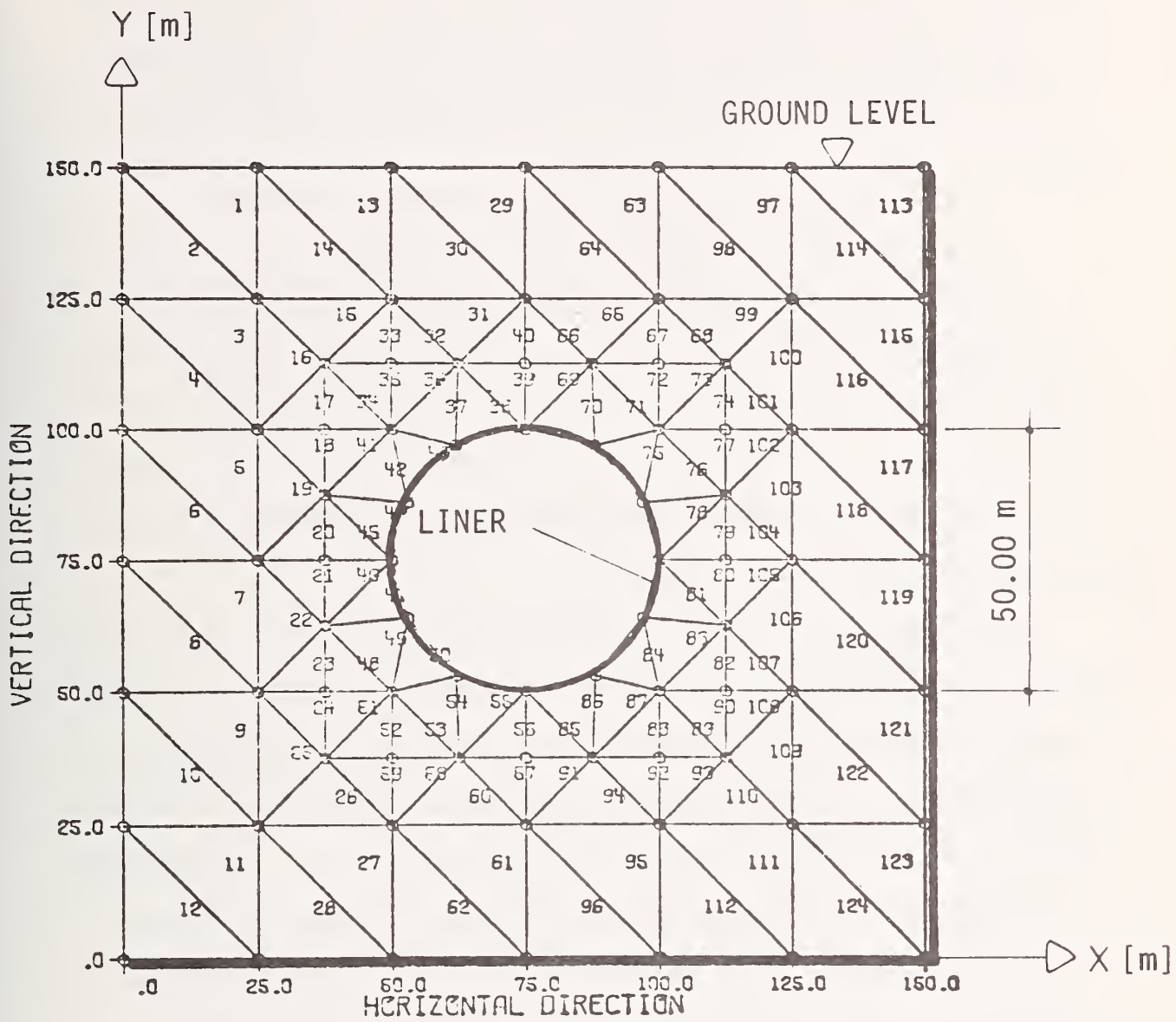


FIGURE 6.2 A MESH SIZING VARIATION SCHEME OF SCALE 2

As far as scale 3 is concerned it is a subset of Scale 1 and Scale 2, and represents the liner which possesses a small mass in comparison with the mass of the surrounding rock. Therefore, the interaction in the dynamic sense between Scales 1 and 2 and Scale 3 is insignificant. Indeed, it can be intuitively seen that no vibrational mode of Scale 3 can in any case influence the vibrational modes of Scale 1 and 2.

6.2.2 Constitutive Relationships

The conceptual basis of the finite element technique being extensively discussed in the literature is not repeated here. Instead, the aspects specific to the rock mechanics application of the F.E.M. are summarized below. The applications reported by Chang (9), are: the 'no tension' analysis, the 'elastoplastic' analysis, the 'viscoelastic' analysis, and the 'joint' analysis.

The 'no tension' analysis was developed by Zienkiewicz (97) to model the fissured rock mass based on the assumption that the rock is incapable of withstanding tensile stresses. However, the convergence of the proposed iterative procedure proved to be very slow, and the effect of the development of cracks on the Poisson's ratio, not adequate.

The 'elasto-plastic analysis' is considered to model realistically the yielding of rock due to the excavation process during the construction phase of the cavity system.

The 'viscoelastic' analysis was developed by Clough (10), to include properties of the rock that are time-dependent. However, the great majority of rocks do not exhibit significant time-dependent behavior within the E.Q. time interval.

In the present study, as said earlier, the emphasis is put on the dynamic phenomenon. Therefore, the following scheme is proposed, Figure 6.3.

1. A nonlinear elastoplastic behavior of the material is considered, during the development of the initial stress field due to the excavation.
2. The dynamic phenomenon is understood to locally perturb the initial stress-level in the σ - ϵ diagram, Fig. 6.3. This justifies a linear behavior as suggested by experimental evidence, Thiel (91), and by the fact that the magnitude of the seismic perturbation is small.

6.3 Finite Elements Used to Discretize the Cavity System

The choice of the type of finite elements is influenced by two factors, namely the accuracy of the solution, and the efficiency of the computational scheme. A best choice should offer a good balance between these two factors. Consequently a triangular constant-strain triangular element is used to represent the rock media as satisfying the following requirements:

- (a) Simplicity in following the correct shape of the boundaries
- (b) Good simulation of the structural response with only six degrees of freedom (d.o.f.). This leaves enough flexibility to perform the uncertainty analysis.

On the other hand the simulation of the liners necessitates the consideration of geometric nonlinearities to increase the sensitivity of the model. Therefore, a beam element using Hermite polynomials is considered for the Scale 3 elements.

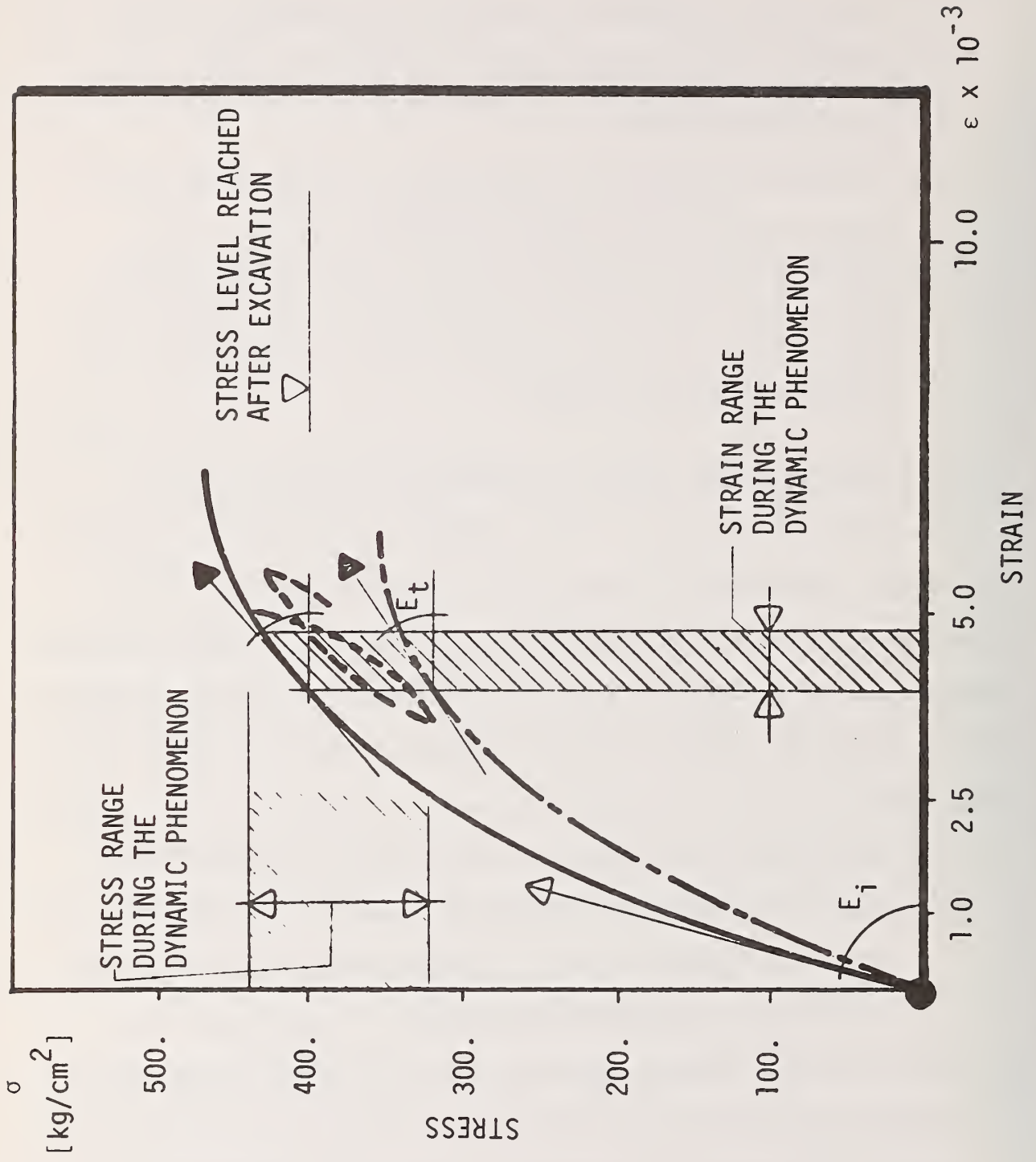


FIGURE 6.3 RANGE OF STRESSES AND STRAINS AT DIFFERENT STAGES OF THE ANALYSIS

The 'joint' analysis is primarily concerned with bedding planes and major geologic discontinuities.

6.3.1 Triangular Element with Six d.o.f.

This element is widely used and the computational details associated with it are given in many textbooks, (98), (18). In the following, basic relations concerning the derivation of the stiffness matrix are given in a condensed form.

The general expression of the displacements at the nodes $\{d\}$, is assumed to be a linear combination of linear functions ϕ_i :

$$\{d\} = \left\{ \sum_{i=1}^3 a_i \phi_i \right\} . \quad (6.1)$$

The displacement field is given by:

$$\{u\} = [N] \begin{Bmatrix} d_1 \\ d_2 \\ d_3 \end{Bmatrix} \quad (6.2)$$

where $[N]$ = matrix of the shape functions

$\{u\}$ = the displacements in the two-dimensional space

$\{d_i\}$ = the vector displacements at the nodes.

Assuming linearity of the strain-displacement relationships also, we have:

$$\begin{Bmatrix} \epsilon_x \\ \epsilon_y \\ \epsilon_{xy} \end{Bmatrix} = [B] \begin{Bmatrix} d_1 \\ d_2 \\ d_3 \end{Bmatrix} \quad (6.3)$$

where:

$$\begin{Bmatrix} \epsilon_x \\ \epsilon_y \\ \epsilon_{xy} \end{Bmatrix} = \begin{Bmatrix} \frac{\partial u}{\partial x} \\ \frac{\partial u}{\partial y} \\ \frac{\partial u}{\partial x} + \frac{\partial u}{\partial y} \end{Bmatrix}$$

$$[B] = \begin{Bmatrix} \frac{\partial N}{\partial x} & 0 \\ 0 & \frac{\partial N}{\partial y} \\ \frac{\partial N}{\partial y} & \frac{\partial N}{\partial x} \end{Bmatrix}$$

It is to be noticed that because of the linearity assumption, matrix $[B]$ is not a function of x and y , so that the stiffness matrix can be simply written:

$$[K] = [B]^T \cdot [D] \cdot [B] \cdot t \cdot A \quad (6.4)$$

6.3.2 Beam Element with Six d.o.f.

The starting point is to write the expression of the Functional representing the Strain Energy developed in the beam:

$$\Pi_S = E \int_V \frac{1}{2} \{\epsilon\}^T \{\sigma\} \cdot dV \quad (6.6)$$

The strain energy Π_S is a function of the strain vector $\{\epsilon\}$, the stress vector $\{\sigma\}$ and the modulus of elasticity E . The integral has to be evaluated over the volume of the element and in our particular case along the Neutral Axis.

The Strain Vector in turn can be separated in three parts, namely the initial strain $\{\epsilon_0\}$, the linear strain $\{\epsilon_L\}$ and the nonlinear strain $\{\epsilon_N\}$:

$$\{\epsilon\} = \{\epsilon_0\} + \{\epsilon_L\} + \{\epsilon_N\} \quad (6.7)$$

where:

$$\{\epsilon_0\} = \begin{Bmatrix} 0 \\ \epsilon_x \\ 0 \\ \epsilon_y \end{Bmatrix}$$

$$\{\epsilon_L\} = \begin{Bmatrix} u_{,x} \\ u_{,y} - v_{,x} \end{Bmatrix} ; \quad u_{,x} = \frac{\partial u}{\partial x} , \quad v_{,x} = \frac{\partial v}{\partial x}$$

$$\{\epsilon_N\} = \begin{Bmatrix} \frac{1}{2}(u_{,x}^2 + v_{,x}^2) \\ u_{,x} u_{,y} + v_{,x} v_{,y} \end{Bmatrix} .$$

Since in our case all expressions are functions of the directional variable X of the beam element, the following relations hold:

$$\begin{aligned} v_{,y} &= 0 \\ u_{,x} &= a_1 - y \cdot v_{,xx} . \end{aligned} \tag{6.8}$$

Furthermore, using the Navier's assumption about the planarity of the cross-section after bending, we can write:

$$\begin{aligned} u(x,y) &= -y \frac{\partial v}{\partial x} \\ \epsilon_x &= -y \frac{\partial^2 v}{\partial x^2} + \text{Nonlinear part} . \end{aligned} \tag{6.9}$$

After substitution, Eq. 6.7 becomes:

$$\{\epsilon\} = \begin{Bmatrix} 0 \\ \epsilon_x \\ 0 \\ \epsilon_{xy} \end{Bmatrix} + \begin{Bmatrix} u_{,x} \\ 0 \end{Bmatrix} + \begin{Bmatrix} \frac{1}{2}(u_{,x}^2 + v_{,x}^2) \\ -u_{,x} \cdot v_{,x} \end{Bmatrix} . \tag{6.10}$$

The stress vector is given by:

$$\{\sigma\} = \begin{bmatrix} E & 0 \\ 0 & G \end{bmatrix} \cdot \{\epsilon\} . \tag{6.11}$$

The strain energy defined in Eq. 6.6 is computed in Appendix C taking into consideration the nonlinear terms of the strain as defined in Eq. 6.11. Its linear and nonlinear components are given in Table 6.1 as a function of the terms:

$$\int_x v_{,x} dx , \quad \int_x v_{,x}^2 dx \quad \text{and} \quad \int_x v_{,xx}^2 dx$$

TABLE 6.1 LINEAR AND NONLINEAR COMPONENTS OF THE STRAIN ENERGY OF A BEAM ELEMENT

$$\Pi_S = E[\frac{1}{2}(F_2 + F_3) + F_4 + F_5 + F_6] + \Pi_I$$

EXPRESSIONS	TERMS INDEPENDENT OF v	COEFFICIENTS OF v, x	COEFFICIENTS OF v, x ²	COEFFICIENTS OF v, xx ²
$\frac{1}{2} F_2$	$\frac{1}{2} A a_1^2 \cdot L$			$\frac{1}{2} I \cdot L$
$\frac{1}{2} F_3$	$1/8 A a_1^4 \cdot L$		$\frac{1}{4} A a_1^2 + \frac{1}{2} \rho A a_1^2$	$3/4 I a_1^2$
F_4	$\epsilon_x^0 A a_1$			
F_5	$\frac{1}{2} \epsilon_x^0 A a_1^2$	$-\rho \epsilon_{xy}^0 A a_1$	$\frac{1}{2} \epsilon_x^0 A$	$\frac{1}{2} \epsilon_x^0 I$
F_6	$\frac{1}{2} A a_1^3$		$\frac{1}{2} A a_1$	$3/2 I a_1$

In the F_3 expression we have neglected the following terms

$$\frac{I}{4} \int v, xx^4 dx, \quad \frac{A}{4} \int v, x^4 dx, \quad \frac{I}{2} \int v, xx^2 dx$$

where: ρ = Mass density A = Area of the cross section of the beam
 I = Inertia of Section A E = Modulus of Elasticity
 Π_S = Strain Energy Π_I = Initial Strain Energy

They are computed after having defined in an apriori way the function $v(x)$ approximating the vertical deformation of the beam.

Hermite polynomials are found to be the best choice (17) to represent this vertical deformation. The following basis is proposed:

$$v(x) = \alpha_1 \phi_1(x) + \alpha_2 \phi_2(x) + \alpha_3 \phi_3(x) + \alpha_4 \phi_4(x) \quad x \in [0, L] \quad (6.12)$$

where: α_i = coefficients to be determined by the finite element procedure

$\phi_i(x)$ = apriori given functions as illustrated in Figure (6.5)

L = length of the element.

The reason for constructing such a basis is the simplicity of the inner products encountered in the expression of the strain energy,

Eq. 6.6:

$$(\phi_i, \phi_j) = \int_0^L \phi_i(x) \cdot \phi_j(x) dx \quad (6.13)$$

$$\left(\frac{\partial \phi_i}{\partial x}, \frac{\partial \phi_j}{\partial x} \right) = [n_1] \quad (6.14)$$

$$\left(\frac{\partial^2 \phi_i}{\partial x^2}, \frac{\partial^2 \phi_j}{\partial x^2} \right) = [n_2] \quad (6.15)$$

where the symmetric matrices $[n_1]$ and $[n_2]$ are, (as computed in Appendix C):

$$[n_1] = L \begin{bmatrix} 0 & 0 & 0 & 0 \\ 0 & 1 & 0 & 0 \\ 0 & 0 & 1/3 & 0 \\ 0 & 0 & 0 & 1/20 \end{bmatrix}$$

$$[n_2] = \frac{1}{L} \begin{bmatrix} 0 & 0 & 0 & 0 \\ 0 & 0 & 0 & 0 \\ 0 & 0 & 4 & 0 \\ 0 & 0 & 0 & 3 \end{bmatrix}$$

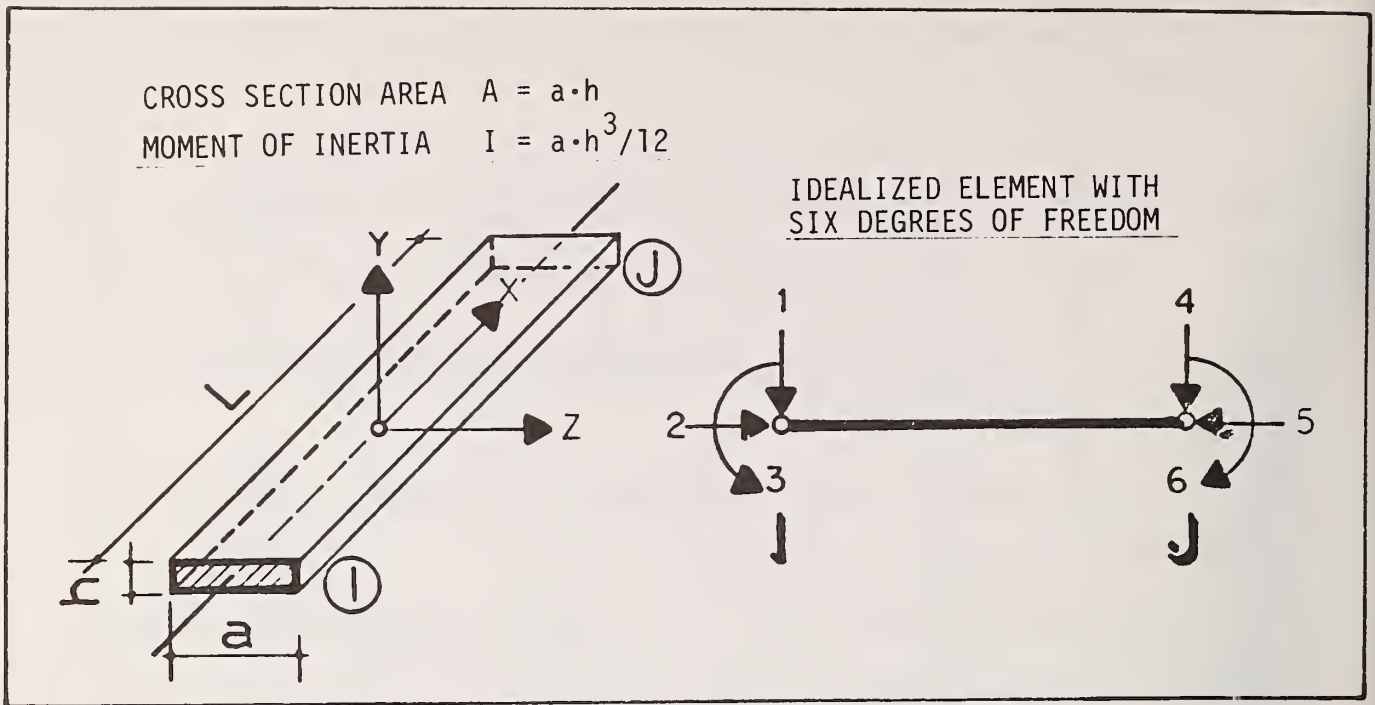


FIGURE 6.4 ILLUSTRATION OF THE BEAM FINITE ELEMENT

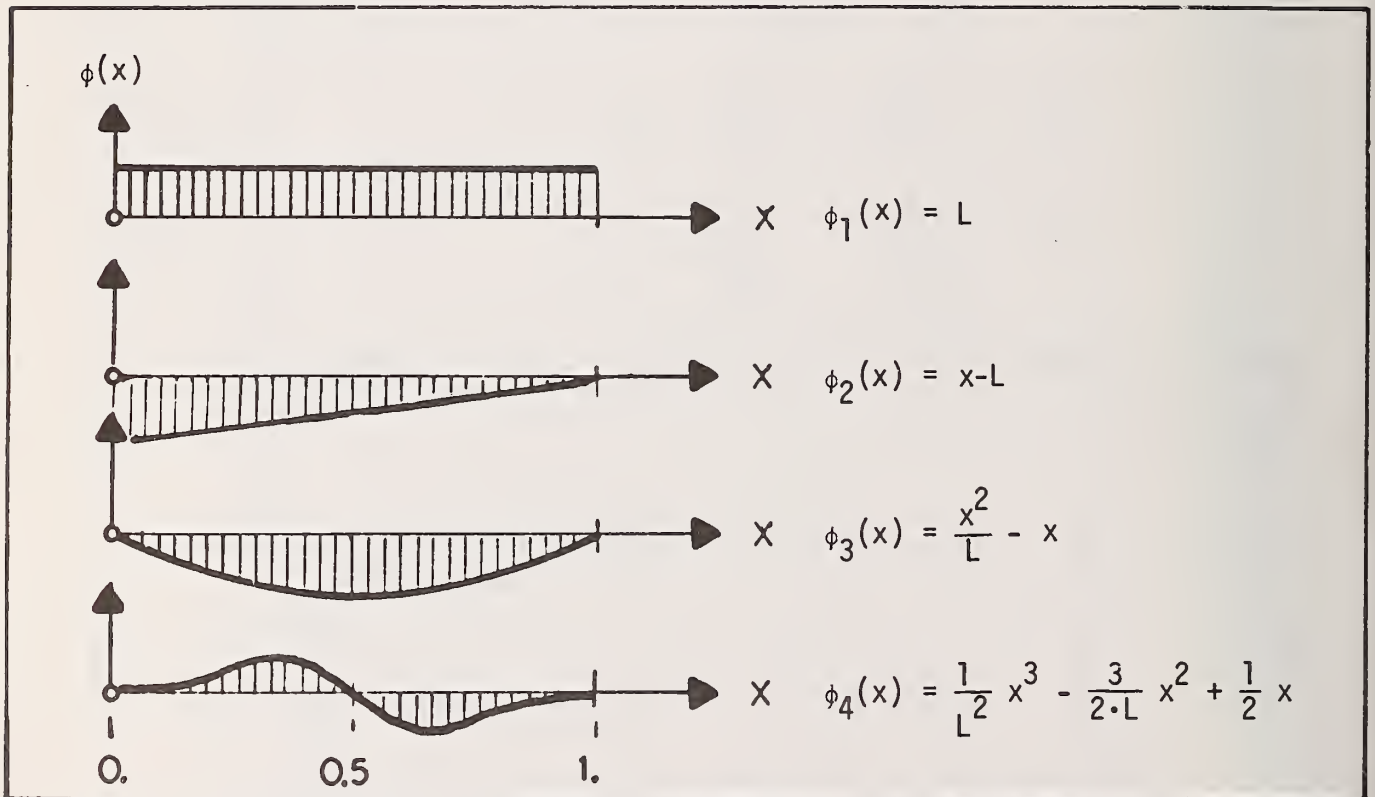


FIGURE 6.5 HERMITE POLYNOMIALS APPROXIMATING $v(x)$

Their simple form clearly justifies the use of Hermite polynomials, and reduces considerably the computations. The stiffness matrix [NK] is obtained by minimizing the strain energy (Eq. 6.6) with respect to the displacement vector {u} in the global coordinate system:

$$\frac{\partial \Pi_s}{\partial \{u\}} = 0 . \quad (6.16)$$

It is to be noticed that the stiffness matrix [NK] is nonlinear with respect to the displacement vector {u}, leading to a nonlinear system of equations that is solved using the NEWTON RAPHSON Iterative procedure. At each iteration, a different linear system of equations is solved, defined in terms of the derivatives of Matrix [NK] with respect to the displacement vector {u}. The computational details are given in Appendix C.

6.4 Uncertainty Analysis Related to the Underground Flow Problem

In the definition of the overall analytical model, the flow problem was considered to be independent of the dynamic problem. Indeed even if the water table was to vary following an earthquake, this would occur much later than the vibratory motion of the cavity. However, it is important to know the effect of the water on the stress field surrounding the cavity at the moment an earthquake would strike. This effect can be estimated if the position of the water table is known from in situ measurements. In that case the flow can be considered as steady and confined, which can be handled computationally by a F.E.M. approach.

Let ϕ be the total head [m]. Its value inside a triangular element can be obtained by:

$$\{\phi\} = [N]^T \{\phi\}^e \quad (6.16)$$

where: $[N]^T = [N_1, N_2, N_3]$ are the shape functions, and
 $\{\phi\}^e$ = the nodal heads of a triangular element.

The conservation law as applied to fluids gives the following Laplace's equation for a two-dimensional flow:

$$\frac{\partial^2 v_x}{\partial x^2} + \frac{\partial^2 v_y}{\partial y^2} + f = 0 \quad (6.17)$$

where: f = the net inflow into the differential volume $dx \cdot dy$.

By Darcy's law the velocity in the x and y direction is given by:

$$v_x = k_x i_x = k_x \frac{\partial \phi}{\partial x}$$

$$v_y = k_y i_y = k_y \frac{\partial \phi}{\partial y} \quad (6.18)$$

where: k_x, k_y = coefficients of permeability in x and y directions,
 i = hydraulic gradient.

Consequently, the Laplace's equation becomes

$$\frac{\partial}{\partial x} \left(k_x \frac{\partial \phi}{\partial x} \right) + \frac{\partial}{\partial y} \left(k_y \frac{\partial \phi}{\partial y} \right) + f = 0 \quad (6.19)$$

The corresponding variational functional is given by:

$$E = \frac{1}{2} \int_A \left[k_x \left(\frac{\partial \phi}{\partial x} \right)^2 + k_y \left(\frac{\partial \phi}{\partial y} \right)^2 - f \cdot \phi \right] dx \cdot dy \quad (6.20)$$

This energy expression has to be minimized with respect to the total head ϕ leading to the expression, Desai (18):

$$\frac{\partial E}{\partial \phi} = \int_A \left\{ k_x \frac{\partial \phi}{\partial x} \frac{\partial}{\partial \phi} \left(\frac{\partial \phi}{\partial x} \right) + k_y \frac{\partial \phi}{\partial y} \frac{\partial}{\partial \phi} \left(\frac{\partial \phi}{\partial y} \right) - f \cdot \frac{\partial \phi}{\partial \phi} \right\} dx \cdot dy \quad (6.21)$$

where: A = the domain of flow (finite element).

The stationary condition applied at all the nodes, leads to the following system of equations:

$$[K] \cdot \{\phi\} = \{F\} \quad (6.22)$$

where: $[K]$ = the permeability matrix

$\{\phi\}$ = the unknown total head at the nodes

$\{F\}$ = the quantity of flow.

In order to obtain a solution the following boundary conditions are necessary:

1. At the boundaries of the flow region: known head, unknown flow
2. Within the flow region: unknown head, known flow.

The uncertainty analysis is carried out assuming that the coefficients of permeability k_x and k_y are statistically independent and that the statistical characteristics of the known quantities k_x and k_y are obtained from a site investigation by means of an Inference model. The objective then of this procedure is to establish the statistical characteristics of the unknown head ϕ . The following Algorithm is used to this effect, as shown in the flow chart of Fig. 6.6.

ALGORITHM

Step 1 Set the permeabilities' mean values \bar{k}_x, \bar{k}_y (from the Inference model).

Solve the conventional linear system

$$[K] \{\bar{\phi}\} = \{F\}.$$

Step 2 Form the vectors

$$\frac{\partial [K]}{\partial k_x}, \quad \frac{\partial [K]}{\partial k_y}$$

and solve the following two systems of equations:

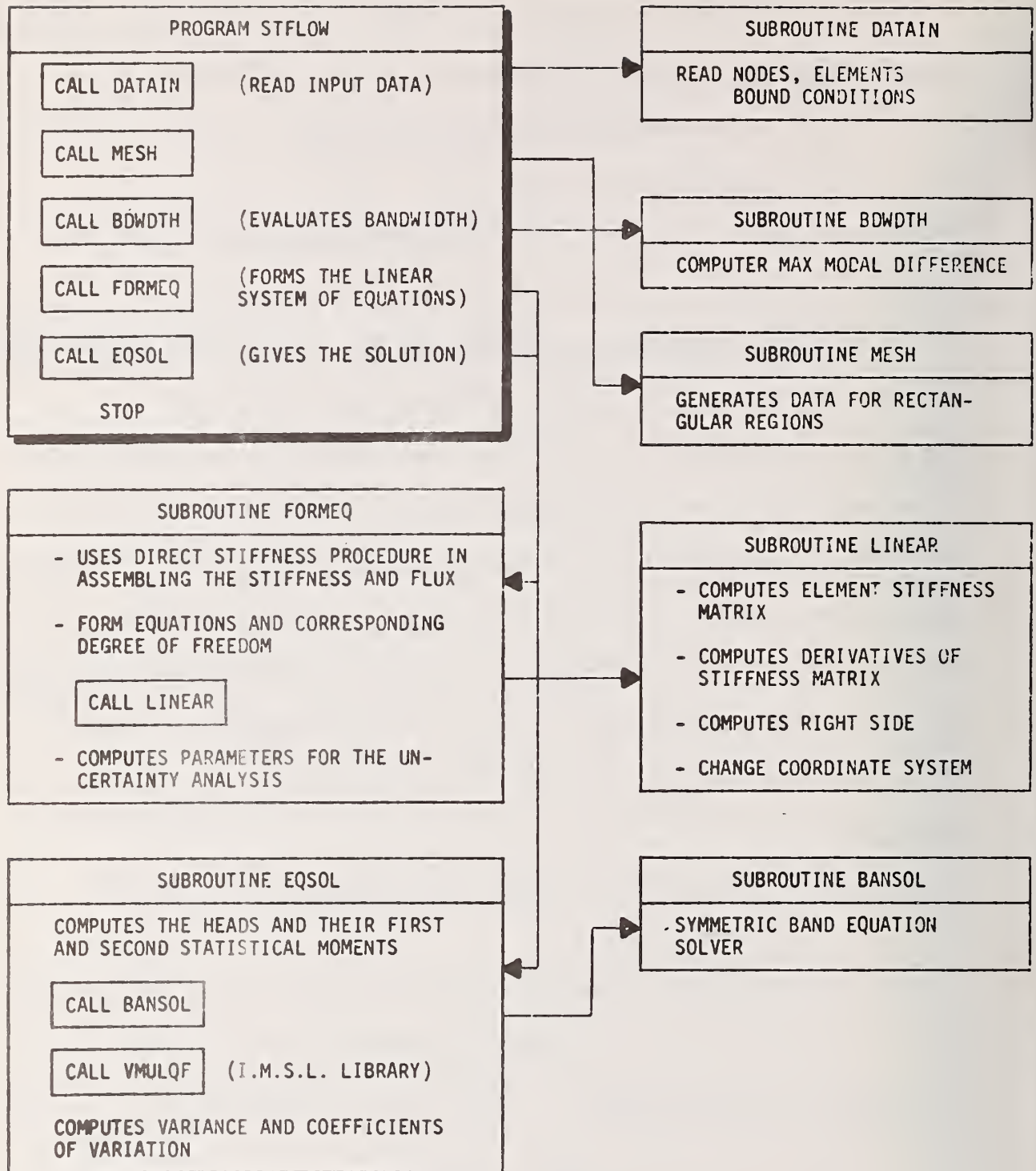


FIGURE 6.6 FLOW CHART OF PROGRAM STFLOW

$$[K] \frac{\partial \bar{\phi}}{\partial k_x} = - \frac{\partial [K]}{\partial k_x} \{\bar{\phi}\} \quad (6.23)$$

$$[K] \frac{\partial \bar{\phi}}{\partial k_y} = - \frac{\partial [K]}{\partial k_y} \{\bar{\phi}\} \quad (6.24)$$

Step 3 Find the variance of ϕ according to a previously defined approximated relation, Eq. 5.19.

Program STFLOW is written based on the above algorithm. Triangular finite elements are used and a special resolution scheme is adopted to optimize the Central Memory space requirements.

6.5 Uncertainty Analysis of Initial Stress Conditions Created by the Excavation

The initial conditions with respect to the dynamic analysis are the result of the excavation of the cavity system that leads to a redistribution of stresses. A number of procedures were developed to evaluate this redistribution, Obert and Duvall (64). However, the finite element method has been most commonly used. This is particularly true for the case of a nonlinear material behavior. Indeed the non-linearity is approximated by assigning different values for the modulus of elasticity and Poisson's ratio at each element, consistent with the stress values of the element. The analysis is performed using an incremental piece-wise linearization of the stress-strain relationship.

The excavation operation can be adopted from Clough and Duncan (10). The following operations are defined:

1. The rock is assumed to be in equilibrium and at rest and the initial state of stresses is provided by the Inference model.
2. The excavation is simulated as follows: the stresses before excavation, on the surface of the opening are evaluated, as well as the

equivalent forces at the nodes of the finite elements. Then, reversing the signs of the forces and applying them to the finite elements surrounding the excavation, the corresponding displacements can be evaluated, using adequate tangent modulus of elasticity and Poisson's ratio.

3. The computed stresses, strains and displacements are then added to the original values to obtain the final configuration of the cavity system before the introduction of a dynamic effect.

The main problem encountered with the F.E.M. idealization for this specific problem is the effect of the finite boundaries of the area of interest. Indeed its location will influence the results obtained in the analysis. A brief investigation showed that at a distance greater than two radii from the opening the boundaries do not affect the solution, Figure 6.7.

The uncertainty analysis is performed with respect to the tangent modulus of elasticity and the initial Poisson's ratio for the state of stresses obtained from the Inference model. Indeed according to results obtained by Kulhawy (50) the Poisson's ratio varies insignificantly with the increase of stresses, Figure 6.8. The following Algorithm gives the adopted computational steps.

Step 1 Evaluation of first and second moments of the stress field from the Inference model.

Step 2 Computation of the tangent modulus of each element according to the following relation given by Kulhawy (50).

$$E_t = \frac{1/E_i}{\left[\frac{1}{E_i} + \frac{R_f \cdot \epsilon}{\sigma_1 - \sigma_3} \right]^2} \quad (6.24)$$

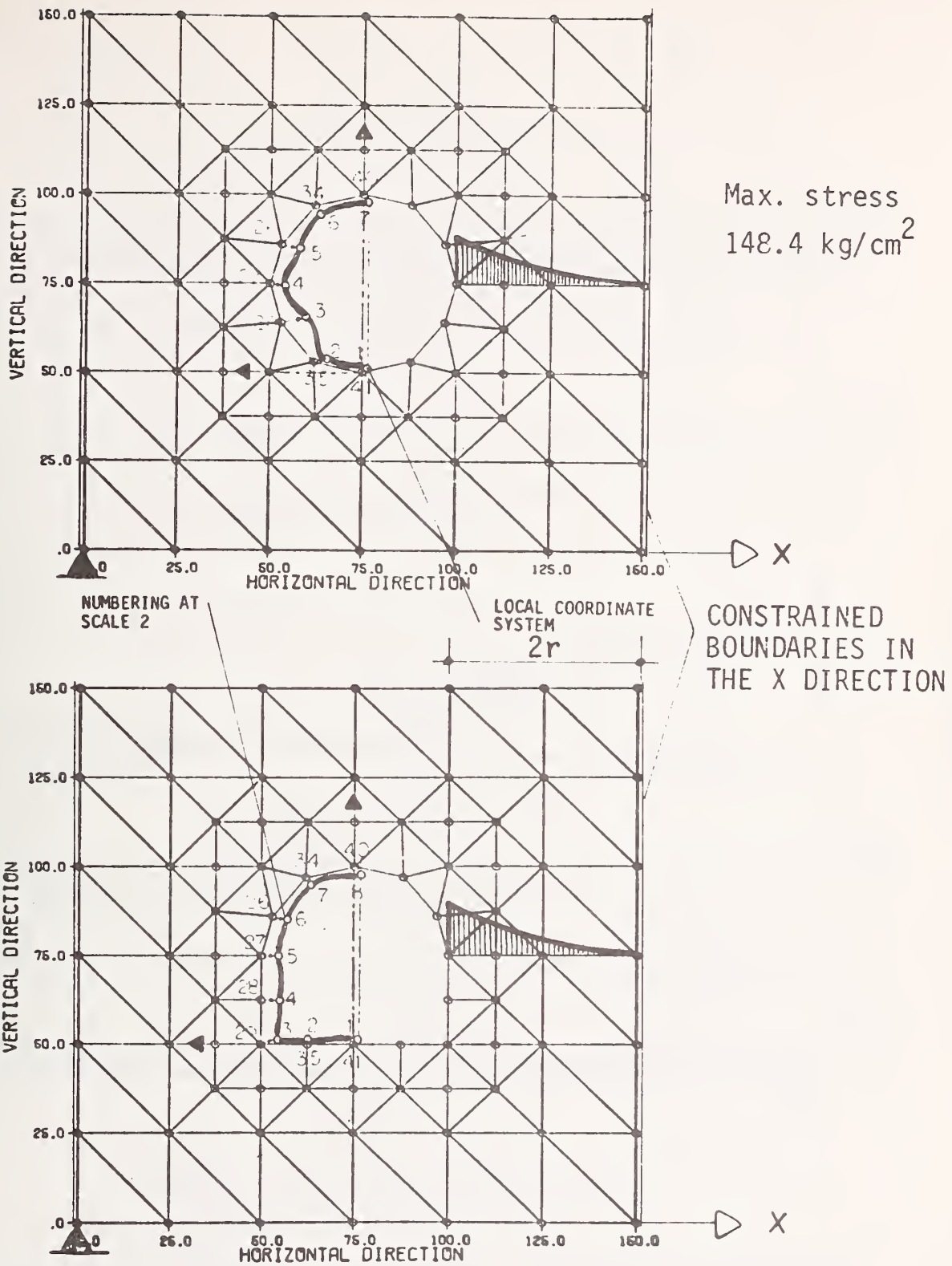


FIGURE 6.7 STRESS FIELD AROUND THE EXCAVATION

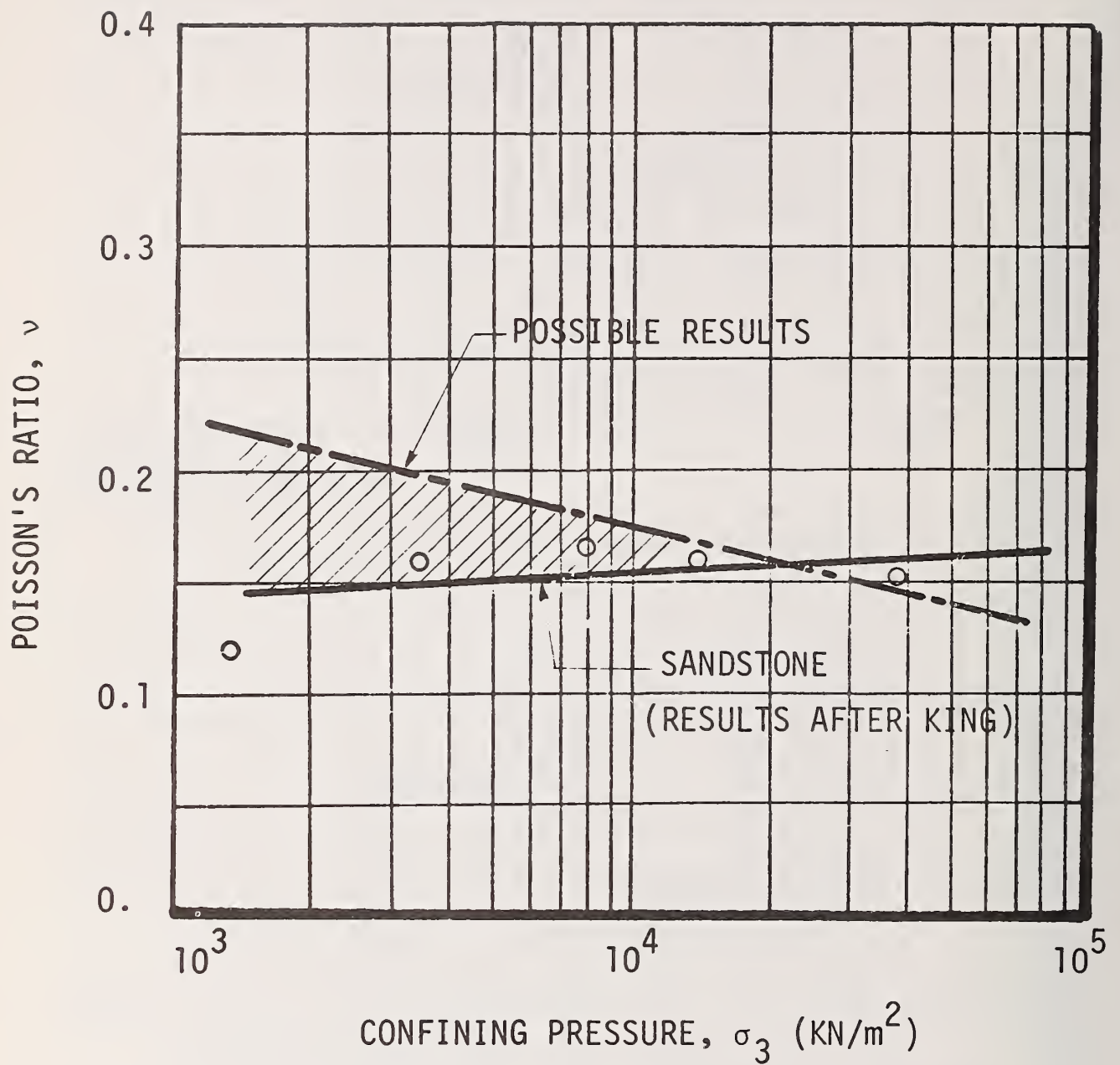


FIGURE 6.8 POISSON'S RATIO VS. STRESSES IN THE ROCK

where: E_i = initial modulus of elasticity
 R_f = failure ratio
 $\sigma_1 - \sigma_3$ = deviator stress
 ϵ = axial strain.

Then compute the first and second moments of E_t , Appendix C.

Step 3 Resolution of the system

$$[K] \{\bar{u}\} = \{F\} \quad (6.25)$$

following the F.E.M. with the appropriate boundary conditions. The load vector $\{F\}$ is evaluated considering the effect of the excavation.

Step 4 Evaluation of the quantities

$$\frac{\partial \{\bar{u}\}}{\partial E} , \frac{\partial \{\bar{u}\}}{\partial \nu}$$

according to the relations:

$$[K] \cdot \frac{\partial \{u\}}{\partial E} = \frac{\partial \{F\}}{\partial E} - \frac{\partial [K]}{\partial E} \{\bar{u}\} \quad (6.26)$$

$$[K] \cdot \frac{\partial \{u\}}{\partial \nu} = \frac{\partial \{F\}}{\partial \nu} - \frac{\partial [K]}{\partial \nu} \{\bar{u}\} .$$

Step 5 Evaluation of the stress tensor according to Zienkiewicz (97)

$$\{\sigma\} = [D] \cdot [B] \cdot \{\bar{u}\} \quad (6.27)$$

where: $\{\bar{u}\}$ = mean value of the displacements

$[D]$ = the elasticity matrix

$[B]$ = the influence matrix.

Then, evaluation of the expressions:

$$\frac{\partial \sigma}{\partial E} , \frac{\partial \sigma}{\partial \nu}$$

according to

$$\frac{\partial \sigma}{\partial E} = \frac{\partial [D][B]}{\partial E} \{\bar{u}\} + [D][B] \frac{\partial \{\bar{u}\}}{\partial E} \quad (6.28)$$

$$\frac{\partial \sigma}{\partial \nu} = \frac{\partial [D][B]}{\partial \nu} \{\bar{u}\} + [D][B] \frac{\partial \{\bar{u}\}}{\partial \nu} . \quad (6.29)$$

Step 6 Evaluation of the variances of the displacements and stressed using the first order approximation as defined previously, Eq. 5.19.

The programming details are given in the flow chart of Figure 6.9.

6.6 Uncertainty Analysis Related to the Modal Dynamic Analysis

The equations of motion can be uncoupled and the solution of the dynamic problem obtained by rearranging them in terms of the dynamic modes of the modes of the system. This is done by solving a classical eigenvalue problem from which the natural modes and the corresponding frequencies are determined. The uncertainty is introduced through the following physical parameters: the damping parameter and the natural frequencies.

On the other hand the motion prescribed at the boundaries is not uniform and phase differences exist in the motions at points located across the boundaries of the cross section shown in Figure 6.10. The motion perpendicular to the cross section is assumed negligible and the dynamic response is assumed to correspond to a plain strain condition over the examined cross section. Therefore, the prescribed horizontal motion at the boundaries is given by the following equations, neglecting the vertical component:

$$\ddot{u}_B(t) = \ddot{u}(t - \frac{L_B}{\bar{v}}) \quad (6.30)$$

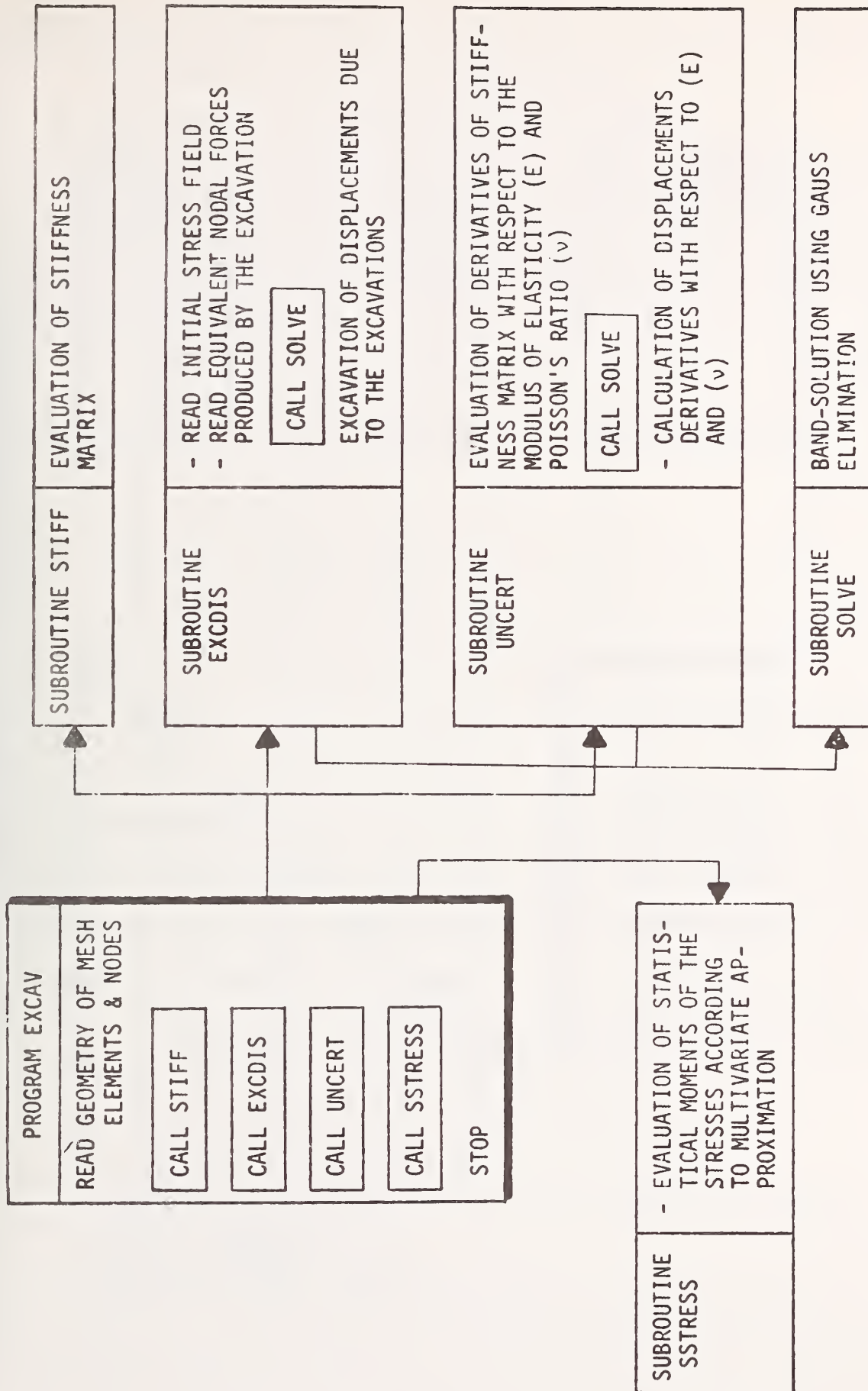
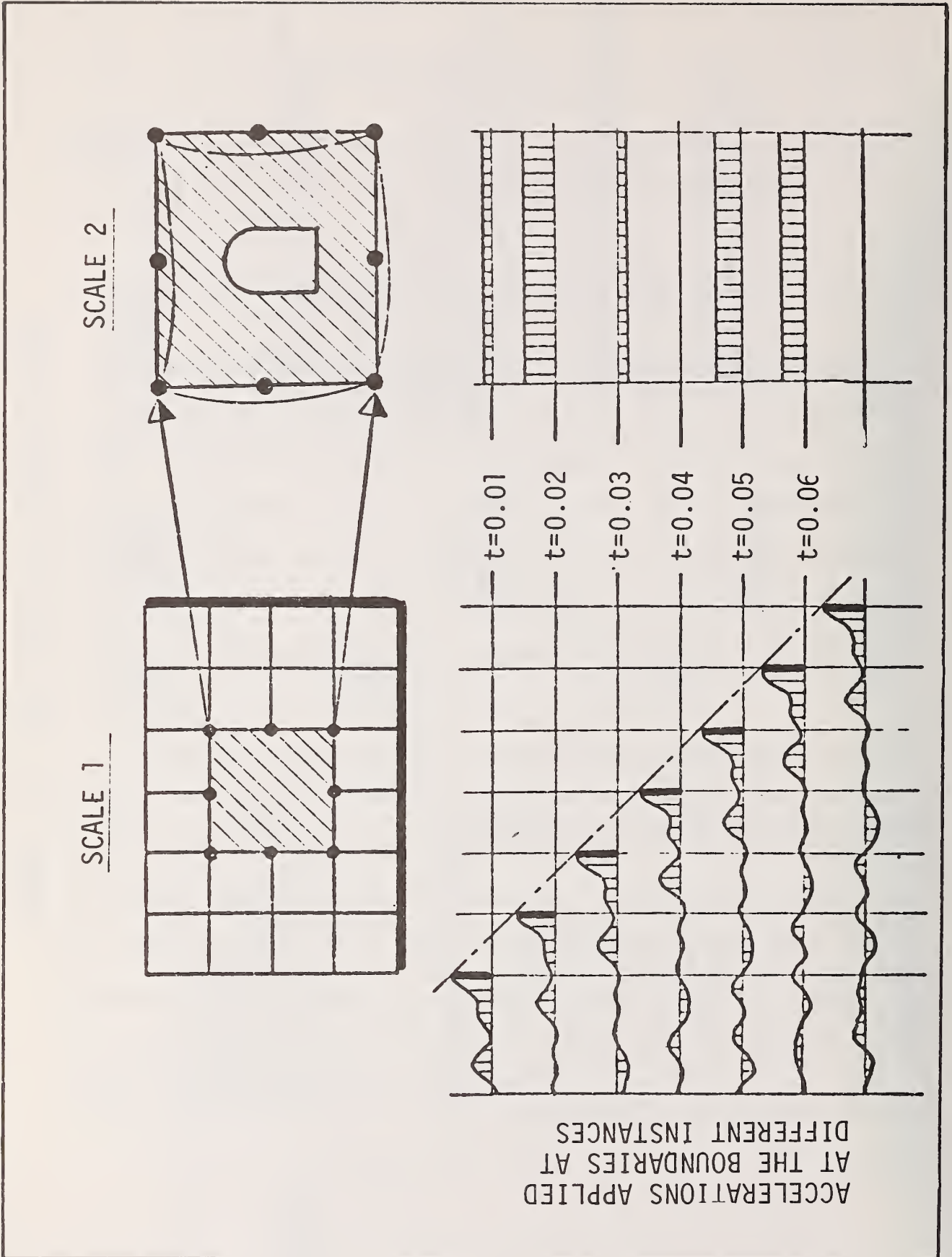


FIGURE 6.9 FLOW CHART OF PROGRAM EXCAV



ACCELERATIONS APPLIED
AT THE BOUNDARIES AT
DIFFERENT INSTANCES

FIGURE 6.10 EXISTING PHASE DIFFERENCES IN THE MOTION AT THE BOUNDARIES

where: L_B = distance between adjacent nodes
 \bar{V} = mean velocity of the propagated wave
 \ddot{u}_B = horizontal acceleration at the basement.

A standard finite element procedure is used and the cross section of interest is divided into triangular elements, Figure 6.11. The unknown variables are the displacements at each node with an horizontal and vertical component:

$$\{d_i(t)\} = \{u_i(t) \ , \ v_i(t)\} \ . \quad (6.31)$$

These displacements can be decomposed into two distinctive parts

$$\{d_i(t)\} = \{d_i^B(t)\} + \{d_i^{IN}(t)\} \quad (6.32)$$

where: $\{d_i^B\}$ = represents the displacement of node 'i' due to the perturbation of the boundaries and could be considered as a quasistatic displacement vector, and

$\{d_i^{IN}(t)\}$ = represents the inertial contribution to the displacement of the node.

Then, distinguishing the free nodes from the constrained nodes, the latter being the nodes lying on the boundaries of the examined cross section, the following equation of motion is obtained, (see Appendix C in relation with Figure C.1).

$$[m_F] \{\ddot{d}_F^{IN}\} + [K_{11}] \{d_F^{IN}\} = - [m_F] \{\ddot{d}_F^B\} \quad (6.33)$$

where: $[m_F]$ = the mass matrix of the free nodes

$[K_{11}]$ = the stiffness matrix

$\{d_F^{IN}\}$ = the inertial component of the unknown displacement vector

$\{d_F^B\}$ = the quasistatic component of the displacement vector.

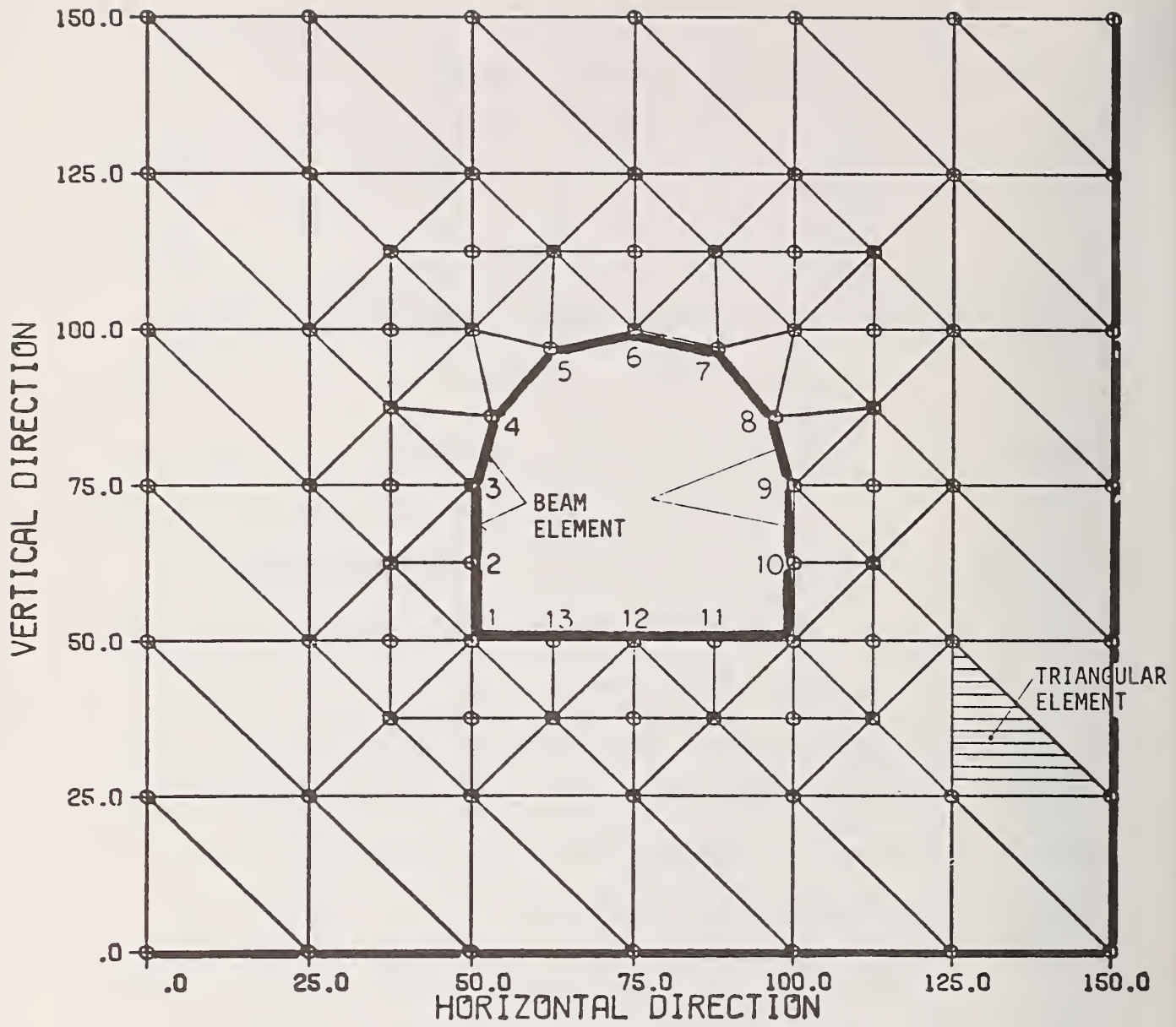


FIGURE 6.11 TYPES OF FINITE ELEMENTS

The above equation is valid under the following assumptions:

1. The damping ratio is defined as a function of the mode of vibration, as specified in section 4.4.3.
2. The material is assumed to behave linearly during the seismic perturbation.

Both assumptions are close to reality according to experimental evidence, (56).

To proceed with the solution of the above equation, the normal mode shapes and frequencies of the free vibration have to be determined first:

$$[m_F] \{\ddot{d}_F^{IN}\} + [K_{11}] \{d_F^{IN}\} = 0 . \quad (6.34)$$

By performing a judicious change of variables we can obtain the displacement vector in terms of the natural modes of vibration of the domain under consideration. Writing $\{d_F^{IN}\}$ as follows:

$$\{d_F^{IN}\} = [A] \{Q_F\} \quad (6.35)$$

where: $\{Q_F\}$ is a dimensionless modal vector,
the free vibration equation of motion becomes:

$$\{\ddot{Q}_F\} + [A]^{-1} [\Omega^2] [A] \{Q_F\} = 0 \quad (6.36)$$

where: $[\Omega^2] = \frac{[K_{11}]}{[m_F]}$.

The uncoupling of the above equation is achieved by means of diagonalization of matrix $[\Omega^2]$. A theorem states that there always exists a matrix $[A]$ such that:

$$[A]^{-1} [\Omega^2] [A] = \begin{bmatrix} \omega_1 & & & \\ & \omega_2 & & \\ & & \ddots & \\ & & & \omega_n \end{bmatrix} \quad (6.37)$$

Only the lower frequencies are expected to be of interest in our case. The corresponding normal modes provide the node displacements in the cavern's vicinity. Matrix [A] is defined in terms of these first frequencies. Substituting in Equation 6.33, the following relation is obtained:

$$[A]^T [m_F] [A] \{\ddot{Q}\} + [A]^T [K_{11}] [A] \{Q\} = -[A]^T [m_F] \{\ddot{d}_F^B\} . \quad (6.38)$$

Using the following simplifications:

$$[M] = [A]^T [m_F] [A]; \quad [K] = [A]^T [K_{11}] [A]; \quad \{F\} = -[A]^T [m_F] \{\ddot{d}_F^B\}$$

and introducing a linear viscous damping coefficient as suggested by Penzien (19), a set of uncoupled equations is obtained:

$$[M] \{\ddot{Q}\} + 2[M] \cdot \omega_i \cdot \xi_i \{\dot{Q}\} + [K] \{Q\} = \{F\} \quad (6.39)$$

where: ω_i = the natural frequencies, and

ξ_i = the damping ratio for the corresponding natural frequency.

The general solution for zero initial conditions, and for each vibrational mode 'i' is given by, Newmark (63):

$$Q_i(t)_j = \frac{1}{\omega_{di} \cdot M_j} \int_0^t F_j(\tau) e^{-\xi_i \cdot \omega_i (t-\tau)} \cdot \sin \omega_{di} (t-\tau) \cdot d\tau \quad (6.40)$$

where: $\omega_{di} = \omega_i (1 - \xi_i^2)^{\frac{1}{2}}$.

Finally, introducing Q into Equation (6.35) and after adequate substitutions, the dynamic displacement vector is given by:

$$\{d_F^{IN}\}_i = \frac{[A]_i}{\omega_{di}} \int_0^t -[A]_i^T \frac{[m_F]}{[M]} \{\ddot{d}_F^B\} \cdot e^{-\xi_i \cdot \omega_i (t-\tau)} \cdot \sin \omega_{di} (t-\tau) \cdot d\tau . \quad (6.41)$$

The quasistatic component of the acceleration \ddot{d}_F^B , can be related to the boundary accelerations by an influence matrix [S] as follows:

$$\{\ddot{d}_F^B\} = [S] \{\ddot{d}_B\} \quad (6.42)$$

Matrix [S] can be obtained through a conventional static analysis.

Substituting into the above equation we obtain:

$$\{d_F^{IN}\}_i = [A]_i \frac{[A]_i^T}{[M]} [m_F] [S] \int_0^t -\{\ddot{d}_B(t - \frac{L}{V_B})\} \cdot e^{-\xi_i \omega_i (t-\tau)} \cdot \sin \omega_{di} (t-\tau) d\tau \quad (6.43)$$

or

$$\{d_F^{IN}\}_i = [A]_i [B]_i^T \cdot \{R_i\} \quad (6.44)$$

where:

$$[B]_i^T = \frac{[A]_i^T}{[M]} [m_F] \cdot [S] \quad , \quad \text{and}$$

$$\{R_i(t)\} = \frac{-1}{\omega_{di}} \int_0^t \{\ddot{d}_B(t - \frac{L}{V_B})\} \cdot e^{-\xi_i \omega_i (t-\tau)} \sin \omega_{di} (t-\tau) d\tau \quad .$$

The loading factor $R_i(t)$ can be computed either by Newmark's (63) technique or by Wilson's (95) step-by-step integration in the time domain.

The uncertainty in the evaluation of the dynamic displacements $\{d_F^{IN}\}$ is induced by the natural frequencies of the system obtained from the modal analysis and the damping parameters. A perturbation technique is used to determine the variance of the natural frequencies for each vibrational mode, in a similar fashion as Hoshiya's (33) procedure. In the equation of free vibration, Equation 6.34, we assume that to the physical quantities $[m_F]$ and $[K_{11}]$ corresponds a mean and a fluctuating component as follows:

$$[m_F]_i = [m_0]_i + \sum_{r=1}^n \alpha_r \delta_{ir} [m_0]_i ; \quad i = 1, n \quad (6.45)$$

$$[K_{11}]_i = [K]_i + \sum_{r=1}^n \beta_r \delta_{ir} [K]_i ; \quad i = 1, n \quad (6.46)$$

where: δ_{ir} = Kronecker delta, and

α, β = fluctuating parameters.

Assuming the fluctuating component of the stiffness matrix (K_i), Eq. 6.46, to be negligible, the solution to Eq. 6.39 takes the following series form, Bolotin (4), neglecting the damping term:

$$Q = Q_0 + \sum_{r=1}^n \pi_r \alpha_r , \quad \omega = \omega_0 + \sum_{r=1}^n \eta_r \alpha_r . \quad (6.48)$$

Substituting into Equation 6.39 (see Appendix C), the following expression of the variance is obtained for the j^{th} natural frequency:

$$\text{VAR}(\omega_j) = \sum_{r=1}^n \{ (\eta_r)_j^2 \cdot \sigma_{\alpha r}^2 \} \quad (6.49)$$

where: $\sigma_{\alpha r}^2$ = the variance of the fluctuating parameter α_r , and

$$(\eta_r)_j = \frac{\omega_{0j} \{Q_0\}_j^T \begin{bmatrix} m_1 & \delta_{1r} & & \\ & & & \\ & & m_n & \delta_{nr} \\ & & & \end{bmatrix} \{Q_0\}_j}{2 \{Q_0\}_j^T \begin{bmatrix} m_0 \\ \end{bmatrix} \{Q_0\}_j} .$$

The algorithm then follows the following steps.

- Step 1 Evaluation of the quasistatic displacement vector
- Step 2 Evaluation of the dynamic displacement vector performing the modal analysis
- Step 3 Evaluation of the statistical characteristics of the natural frequencies
- Step 4 Evaluation of the second moment of the dynamic stresses according to:

$$\frac{\partial \sigma}{\partial \omega_j} = [D] [B] \frac{\partial \{d_F^{IN}\}}{\partial \omega_j} \quad (6.50)$$

for $j = 1, \dots, n$ modes.

The detail of the computations is given in Appendix C. Program DYNMODE is written conformal to the above conceptual basis. Triangular elements are used and the computations are performed in the time-domain. In the flow-chart of Figure 6.12 the details concerning the computational organization is given as well as the needed input information.

6.7 Uncertainty Related to the Stability of the Liner

From the dynamic point of view it is assumed that the liner does not have any effect on the surrounding the cavity media. Consequently, at every time step a static analysis is performed to compute the effect of the rock media, subjected to a seismic perturbation, on the liner.

The behavior of the liner is of primary importance. This is the reason of adopting a geometric nonlinearity procedure leading to a stability analysis of the structure.

As previously seen, section 6.3, the stiffness matrix of the structure is given as a function of the displacements. Therefore, the equilibrium conditions produce nonlinear expressions, forming a system of nonlinear equations. This system of nonlinear equations can be solved using Newton Raphson's iterative procedure (see Appendix C).

At the n^{th} iteration the following relation is obtained:

$$\left[\frac{\partial NK(u^n)}{\partial u} \right] \{u^{n+1} - u^n\} = \{F\} - \{NK(u^n)\} \quad (6.51)$$

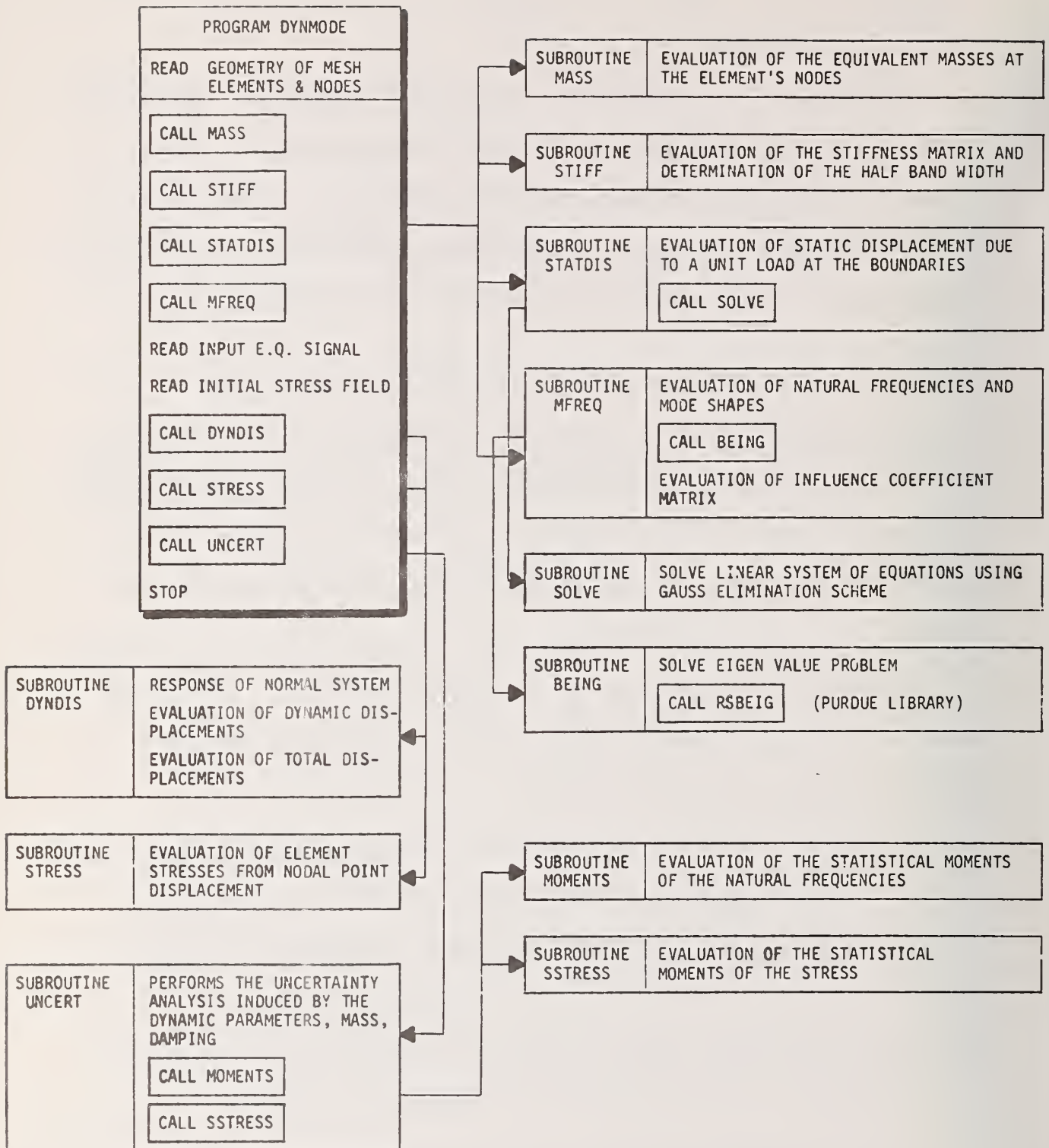


FIGURE 6.12 FLOW CHART OF PROGRAM DYNMODE

where: $[NK(u^n)]$ = the nonlinear stiffness matrix defined at the n^{th} iteration

$\{F\}$ = the load vector

$\{u^n\}$ = the displacement vector at the n^{th} iteration.

If u^n is known then u^{n+1} can be determined by solving the above linear system of equations. From Taylor's expansion:

$$\{NK(u^n)\} = \{NK(u^{n-1})\} + \frac{\partial NK(u^{n-1})}{\partial u} \{u^n - u^{n-1}\} \quad (6.52)$$

Furthermore, setting:

$$\{u^{n+1} - u^n\} + \{u^{n-1}\} - \{u^{n+1}\} = \lambda \{u^{n+1} - u^n\} \quad (6.53)$$

and substituting Eqs. (6.52) and (6.53) in Eq. (6.51) (Appendix C), the following relation is obtained:

$$\left[\frac{\partial NK(u^n)}{\partial u} \right] - \lambda \left[\frac{\partial NK(u^{n-1})}{\partial u} \right] \{\Delta u\} = \{\Delta F\} \quad (6.54)$$

If to a virtual displacement Δu the external loads remain constant, i.e. $\Delta F = 0$, then Eq. (6.54) represents the classical structural stability equation.

Matrix $\lambda \left[\frac{\partial NK(u^{n-1})}{\partial u} \right]$ is also known as the geometric stiffness matrix, Cook (11), and $\frac{\partial NK(u^{n-1})}{\partial u}$ represents a specific force due to initial strain conditions.

In our particular case the following simplification can be made:

$$\frac{\partial NK(u^{n-1})}{\partial u} = C(M) \quad (6.55)$$

that is, the uniaxial force is proportional to the liner's mass. The constant (C) can be eventually determined experimentally. Figure 6.13 gives an illustration of the various parameters.

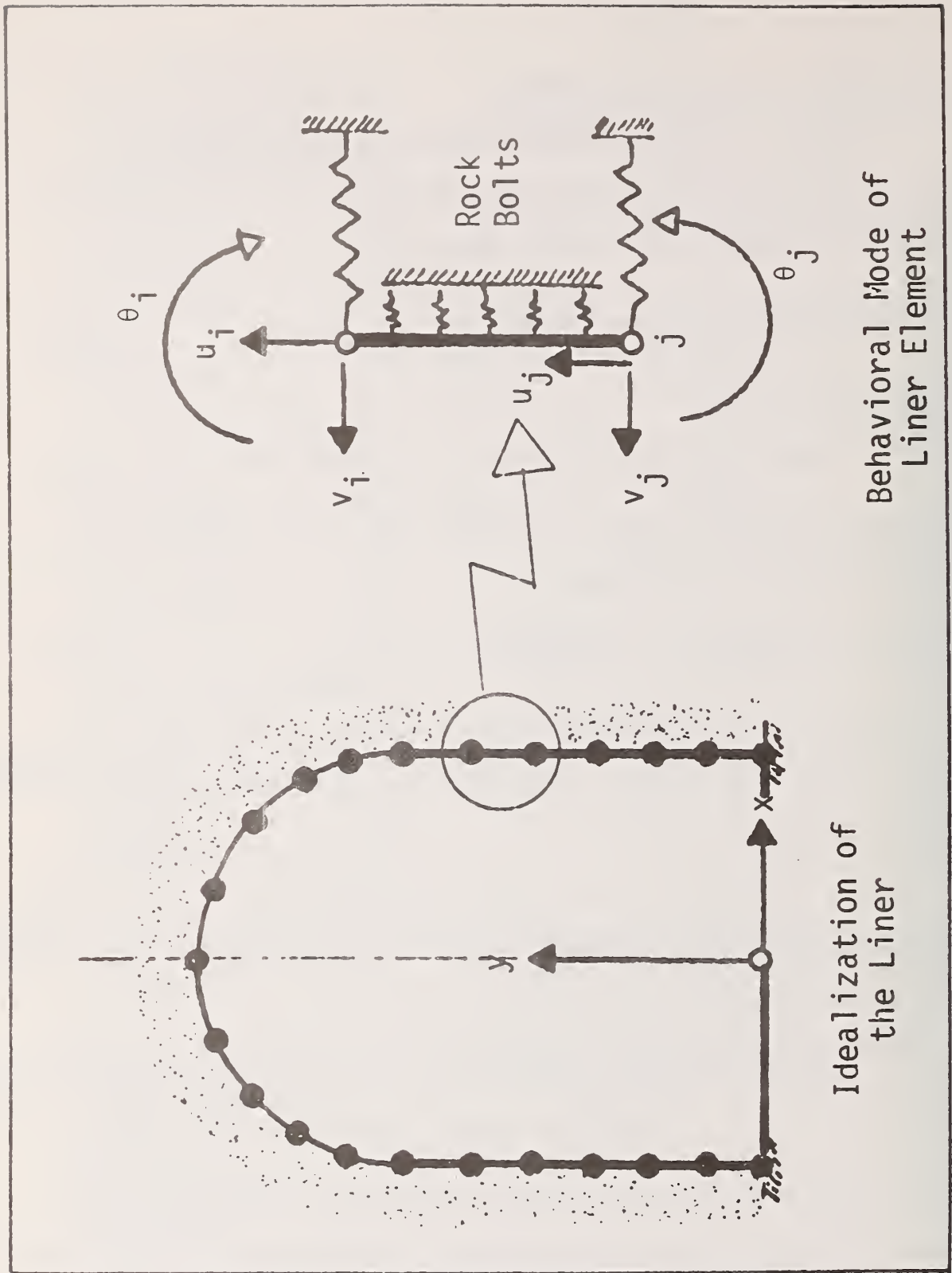


FIGURE 6.13 PARAMETERS DESCRIBING THE LINER'S BEHAVIOR

Setting $\Lambda^2 = \lambda \cdot c$, Eq. 6.54 becomes:

$$\{[K] - \Lambda^2[M]\} \Delta u = 0 \quad (6.56)$$

which is an eigenvalue problem, Λ being the eigenvalues.

The uncertainty in the analytical model is introduced by the physical parameters characterizing the liner i.e. the mass and stiffness.

As previously seen with the modal analysis a perturbation technique is adopted here also. Thus the general shape of the structure in the instable configuration is assumed to be of the form:

$$\Delta u_i = u_i \sin(\Lambda X) . \quad (6.57)$$

The physical parameters are defined as previously in Equations 6.45 and 6.46, leading to the series forms for Λ and u_i :

$$u_i = u_{0i} + \sum_{k=1}^n (U_{1ik} \alpha_k + U_{2ik} \beta_k) \quad (6.58)$$

$$\Lambda = \Lambda_0 + \sum_{k=1}^n (L_{1k} \alpha_k + L_{2k} \beta_k) . \quad (6.59)$$

Substituting Eqs. 6.58 and 6.59 into Eq. 6.56 and comparing the terms containing identical powers of the parameters α and β , we obtain the set of equations:

$$\begin{aligned} -\Lambda_0^2 m_i u_{0i} + K_i u_{0i} &= 0 \\ \{-\Lambda_0^2 m_i U_{1ik} + K_i U_{1ik}\} \sum_{k=1}^n \alpha_k &= \{2\Lambda_0 L_{1k} m_i u_{0i} + \Lambda_0^2 m_i u_{0i}\} \sum_{k=1}^n \alpha_k \\ \{-\Lambda_0^2 m_i U_{2ik} + K_i U_{2ik}\} \sum_{k=1}^n \beta_k &= \{2\Lambda_0 L_{2k} m_i u_{0i} + K_i u_{0i}\} \sum_{k=1}^n \beta_k \end{aligned} \quad (6.60)$$

Matrices $[L_{1k}]$ and $[L_{2k}]$ representing the influence of the stiffness and mass fluctuation on the eigenvalues Λ are computed in Appendix C. The variance then of each eigenvalue is given by:

$$\text{VAR}(\Lambda_j) = \sum_{k=1}^n \{ (L_{1k})_j^2 \sigma_{\alpha k}^2 + (L_{2k})_j^2 \sigma_{\beta k}^2 \} \quad (6.61)$$

where: $\sigma_{\alpha k}, \sigma_{\beta k}$ = the variance of the fluctuating parameters α_k and β_k ,

$$(L_{1k})_j = \frac{\Lambda_{0j} \{u_0\}_j^T \begin{bmatrix} m_1 \delta_{1k} \\ \vdots \\ m_n \delta_{nk} \end{bmatrix} \{u_0\}_j}{2 \{u_0\}_j^T [m_0] \{u_0\}_j} \quad (6.62)$$

and

$$(L_{2k})_j = \frac{\{u_0\}_j^T \begin{bmatrix} -k_1 \delta_{1k} \\ \vdots \\ k_n \delta_{nk} \end{bmatrix} \{u_0\}_j}{2 \Lambda_{0j} \{u_0\}_j^T [m_0] \{u_0\}_j} \quad (6.63)$$

The algorithmic procedure is defined in the following steps.

- Step 1 Prepare the input loads at every time increment
- Step 2 Perform the analysis considering the geometric non-linearity at every increment of time
- Step 3 Find the most unfavorable configuration of the liner's displacement and perform the stability analysis
- Step 4 Find the statistical characteristics of the eigenvalues representing the stability factor of the structure
- Step 5 Evaluate the liner's moments and their statistical characteristics.

The flow chart of the corresponding program is given in Figure 6.14.

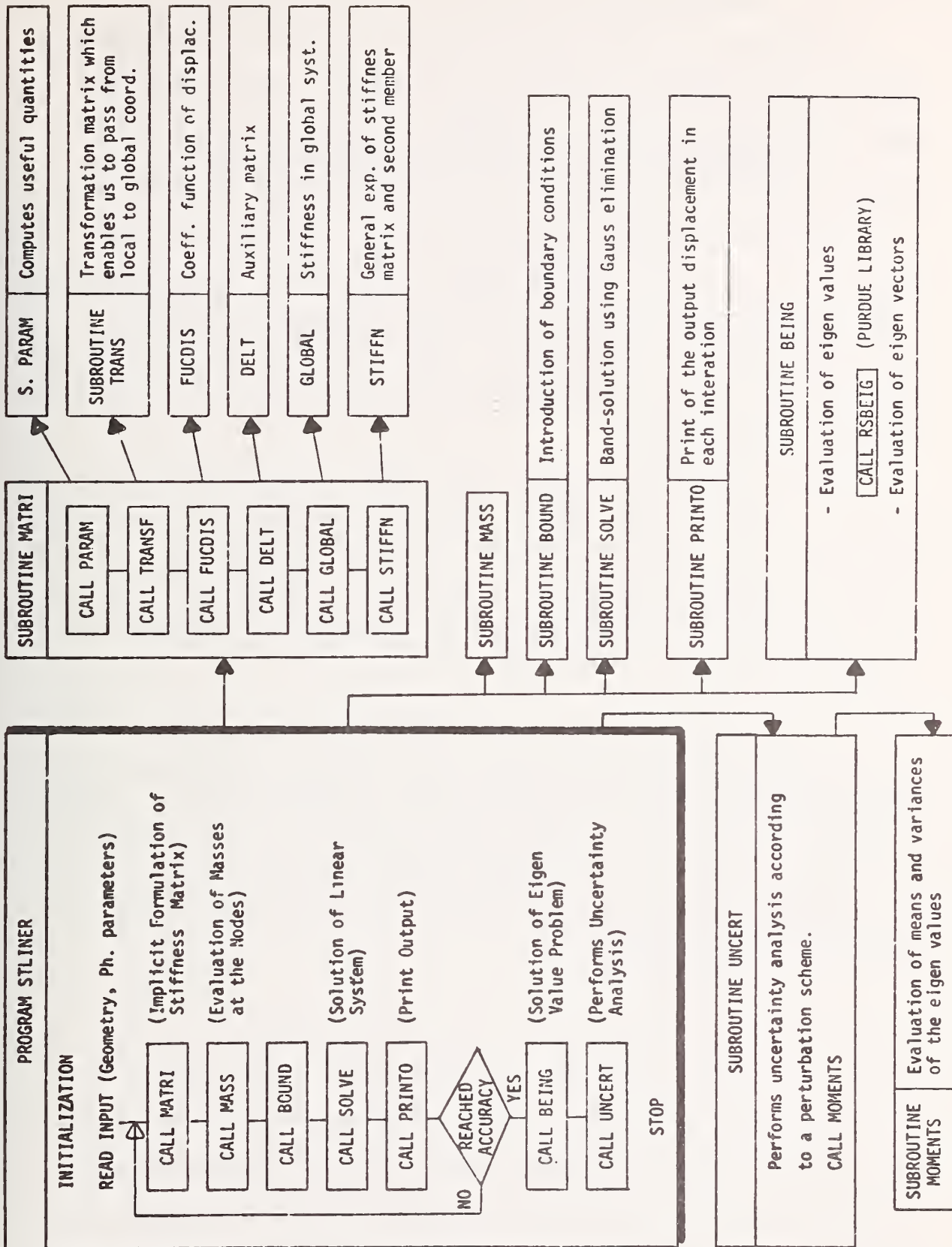


FIGURE 6.14 FLOW CHART OF PROGRAM STLINER

6.8 Remarks Concerning the Given Computational Scheme

The main goal in the proposed scheme is to perform an uncertainty analysis with respect to the physical parameters. This is done by means of the modal analysis. It is particularly well fitted to our problem because of its moderate central memory storage requirements.

The dynamic interaction between the rock and the liner is considered to be negligible because of the corresponding vibrating masses are disproportional. Therefore, only the very high frequencies are affecting the interaction phenomenon - a situation which never takes place during earthquakes.

On the other hand the static interaction is considered in its most simple form since the dimensions of the opening are much larger than the thickness of the liner. Under these conditions the liner would rather act as a membrane requiring, therefore, a stability analysis.

The input seismic load necessary to perform the previously mentioned computations is evaluated in the following chapter. Finally in Chapter 9 a complete treatment of a case study is provided along with some additional details concerning the sequence in which the computations are performed.

CHAPTER 7
MODEL PROVIDING THE INPUT SEISMIC DISTURBANCE

7.1 Introduction

A model for generating earthquake accelerations was seen to be necessary in section 3.5. Indeed a two degree of freedom system was considered sufficient for simulating the vibration of the cavity under a seismic perturbation. One of the degrees of freedom is assumed to represent the behavior of the media surrounding the opening. It is the a priori component of the model. On the other hand the second degree of freedom constitutes the a posteriori component which links together the vibrational mode of the examined cavity and the expected earthquake signal at the surface of the earth.

The analysis proposed in the subsequent sections is based on the following physical parameters: the natural frequency and the damping ratio. They constitute the basic elements of the model. In what follows the detailed derivation of the a priori, coupled with the a posteriori component is given, as well as a brief parametric study of the physical parameters, that enable us to define the limits of applicability of the model. The a posteriori component adopted here is the one developed by Ruiz and Penzien (80). Their fitting parameters and analytical results are used for the generation of the earthquake signal. Finally the retained sequence of operations and the obtained acceleration signal are presented both at the earth surface and at depth.

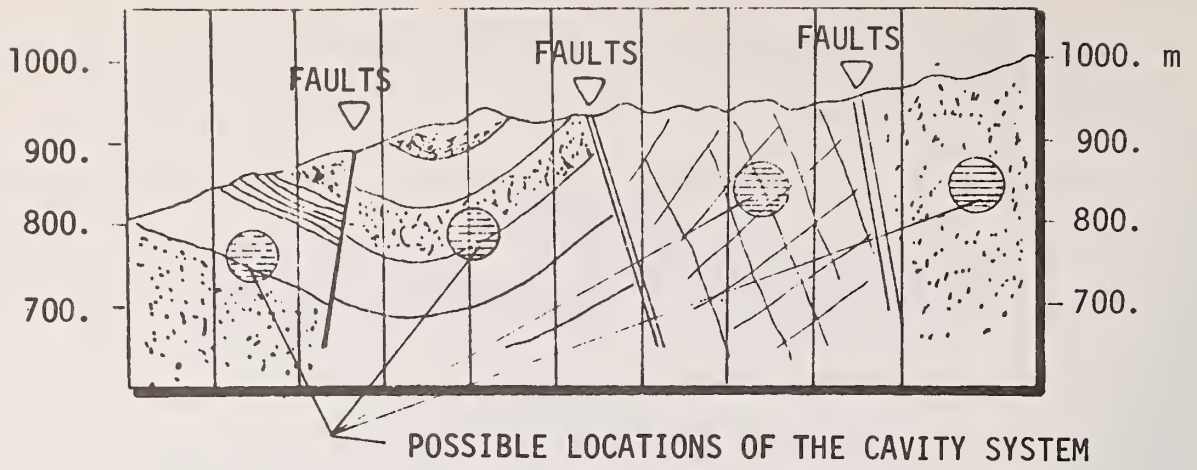


FIGURE 7.1 ILLUSTRATION OF DIFFERENT GEOLOGICAL ENVIRONMENT

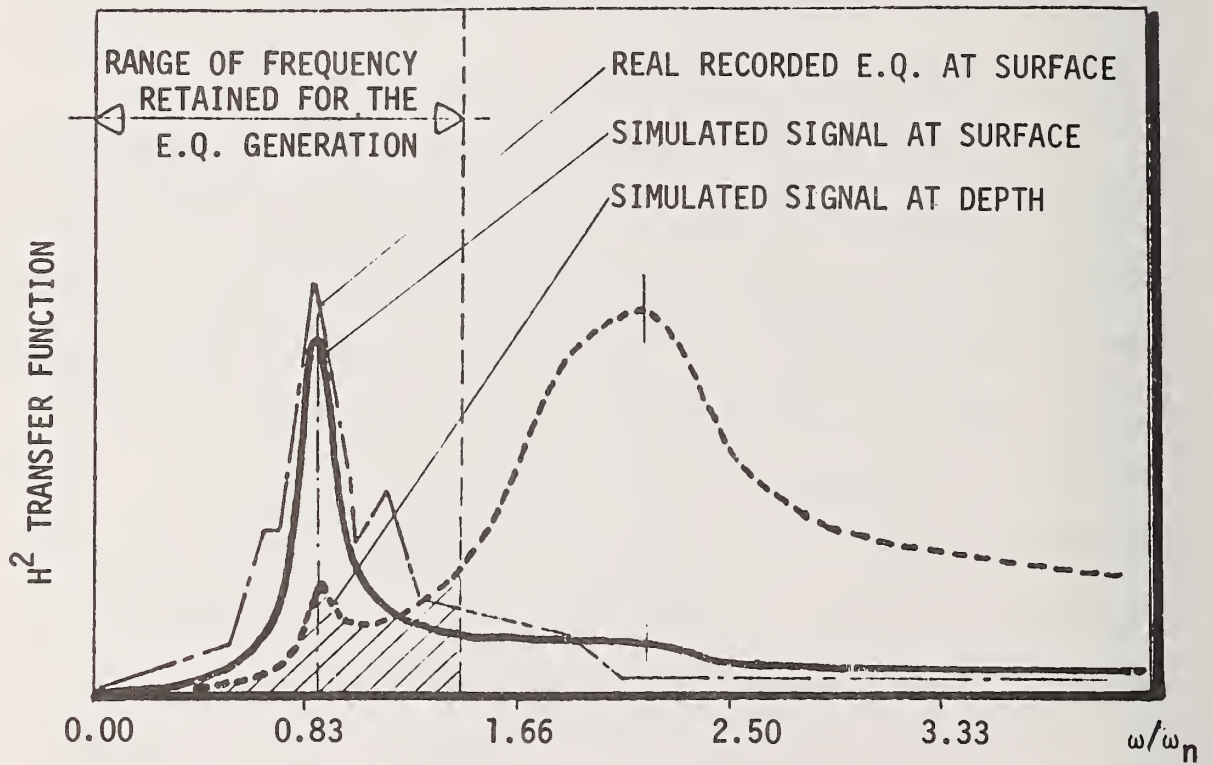


FIGURE 7.3 TRANSFER FUNCTIONS H^2

7.2 Analytical Treatment of the Model

The main objective in defining the a priori characteristics of the model is to obtain the scale factor to be applied to the acceleration at the earth's surface so as to obtain the acceleration signal the depth of scale one as defined in section 3.2.3. Clearly the input acceleration to Scale One must be influenced by the size of Scale One and its physical parameters. To simplify the analysis Scale One is assumed to represent a discrete vibrating mass M , connected with the cavity base through a spring of constant K and a dashpot with a damping ratio ξ . This approximation seems to be close to the real behavior of the media, at least as far as the first vibrational mode is conceived. Indeed, the rock mass enclosed in Scale One bound by faulting systems, vibrates as a discrete entity. The above heuristic argument is to a certain extent confirmed by the real data of recorded earthquake signals (see Figures 3.6 and 7.1).

However there are several physical constraints that influence the vibration of mass M , which can be difficultly quantified. One such constraint could well be the damping effect of the faulting system, or the effect of the surrounding Scale One media, etc. Therefore an a posteriori component possessing a mass m , a spring constant k , and a damping ratio ξ , is coupled in series with the above mentioned a priori component. The related equations of motion then are given by Equations (3.5) and (3.6). After a few computational simplifications, these equations become (see Appendix D):

$$M\ddot{x} + C\dot{x} + Kx + c(\dot{x}-\dot{z}) + k(x-z) = -M\ddot{y} \quad (7.1)$$

$$m\ddot{z} - c(\dot{x}-\dot{z}) - k(x-z) = -m\ddot{y} \quad (7.2)$$

Now setting: $M = \frac{m}{M} =$ the mass ratio

$\omega_n^2 = \frac{k}{m} =$ the natural frequency of the a posteriori component

$\Omega_n^2 = \frac{k}{M} =$ the natural frequency of the a priori component,
(value obtained from the modal analysis of scale one)

$c = 2 \xi m \omega_n =$ the a posteriori damping coefficient

$C = 2 \Xi M \Omega_n =$ the a priori damping coefficient

$\xi =$ the a posteriori damping ratio

$\Xi =$ the a priori damping ratio

the following expressions are obtained:

$$\ddot{x} + 2(\Xi)(\Omega_n) \dot{x} + (\Omega_n^2) x + 2(\xi)(\omega_n) M(\dot{x}-\dot{z}) + \omega_n^2 M(x-z) = -\ddot{y} \quad (7.3)$$

$$\ddot{z} - 2(\xi)(\omega_n)(\dot{x}-\dot{z}) - \omega_n^2(x-z) = -\ddot{y} \quad (7.4)$$

which represent a system of linear differential equations with x and z being the unknown variables, and \ddot{y} the acceleration of the cavity base, as shown in Figure (7.1).

Making use of the Fourier Transform technique, and working in the frequency domain the amplitude of the transfer functions of the system of two masses previously specified, are: (see derivation in Appendix D)

For the A Posteriori Component

$$\left| \frac{z}{y} \right|^2 = \frac{\left[(\Omega_n^2 - \omega^2) + \omega_n^2(M+1) \right]^2 + \left[2(j\omega)(\omega_n) \left(\frac{\xi(M+1)}{\omega_n^2} + \frac{(\Xi)(\Omega_n)}{\omega_n} \right) \right]^2}{A^2 + B^2} \quad (7.5)$$

where: j = imaginary unit

and

$$A = (\Omega_n^2 - \omega^2) \left(\frac{\omega_n^2}{\omega^2} - 1 \right) - \omega_n^2 M - 4(\xi)(\Xi)(\Omega_n)(\omega_n)$$

$$B = j2 \left[\xi(\Omega_n^2 - \omega^2) \cdot \left(\frac{\omega_n}{\omega} \right) - \xi(\omega_n) \omega \cdot M + (\Xi)(\Omega_n) \cdot \omega \left(\frac{\omega_n^2}{\omega^2} - 1 \right) \right]$$

Equation 7.5 is also known as the complex transfer function $H(j\omega)$.

Indeed $\left| \frac{z}{y} \right|^2 = |H(j\omega)|^2$.

For the A Priori Component

$$\left| \frac{x}{y} \right|^2 = \frac{(M \cdot \omega^2)}{D^2} \left| \frac{z}{y} \right|^2 + \frac{[(M+1) \cdot \omega^2]^2}{2} = |H_D(j\omega)|^2 \quad (7.6)$$

where: $D = (\Omega_n)^2 + 2j(\xi)(\Omega_n)(\omega) - \omega^2$

As it can be observed from Equations (7.5) and (7.6) the amplitude of the transfer functions are dependent on the following four parameters:

M = the mass ratio $\frac{M}{m}$

ξ, Ξ = the damping ratios of masses m and M respectively

and F = the frequency ratio $\frac{\Omega_n}{\omega_n}$

These quantities constitute the input to Program EQGEN implementing the above scheme. The corresponding flow chart is given in Figure 7.2 and the computational details in section 7.5.

The transfer function given by Equation 7.5 is illustrated in Figure 7.3. Interestingly enough, it has the same shape as the one-degree-of-freedom transfer function defined by Ruiz (80), based on a simple a posteriori technique. It seems appropriate then to adopt his

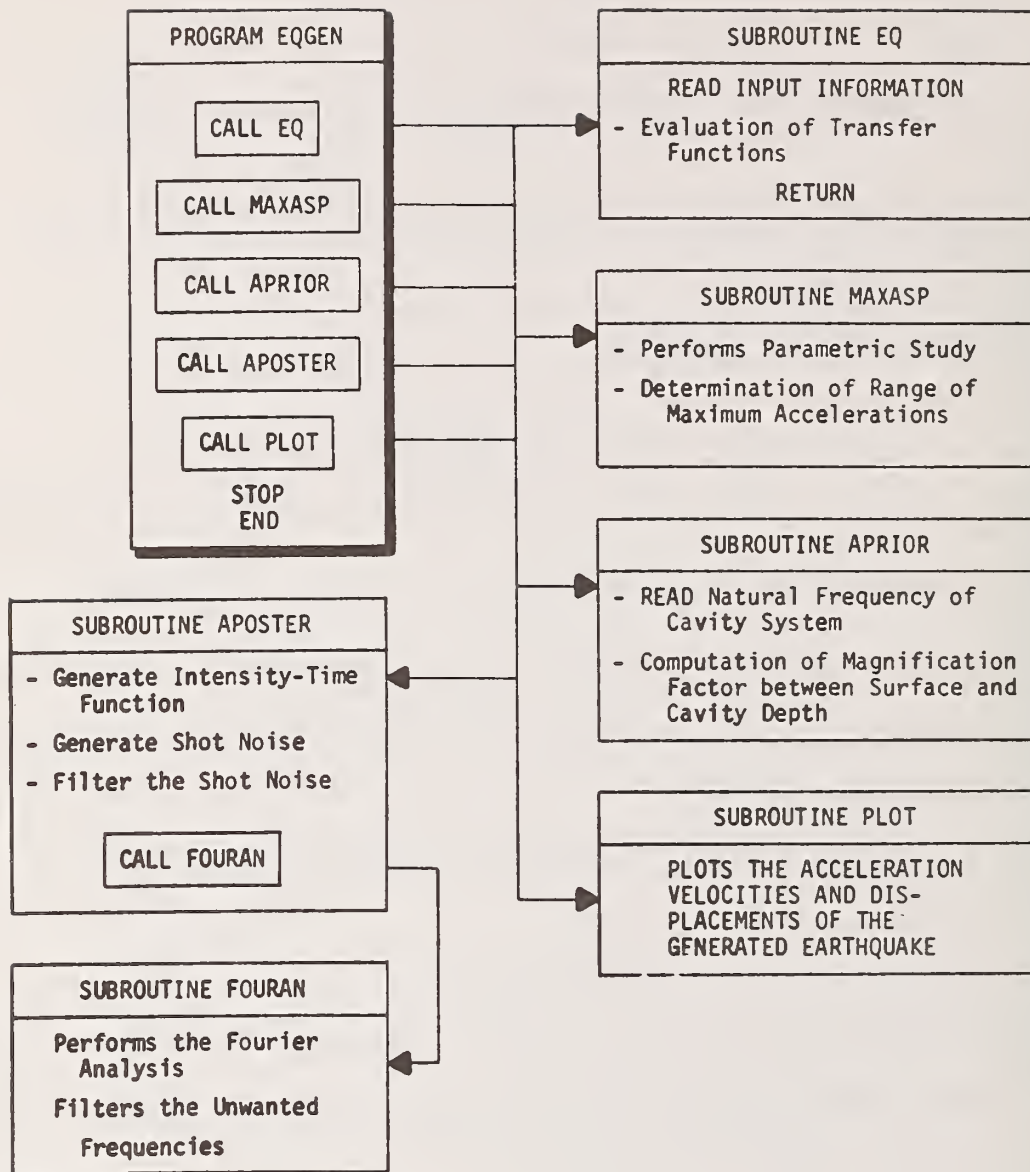


FIGURE 7.2 COMPUTATIONAL SCHEME OF THE EARTHQUAKE GENERATION MODEL

values concerning the governing parameters m , k , and ω_n for generating the earthquake signal at the surface of the earth. On the other hand a scale factor is used to evaluate the corresponding earthquake signal at the level of the cavity. This factor is determined by Equation (7.6). Simply speaking it is the ratio between the maximum acceleration at the ground surface and at depth.

Ruiz and Penzien defined their a posteriori model taking into consideration the random nature of the earthquake phenomenon. In the following the adopted statistical assumptions are presented as borrowed from their analysis (80).

7.3 A Posteriori Component

The most commonly used practice is to consider a gaussian nonstationary shot noise to represent the earthquake acceleration. This process simulates the effect of random pulses arriving as seismic waves. The nonstationarity characterizes the variability of the random interarrival times of the above mentioned pulses. The acceleration at the cavity's level is evaluated by passing the above mentioned gaussian shot noise through the filter that constitutes the previously defined two-degrees-of-freedom mechanical model. The process is completely defined as soon as the model's parameters are known as well as the variance intensity function $\phi(t)$ of the shot noise. These parameters must therefore be representative of a specific site location in order to generate earthquake records corresponding to earthquakes occurring in similar geologic conditions, namely epicentral distance and magnitude.

Following this general order of ideas the natural frequency (ω_n), the damping ratio (ξ) and the variance intensity function ($\phi(t)$) are

estimated in such a way as to give the best fit to known past seismic records. Formally the output process in the frequency domain can be expressed as:

$$z(j\omega) = H(j\omega) \cdot y(j\omega) \quad (7.7)$$

where: $z(j\omega)$ is the output process

$y(j\omega)$ is the input process

$H(j\omega)$ is the complex frequency response function of the filter as previously defined.

In the time domain, by the inverse Fourier transform we obtain:

$$z(t) = \int_{-\infty}^{\infty} y(\tau) h(t-\tau) d\tau \quad (7.8)$$

where: $h(t)$ is the unit impulse response function of the filter.

Since the excitation process is assumed to be gaussian, the output process will also be gaussian for our linear system, and thus fully described by its covariance function:

$$\text{Cov}_z(t_1, t_2) = \int_{-\infty}^{\infty} \int_{-\infty}^{\infty} \text{Cov}_y(\tau_1, \tau_2) \cdot h(t_1 - \tau_1) \cdot h(t_2 - \tau_2) d\tau_1 d\tau_2 \quad (7.9)$$

But:
$$\text{Cov}_y(\tau_1, \tau_2) = \phi(\tau_1) \delta(\tau_1 - \tau_2) \quad (7.10)$$

where: $\delta(\tau_1)$ is the Dirac delta function

$\phi(\tau_1)$ is the variance intensity function of a shot noise process equal to:

$$\phi(\tau_1) = \pi S_0 p(\tau_1) \quad (7.11)$$

where: S_0 is the power spectral density function.

The following values are taken from Ruiz (80) as well as Tajimi (65) for the above mentioned fitting parameters:

Natural frequency ω_n	= (4.8 to 5.0) π
Damping ratio	= 0.6 to 0.62
Variance intensity parameter ϕ_0	= 5.1×10^{-5} sec
Fitting constant c	= 0.15 sec^{-1}
t_0	= 5.0 sec

7.4 A Priori Component and Parametric Study

The parameters defining the a priori component are the natural frequency ω_n of Scale One, and the damping ratio ξ . The natural frequency ω_n is evaluated in the modal analysis of the cavity system and its range varies between the following values:

Case of a Shallow Cavity	ω_n	7.76	25.6	32	Hertz
	F	1.55	5.1	6.4	
Case of a Deep Cavity	ω_n	9.48	27.42	35.46	Hertz
	F	1.89	5.48	7.09	

The damping ratio ξ is dependent on the behavior of the rock environment. It can be estimated from in situ tests as suggested in Chapter 4. However all the existing studies consider ξ to lie between 0.05 and 0.25.

At this point the frequency ratio $F = \frac{\omega_n}{\omega_n}$ can be evaluated leaving the mass ratio $M = \frac{M}{m}$ to be the only undetermined parameter. Its determination is at least difficult, if not impossible. Indeed how can anyone, accurately evaluate the mass M of a rock medium contained within an area of one square kilometer. Moreover, the equivalent mass m is even more difficult to determine. Therefore a parametric study is

reformed to observe the influence of this parameter in the evaluation of the transfer function $|H|^2$. The results are illustrated in Figure 7.4 as obtained from Subroutine MAX. As it can be seen, the influence of M is small for the range of F values between 1 and 4 and for damping ratios of $\xi = 0.05$ and $\varepsilon = 0.05$. It can be concluded then, that the important parameter influencing the evaluation of the transfer function $|H|^2$ is the frequency ratio F . Figure 7.5 shows the results obtained for the transfer function when F varies between 1 and 3.

Interestingly enough, for values of the Natural frequency ω_n of the a priori component, three times larger than the frequency ω_n of the a posteriori component, the surface measurements can not be used to estimate the accelerations at depth, which is in concordance with the common sense. On the other hand, for F ranging between 0.8 and 1.3, - a much more realistic case - the surface motion can effectively give an indication of the underground movement.

At this point all the elements exist to proceed to the generation of earthquakes signals.

7.5 Generation of Pseudo-Earthquakes

The model described so far follows Ruiz's procedure of filtering a digitally obtained white noise. Indeed, a sequence of white numbers possessing a gaussian distribution with a zero mean and a unit variance, is commonly obtained from the following expressions:

$$\begin{aligned} n_i &= (-2 \ln r_i)^{-1/2} * \cos (2\pi r_{i+1}) \\ n_{i+1} &= (-2 \ln r_i)^{-1/2} * \sin (2\pi r_{i+1}) \end{aligned} \quad (7.13)$$

where: r_i is a sequence of independent random numbers uniformly distributed in the interval (0,1).

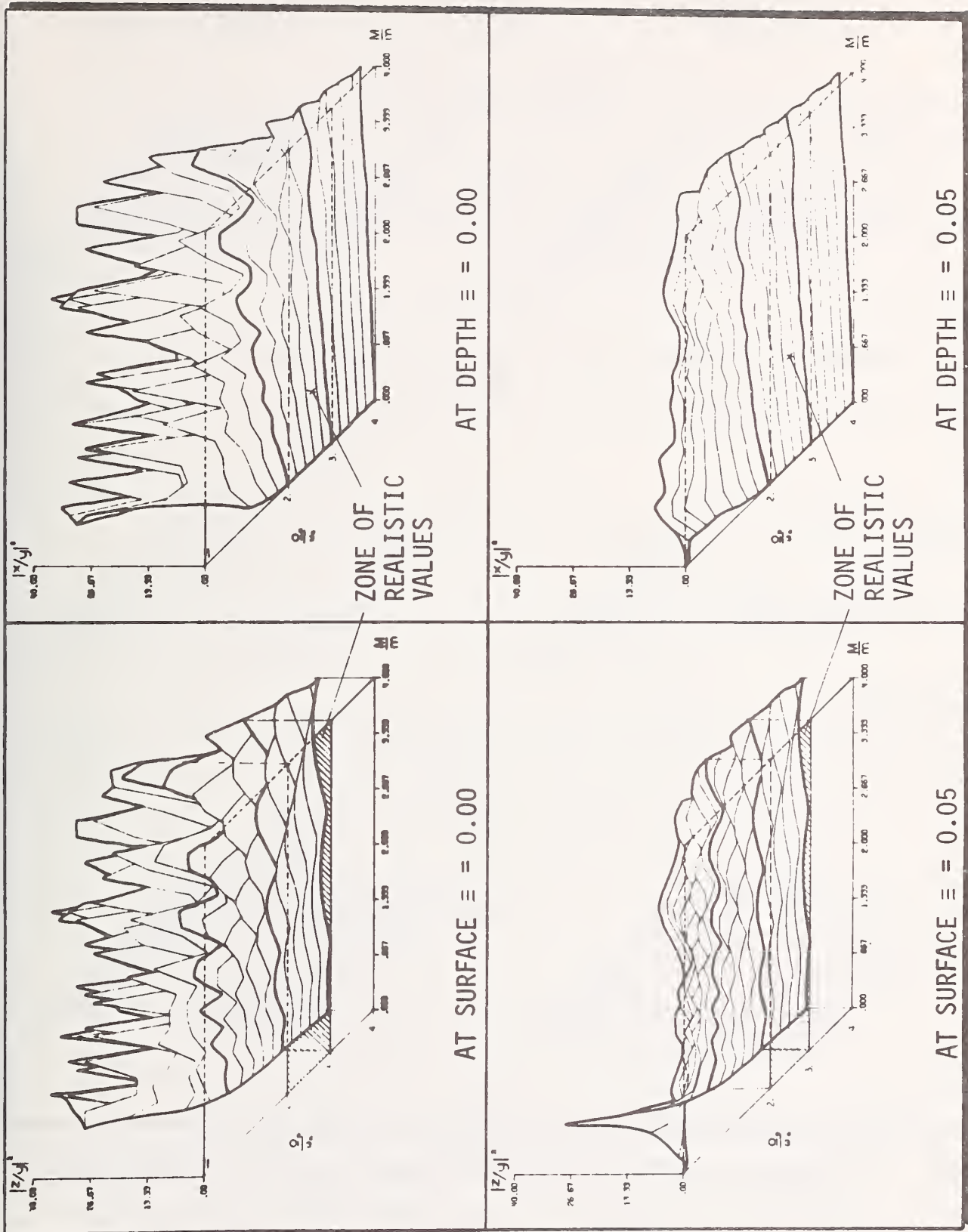


FIGURE 7.4 MAXIMUM VALUES OF THE TRANSFER FUNCTION H^2

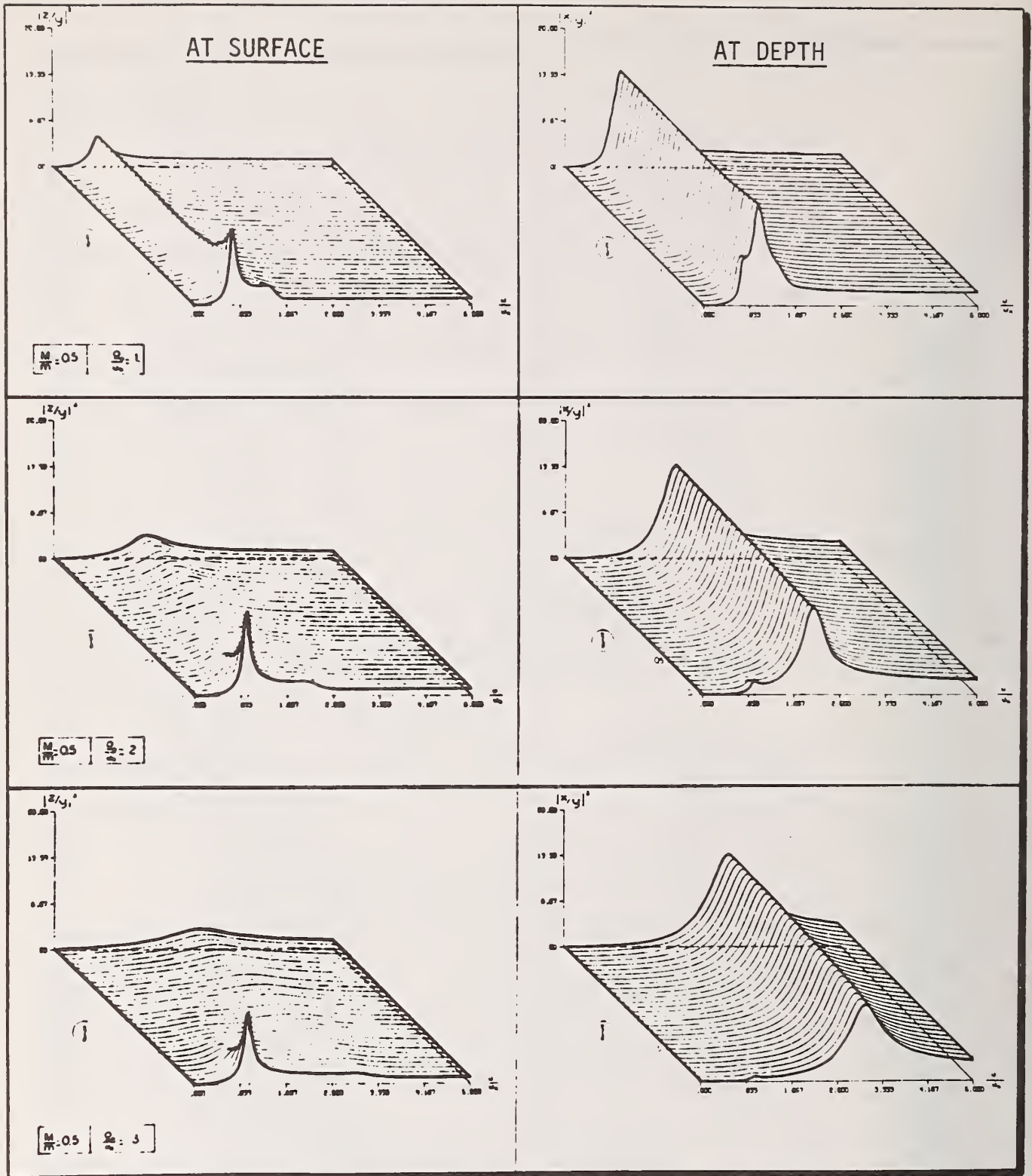


FIGURE 7.5 TRANSFER FUNCTION $(H)^2$ FOR DIFFERENT VALUES OF THE FREQUENCY RATIO F

The nonstationarity is obtained by multiplying n_j by a shaping function $SF(t)$ which is defined in terms of the variance intensity function $\phi(t)$ (given in Equation 7.12), as follows:

$$SF(t) = \left[\frac{\phi(t)}{\pi S_0} \right]^{\frac{1}{2}} \quad (7.18)$$

where: S_0 is the intensity of the white noise.

Finally the input to the model is provided by the following expression:

$$\ddot{y}(t) = \frac{\phi(t)}{\Delta t}^{\frac{1}{2}} n(t) \quad (7.19)$$

If initial conditions of zero velocity and zero displacement are assumed, then the acceleration at the cavity's depth can be expressed as the convolution:

$$\ddot{x}(t) = \int_{-\infty}^{\infty} \ddot{y}(t) \cdot h_D(t-\tau) dz \quad (7.20)$$

where $h_D(t-\tau)$ is the inverse Fourier transform of the complex transfer function $H_D(j\omega)$ defined by Equation 7.6.

It is to be noticed that the a priori component is present only through the function $h_D(t)$ and acts like a scale factor of the geologic environment, while the a posteriori component both, influences the variance intensity function $\phi(t)$, and scales the pseudo-earthquake according to recorded earthquake signals.

The last operation consists of decomposing the obtained pseudo-acceleration into two signals according to the scheme suggested in Chapter 3. Such a decomposition is illustrated in Figure 7.6, in which the low frequency content and the high frequency content signals are plotted. The low frequency content signal constitutes the input acceleration for Scale One, while the high frequency content signal provides the input to Scale Two. The results of this procedure, Figure 7.5,

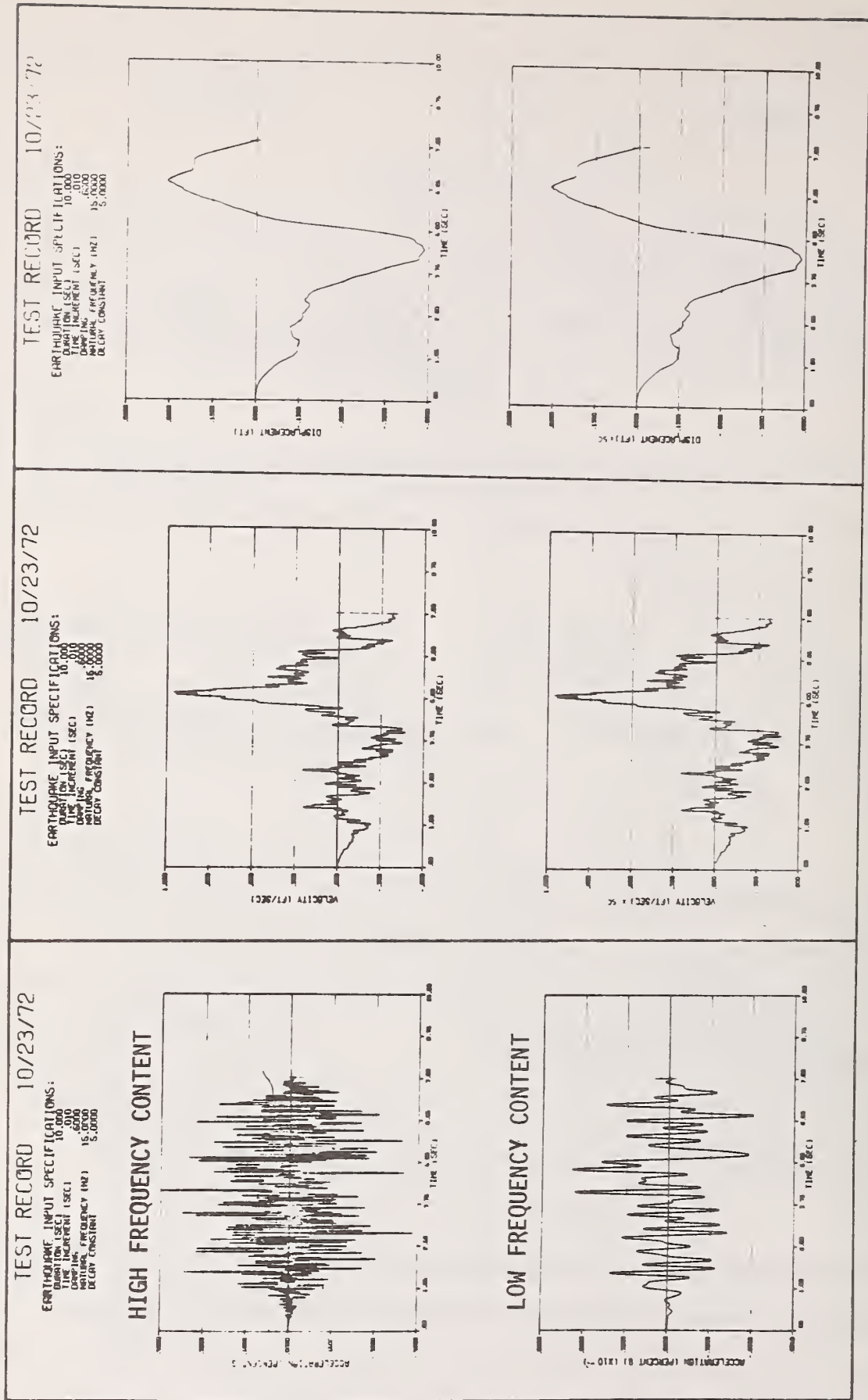


FIGURE 7.6 DECOMPOSITION OF THE GENERATED ACCELERATION SIGNAL

exhibit an overall similarity with the work of Kanai et al., (45). Specifically they represent the frequency distribution of the acceleration signal by plotting the number of 0-line crossings of the signal vs. the length of the corresponding time intervals, Figure 7.7. It is believed that there exists a direct analogy between the numbers of 0-line crossings and the transfer function of the signal, while frequencies and periods are related by an inverse relationship. An interesting similarity is thus seen to exist between the proposed generated signals and observed earthquake signals.

OBSERVED EQ. SIGNALS (after Kanai (45))

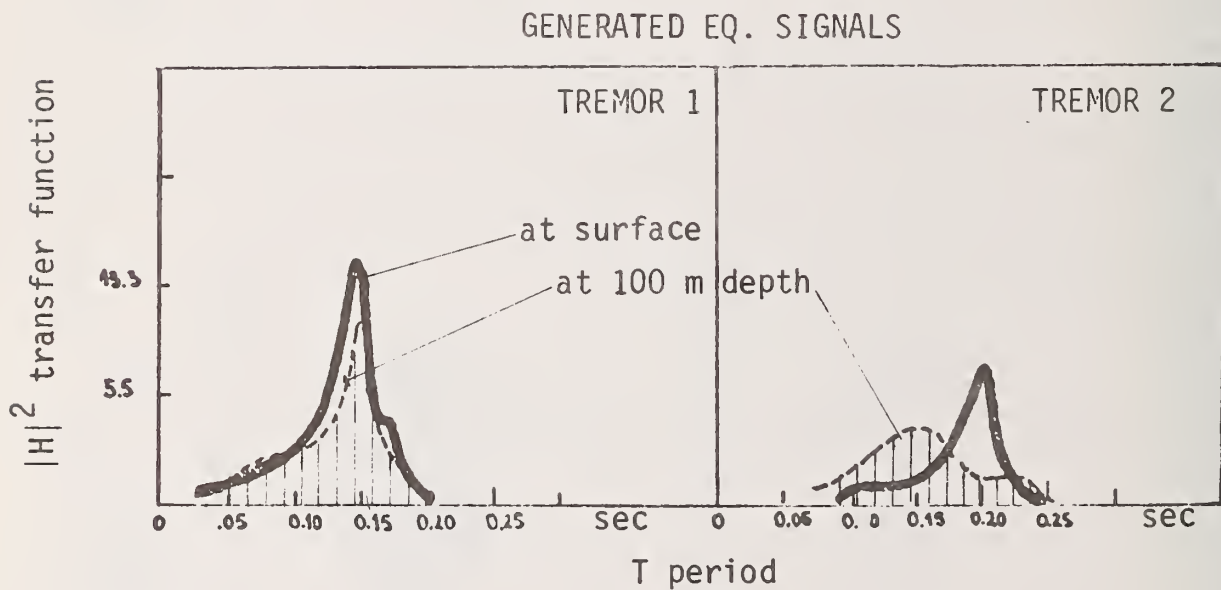
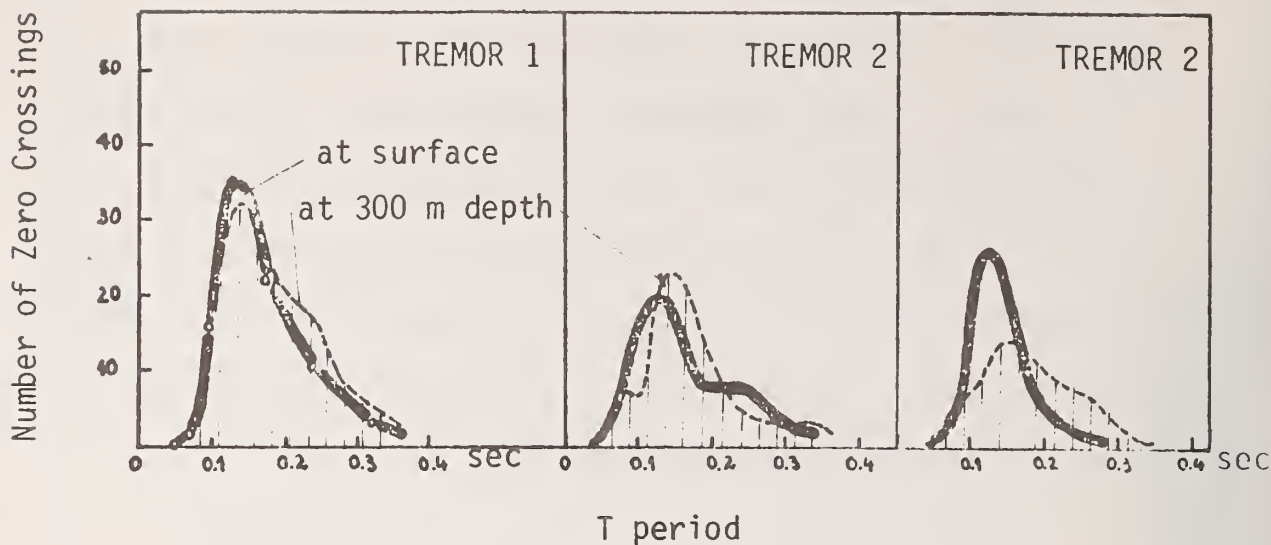


FIGURE 7.7 OBSERVED SIMILARITY BETWEEN PROPOSED GENERATED SIGNALS AND OBSERVED EARTHQUAKES

CHAPTER 8
EVALUATION OF DESIGN ALTERNATIVES

8.1 Introduction

The analytical model defined in the previous chapters provides the required quantification to evaluate the performance of a given cavity system under seismic conditions. However for a given geologic site and an expected earthquake perturbation many engineering alternatives exist. The need is then to justify the selection of one of these, based on a number of criteria. Strictly speaking this is an optimization problem in the general sense of the term. It is recognized though that for large engineering projects it is difficult to incorporate in an optimization scheme the great amount of detail and complex mechanism involved in the physical-engineering system.

A way around this difficulty is by using accumulated experience and technological knowledge to identify an exhaustive list of performance criteria to make possible the comparison of different classes of technological alternatives. Finally a sorting among the discrete number of alternatives permits their listing in a decreasing order of attractiveness. The sorting of the cavity system alternatives can be performed on the basis of the merit of each alternative as summarized by a performance profile over the previously mentioned criteria. A computational scheme performing such a "sorting" operation exists in ELECTRE developed by B. Roy (79).

The two major steps in implementing the above sorting scheme are primarily the determination of all possible technological alternatives for the engineering project at hand, and the definition of adequate criteria of selection. These steps are essential in order to obtain a sound alternative selection. They are presented in the following sections for the case of underground cavity systems.

8.2 Classes of Alternatives for Cavity Systems

There are three specifications in cavity systems that permit isolation of the possible classes of alternatives, namely the geometry of the opening, the structural system for the stability of the opening, and the depth of excavation.

Two geometric configurations typical of existing underground facilities are retained here for the cavity system: The horseshoe shape and the circular shape.

The systems most commonly used to maintain stability of the opening are a simple concrete liner or the combined system of a concrete liner and rock bolts.

Finally an important decision concerns the depth of excavation of the cavity system. In this study only a shallow cavity system will be compared to a deep one. Both locations are anticipated to offer advantages and drawbacks.

A combination of the above proposed possibilities leads to a total of eight different alternatives. This number does not represent an upper limit of all possible different alternatives. It is only selected for convenience of the analysis. However it is emphasized that the retained alternatives must represent a set of

homogeneous equal candidates. Each such alternative should optimally satisfy a given number of specifications such as cost-effectiveness, efficiency, level of reliability etc.

8.3 Classes of Criteria of Selection

All human activities ultimately can be described as a sequence of consecutive decision-making processes of varying importance, parties interested, extent of impact, etc. This is particularly true for large engineering projects whose impact may be felt over a large portion of society not to mention the natural environment itself. Appropriately then the final decisions over such issues impinge on the collectivity by means of decision-making bodies, agencies etc. While engineers cannot be substituted for these decision-making bodies, the engineers' role is becoming increasingly important in providing necessary, relevant and adequate information about the project at hand. Indeed, different levels of decisions can be recognized, from the basic decision of whether to accept a project or not, to detailed decisions about a specific component. Accordingly, different sets of objectives and criteria suit the different levels of decisions. An example of such criteria of selection can be taken from the following partial list: economic, technologic, aesthetic, environmental impact, flexibility, and even political. Obviously engineers are primarily involved with the technologic criteria. Yet, limited as the list of technologic criteria alone may be, the associated decision process remains complex, further complicated by the accumulation of knowledge in the intangible form of experience. This study attempts to rationalize the traditional engineering judgement based on knowledge and experience.

From the technical point of view, the performance of a given engineering project can be described or characterized by a number of parameters generally defined as attributes. A number of these attributes can be retained to be used as criteria of technical performance. For the case of the performance of underground openings three categories of such attributes can be distinguished, namely, the initial physical conditions, the dynamic response of the cavity system, and the reliability attained at different points on the wall of the opening. More specifically, for each category the following attributes are retained:

a. Initial Physical Conditions (Static Analysis)

R.Q.D. - Rock Quality Designation,

Stress field created by the excavation, and the corresponding Stability Factor of the liner

b. Dynamic Response (Dynamic Analysis)

Natural Frequency of the cavity system,

Input Dynamic Signal, and

Maximum stress level reached during the earthquake

c. Reliability Conditions (Conventional Approach)

Safety Factor at the walls of the opening

Safety Factor at the roof of the opening

The previously mentioned subjectivity in an expert's judgment, attributed to his accumulated experience and resulting in a different value attached to each one of the above attributes, can be quantified by means of a set of weight coefficients. Moreover, two components for each weight coefficient can be imagined, the one heuristic translating the expert's experience and intuition, the other deterministic

translating the expert's 'confidence' in the numerical prediction or estimation of every specific attribute. This is particularly true for parameters having a statistical character as is the case for the performance of the cavity system under seismic conditions. Such 'confidence' can be quantified by means of the coefficient of variation of the corresponding attribute. Alternately, the notion of entropy, as used in Information Theory (97), can provide a measure of the above 'confidence'. Summarizing, the weight coefficient $W(p)$ attached to attribute p is given as follows:

$$W(p) = H(p) \oplus CVR(p) \quad (1)$$

where: $W(p)$ is the weight coefficient of attribute p
 $H(p)$ is the heuristic component of the weight coefficient of p
 $CVR(p)$ is the deterministic component of the weight coefficient of p , for example coefficient of variation of attribute, or entropy of attribute,
 \oplus denotes a law of composition of the two above components. Simple addition is self-justified in the case of weight coefficients.

8.4 Formalization of Sorting Algorithm

The proposed procedure can be described as a "multiobjective optimization" or as a "choice with multiple criteria." The latter description shows that the method proposed by B. Roy (79) can handle also qualitative information.

In order to describe the algorithm that is used in the search for the more adequate structural configuration for the cavity system, first the problem components have to be defined.

8.4.1 Problem Components and Nomenclature

The problem components, nomenclature and proposed procedure, is given in point form as follows:

1. A set of 'n' alternatives

$$(A_1, A_2, \dots, A_n) = (A) \quad (8.2)$$

As such is considered the discrete sequence of alternatives as defined at the beginning of this chapter, one of which has to be selected upon its performance over the selection criteria.

2. A set of 'm' criteria

$$(p_1, p_2, p_m) = (p) \quad (8.3)$$

They are extensively defined in section 6.3.

3. The application of the 'm' criteria to each of the 'n' alternatives produces the multidimensional profile of performance of the 'n' alternatives at hand.

4. The relative importance of the criteria is expressed in terms of a weighting coefficient $W(p)$, $p = 1, \dots, m$.

5. An ordering γ_p among alternatives, according to criterion p is defined as a mapping

$$\gamma_p: (A_i) \rightarrow K_p \quad p = 1, \dots, m, \quad (8.4)$$

K_p being the change line ordering according to criterion p . The elements and procedural steps of the method being given above, the goals of the method are two-fold:

1. Permit the selection of the "best" alternative (A_i)
2. Produce a finer ranking of the top alternatives so that the introduction of new criteria will permit the ultimate selection of the "best" alternative.

8.4.2 Outranking Relation and Basic Assumptions

The method used to achieve the above two goals is to determine a partial order stronger than the product of the 'm' complete orders associated with the 'm' criteria.

Such a partial order is achieved in the present algorithm by defining an outranking relation R, such that a dichotomy operated on the set of alternatives (A_j), the one subset called the "core" or "kernel" containing a small number incomparable among themselves but altogether better than the remaining subset of rejected alternatives. The outranking relation R is defined in three successive steps developed hereafter. It is based on the concord and discord indices concept which is central to the whole method.

Step No. 1. It can be shown (78), that the complete orderings γ_p according to criterion p form one "oriented graph" $G_p = (A, U_p)$ whose nodes represent the alternatives (A_j) and the arcs U_p are defined by:

$$\text{Arc } (A_i, A_j) \in U_p \text{ if and only if } \gamma_p(A_i) \geq \gamma_p(A_j)$$

that is arc $A_i \rightarrow A_j$ signifies that alternative A_i is higher ranked than A_j . There is one such graph for each criterion p. These complete order graphs display the properties of transitivity and completeness.

Step No. 2. At this point, the 'p' G_p graphs need to be reduced to a unique graph $G = (A, U)$ synthesizing the p different criteria.

First we notice that all orders $A_i \rightarrow A_j$ satisfying all 'p' criteria (unanimity condition), belong to $G(A, U)$:

$$(A_i, A_j) \in U_p \quad \forall p = 1, \dots, m \quad \rightarrow \quad (A_i, A_j) \in U$$

In fact, this partial order unanimity graph $G_0 = (A, U_0)$, where $U_0 = \bigcap_{p=1}^m U_p$, is a subset of $G = (A, U)$ containing an extremely small number of alternatives. Often times there is no alternative satisfying the unanimity condition. This is a serious limitation overcome by defining indicators of concord or discord among the different criteria, allowing relaxation of the too stringent unanimity condition. To this effect, a Concord Index and a Discord Index are defined as follows:

Concord Index c_{ij} . It is meant to measure how well the hypothesis is that alternative A_i outranks alternative A_j . It is defined as the percentage of criteria in favor of the above hypothesis:

$$c_{ij} = \frac{\sum_{p \in C(i,j)} W(p)}{\sum_{p=1}^m W(p)} \quad (8.5)$$

where: $C(i,j)$ is the class of criteria according to which A_i outranks A_j

$W(p)$ is the weight coefficient of criterion p

The Concord Index c_{ij} displays the following properties:

$$\frac{0 \leq c_{ij} \leq 1}{c_{ij} = 1 \leftrightarrow (A_i, A_j) \in U_0} \quad (8.5)$$

Discord Index $d_{ij}(s)$. It is meant to measure how strong the opposition is, to the assertion that A_i outranks A_j . Designating by $D(i,j)$ the class of criteria according to which A_i does not outrank A_j , the Discord Index is defined as:

$$d_{ij}(s) = \text{the } s^{\text{th}} \text{ element of the decreasing ordered set } T \quad (8.7)$$

$$T = \left\langle r_p : r_p = \frac{|\gamma_p(i) - \gamma_p(j)|}{R_{\text{MAX}}} \quad \forall p \in D(i,j) \right\rangle$$

where: $\gamma_p(i)$ = scale value appreciation of alternative A_i according to criterion 'p'

RMAX = absolute max scale range among all criteria

For a pair of alternatives A_i, A_j satisfying the unanimity condition, we have:

$$D(i,j) = s - (A_i, A_j) \in U_0 \iff d_{ij} = 0 \quad (8.8)$$

also

$$0 \leq d_{ij}(s) \leq 1$$

Step No. 3. On the basis of the two indices introduced above, the outranking relation R is defined as:

$$\left. \begin{array}{l} A_i R A_j \\ (A_i \text{ outranks } A_j) \end{array} \right\} \iff \left\{ \begin{array}{l} c_{ij} \geq p; \quad 0 \leq p \leq 1, \text{ close to } 1 \\ \text{and} \\ d_{ij} \leq q; \quad 0 \leq q \leq 1, \text{ close to } 0 \end{array} \right. \quad (8.9)$$

and the associated graph $G(p,q,s) = (A, U(p,q,s))$ defined so that:

$$(A_i, A_j) \in U(p,q,s) \iff \left\{ \begin{array}{l} c_{ij} \geq p \\ c_{ij}(s) \leq q \end{array} \right. \quad (8.10)$$

It is to be noticed that the outranking relation R is defined in terms of three parameters, namely p, q and s, which permit parametric calibration of its severity.

The following properties can be readily established:

1. If $p \leq p'$, and $q \geq q'$, then $G(p', q', s) \subset G(p, q, s)$ that is, p', q' is a more restrictive set of parameter values.
2. $G(1, q, s) = G(p, 0, s); \forall s$ (unanimity graph)
3. R is not transitive, that is

$$A_i R A_j; \text{ and } A_j R A_k \not\Rightarrow A_i R A_k$$

4. The graph G may not be complete, that is circuits might appear.

5. Reducing the value of 'p' is equivalent to relaxing the requirements of agreement among criteria, concerning the hypothesis $A_i \rightarrow A_j$.
6. Increasing the value of q is equivalent to relaxing the requirements concerning the discordance of the above hypothesis.

Having at this point obtained a unique graph (G) (not complete and not transitive), reflecting the outranking relation R and operating a synthesis of the 'm' complete and transitive graphs of each criterion, the next task is to extract from this G the core or kernel containing in a classified order the definitively best alternatives.

Defining the core (or kernel) of the graph G(p,q,s)

The core 'S' of a graph is the subset of nodes (alternatives), satisfying the two following conditions:

1. External stability

$$\forall A_j \in \{A - S\}, \quad \exists A_i \in S \text{ such that } (A_i, A_j) \in U(p,q,s) \quad (8.11)$$

In other words, all eliminated alternatives are outranked by at least one alternative of the core.

2. Internal Stability

$$\forall A_j \in S \text{ and } \forall A_k \in S: \quad (A_j, A_k) \notin Y(p,q,s) \quad (8.12)$$

in other words, no alternative of the core is outranked by any other alternative of the core.

Since a complete and circuit-free graph admits one and only one core (kernel), eliminating the circuits from the graph G(p,q,s) is equivalent to "shrinking" or reducing the original graph G into G' whereby the circuits, as formed by equivalent alternatives are eliminated. The reduced graph G' then admits a unique core containing the

ultimately best alternatives. Consequently the strategy followed in ELECTRE consists of establishing the outranking relation R and the corresponding graph G , identifying and eliminating the circuits reducing G to G' and finally isolating the core or kernel of the reduced graph G' . This is shown in the flow chart of Fig. 8.2.

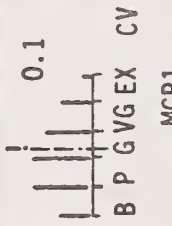
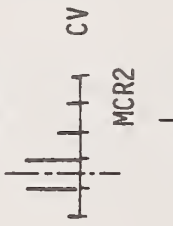
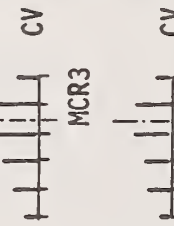
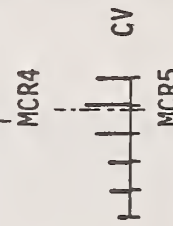
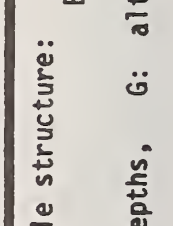
The basic assumptions required in the above procedure are summarized as follows:

1. The different criteria of performance assume a certain hierarchy of importance translated by a set of weight coefficients.
2. By means of these weight coefficients, the above criteria become comparable.
3. Moreover the criteria are assumed to be additively comparable for the purpose of defining the outranking relation.
4. A complete order of preference is assumed to exist for every criterion individually.
5. All criteria are assumed to admit a scale-structure, even though it may be a qualitative one.

8.5 Example of Application

Following the general ideas displayed above a hypothetical example is given here, as introduced in sections 8.2 and 8.3. It is only meant to provide a clear illustration of the program's implementation. A more complete case study is presented in Chapter 9.

All the elements of the study are presented in Figure 8.1 for hypothetical values. Only five criteria are taken into consideration among which the safety factor of the roof exhibits the least variability. Indeed the mean value of its coefficient of variation is the smallest

WEIGHT COEFFICIENT % of MAX. RANGE	DISTRIBUTION OF COEFF. OF VARIAT.	At 300 m. Depth		At 250 m. Depth				CRITERIA OF PERFORMANCE			
		⑧	⑦	⑥	⑤	④	③		②	①	
2		P*	B	P	G	G	VG	VG	EX	EX	Initial Stresses Before Dynamic Disturb.
1		G	EX	G	VG	P	P	B	B	CR2	Natural Frequency of Structure
2		EX	VG	VG	G	G	P	P	P	CR3	Input Dynamic Signal
2		G	G	P	B	B	VG	VG	EX	EX	Max. Stress Level After Seismic Load
3		B	G	G	EX	EX	P	G	G	CR5	Safety Factor Distribution

*qualitative scale structure: EX VG G P B
 Excellent Very Good Good Poor Bad

**D: alternate depths, G: alternate geometry, L: alternate Liner System

FIGURE 8.1 ILLUSTRATIVE EXAMPLE

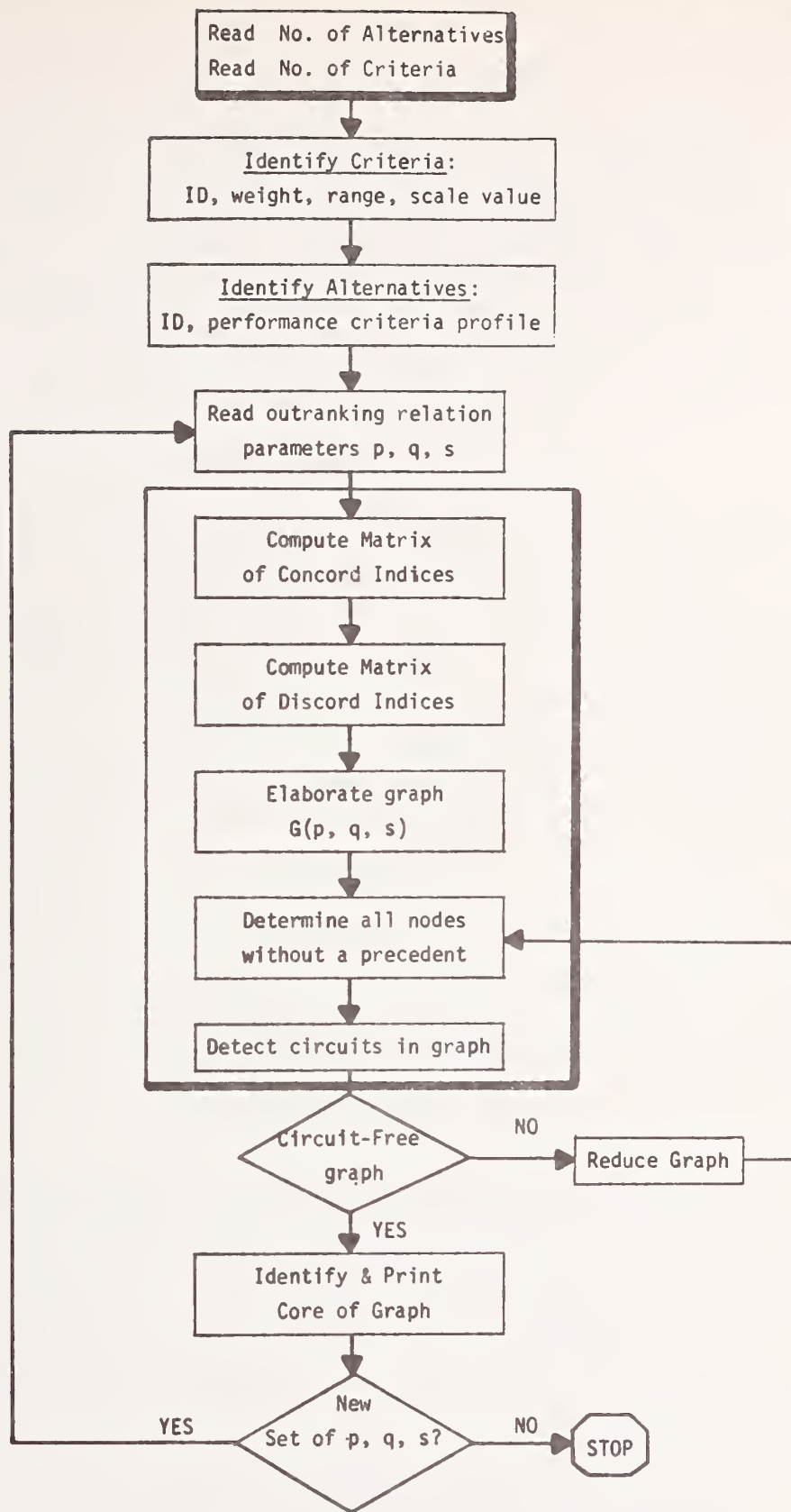


FIGURE 8.2 FLOW CHART OF PROGRAM DELECTRE

and therefore its corresponding weight coefficient is large. On the other hand the natural frequency of the structure exhibiting the largest variability assumes the smallest weight coefficient.

Another way to determine the weight coefficients attributed to the different criteria is by means of the entropy of information as suggested in section 2.3. It is given by the following expression

$$E = - \int_{-\infty}^{\infty} p(f) \log_2 p(f) df \quad (8.13)$$

where $p(f)$ is the probability density function of f . f is a random variable characterizing the criterion under consideration. At this stage $p(f)$ is unknown. It is determined according to the following maximization scheme (Maximum Entropy Criterion).

Maximize E subject to the following three constraints.

$$1. \quad \int_{-\infty}^{\infty} p(f) df = 1 \quad (8.14)$$

$$2. \quad \int_{-\infty}^{\infty} p(f) f df = \bar{f} \quad (8.15)$$

$$3. \quad \int_{-\infty}^{\infty} p(f) (f - \bar{f})^2 df = \sigma_f^2 \quad (8.16)$$

where \bar{f} is the mean and σ_f^2 the variance of the random variable f . Both these statistical estimates are provided by the uncertainty finite element analysis. The computational details of the above maximization problem are given in Appendix E. The probability density thus obtained is seen to be normal.

The corresponding maximal entropy is given by Eq. E.5. At this point each criterion has a particular maximal entropy value for each

one of the design alternatives under consideration. Therefore it seems plausible that the randomness of each criterion be reflected by the mean value of the entropy over the different design alternatives. Thus the previously mentioned weight coefficients attributed to each criterion can be determined making use of this mean value of the entropy. A low weight coefficient corresponds to a high entropy value and a high weight coefficient corresponds to a low entropy value. In other words the weight coefficients provide a measure of the confidence that one has to every specific performance criterion.

It was noted earlier that for the particular values of the triplet (p,q,s) of $(1,0,1)$, the graph G was reduced to the unanimity graph G_0 . It is then appropriate to use a number of combinations of p , q , and s so as to obtain a number of results corresponding to different levels of relaxation of the ordering relation. Such an example is shown in Fig. 8-3 where ELECTRE was used in conjunction with the above illustrative example for the two sets of values of (p,q,s) of $(.66, .40, 1)$ and $(.60, .30, 2)$. The effect of relaxation of the outranking relation is clearly illustrated. In fact a complete and orderly sensitivity analysis over the range of possible values of the parameters p , q , and s would seem necessary so as to qualify a final choice for the 'best' alternative by a measure of the statistical confidence of such a decision, as illustrated in Fig. 8.4.

Finally, it must be stressed here that the goal of the above procedure is not merely to give an answer to a decision problem, but rather to provide a general and justifiable methodology for handling rationally, often complex engineering decision problems.

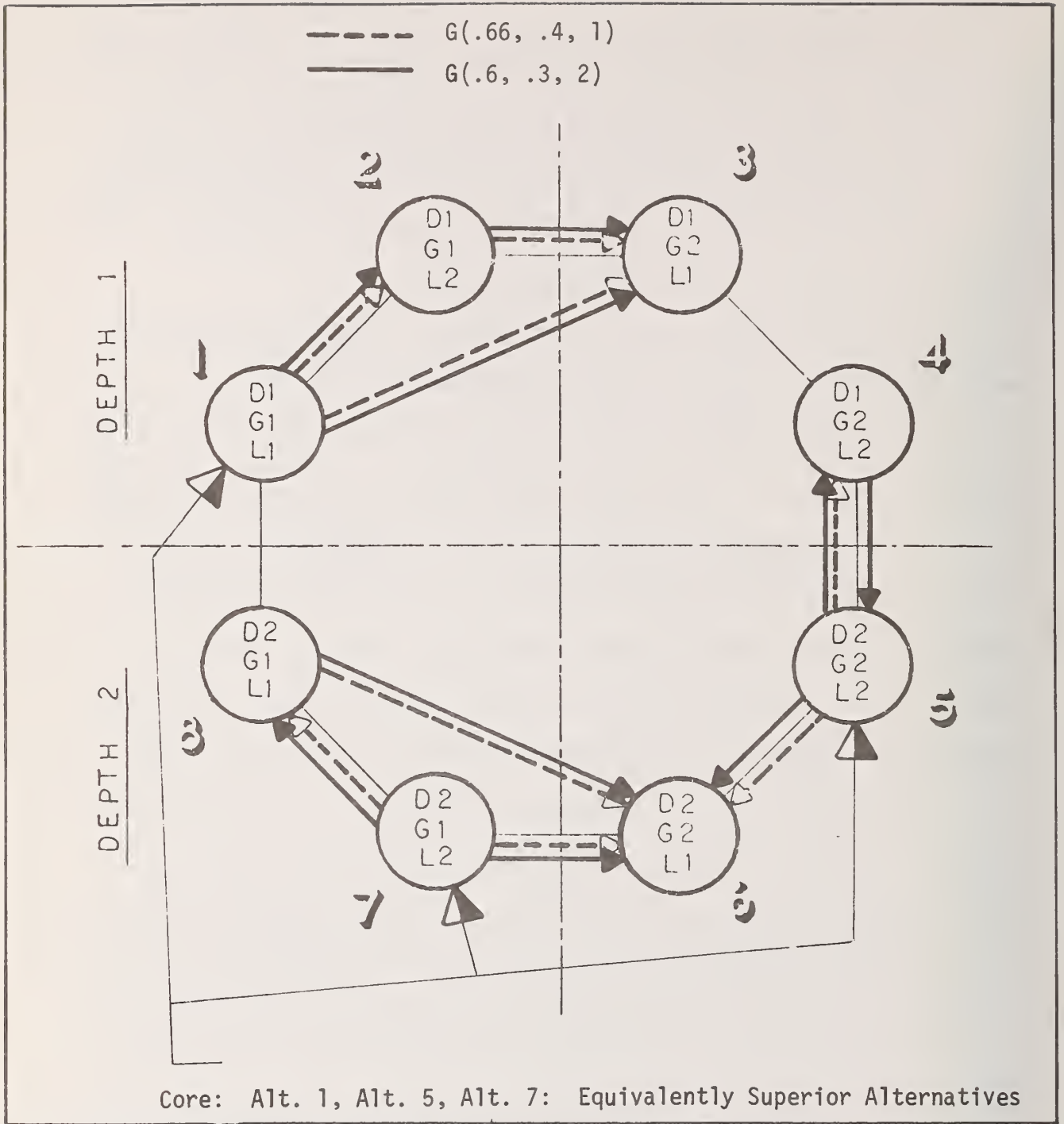


FIGURE 8.3 EXAMPLE OF APPLICATION OF DELECTRE

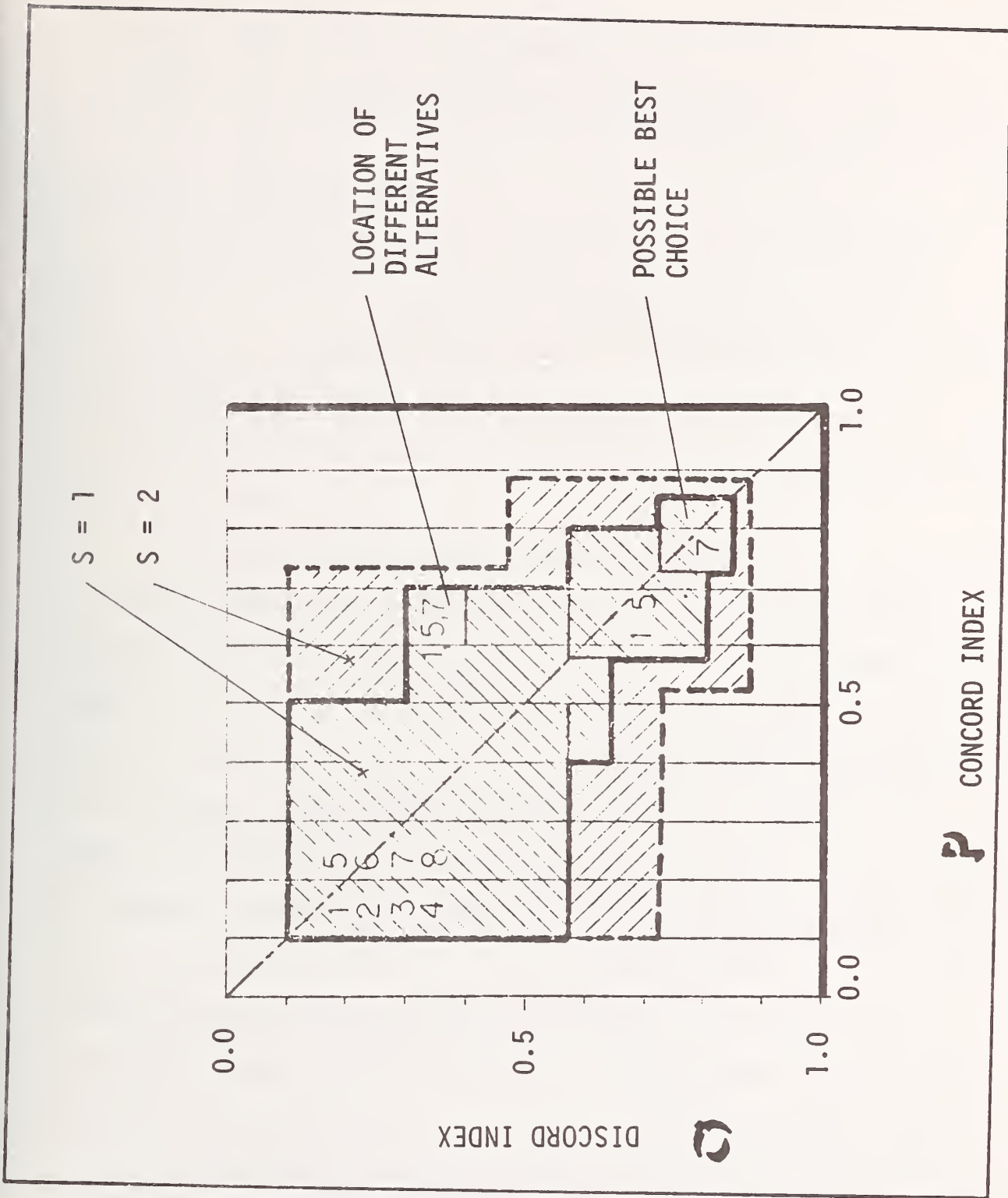


FIGURE 8.4 INTERPRETATION OF THE OUTPUT FROM DELECTRE

CHAPTER 9

EXAMPLE OF APPLICATION OF THE MODEL

The treated example is inspired from the following case histories:

1. The Poatina underground power stations in Tasmania (21),
2. The Swedish power producers study (88).

The main body of data concerning the physical parameters of the rock media are taken from the proceedings of the Johannesburg conference on site exploration (27).

9.1 Geologic Structure of the Site

The power station is located at the foot of a well defined and steep escarpment (Figure (3.4)). The stratigraphic investigation revealed a thick sandstone forming a resistant cap overlying horizontally bedded mudstones and siltstones.

The main fault forming the original escarpment has a length of about 1 km and follows a N-NW trend. Also in the area there are a number of smaller faults that follow this same direction and a further group of faults with a N-E trend.

An exploratory shaft showed that the rock throughout the 200 meters depth was stable and competent with however extensive water inflows in the upper and middle section.

The rocks in the middle and upper sections of the shaft are thick-bedded, compact homogeneous sandstones. These thickbedded series are open jointed and some formations have considerable lateral permeability.

At a deeper level the rock formations are dense, fine grained massive mudstones.

9.2 Input Data for the Analytical Treatment

Eight different alternatives are retained for a preliminary design of a nuclear power plant which will require a large underground excavation with a span of 50 meters.

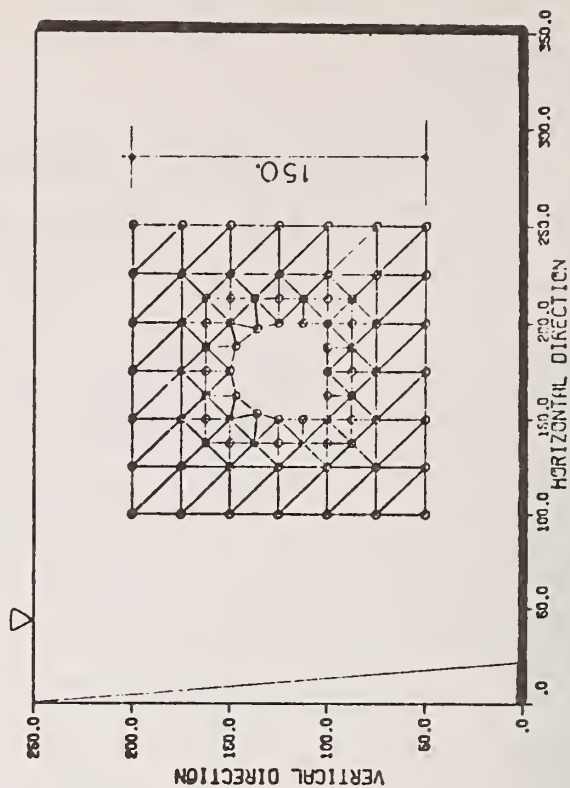
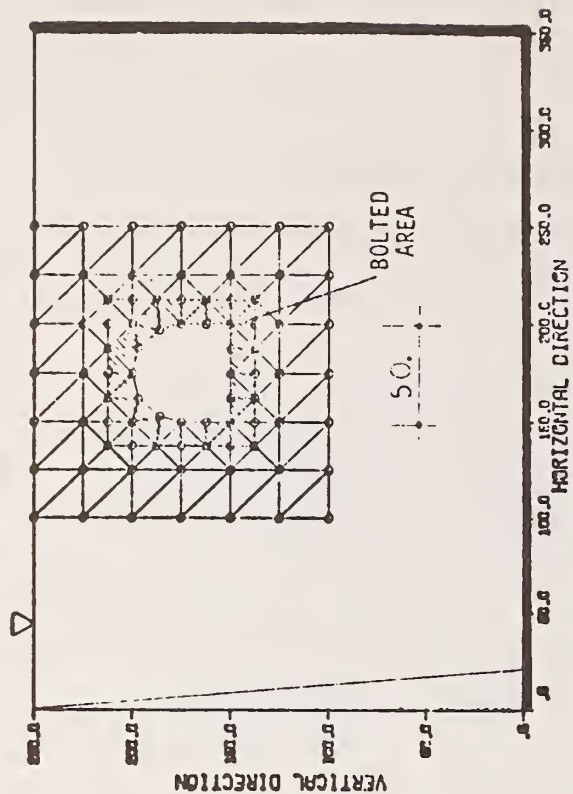
Two geometric configurations are retained, namely the horseshoe shape and the circular shape. Also two systems are retained for the stability of the opening, a simple concrete liner and a combined system of a concrete liner and rock bolts.

Finally two depths appeal to the designers: 75 meters and 125 meters (Figure (9.1)).

The complete sequence of computational steps is given in Figure 9.2. It should be noted that the output of each computational unit is checked by the plotting facility MESH to avoid any errors at the early stage of the analysis. Moreover MESH prepares, in an adequate format the data necessary for the next encountered step. Finally at the end of the analysis a computational unit performs the statistical analysis of the different variables under consideration, and describes the behavior of the cavity system. Specifically only the variables related to the finite elements surrounding the opening are retained.

The proposed uncertainty analysis is essentially based on the statistical information obtained from a site investigation. More specifically the fundamental statistical parameter is the variogram, a plot of the semivariance vs. the distance vector $\{d\}$ (see Chapter 5). The determination of the correct variogram curve is of great importance.

HORSESHOE GEOMETRY



CIRCULAR GEOMETRY

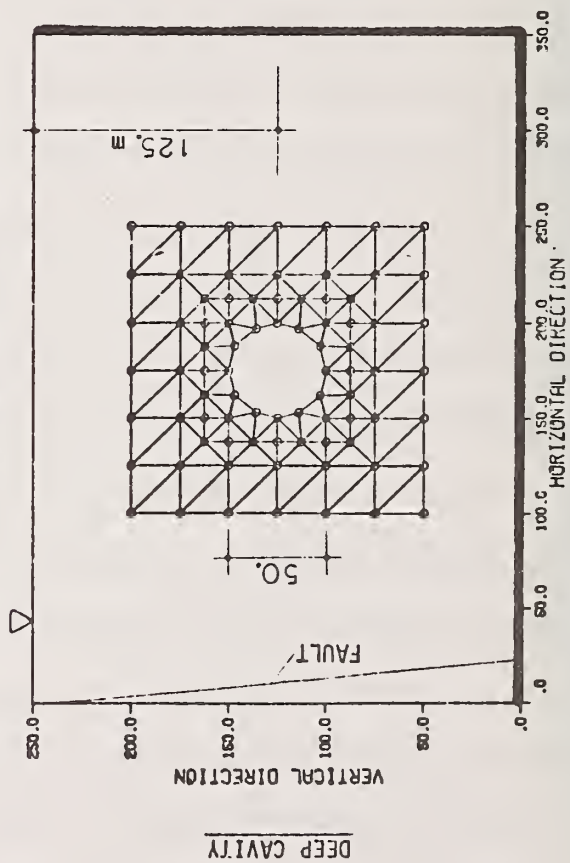
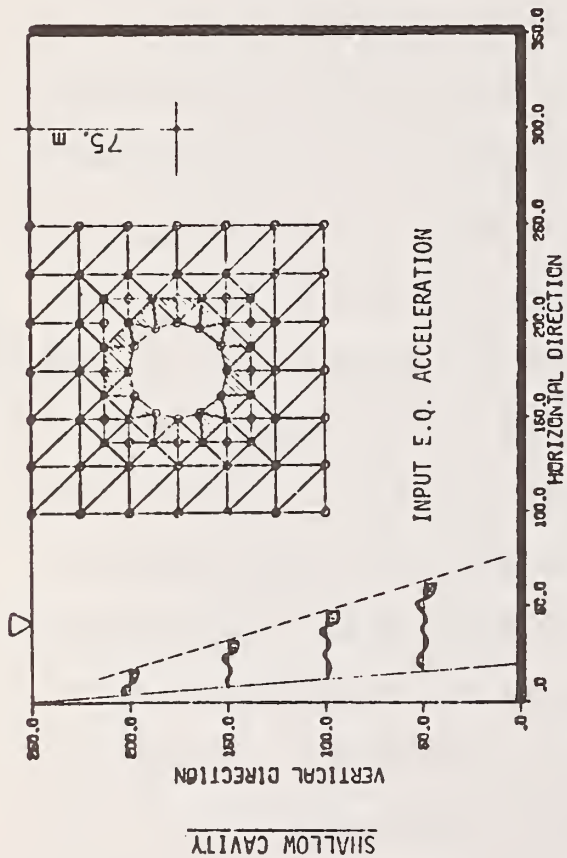


FIGURE 9.1 GENERAL GEOMETRIC CONFIGURATION OF DIFFERENT CONSTRUCTION ALTERNATIVES FOR THE PROPOSED CAVITY SYSTEM

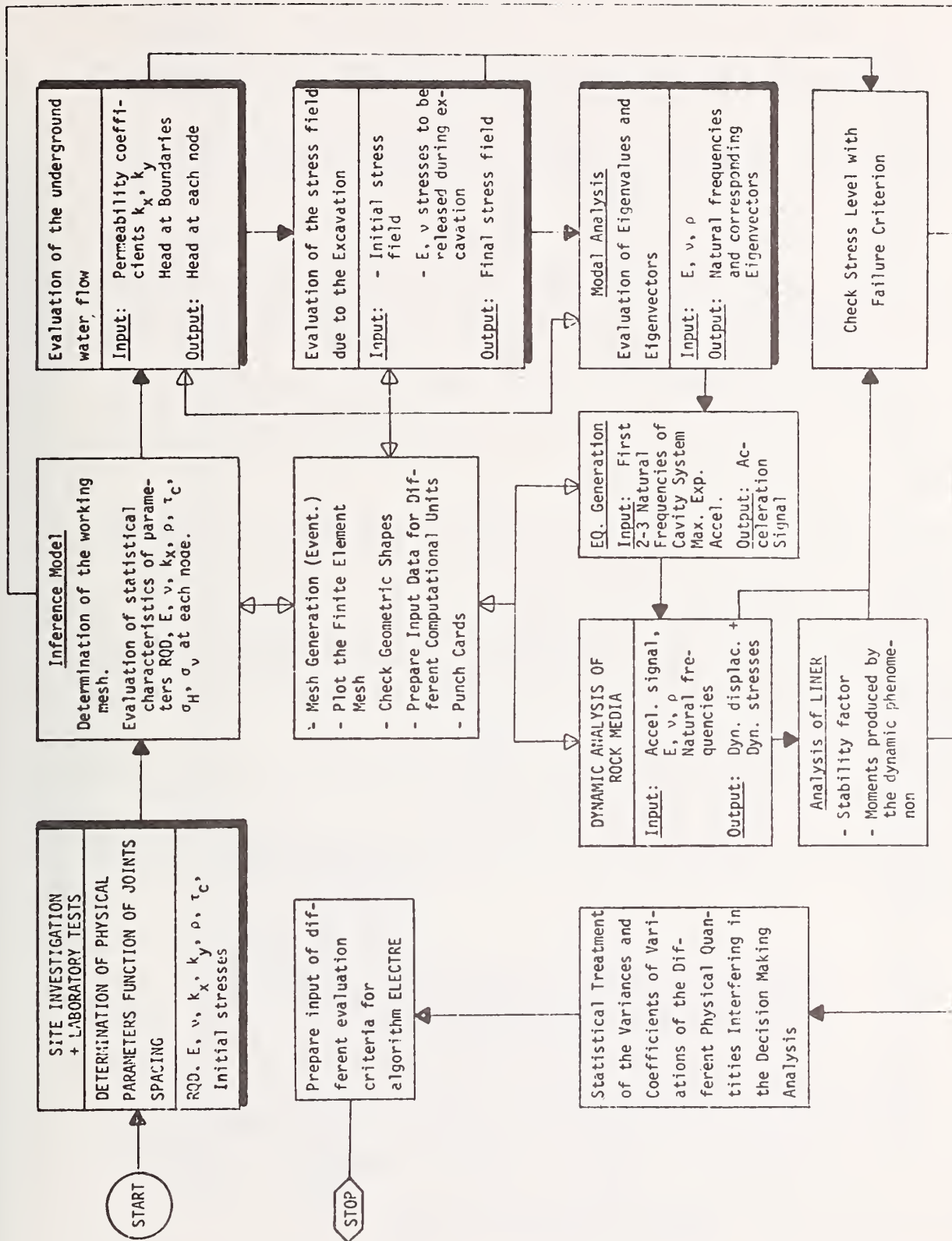


FIGURE 9.2 SEQUENCE OF COMPUTATIONAL STEPS

Figure 9.3 illustrates how to obtain a quick estimate of the variogram from the existing drilling grid of a site investigation. However it should be noted that the above procedure is valid only for the case of statistical isotropy, where the distance vector $\{d\}$ has no angular properties.

The adopted variogram curve in the present model is a linear model for the R.Q.D. (Rock Quality Designation) values and a De Wijs's model so far as the other physical parameters are concerned. The information obtained from a site investigation at 48 particular locations of the rock media are given in Table 9.1. These quantities constitute the input data to the inference model.

Through the computational unit INFMOD the coefficient of variations of the physical parameters under consideration are computed as shown in Table 9.2. They reflect the uncertainty with which the estimation is performed for each parameter. The results are conformal to the findings of other investigators. (see Figure 9.4)

The Poisson's ratio and the mass density exhibit the greatest variability with a maximum coefficient of variation of 0.36 and 0.21 respectively.

9.3 Intermediate Results of the Uncertainty Analysis Coupled with the Finite Element Approach

The organizational scheme of the input data necessary for this part of the study is provided by Table 9.3. The input file for each alternative is specified according to the three computational units related to the finite element procedure.

AREA 1 IN WHICH THE VARIOGRAM IS MEASURED FOR DIFFERENT PHYSICAL PARAMETERS

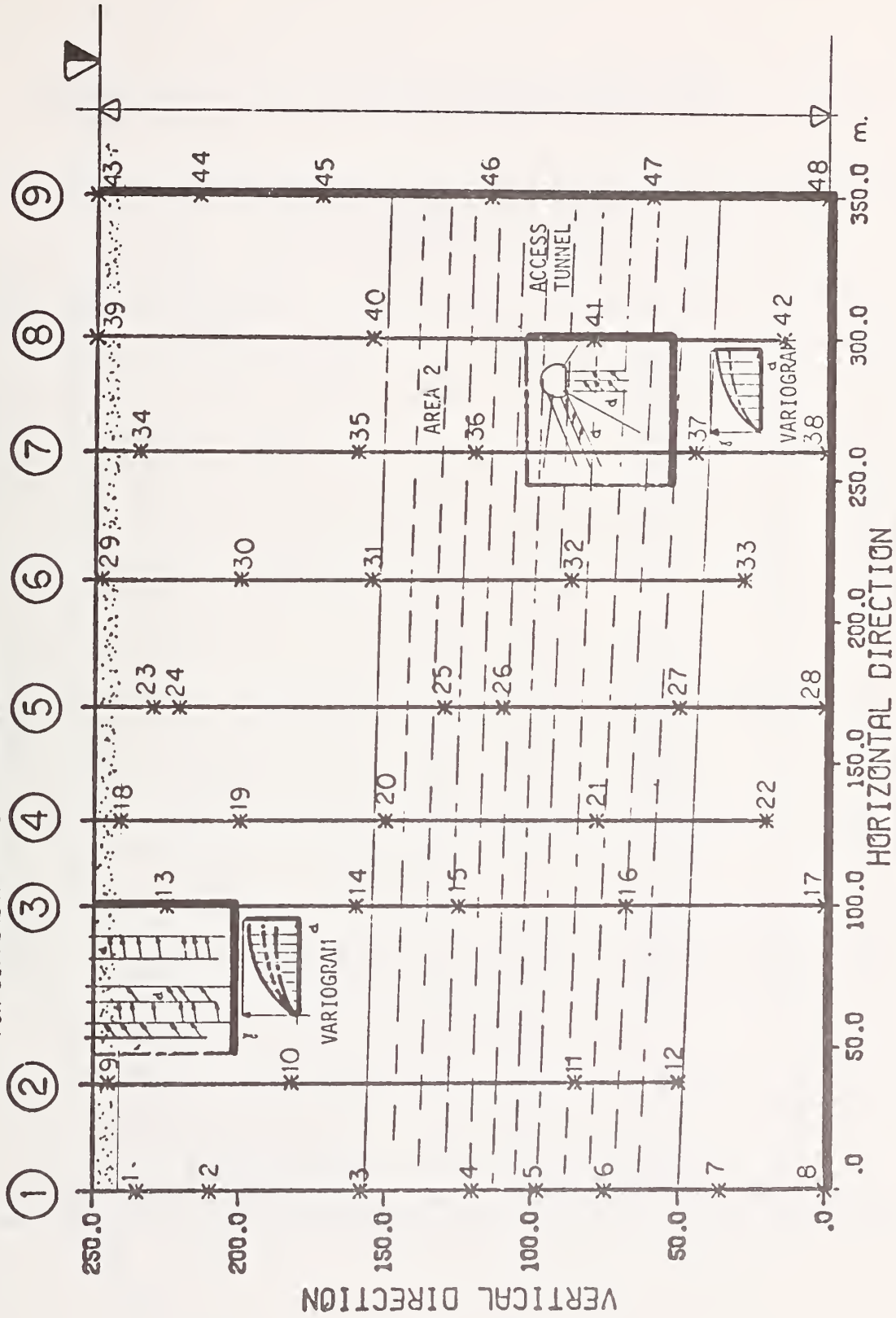


FIGURE 9.3 ORGANIZATIONAL SCHEME OF A SITE INVESTIGATION

TABLE 9.1 INPUT DATA OBTAINED FROM A SITE INVESTIGATION AND LABORATORY TESTS

SAMPLE NUMBER	R.Q.D.	INITIAL HOR. STRESS	INITIAL VERT. STRESS	PERMEABIL. COEFFICIENT	INITIAL MODULUS OF ELASTICITY	POISSON'S RATIO	STRENGTH PARAMETERS		DRY DENSITY	DAMPING RATIO
		$\sigma_H \text{ max}$	σ_V	k_x	E_i	ν	ϕ	τ_c		
	%	10^3 kg/cm^2	10^3 kg/cm^3	log (cm/sec)	10^5 kg/cm^2		DEGREES	kg/cm^2	gr/cm^3	
1	70	0.1	0.01	-4.	1.1	0.1	25.°	3.	2.3	0.12
2	82	0.14	0.02	-4.5	1.2	0.15	26.°	3.5	2.38	0.2
3	85	0.135	0.025	-5.2	3.5	0.25	35.°	5.	2.58	0.14
4	87	0.15	0.042	-5.2	4.0	0.26	38.°	6.	2.61	0.13
5	96	0.15	0.048	-5.0	4.1	0.27	39.4°	7.1	2.68	0.125
6	90	0.155	0.052	-6.	4.22	0.28	40.°	8.	2.71	0.12
7	89	0.16	0.067	-6.5	5.	0.3	41.°	8.1	2.72	0.12
8	97	0.154	0.07	-7.5	4.8	0.31	41.°	8.15	2.74	0.11
9	65	0.06	0.008	-3.8	0.8	0.12	24.°	2.5	2.28	0.23
10	79	0.13	0.017	-4.7	1.1	0.13	28.°	2.9	2.3	0.2
11	89	0.14	0.04	-5.2	4.22	0.28	38.°	8.	2.59	0.14
12	87	0.162	0.054	-6.2	4.28	0.39	39.°	8.1	2.63	0.13
13	73	0.12	0.012	-4.2	1.21	0.128	25.2°	4.2	2.3	0.61
14	80	0.15	0.02	-5.4	1.55	0.17	30.°	4.8	2.45	0.18
15	82	0.145	0.04	-5.2	4.1	0.28	38.°	5.2	2.62	0.14
16	89	0.16	0.06	-6.1	4.5	0.31	40.°	7.1	2.68	0.14
17	96	0.164	0.075	-7.4	5.1	0.34	42.°	8.3	2.71	0.12
18	68	0.08	0.0075	-3.5	0.79	0.1	23.°	2.5	2.29	0.21
19	78	0.12	0.019	-4.6	1.2	0.11	28.°	4.0	2.31	0.17
20	84	0.151	0.022	-5.1	3.9	0.18	32.°	5.2	2.55	0.74
21	90	0.158	0.048	-6.	4.1	0.31	36.°	6.1	2.68	0.13
22	92	0.16	0.063	-6.2	4.5	0.34	44.°	8.3	2.71	0.11
23	66	0.09	0.009	-4.1	1.1	0.13	21.°	3.8	2.44	0.22
24	69	0.10	0.010	-4.4	1.0	0.12	28.°	4.	2.44	0.21
25	74	0.14	0.038	-5.1	3.5	0.22	29.°	5.7	2.6	0.15
26	80	0.153	0.042	-5.3	3.8	0.25	35.°	6.2	2.61	0.14
27	94	0.16	0.05	-6.1	4.0	0.3	40.°	8.	2.69	0.12
28	97	0.16	0.072	-7.1	4.5	0.31	41.°	10.	2.72	0.1
29	64	0	0.06	-3.	0.82	0.1	20.°	2.3	2.9	0.2
30	75	0.10	0.018	-4.4	1.22	0.13	29.°	3.1	2.33	0.18
31	76	0.148	0.02	-5.0	3.4	0.24	34.°	4.8	2.54	0.13
32	85	0.13	0.04	-4.9	4.15	0.3	38.°	5.2	2.61	0.1
33	96	0.158	0.058	-6.1	4.6	0.34	41.°	6.2	2.69	0.1
34	68	0.092	0.008	-4.0	1.	0.14	26.°	3.5	2.35	0.2
35	72	0.142	0.018	-5.3	1.4	0.21	28.°	4.1	2.41	0.17
36	84	0.148	0.038	-5.1	3.8	0.28	34.°	5.4	2.53	0.15
37	93	0.156	0.048	-6.4	4.2	0.34	39.°	6.8	2.68	0.12
38	94	0.17	0.07	-7.0	5.1	0.35	42.°	8.	2.72	0.1
39	67	0.	0.	-3.3	1.	0.12	25.°	3.8	2.32	0.18
40	74	0.146	0.018	-4.8	1.9	0.15	29.°	4.4	2.37	0.14
41	87	0.16	0.044	-5.1	4.1	0.3	32.°	5.6	2.62	0.14
42	96	0.157	0.06	-6.3	5.3	0.38	40.°	8.	2.7	0.12
43	69	0.03	0.	-3.1	1.2	0.13	26.°	4.2	2.4	0.22
44	75	0.12	0.009	-4.3	1.4	0.15	28.°	4.7	2.52	0.2
45	86	0.13	0.015	-4.6	2.1	0.2	30.°	4.9	2.63	0.17
46	85	0.158	0.038	-5.2	3.85	0.29	38.°	5.7	2.69	0.14
47	92	0.142	0.047	-6.	4.25	0.31	40.°	6.	2.72	0.12
48	92	0.16	0.08	-7.2	5.2	0.34	40.°	8.4	2.74	0.08

TABLE 9.2 RESULTS OF THE INFERENCE MODEL

No. Nodes	COORDINATES		RQD		MODULUS OF ELASTICITY E		POISSON'S RATIO ν		MASS DENSITY ρ		PERMEABILITY COEFF. k_y	
	x	y	Expected Value	Coeff. of Variation	Expected Value	Coeff. of Variation	Expected Value	Coeff. of Variation	Expected Value	Coeff. of Variation	Expected Value	Coeff. of Variation
	[m]	[m]	%		10^5 kg/cm^2				gr/cm^3		$\log(\text{cm/sec})$	
1	150.	200.	76.89	0.008	1.70	0.3	0.14	0.36	2.38	0.21	4.64	0.11
2	175.	200.	75.53	0.005	1.66	0.19	0.14	0.22	2.39	0.13	4.56	0.069
3	200.	200.	75.03	0.009	1.61	.27	0.14	0.3	2.38	0.18	4.45	0.09
4	150.	175.	83.11	0.018	2.39	0.11	0.19	0.14	2.41	0.11	4.99	0.057
5	175.	175.	71.94	0.02	2.29	0.22	0.17	0.30	2.52	0.20	5.04	0.103
6	200.	175.	78.31	0.014	2.46	0.14	.19	0.17	2.43	0.14	4.76	0.073
7	150.	150.	84.06	0.015	3.44	0.098	.23	0.14	2.54	0.13	5.09	0.066
8	175.	150.	78.63	0.003	3.41	0.077	.23	0.11	2.56	0.10	5.05	0.052
9	200.	150.	75.14	0.005	3.45	0.15	.22	0.22	2.58	0.20	5.04	0.10
10	150.	125.	80.12	0.016	3.82	0.11	.26	0.16	2.60	0.16	5.29	0.08
11	175.	125.	75.85	0.003	3.58	0.08	.23	0.13	2.59	0.12	5.12	0.062
12	200.	125.	78.07	0.008	3.88	0.06	.26	0.10	2.58	0.10	4.95	0.054
13	150.	100.	83.74	0.013	3.81	0.11	.267	0.15	2.64	0.16	5.57	0.076
14	175.	100.	81.98	0.008	3.89	0.11	.266	0.16	2.62	0.16	5.24	0.085
15	200.	100.	82.20	0.002	4.03	0.07	.277	0.10	2.60	0.11	5.08	0.058
16	150.	75.	90.29	0.008	3.95	0.09	.29	0.12	2.67	0.13	6.0	0.062
17	175.	75.	88.21	0.006	4.029	0.17	.29	0.15	2.65	0.17	5.48	0.084
18	200.	75.	87.59	0.009	4.12	0.11	.29	0.16	2.63	0.17	5.21	0.091

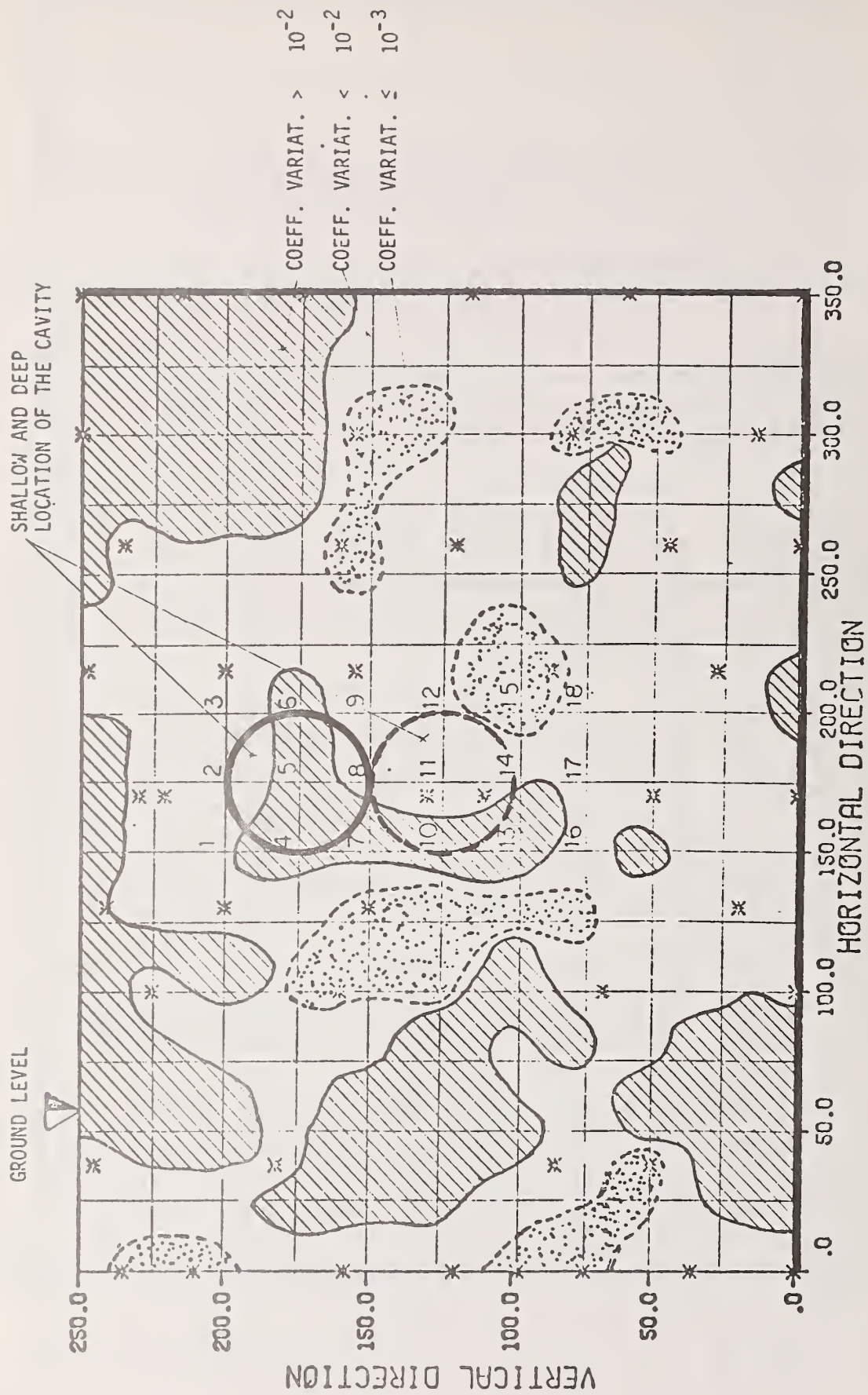


FIGURE 9.4 RESULTS OF INFMD (SPATIAL DISTRIBUTION OF COEFFICIENT OF VARIATION OF R.Q.D.)

TABLE 9.3 ORGANIZATIONAL SCHEME OF THE INPUT DATA RELATED TO THE F.E. ANALYSIS

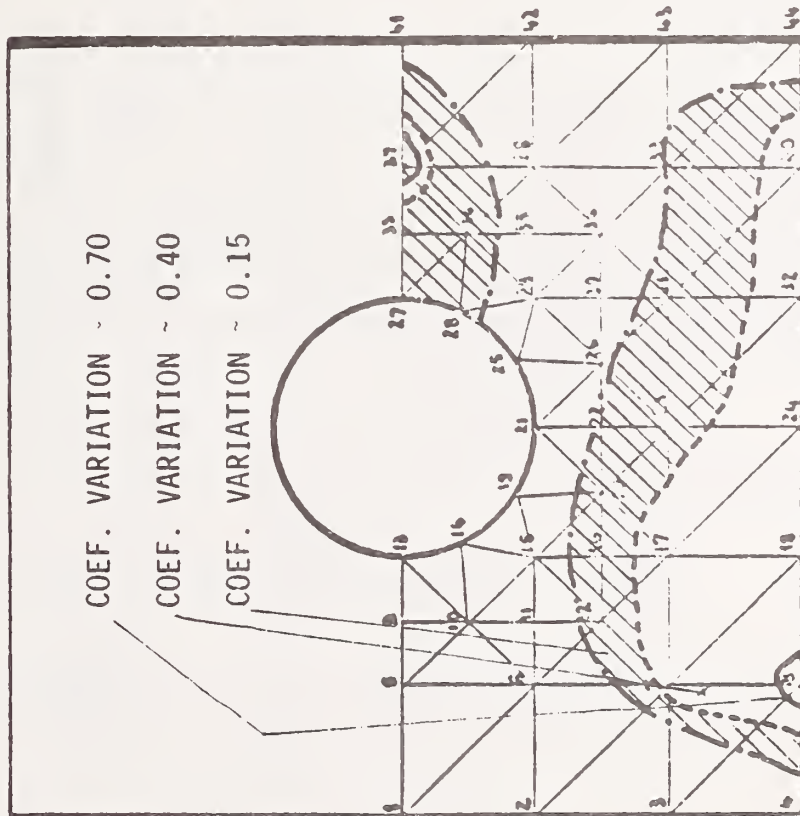
		DATA FILES OF STRUCTURAL CASES FOR THE FINITE ELEMENT ANALYSIS												
		SHALLOW, CAVITY						DEEP, CAVITY						
		GEOMETRY A			GEOMETRY B			GEOMETRY A			GEOMETRY B			
PERFORMED ANALYSIS	R. CONCRETE LINER	R. CONCRETE + BOLTS	R. CONCRETE LINER	R. CONCRETE + BOLTS	R. CONCRETE LINER	R. CONCRETE + BOLTS	R. CONCRETE LINER	R. CONCRETE + BOLTS	R. CONCRETE LINER	R. CONCRETE + BOLTS	R. CONCRETE LINER	R. CONCRETE + BOLTS	R. CONCRETE LINER	R. CONCRETE + BOLTS
	SCALE 1	SCALE 2	SCALE 1	SCALE 2	SCALE 1	SCALE 2	SCALE 1	SCALE 2	SCALE 1	SCALE 2	SCALE 1	SCALE 2	SCALE 1	SCALE 2
STFLOW EFFECT OF UNDERGROUND WATER	UFSA		UFSA		UFSA		UFSA		UFDA		UFDA		UFDB	
	ESA2	ESA2B	ESA2	ESA2B	ESB2	ESB2B	ESB2	ESB2B	EDA2	EDA2B	EDA2	EDA2B	EDB2	EDB2B
EVALUATION OF STRESS FIELD AFTER EXCAVATION	DSA1	DSA1B	DSA1	DSA1B	DSB1	DSB1B	DSB1	DSB1B	DDA1	DDA1B	DDA1	DDA1B	DDB1	DDB1B
	DSA2	DSA2B	DSA2	DSA2B	DSB2	DSB2B	DSB2	DSB2B	DDA2	DDA2B	DDA2	DDA2B	DDB2	DDB2B
DYNMODE MODAL ANALYSIS EVALUATION OF DYNAMIC STRESSES	LSA	LSAB	LSA	LSAB	LSB	LSBB	LSB	LSBB	LDA	LDAB	LDA	LDAB	LDB	LDBB
	STLINER		STLINER		STLINER		STLINER		STLINER		STLINER		STLINER	

First the effect of the underground flow is considered. Different heads at the boundaries are considered in accordance with the observed water table variation. The results of the computational unit STFLOW are illustrated in Figure 9.5 and given in Table 9.4. As can be seen the zone in which the coefficient of variation is large has smoother boundaries for the circular shape than the horseshoe shape. The obtained mean value of the coefficient of variation is almost identical for the two proposed shapes but can vary significantly at particular locations as the corner of the horseshoe shape. Interesting results are obtained for increasing permeabilities. Indeed as they become larger the head increases slightly, but the coefficients of variation decrease indicating that the flow conditions are steadier. The evaluation of the flow heads permit definition of the water pressure at any location of the cavity system, a quantity which is necessary for the evaluation of the shear strength.

In the next computational unit the effect of the excavation is estimated, either by releasing an equivalent to the initial amount of stress or by considering the displacements read on extensometers installed at the boundaries of the openings. The latter approach is adopted and the displacements used to evaluate the change of stresses are given in Table 9.5 (Figure 9.6).

The computations performed so far concern the static analysis of the cavity system and are related to scale 2. In the following the dynamic analysis is presented considering the effect of both scale one and scale two.

CIRCULAR CAVITY



HORSESHOE CAVITY

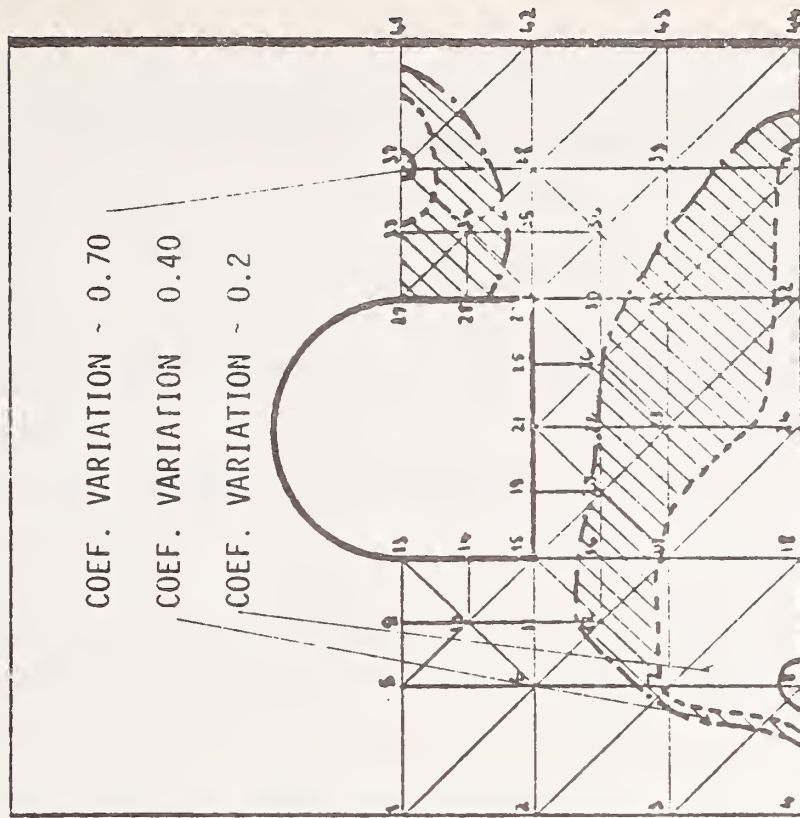


FIGURE 9.5 RESULTS OF UNDERGROUND FLOW FOR DIFFERENT CASES

TABLE 9.4 RESULTS OF THE UNDERGROUND FLOW ANALYSIS

No. Nodes	Coordinates/Local Ref. System		HEAD DIFF. = 14 m COEFF. OF PERMEABILITY k_y				HEAD DIFF. = 15 m $10k_y$		HEAD DIFF. = 20 m k_y	
	x	y	CIRCULAR GEOMETRY		HORSESHOE GEOMETRY		CIRCULAR GEOMETRY		HORSESHOE GEOMETRY	
	[m]	[m]	Total Head Expected Value	Coeff. of Variation	Total Head Expected Value	Coeff. of Variation	Total Head Expected Value	Coeff. of Variation	Total Head Expected Value	Coeff. of Variation
13	50.	75.	35.13	0.28	36.75	.29	35.96	0.027	41.96	.24
14	50.	62.5	39.08	0.31	37.49	.31	37.90	0.03	42.64	.26
15	50.	50.	39.83	.39	39.68	.39	40.62	0.038	44.52	.32
16	50.	37.5	43.14	.67	42.13	.58	43.88	.065	46.62	.48
17	50.	25.	44.64	.88	44.30	.88	45.34	.085	48.71	.76
18	50.	0.	47.2	1.40	47.22	1.43	47.90	.137	51.51	1.2
19	62.5	50.	39.94	.38	40.71	.42	40.61	.037	44.50	.36
20	62.5	37.5	41.52	.58	41.50	.54	42.15	.051	45.25	.47
21	75.	50.	39.55	.34	40.14	.37	40.06	.033	43.11	.33
22	75.	37.5	40.38	.48	40.66	.47	40.88	.047	43.63	.42
23	75.	25.	41.72	.77	41.82	.74	42.23	.076	44.90	.65
24	75.	0.	44.0	1.33	44.05	1.31	44.52	0.13	47.25	1.18
25	87.5	50.	36.97	.23	38.43	.27	37.26	0.024	40.39	.28
26	87.5	37.5	38.83	.38	39.29	.38	39.16	0.038	41.29	.39
27	100.	75.	32.60	.49	31.76	.58	32.77	0.049	32.59	.57
28	100.	62.5	33.61	.44	32.69	.52	33.80	0.044	33.58	.51
29	100.	50.0	35.8	.21	35.81	.21	36.01	0.021	37.00	.21
30	100.	37.5	38.24	.29	38.34	.29	38.47	0.038	39.71	.32
31	100.	25.	40.38	.56	40.41	.55	40.60	0.05	41.7	.6
32	100.	0.	44.47	1.18	44.48	1.18	44.69	0.11	45.77	1.2

TABLE 9.5 DISPLACEMENTS DUE TO THE EXCAVATION

NODAL POINTS	CIRCULAR GEOMETRY				HORSESHOE GEOMETRY			
	Shallow Cavity		Deep Cavity		Shallow Cavity		Deep Cavity	
	x	y	x	y	x	y	x	y
	[mm]	[mm]	[mm]	[mm]	[mm]	[mm]	[mm]	[mm]
28	6.4	-0.2	8.2	-0.2	7.5	-0.1	8.7	-0.1
27	5.38	-0.18	5.47	-0.18	6.0	-0.08	6.5	-0.08
26	4.1	-0.1	5.0	-0.1	4.12	-0.1	5.0	-0.1
35	3.49	+0.08	4.1	+0.08	0.001	+0.095	0.001	+0.095
34	-0.01	-0.01	-0.04	-0.01	-0.01	-0.01	-0.04	-0.01
41	0.0	+0.085	0.0	+0.088	0.0	+0.098	0.0	+0.098
40	0.0	-0.01	0.0	-0.01	0.0	-0.01	0.0	-0.01

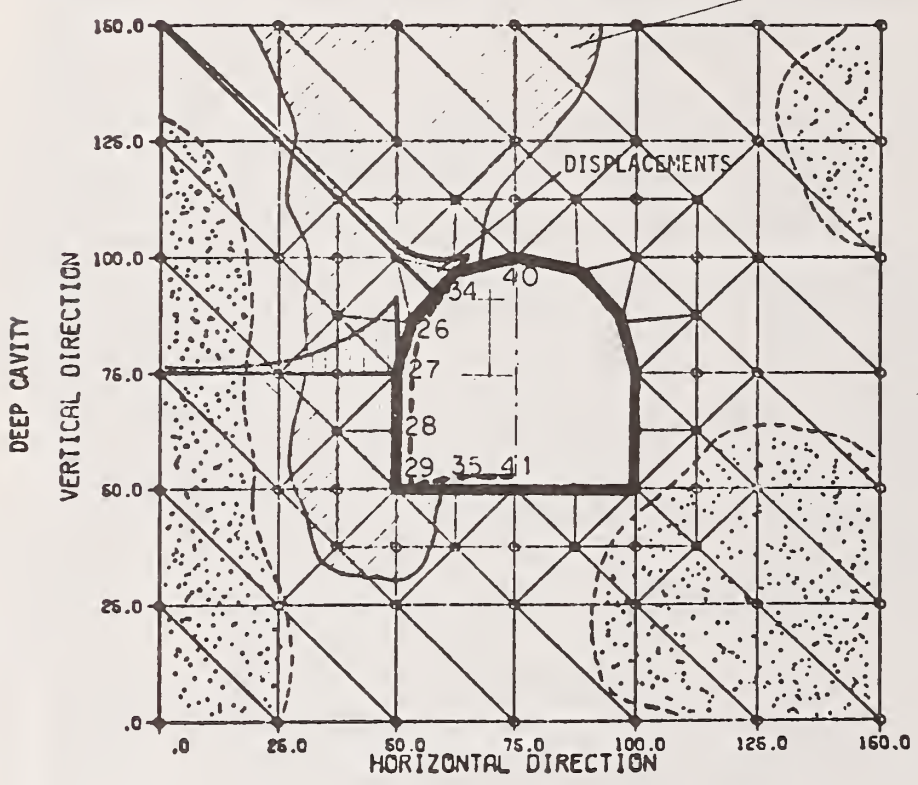
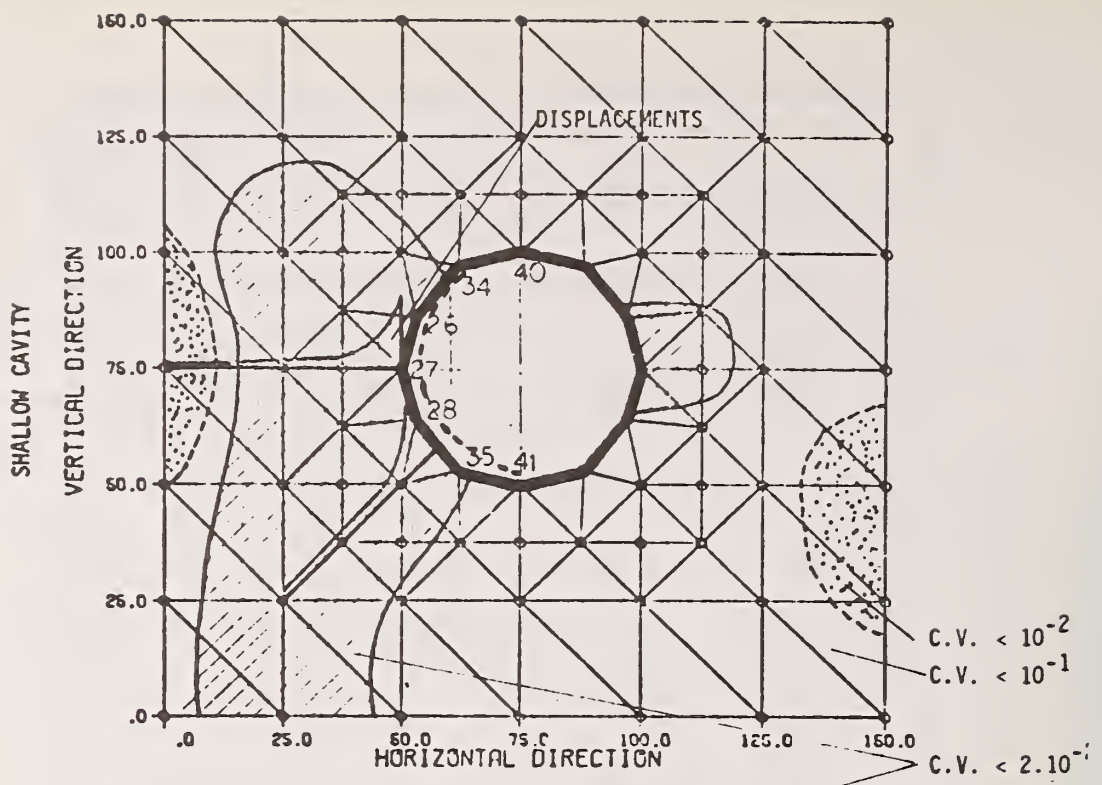


FIGURE 9.6 RESULTS OF THE EXCAVATION

The computational unit MODAN provides the first 15 natural frequencies of both scales as well as their corresponding coefficient of variation (see Table 9.6).

The first two natural frequencies of scale one are in turn used to compute the adequate earthquake acceleration to be applied at the physical boundaries defined by the existing fault and according to the procedure suggested in Chapter 7. A horizontal perturbation is considered in the present treatment as illustrated in Figure 9.1.

The scale factor between the ground motion at the surface and at cavity depth is estimated to be between 1.5 and 2. (Figure 9.7). The generated accelerations considered hereafter have a maximum value of 0.25 g.

Using the modal analysis as described in Chapter 6 the stresses are computed based on the values of both the displacements obtained in scale one and in scale two (Table 9.7). This is justified since the model is linear and the superposition principle valid. The time interval adopted is between 3 and 4 sec and an increment of time of 0.01 sec is used. This range is adopted for computational simplicity. The computed stresses are illustrated in Figure 9.10 and the whole evolution of the stress field in the rock media surrounding the opening are provided in Table 9.8.

The evolution of the dynamic phenomenon is also illustrated in Figure 9.9 in which the curves of equal displacements at different times is shown. In Figure 9.8 the response spectra of the cavity system is provided.

Finally the liner and bolting system is considered. It is assumed that the rock bolts will affect only the strength parameters of

TABLE 9.6 NATURAL FREQUENCIES OBTAINED FROM THE MODAL ANALYSIS

MODE NUMBER	SCALE 1						SCALE 2					
	SHALLOW CAVITY		DEEP CAVITY		CIRCULAR GEOMETRY		CIRCULAR GEOMETRY		HORSE SHOE GEOMETRY		HORSE SHOE GEOMETRY	
	Expected Natural Frequency	Coefficient of Variation	Expected Natural Frequency	Coefficient of Variation	Expected Natural Frequency	Coefficient of Variation	Expected Natural Frequency	Coefficient of Variation	Expected Natural Frequency	Coefficient of Variation	Expected Natural Frequency	Coefficient of Variation
1	HERTZ	10^{-3}	HERTZ	10^{-3}	HERTZ		HERTZ		HERTZ		HERTZ	
2	3.88	1.14	4.74	5.02	10.65		10.34		10.34		10.34	
3	12.80	2.96	13.71	5.41	25.62		25.08		25.08		25.08	
4	16.092		17.7		36.50		36.43		36.43		36.43	
5	26.72		26.98		47.00		46.17		46.17		46.17	
6	31.21		30.16		48.04		46.91		46.91		46.91	
7	33.65		31.20		48.95		48.44		48.44		48.44	
8	35.72	6.21	34.70	4.98	71.78		71.55		71.55		71.55	
9	37.43		36.65		74.68		73.11		73.11		73.11	
10	43.07	7.69	43.65	8.86	83.59		81.80		81.80		81.80	
11	46.49		46.26		89.85		89.70		89.70		89.70	
12	47.70		49.53		98.58		98.35		98.35		98.35	
13	52.59		52.32		100.89		100.25		100.25		100.25	
14	58.41		55.63		103.36		102.46		102.46		102.46	
15	59.65		58.32		112.02		111.62		111.62		111.62	
15	61.56		59.39		118.89		117.64		117.64		117.64	

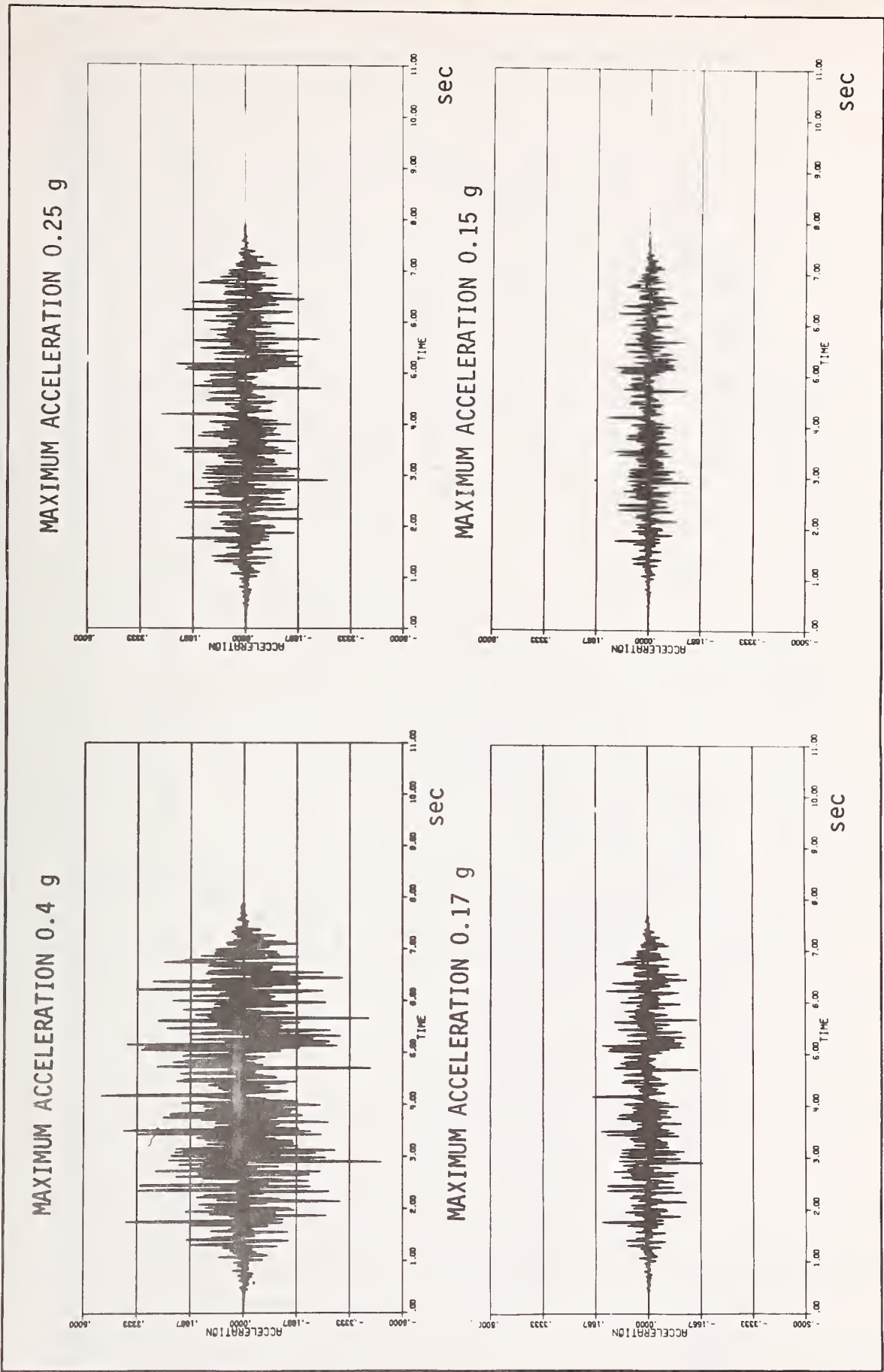


FIGURE 9.7 ACCELERATION SIGNALS

TABLE 9.7 DISPLACEMENTS DUE TO THE SEISME

NODAL POINT	CIRCULAR GEOMETRY						HORSESHOE GEOMETRY									
	SHALLOW CAVITY			DEEP CAVITY			SHALLOW CAVITY			DEEP CAVITY						
	Concrete Liner		Conc. Liner + R. Bolts	Concrete Liner		Conc. Liner + R. Bolts	Concrete Liner		Conc. Liner + R. Bolts	Concrete Liner		Conc. Liner + R. Bolts				
	x	y	x	y	x	y	x	y	x	y	x	y				
	10^{-2} cm	10^{-2} cm	10^{-2} cm	10^{-2} cm	10^{-2} cm	10^{-2} cm	10^{-2} cm	10^{-2} cm	10^{-2} cm	10^{-2} cm	10^{-2} cm	10^{-2} cm				
28	23.22	2.	23.2	2.0	19.99	1.71	19.88	1.46	22.9	1.80	22.8	1.73	19.62	1.54	19.54	1.32
27	6.85	1.07	6.84	1.05	5.87	0.91	5.86	0.78	6.72	1.01	6.7	2.77	5.76	0.86	5.74	0.73
26	12.33	2.85	12.3	2.81	10.56	2.44	10.54	2.09	12.1	2.81	12.0	1.70	10.37	2.40	10.28	2.05
35	1.43	1.16	1.47	1.11	1.22	0.99	1.20	0.84	1.39	1.21	1.38	1.14	1.19	1.03	1.18	0.88
34	0.49	0.47	0.48	0.44	0.42	0.40	0.36	0.34	0.55	0.49	0.54	0.45	0.47	0.42	0.46	0.36
41	13.57	0.30	13.5	0.35	11.63	0.25	9.96	0.21	13.69	0.13	13.6	0.19	11.73	0.11	11.65	0.09
40	7.09	1.0	7.07	0.97	6.07	0.85	6.06	0.72	7.03	1.04	7.01	1.01	6.02	0.89	6.00	0.76
47	1.16	0.64	1.15	0.61	0.99	0.54	0.98	0.46	1.14	0.42	1.13	0.38	0.97	0.36	0.96	0.30
46	0.66	0.35	0.65	0.33	0.56	0.30	0.55	0.25	0.71	0.23	0.69	0.20	0.60	0.19	0.53	0.16
55	2.29	0.55	2.28	0.53	1.96	0.47	1.95	0.40	2.4	0.67	2.4	0.66	2.05	0.57	2.05	0.48
54	1.23	0.62	1.22	0.61	1.05	0.53	1.04	0.45	1.25	0.68	1.24	0.67	1.07	0.58	1.06	0.49
53	1.87	1.52	1.85	1.51	1.60	1.30	1.58	1.11	1.78	1.64	1.75	1.62	1.52	1.40	1.50	1.20

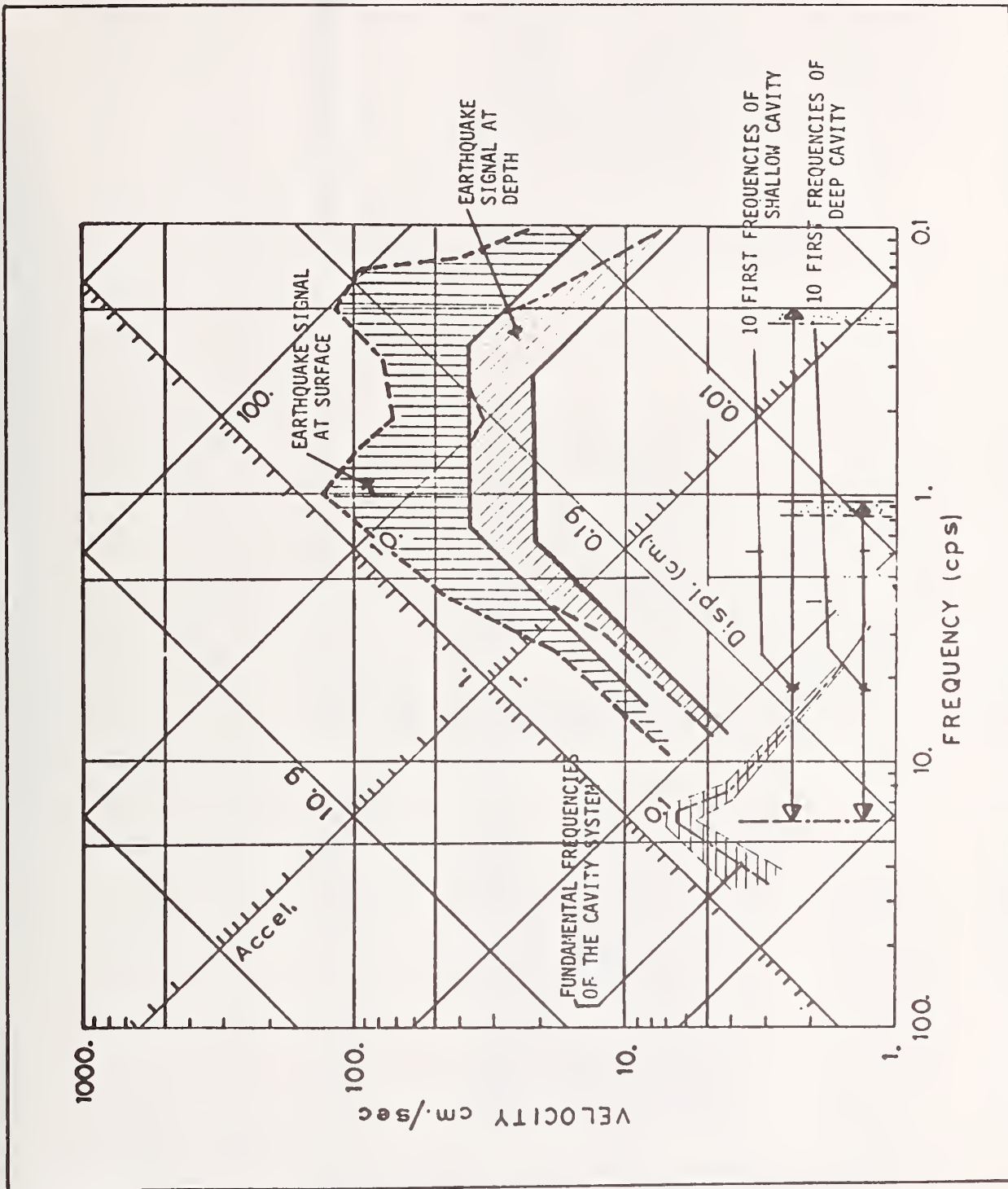
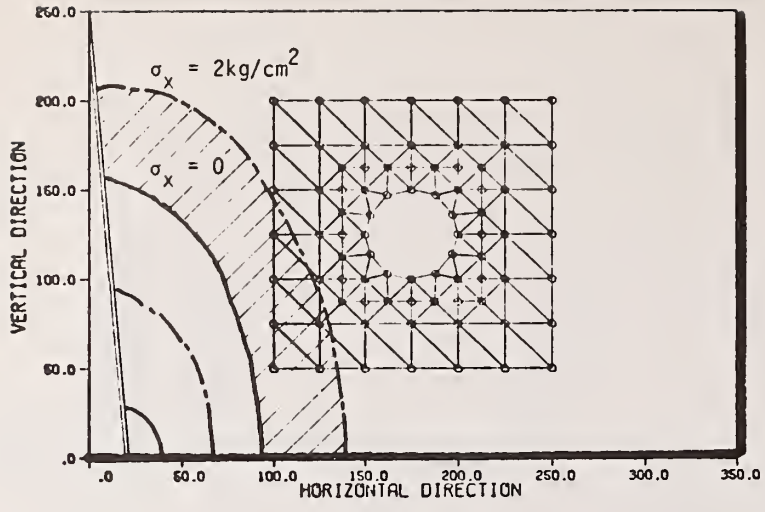
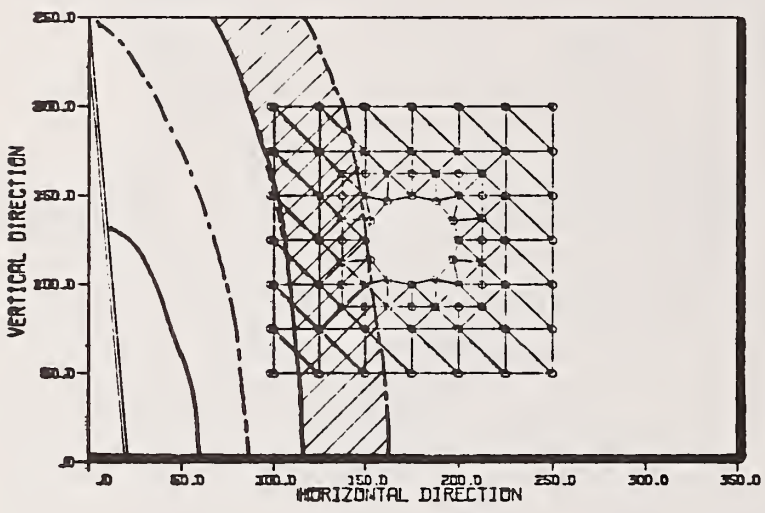


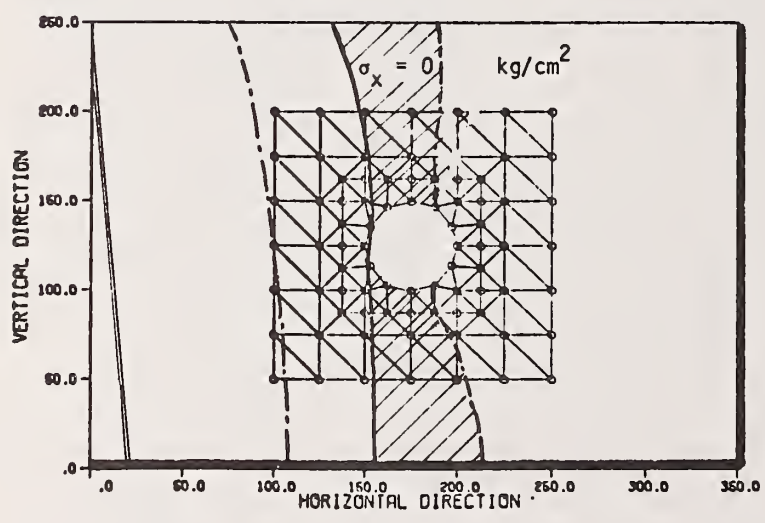
FIGURE 9.8 GROUND MOTION RESPONSE SPECTRA



t = 0.5 sec



t = 1.0 sec



t = 1.5 sec

FIGURE 9.9 PROPAGATION OF THE SEISMIC PERTURBATION

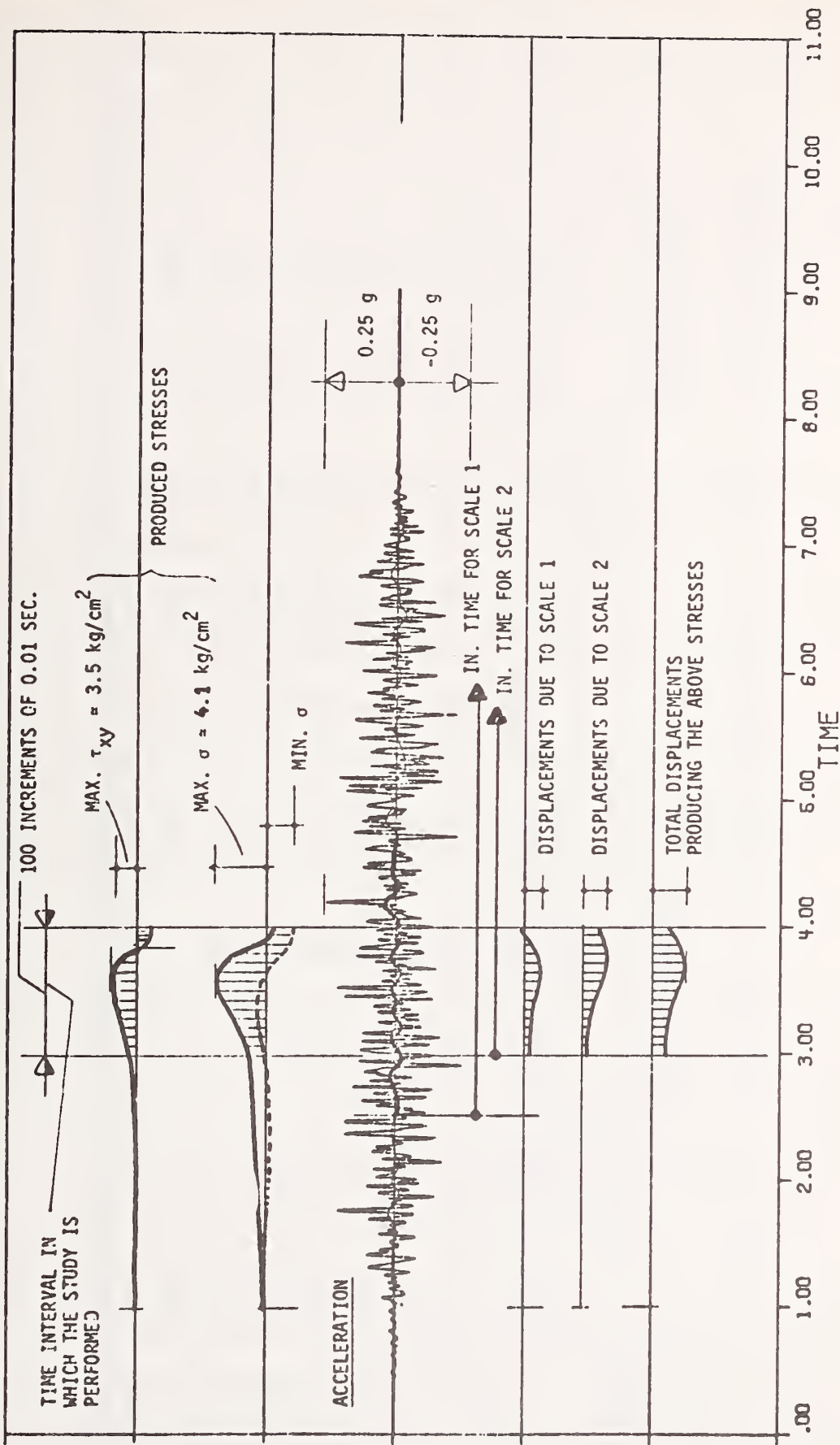


FIGURE 9.10 VARIATION OF STRESSES

TABLE 9.8 EVOLUTION OF MAXIMUM COMPRESSIVE STRESSES IN THE ROCK MEDIA

ELEMENT NUMBER	CIRCULAR GEOMETRY						HORSESHOE GEOMETRY					
	SHALLOW CAVITY			DEEP CAVITY			SHALLOW CAVITY			DEEP CAVITY		
	Initial Stress Field	Stresses After Excav.	Dynamic Stresses	Initial Stress Field	Stresses After Excav.	Dynamic Stresses	Initial Stress Field	Stresses After Excav.	Dynamic Stresses	Initial Stress Field	Stresses After Excav.	Dynamic Stresses
	kg/cm ²	kg/cm ²	kg/cm ²	kg/cm ²	kg/cm ²	kg/sm ²	kg/cm ²	kg/cm ²	kg/cm ²	kg/cm ²	kg/cm ²	kg/cm ²
29	121.	2.6	3.76	140.	2.62	3.4	121.	2.65	3.76	140.	2.68	3.68
30	143.	2.8	3.81	144.	2.81	3.5	143.	2.7	3.80	144.	2.72	3.72
31	146.	2.4	3.62	145.	2.4	3.48	146.	2.65	3.60	145.	2.4	3.58
32	147.	1.5	3.72	145.	1.4	3.33	147.	2.62	3.62	145.	2.45	3.53
33	147.	2.4	3.5	147.	2.36	3.4	155.	2.63	3.63	147.	2.48	3.50
34	155.	2.6	4.0	150.	2.45	3.7	155.	2.64	3.7	160.	2.5	3.6
35	155.	2.72	4.1	165.	2.68	3.7	160.	2.64	3.8	165.	2.6	3.6
36	160.	2.7	4.	165.	2.7	3.8	160.	2.7	3.8	165.	2.68	3.71

the rock media and will slightly modify the modulus of elasticity. On the other hand they will homogenize the statistical characteristics of the rock.

The displacements of the concrete liner are computed only under dynamic conditions without the possible effect of rock creep.

Half of the opening is examined and only the induced dynamic efforts are considered with respect to the relative position of nodes 40 and 41 of scale 2.

The maximum efforts are induced at 3.80 sec. causing the displacements shown in Table 9.9 and illustrated in Figure 9.11.

At this deformed configuration a stability analysis is performed showing that the circular shape is more stable than the horseshoe shape. This is in accordance with the common belief.

The shear strength of the rock media surrounding the opening is computed based on the Mohr-Coulomb criterion. The conventional factor of safety lies within the range of 5. to 10.

9.4 Comparison of Different Alternatives

All the elements of the study are presented in Table 9.11. Five static criteria and three dynamic independent criteria are retained. The corresponding weight coefficients are computed based on the statistical analysis of the coefficient of variation obtained previously for each criterion. The criterion exhibiting the largest variability assumes the smallest weight coefficient.

The other way to sort the different criteria is the entropy function according to a scheme given in section 8.5. The results are presented in Table 9.12 and illustrated in Figure 9.12. A mean entropy

TABLE 9.9 MAXIMUM DEFORMATIONS IN THE LINER

NODE NUMBER	CIRCULAR GEOMETRY			HORSESHOE GEOMETRY		
	RELATIVE DISPLACEMENTS		ROTATION	RELATIVE DISPLACEMENTS		ROTATION
	x	y		x	y	
	[cm]	[cm]		[cm]		
1	0.	0.	6×10^{-5}	0.	1.6×10^{-4}	
2	0.02	0.078	1×10^{-4}	0.0004	1×10^{-4}	
3	0.117	0.176	-2×10^{-5}	0.0008	-1.2×10^{-4}	
4	0.067	0.161	9×10^{-5}	0.218	-1.5×10^{-4}	
5	-0.017	0.192	-9×10^{-5}	0.269	6×10^{-5}	
6	-0.048	0.198	1.1×10^{-4}	0.143	-1.5×10^{-4}	
7	0.	0.	-2×10^{-4}	0.002	6×10^{-5}	
8	-	-	-	0.	2×10^{-5}	

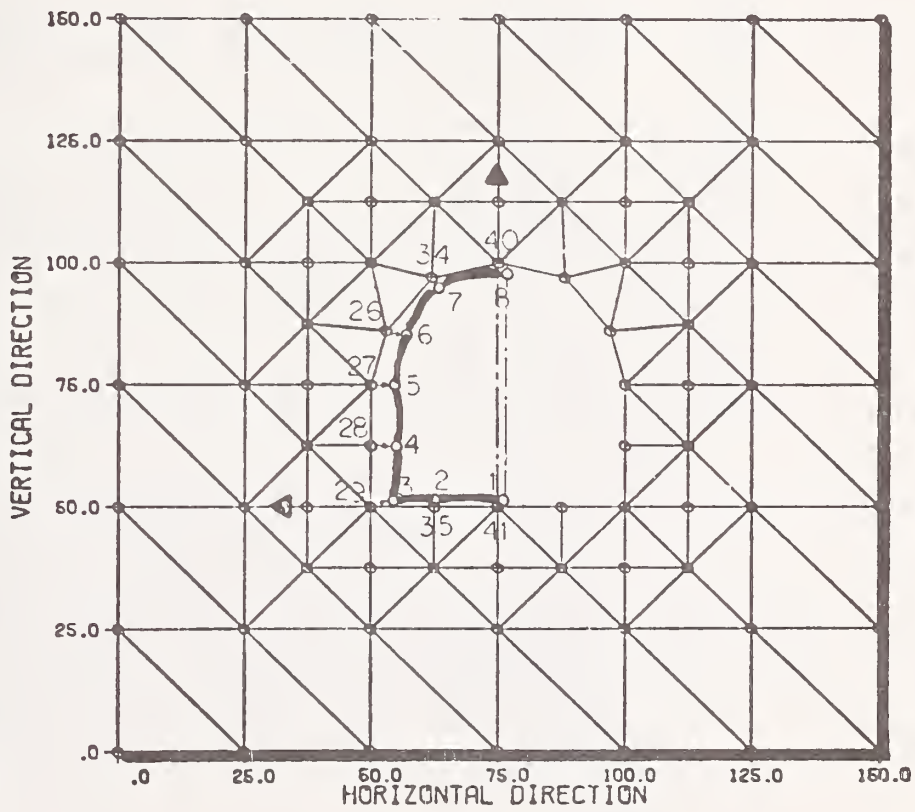
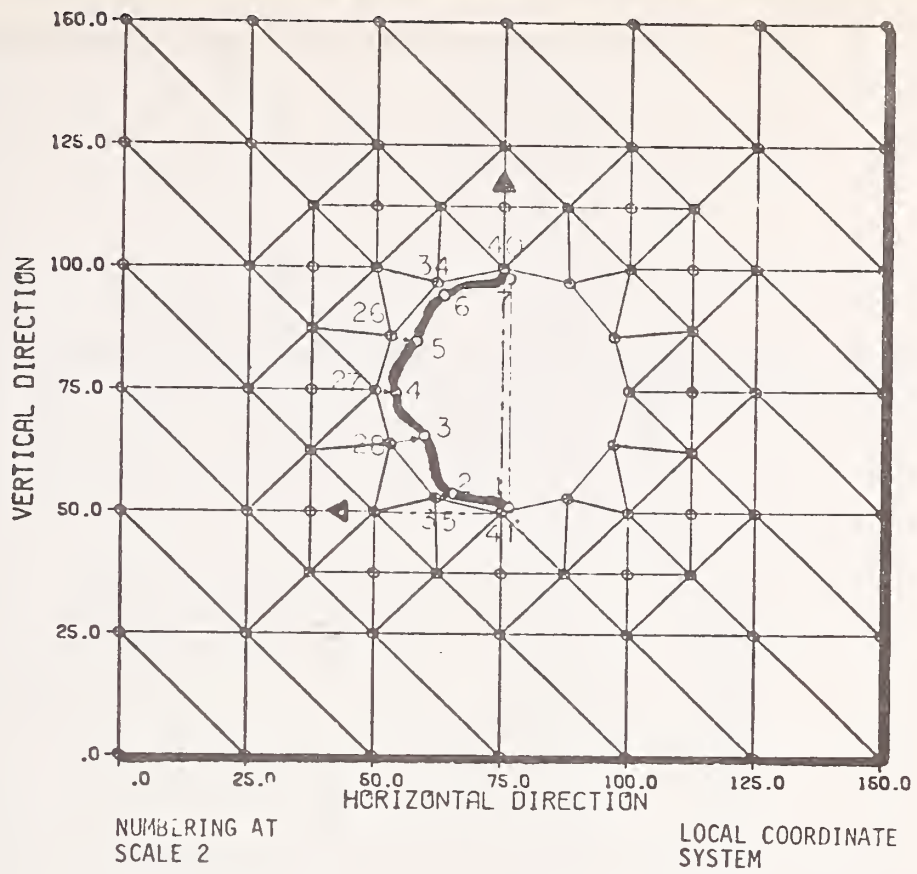


FIGURE 9.11 DEFORMATION OF THE LINER (TIME = 3.80)

TABLE 9.10 SHEAR STRENGTH IN THE ROCK MEDIA

ELEMENT NUMBER	SHALLOW CAVITY					DEEP CAVITY				
	Apparent Cohesion kg/cm ²	Angle of Friction	Normal Stress kg/cm ²	Water Pressure kg/cm ²	Shear Strength kg/cm ²	Apparent Cohesion kg/cm ²	Angle of Friction	Normal Stress kg/cm ²	Water Pressure	Shear Strength kg/cm ²
29	1.74	22.21	110	0.	46.65	4.19	28.41	107.	16.75	53.01
30	4.2	25.2	112	0.	56.90	4.80	32.33	108.	17.49	53.76
31	3.92	26.97	113	0.	61.42	5.22	38.00	110.	19.68	75.79
32	4.19	28.41	115	0.	66.40	5.82	39.22	116.	22.13	82.43
33	4.8	32.33	112	15.13	66.11	6.37	39.26	117.	24.30	82.14
34	5.2	38.00	113.5	17.08	80.53	7.55	40.38	119.	27.2	82.58
35	5.78	39.22	116	19.83	84.27	8.5	41.76	120.	20.71	89.65
36	6.9	40.79	118	23.14	88.75	8.3	42.	122.	21.50	90.44

TABLE 9.11 INPUT DATA FOR ALGORITHM ELECTRE
(WITH COEFFICIENT OF VARIATION)

	INITIAL CONDITIONS IN ROCK MEDIUM				EFFECT OF THE EXCAVATION				EFFECT OF SEISME					
	RQD		Modulus of Elast. E		Mean Hor. Displacements		Natural Frequencies of Und. Flow		Seisime G.		Dynamic Displacements		Stability of Liner	
	EV.	10^5 kg/cm^2	EV.	mm	EV.	Hertz	m	EV.	mm	EV.	mm	EV.	EV.	
<u>ALTERNATIVE 1</u> Shallow Cavity Circular Geometry Concrete Liner	75% 4	2.0	5	6.4	1	31.21 48.01	4	38.0	1	23.33	4	2.14	1	
<u>ALTERNATIVE 2</u> Shallow Cavity Circular Geometry Conc. Liner + R. Bolts	75% 4	2.51	4			31.21 48.04	4	38.0	1	23.2	4	2.14	1	
<u>ALTERNATIVE 3</u> Shallow Cavity Horsesh. Geometry Concrete Liner	77% 3	1.9	5	8.6	3	31.21 46.91	2	38.9	2	22.9	3	1.99	2	
<u>ALTERNATIVE 4</u> Shallow Cavity Horsesh. Geometry Conc. Liner + R. Bolts	77% 3	2.4	4			31.21 46.91	2	38.9	2	22.9	3	1.99	2	
<u>ALTERNATIVE 5</u> Deep Cavity Circular Geometry Concrete Liner	83% 2	3.58	2	7.5	2	30.16 48.04	1	45.0	3	19.99	2	2.14	1	
<u>ALTERNATIVE 6</u> Deep Cavity Circular Geometry Conc. Liner + R. Bolts	83% 2	3.70	1			30.16 48.04	1	45.0	3	19.83	2	2.14	1	
<u>ALTERNATIVE 7</u> Deep Cavity Horsesh. Geometry Concrete Liner	84% 1	3.4	3	8.7	4	30.16 46.91	3	47.0	4	19.62	1	1.99	2	
<u>ALTERNATIVE 8</u> Deep Cavity Horsesh. Geometry Conc. Liner + R. Bolts	84% 1	3.48	3			30.16 46.91	3	47.0	4	19.54	1	1.99	2	
Mean Value of the Coefficient of Variation	$1. \times 10^{-2}$	1.1×10^{-1}	1.5×10^{-1}	4.9×10^{-3}	3.5×10^{-1}	$6. \times 10^{-1}$	$< 10^{-3}$	1.3×10^{-2}						
Weight Coefficient	0.5	1.	1.5	0.5	1.5	2.	2.	1.5	2.	2.	2.	1.	1.	

TABLE 9.12 INPUT DATA FOR ALGORITHM ELECTRE (with Entropy)

	INITIAL CONDITIONS IN ROCK MEDIUM				EFFECT OF THE EXCAVATION				EFFECT OF SEISME							
	RQD	Modulus of Elast. E		Mean Hor. Displacements	Natural Frequencies	Mean Head of Und. Flow	Seisime G.	Dynamic Displacements	Stability of Liner	EV.	EV.	EV.	EV.			
		EV.	EV.													
<u>ALTERNATIVE 1</u> Shallow Cavity Circular Geometry Concrete Liner	.88	4	7.3	5	2.38	1	2.36	4	4.12	1	1.6	2	1.33	4	1.43	1
<u>ALTERNATIVE 2</u> Shallow Cavity Circular Geometry Conc. Liner + R. Bolts	0.88	4	7.39	4			2.36	4	4.12	1			1.33	4	1.43	1
<u>ALTERNATIVE 3</u> Shallow Cavity Horsesh. Geometry Concrete Liner	0.89	3	7.47	5	3.11	3	2.342	2	4.13	2			1.31	3	1.4	2
<u>ALTERNATIVE 4</u> Shallow Cavity Horsesh. Geometry Conc. Liner + R. Bolts	0.89	3	7.38	4			2.342	2	4.13	2			1.31	3	1.4	2
<u>ALTERNATIVE 5</u> Deep Cavity Circular Geometry Concrete Liner	0.92	2	7.55	2	3.05	2	2.36	1	4.19	3			1.26	2	1.43	1
<u>ALTERNATIVE 6</u> Deep Cavity Circular Geometry Conc. Liner + R. Bolts	0.92	2	7.56	1			2.36	1	4.19	3			1.26	2	1.26	1
<u>ALTERNATIVE 7</u> Deep Cavity Horsesh. Geometry Concrete Liner	0.93	1	7.53	3	3.113	4	2.32	3	4.188	4			1.25	1	1.4	2
<u>ALTERNATIVE 8</u> Deep Cavity Horsesh. Geometry Conc. Liner + R. Bolts	0.93	1	7.54	3			2.32	3	4.188	4			1.24	1	1.4	2
Mean Value of Entropy	0.90		7.40		3.05		2.34		4.15		1.8		1.26		1.47	
Weight Coefficient	0.5		1.		1.5		0.5		1.5		2.		2.		1.	

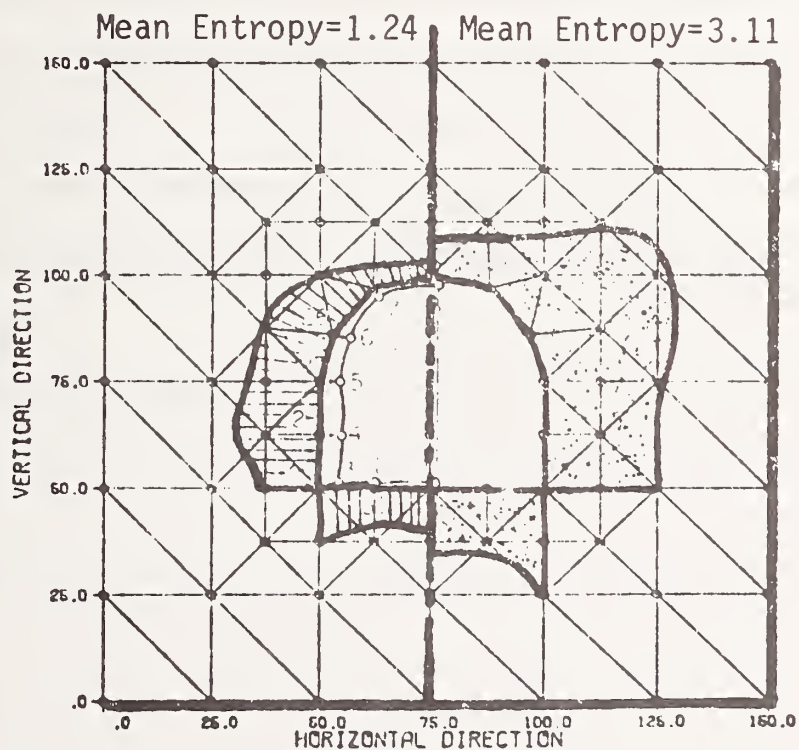
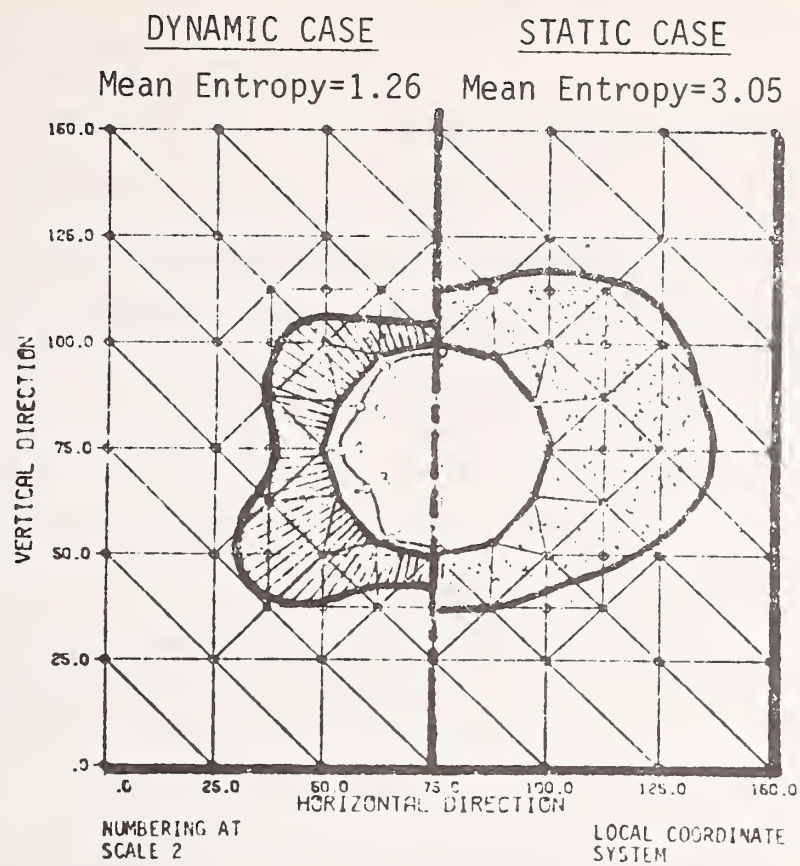


FIGURE 9.12 DISTRIBUTION OF THE ENTROPY OF INFORMATION OF THE STATIC AND DYNAMIC DISPLACEMENTS (CASE OF DEEP CAVITY)

value is evaluated for each design alternative by averaging the entropies of the variables characterizing each criterion, at the surrounding the opening finite elements. Then the average of the mean entropy values is the factor to judge the performance of each criterion and to determine accordingly the weight coefficients.

Two different cases are considered:

Case A - The static criteria

Case B - The static plus the dynamic criteria.

Case A and B are treated using the finite uncertainty analysis as developed in Chapter 6. The computer programs and subroutines related to the different computational units are provided in Appendix F.

The above mentioned two approaches to sort the different criteria were found to be equivalent. However the entropy procedure offers a more refined sorting than the coefficient of variation. In addition it provides the probability density function of the examined parameter. This quantity is essential if a combinatorial reliability analysis is foreseen.

Both cases are run for different combinations of the values of the triplet (p, q, s) corresponding to different levels of relaxation of the ordering relation.

The results are illustrated in Figures 9.13 and 9.14 respectively for cases A and B.

The unanimity graph as expected is never achieved. This proves the need of a multiobjective selection approach to rank the alternate design solutions as suggested in Chapter 8.

For Case A (STATIC ANALYSIS)

The circular shallow cavity shows a better performance with a coefficient of relaxation $p = 0.4$ and $s = 1$.

For Case B (STATIC AND DYNAMIC ANALYSIS)

The deep cavity with the horseshoe shape is more appealing, having a coefficient of relaxation $p = 0.6$ and $s = 2$.

The above two options constitute, as a matter of fact, two opposing design alternatives. In effect for the static case alone the shallow circular cavity offers the greater advantages while for the combined static and dynamic case the deep horseshoe cavity is without doubt the best choice. Therefore for the particular geological site at hand and seismic conditions a designer would prefer the horseshoe geometry.

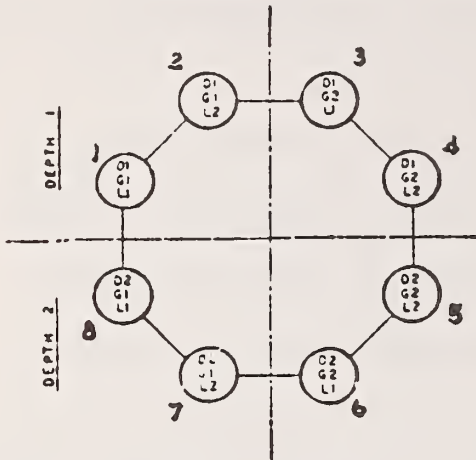
However, it must be pointed out that the above conclusions are only valid for the assumptions under which the analysis is performed.

More specifically the limitations imposed in this study for the comparison of the different design alternatives are:

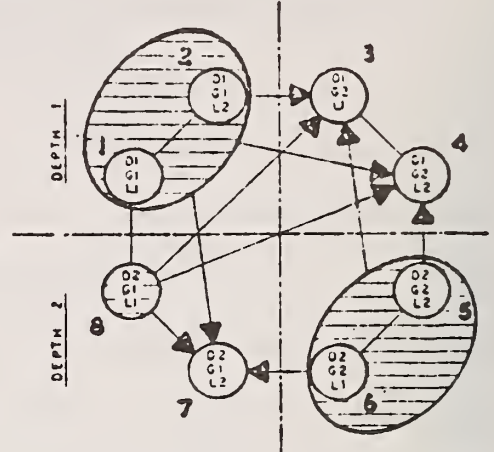
1. Only the uncertainty of the different criteria is adopted as a means to compare. The economic, technologic and construction criteria are not considered.
2. The discord and concord indices are defined with respect to the relative maximum and minimum values of each examined criterion.
3. The confidence limits for each best choice is not considered since the answer to that problem necessitates a deep study of the system reliability.
4. The sensitivity of the model is not examined and the effect of the weight coefficients (used to determine the ranking of the different criteria) on the final outcome of the study are partially examined.

UNANIMITY NEVER ACHIEVED

NO POSSIBLE ORDER

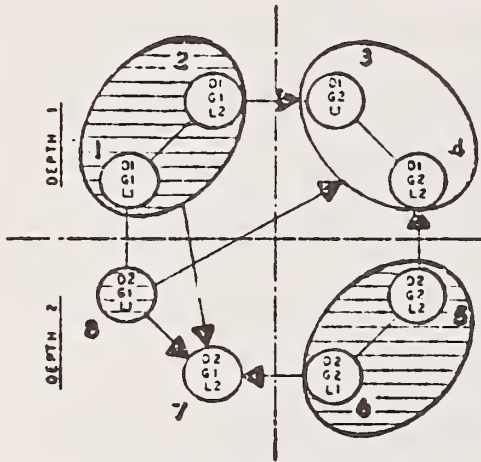


$G(p=1. \ q=0. \ s=1)$

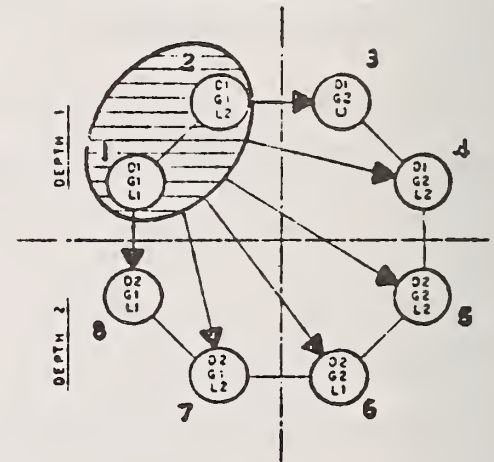


$G(p=0.7 \ q=0.5 \ s=1)$

FINAL REDUCED GRAPH



$G(p=0.66 \ q=0.4 \ s=1)$



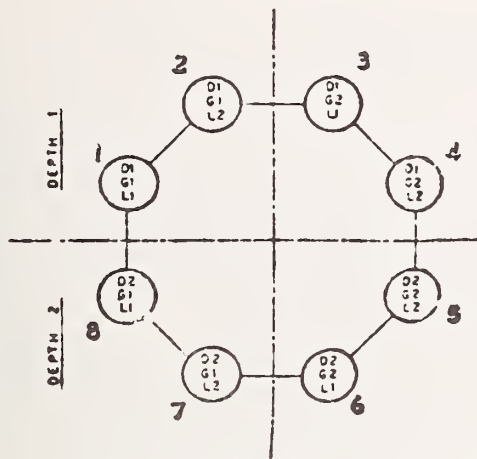
$G(p=0.4 \ q=0.6 \ s=1)$
 $G(p=.7 \ q=0.5 \ s=2)$
 $G(p=.5 \ q=0.6 \ s=3)$

ALTERNATIVE 1+2 (CIRCULAR GEOMETRY) ARE THE MOST APPEALING

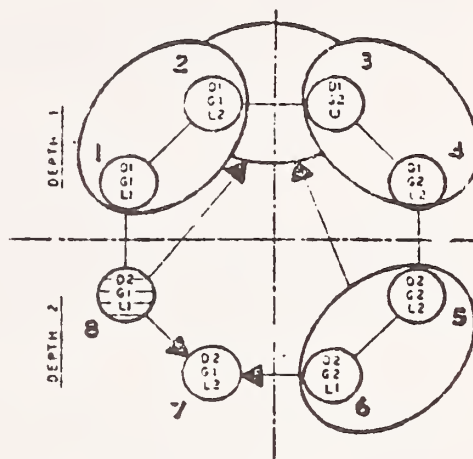
FIGURE 9.13 ILLUSTRATION OF THE RESULTS OBTAINED BY DELECTRE (STATIC CASE)

UNANIMITY NEVER ACHIEVED

NO POSSIBLE CORE

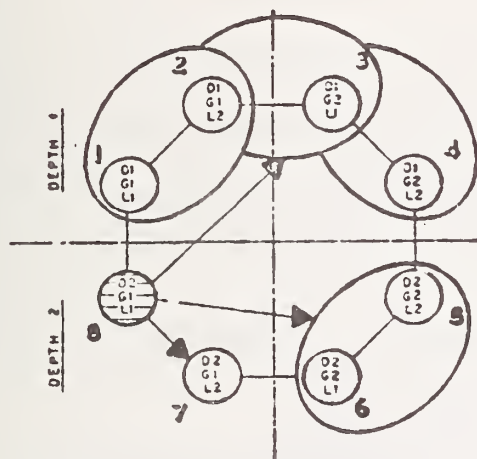


$G(p=1, q=0, s=1)$

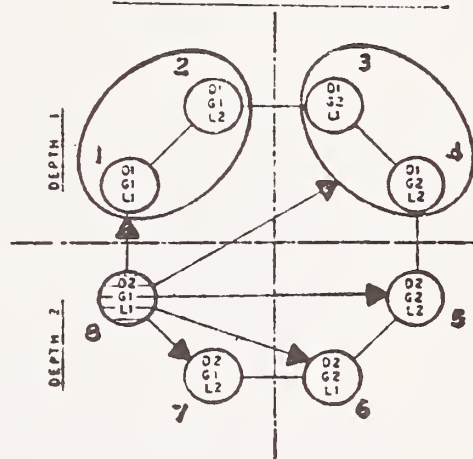


$G(p=0.66, q=.4, s=1)$

FINAL REDUCED GRAPH



$G(p=0.7, q=0.5, s=2)$



$G(p=0.6, q=0.5, s=2)$

ALTERNATIVE 8 (HORSESHOE GEOMETRY) IS CLEARLY THE MOST APPEALING

FIGURE 9.14 ILLUSTRATION OF THE RESULTS OBTAINED BY DELECTRE (DYNAMIC CASE)

On the other hand the following advantages are offered to the designer:

1. The model is very flexible and every component of the system can be changed without difficulty.
2. The parallel structure of the model offers an easy way to evaluate the sensitivity of the model with respect to any desired criterion.
3. The parallel structure does not allow the propagation of an error.
4. The maximum entropy of information offers a means to compute the probability density function of the examined variables.

Indeed if an error is committed in evaluating the quantities of one criterion this error will be kept inside this criterion without affecting the other evaluative criteria. Therefore, the error will only partially influence the overall analysis.

Also the results of the preceding example indicate that the scheme which offers a good computational efficiency is the following.

1. Collect the Data obtained from a site investigation and their spatial distribution.
2. Use an Inference model to couple the results of the site investigation with the available analytical model.
3. Collect the statistical characteristics of the physical parameters to be used in the analytical model.
4. Perform the Static Analysis for each Design alternative
5. Perform the Dynamic Analysis for each Design alternative.
6. Compare the different design alternatives for the desired range of the values of the weight coefficients according to the values of the entropy of information.

CHAPTER 10
CONCLUSIONS AND RECOMMENDATIONS

10.1 Conclusions

An attempt was made in the present study to analyze the behavior of cavity systems under seismic conditions. The results can be summarized in point form as follows:

1. An inference model was developed to rationalize the information obtained from site investigation and to estimate the degree of confidence that one has in the inferred values of the physical parameters describing the rock media.
2. An uncertainty analysis was introduced to deduce the statistical characteristics of the output from the analytical model as dictated by the statistical properties of the input, obtained from the above inference model. The computational part of the analytical model is handled by a Finite Element procedure.
3. The seismic phenomenon was described and earthquake signals generated in a realistic approximation, taking into considerations the natural boundaries created by existing faults in the rock mass surrounding the location where the cavity is planned to be excavated.
4. An algorithm based on an application of Graph Theory in relation to a multiobjective selection approach, permitted the systematic ranking of alternate design solutions according to results obtained from

the uncertainty analysis. It allowed for the comparison between different alternatives based on the evaluation of their respective performance over a set of criteria of comparison.

The above four-step scheme is meant to offer a mechanism for the evaluation of the modes of behavior of a cavity system under seismic loads, leading to the estimation of the safety level reached by the cavity system under seismic conditions. A computer program was developed to handle numerically each one of the above computational units. More specifically:

Unit INFMOD evaluates the statistical moments of the inferred physical parameters of the rock at any particular point of the geometric space. It proved to be sensitive to the spatial distribution of the Known Sample points and thus reliable. It provides the basic input data to units STFLOW, EXCAV and DYNMOD each of which digitally simulates different aspects of the behavior of the cavity system.

STFLOW computes the effects of the underground water flow on the structure and permits the evaluation of the effective stresses around the cavity. Interestingly it locates the regions of possible nonlaminar flow, the region in which the water effect is of importance.

EXCAV computes the stresses created by the excavation, taking into consideration nonlinearities in the behavior of the rock. It provides also the variances of the stress distribution, allowing the designer to identify the zones of potential failure.

DYNMODE performs a modal linear analysis. It computes the first 10 to 20 natural frequencies and their variance allowing the determination of the most critical vibrational mode between different geometric

configurations. The maximum and minimum stresses induced by the dynamic phenomenon are then computed to assess the safety level reached during a seisme. To this effect, the conventional Mohr-Coulomb failure criterion was adopted.

STLINER evaluates the displacements of the adopted liner using a geometric-nonlinearity approach. The stability analysis on the deformed shape is then performed, so as to provide an estimate of the overall stability factor. This is a parameter of interest - if one wishes to compare different geometries for the cavity system.

The partial results of the above programs for each prospective alternative are then introduced to unit DELECTRE. It allows identification of the best choice among the alternatives according to a number of commonly used performance criteria. It represents the most significant part of the study since it provides the tool necessary for the designer to parametrically identify the most sensitive performance criteria in the selection of the most reliable alternative.

In general the proposed methodology offers a means to examine the effects of a seism striking a cavity system on a more realistic basis than offered in existing procedures. Moreover, it couples the uncertainty analysis with the information obtained from site investigations, so that a realistic and reliable simulation of the real geologic environment can be achieved.

10.2 Perspective for Future Work

The emphasis in the present study was put on the development of a general methodology for the analysis and design of a cavity system under seismic conditions. Consequently, numerical procedures as simple

as possible were adopted for the different computational steps. Therefore, a future work could be focused on the following broad two items:

- A. The improvement of the computational scheme;
- B. The inclusion of economic and other technologic criteria in the comparison of the different design alternatives.

More specifically, the following recommendations are made:

1. Concerning the inference computational scheme.

The quadratic form approximating locally the trend of the inferred physical parameter can be more accurately determined by using pattern recognition techniques.

2. Concerning the Finite Element Method. Isoparametric elements with 16 d.o.f can be included improving the results of the uncertainty analysis.
3. Concerning the physical parameters. A CAP model can be included to describe the rock behavior under failure conditions. Also the anisotropy of the rock media can be taken into consideration without any particular problem.
4. The Dynamic analysis can become more efficient by means of an explicit formulation, similar to the existing SAMSON code.
5. A more elaborate technique can be used to generate the earthquake signal taking into consideration the magnitude and of an earthquake.
6. A three dimensional analysis would certainly offer the most realistic simulation of the real world. But, the efficiency of such a scheme is questionable at the present time.

BIBLIOGRAPHY

1. Becker, R. M. et al., "Particle Statistics of Infinite Populations as Applied to Mine Sampling " Bureau of Mines Rept. of Investigations 5669, 1961.
2. Bello, A., Serrano, F., "Measurements of the Behavior of Grouted Bolts Used as Reinforcing Elements for the Support of Underground Openings," Advances in Rock Mechanics, Vol. II, Part A, Proceedings of the 3rd Congress of the International Society of Rock Mechanics, Denver, 1974.
3. Benjamin, J. R., Cornell, C. A., "Probability, Statistics, and Decisions for Civil Engineers," McGraw-Hill Book Company, New York, 1970.
4. Bolotin, V. V., "Statistical Methods in Structural Mechanics," Holden-Day, Inc., 1969.
5. Boyer, R., "Predicting Pavement Performance Using Time Dependent Transfer Functions," Joint Highway Research Project, File: 2-1, Sept. 7, 1972, pp. 13.
6. Broch, I. T., "Effects of Spectrum Nonlinearities upon the Peak Distribution of Random Signals," Brüel and Kjaer reprints from technical review, Jan. 1972, pp. 25.
7. Cambou, B., "Applications of First-Order Uncertainty Analysis in the Finite Elements Method in Linear Elasticity," Proceedings of Applications of Statistics and Probability in Soil and Structural Engineering, 2nd Int. Conf. in Aachen, Vol. 1, Sept. 1975, pp. 67-80.
8. Cannon, R., "Dynamics of Physical Systems," McGraw-Hill, 1967.
9. Chang, C. Y., Nair, K., "A Theoretical Method for Evaluating Stability of Openings in Rock," U.S. Bureau of Mines, Contract Number H0210046, April 1972.
10. Clough, G. W., Duncan, J. W., "Finite Element Analyses of Port Allen and Old River Locks," College of Eng., Office of Research Services, Univ. of Cal., Berkeley, 1969.

11. Cook, R., "Concepts and Applications of Finite Element Analysis," John Wiley & Sons, 1973.
12. Crowley, J. H., Doan, P. L., McCreath, D. R., "Underground Nuclear Plant Siting: A Technical and Safety Assessment," Nuclear Safety Volume 15, No. 5, Sept. 1974, pp. 519.
13. Davis, J. C., "Statistics and Data Analysis in Geology," J. Wiley, 1973.
14. Deere, D. U. et al., "Design of Surface and Near Surface Construction in Rock," In (Failure and Breakage of Rock), Ed. by Fairhurst, C., AIME, NY, 1967, pp. 237-302.
15. Deere, D. U., "Geological Considerations" in "Rock Mechanics in Engineering Practice," edited by Stagg, K. G. and Zienkiewicz, O.C., John-Wiley & Sons, Inc., 1968, pp. 1-27.
16. Deere, D. U., Peck R. B., "Design of Tunnel Liners and Support Systems," Final Report, U. S. Dept. of Transportation, Contr. No. 3-0152, Feb. 1969.
17. Dendrou, B., "Beam Element with Six D.O.F.," Special Project for Prof. Ting E., C.E. Purdue University, 1975.
18. Desai, C. S., Abel, J. F., "Introduction to the Finite Element Method," Von Nostrun-Reinhold, 1972.
19. Dibaj, M., Penzien, J., "Dynamic Response of Earth Dams to Traveling Seismic Waves," U. of Cal., Berkeley, Report No. TE-67-3, Aug. 1967.
20. Duke, C. M., Leeds, D. J., "Effects of Earthquakes on Tunnels," Rand 2nd Protective Symp., March 24-6, 1959, p. 1762.
21. Endersbee, L. A., Hofto, E. O., "Civil Engineering Design and Studies in Rock Mechanics for Poatina Underground Power Station, Tasmania," The Journal of the Institution, Vol. 35, 1963, pp. 187-207.
22. Esteva, L., "Second Moment Analysis of Statically Loaded Nonlinear Structures," Proceedings of Applications of Statistics and Probability in Soil and Structural Engineering, 2nd Int. Conf. in Aachen, Vol. 1, Sept. 1975, pp. 117-129.
23. deFinetti, B., "Theory of Probability, A Critical Introductory Treatment," J. Wiley, 1974.
24. Gallagher, R. H., Zienkiewicz, O. C., editors, "Optimum Structural Design, Theory and Applications," John Wiley and Sons, 1973.

25. Glass, C. E., "Seismic Considerations in Siting Large Underground Openings in Rock," Ph.D. Dissertation, U.C. Berkeley.
26. Gregory, R. D., "An Expansion Theorem Applicable to Problems of Wave Propagation in an Elastic Half-Space Containing a Cavity," Proc. Cambr. Phil. Soc., 63, 1967, pp. 1341-50.
27. "A Guide to Core Logging for Rock Engineering," Proceedings of the Symposium on Exploration for Rock Engineering, Ed. by Biemawski, Z. T., Johannesburg, Nov. 1976.
28. Haimson, B. S., et al., "Site Characterization for Tunnels Housing Energy Storage Magnets," Proceedings of 17th Symposium on Rock Mechanics at Snowbird, Utah, Aug. 1976.
29. Harary, F., "Graph Theory," Addison-Wesley Co., 1972.
30. Hardin, B. O., "Study of Elastic Wave Propagation and Damplog in Granular Materials," Ph.D. Dissertation, Univ. of Florida, Aug. 1961.
31. Harr, M., "Particulate Mechanics," McGraw-Hill, 1977, (to be published).
32. Hofmann, R. B., "Factors in the Specification of Ground Motions for Design Earthquakes in California," Report 3, Miscellaneous Paper S-73-1, June 1974.
33. Hoshiya, M., Chiba, T., "Random Eigenvalues of a Building Structure," Proceedings of Applications of Statistics and Probability in Soil and Structural Engineering, 2nd Int. Conf. in Aachen, Vol. 1, 141-152, Sept. 1975.
34. Hou, S., "Earthquake Simulation Models and Their Applications," M.I.T., Dept. of Civil Eng., Research Report R-68-17, May 1968.
35. Housner, G. W., "Intensity of Earthquake Ground Shaking Near the Causative Fault," Proc. 3rd World Conf. on Earthquake Eng., New Zealand, Vol. 1, pp. III 94-115.
36. Houstis, E. et al., "Development, Evaluation and Selection of Methods for Elliptical P.D.E.," Proceedings of AICA, Int. Symp. on Comp. Methods for P.D.E., June 1975, pp. 1.
37. Idriss I., et al., "QUAD 4," Report No. EERC 73-16, July 1973, University of California, Berkeley.
38. Isenberg, J., et al., "Analytic Modeling of Rock-Structure Interaction," Final Technical Report, Vol. 1, April 1973, U.S. Bureau of Mines, Contract Number H0220035.
39. Isenberg, J., "Part Two: Mechanical Properties of Earth Materials," Defense Nuclear Agency, DNA 1285H2, 12-15, Nov. 1972.

40. Jaeger, J. C., and Cook, N. G. W., "Fundamental of Rock Mechanics," Methuen, London, 1969.
41. Jennings, P. C., Housner, G. W., Tsui, N. C., "Simulated Earthquake Motions for Design Purposes," Proc., 4th World Conf. on Earthquake Eng., Chile, Vol. 1, pp. 145-160, 1972.
42. Judd, W. R., Herrill, R. H., and Workman, J. W., "The Σ Vulnerability of Underground Facilities: Geologic and Rock Mechanics Factors," U.S.A.F. Space and Missile Systems Organization Report BSD-TR-67-241, June 1967.
43. Judd, W. R., "A Synthesis of the Problem in Seismic Coupling," in "ARPA Seismic Coupling Conference," Advanced Research Projects Agency Report, ARPA-T1U-71-13-1d2, pp. 265-279.
44. Judd, W. R., Huber, C., "Correlation of Rock Properties by Statistical Methods," Int. Symposium on Mining Research, Univ. of Missouri, School of Mines and Metall., Feb. 1961.
45. Kanai, K., Osada, K., "Observational Study of Earthquake Motion in the Depth of the Ground, IV (Relation between the Amplitude at Ground Surface and the Period)," Bulletin, Earthquake Research Institute, Volume 31, 1953, p. 228.
46. Kanai, K., Tankaka, T., "Observations of the Earthquake Motion at Different Depths of the Earth," Bulletin, Earthquake Research Institute, Volume 29, 1951, p. 107.
47. Kayser, K., "A New Method for Estimation of Response in Complex Systems," Ph.D., Purdue University, Dec. 1973.
48. Krige, D. G., "Two-Dimensional Weighted Moving Average Trend Surfaces for Ore Valuation," Proc. Symposium on Mathematical Statistics and Computer Applications in Ore Valuation, Johannesburg, 1966, pp. 13-38.
49. Krumbein, W. C., "Analytic Geology," McGraw-Hill Book Company, 1963.
50. Kulhawy, F. H., "Analysis of Underground Opening in Rock by Finite Element Methods," Final Report, U.S. Bureau of Mines, Contract Number H0210029, April 1973.
51. Labrech, D. A., Markow, M. J., Einstein, H. H., "Decision Analysis Applied to Rock Tunnel Exploration," Proceedings of 17th U.S. Symposium on Rock Mechanics, Snowbird, Utah, August 1976.
52. Levy, R., "Random Processes for Earthquake Simulation," Ph.D. Thesis. Polytechnic of Brooklyn, 1969, pp. 1-19.
53. Lew, T. K., "Deep Underground, Lined, Horizontal, Circular Openings in Rock," Civil Eng. Lab. Naval Constr. Batt. Center, Report No. TR-833, DN 544245, Feb. 1976.

54. Luce, R. D., Reiffa, H., "Games and Decisions," John Wiley & Sons, Inc., 1957.
55. Lundborg, N., "A Statistical Theory of the Polyaxial Strength of Materials," Proceedings of the 3rd Congress of the International Society for Rock Mechanics, Vol. II, Part A, Denver, 1974, pp. 180-185.
56. Martin, G. R., Seed, H. B., "An Investigation of the Dynamic Response Characteristics of Ban Tempe Dam, California," Un. of Cal., Berkeley, Dept. of Transportation, Report No. TE-66-2, Feb. 1966.
57. Matheron, G., "Kriging or Polynomial Interpolation Procedures," Canadian Inst. of Mining Bull., V. 60, 1967, p. 1041-1045.
58. Matheron, G., "Le Krigeage Universel," Les Carriers du Centre de Morphologie Mathematique de Fontainebleau, Fascicule 1, 1969.
59. Morgenstern, N. R., "The Influence of Groundwater on Stability," Chapt. 5 in 'Stability in Open Pit Mining' (Ed. C. O. Brawner and V. Milligan, AIME, New York).
60. Moselhi, O. E., "Finite Element Analysis of Dynamic Structure - Medium Interaction with Some References to Underground Nuclear Reactor Containments," M. Eng. Thesis, Men. Un. of Newfoundland, Aug. 1975.
61. Nasu, N., "Comparative Studies of Earthquake Motion above Ground and in a Tunnel, Part 1," Bulletin, Earthquake Research Institute, Volume 1, pp. 456, 1931.
62. Nelson, R. A., "An Experimental Study of Fracture Permeability in Porous Rock," Proceedings of 17th Symposium on Rock Mechanics at Snowbird, Utah, Aug., 1976.
63. Newmark, N. M., Rosenblueth, E., "Fundamentals of Earthquake Engineering," Prentice-Hall Inc., 1971, pp. 14-16.
64. Obert, L., Duvall, W. I., "Rock Mechanics and the Design of Structure in Rock," John Wiley, 1967.
65. Okamoto, S., Tomura, C., "Dynamic Behavior of Rock Ground During Earthquakes," Rock Mechanics in Japan, Vol. 1, 1970, p. 121.
66. Okamoto, S., "Introduction to Earthquake Engineering," J. Wiley, 1973, p. 100.
67. Padilla, J. D., Vanmarcke, E. H., "Settlement of Structures on Shallow Foundations: A Probabilistic Analysis," M.I.T., Dept. of Civil Engineering, Research Report R74-9, Jan. 1974.

68. Papoulis, A., "Probability, Random Variables and Stochastic Processes," McGraw-Hill Book Co., New York, 1965.
69. Peres-Rodrigues, F., "Influence of the Scale Effect over Tock Mass Safety Against Deformability," Proceedings of the 3rd Congress of the International Society for Rock Mechanics, Vol. II, Part A, Denver, 1974, pp. 202-208.
70. Perser, L. N., "Rock Dynamics and Geophysical Exploration," Development in Geotechnical Engineering, Vol. 8, ELSEVIER, 1975.
71. Phillips, D. T., et al., "Operations Research, Principles and Practice," John Wiley & Sons, 1975.
72. Priest, S. D., Hudson, J. A., "Discontinuity Spacings in Rock," Int. J. Rock Mech. Min. Sci. & Geomech. Abstr., Vol. 13, Pergamon Press, 1976, pp. 135-148.
73. Rea, D., "Proceedings of the Universities Council for Earthquake Engineering Research," Un. of British Columbia, Report No. UCEER-4, 45-46, June 28-29, 1976.
74. Richart, F. E., et al., "Vibrations of Soils and Foundations," Prentice-Hall, Inc., 1969, pp. 300-305.
75. Rinehart, B., "Model Experiments Pertaining to the Design of Underground Openings Subjected to Intense Ground Shocks," Res. Round., Colo. Sch. of Mines, Goldon, CO, Jan. 1960.
76. Rocha, M. et al., "Application of Advanced Techniques to the Study of the Foundations of Sao Simao Dam," Proc. of the 3rd Congress of the Inter. Soc. of Rock Mechanics, Denver, 1974, pp. 913-921.
77. Rosenblueth, E., "Design Philosophy," Proceedings of Applications of Statistics and Probability in Soil and Structural Engineering, 2nd Int. Conf., in Aachen, September 1975, Vol. 3, pp. 42-61.
78. Roy, B., "Algèbre Moderne et Theorie des Graphes," Dunod Paris, 1969.
79. Roy, B., Problems and Methods with Multiple Objective Functions," Math. Progr., 1(2), 1971, pp. 239-266.
80. Ruiz, P., Penzien, J., "Probabilistic Study of the Behavior of Structures during Earthquakes," Report for the National Science Foundation, Grant NSF-GK-1379, March 1969.
81. Sandler, I. S., "The CAP Model for Static and Dynamic Problems," Proceedings of 17th Symposium on Rock Mechanics, at Snowbird, Utah, Aug. 1976.
82. Schlaifer, R., "Analysis of Decisions Under Uncertainty," McGraw-Hill Book Co., 1969.

83. Seed, H. E., Idriss, I. M., Kiefer, F. W., "Characteristics of Rock Motions During Earthquakes," Jour. of Soil Mech. and Found. Div., ASCE, Vol. 95, No. SM6, Nov., pp. 105-134.
84. Seed, H. E., "The Influence of Local Soil Conditions on Earthquake Damage," Proceedings of Specialty Session II, Soil Dynamics, 7th International Conference on Soil Mechanics and Foundation Engineering, Mexico City, 1969, pp. 33-66.
85. Serrano, J. Castillo, E., "A New Concept about the Stability of Rock Masses Advances in Rock Mechanics, Vol. II, Part B, Proceedings of the 3rd Congress of the International Society for Rock Mechanics, Denver, 1974, pp. 820-826.
86. Shima, E., "Modifications of Seismic Waves in Superficial Soil Layers as Verified by Comparative Observations on and beneath the Surface," Bulletin, Earthquake Research Institute, Vol. 40, Part 2, 1962.
87. Staunton, W. F., "Effects of an Earthquake in a Mine at Tombstone, Arizona," Bull. Seis. Soc., Amer., Vol. 8, 1918, pp. 25-27.
88. Swedish Underground Construction Mission, to the United States of America, Oct. 1976.
89. Talobre, J. A., "La Mecanique des Roches," DUNOD, 1967, pp. 197-198.
90. "The Committee of Experts UNESCO: Koyno Earthquake, December 11, 1967," Report of the Committee of Experts of UNESCO, 1968.
91. Thiel, K., "Influence of the System Load on Deformability of Rocks in Field Tests," Proc. of the 3rd Congress of the Inter. Soc. of Rock Mechanics, Denver, 1974, p. 209-215.
92. Vaish, A., Chopra, A., "Earthquake Analysis of Structure - Foundation Systems," Report to the Office of the Chief of Engineers, Dept. of the Army, Washington, Report No. EERC 73-9, May 1973.
93. Vichneretsky, R., and Peiffer, B., "Error Waves in Finite Element and Finite Difference Methods for Hyperbolic Equations," Proceedings of the AICA, Int. Symp. on Comp. Methods for P.D.E., June, 1975, pp. 53.
94. Whitten, E. H. T., "The General Linear Equation in Prediction of Gold Content in Witwatersrand Rocks," South Africa, Proc., Symposium on Mathematical Statistics and Computer Applications in Ore Valuation, Johannesburg, 1966.
95. Wilson, E. L., and Clough, R. W., "Dynamic Response by Step-by-Step Matrix Analysis," Symposium on the Use of Computers in Civil Engineering, Lisbon, Portugal, Oct. 1962.

96. Wilson, E. L., "Finite Element Analysis of Two-Dimensional Structures," Inst. of Eng. Res., Report No. 63-2, Un. of Cal., Berkeley, June 1963.
97. Yu, F.T.S., "Optics and Information Theory," John Wiley, 1976.
98. Zienkiewicz, "The Finite Element Method in Engineering Science," McGraw-Hill, 1967.

Appendix A

Expression Allowing the Evaluation of the Dynamic Modulus of Elasticity

From the known relations giving the velocities of the compression and the shear wave one can obtain:

$$V_p^2 = \frac{\lambda + 2G}{\rho}$$

or

$$\rho V_p^2 = \frac{E \cdot \nu}{(1+\nu)(1-2\nu)} + 2 \left[\frac{E}{2(1-\nu)} \right] = \frac{E(1-\nu)}{(1+\nu)(1-2\nu)}$$

then the Modulus of Elasticity is equal to:

$$E = \rho V_p^2 \frac{(1+\nu)(1-2\nu)}{(1-\nu)} \quad (A.1)$$

where: V_p = the velocity of the compression wave

ρ = mass density

ν = Poisson's ratio

but

$$V_s^2 = \frac{G}{\rho} = \frac{E}{2\rho(1+\nu)}$$

or

$$E = 2\rho(1+\nu)V_s^2 \quad (A.2)$$

where: V_s = the velocity of the shear wave

G = the shear modulus

Now coupling Equations (A.1) and (A.2) we obtain the Poisson's ratio in terms of the measured velocities

$$V_p^2 \frac{(1+\nu)(1-2\nu)}{1-\nu} = 2\rho(1+\nu)V_s^2$$

or

$$\nu = \frac{1}{2} \left[\frac{\frac{V_c}{V_s} - 2}{\frac{V_p}{V_s} - 1} \right] \quad (A.3)$$

Replacing Eq. (A.3) in Eq. (A.2) one obtains

$$\bar{E} = V_s^2 \frac{(3V_p^2 - 4V_s^2)}{V_p^2 - V_s^2} \quad (A.4)$$

which is the expression of Modulus of Elasticity in terms of the measured velocities V_p and V_s .

Appendix B

Computations Related to the Inference Model

1. Relationship between Covariance and Variogram

Using the general expression of the second statistical moment one can obtain

$$\begin{aligned} E \left[(Z_x - Z_y) - (\hat{Z}_x - \hat{Z}_y) \right]^2 &= E (Z_x - Z_y)^2 + E (\hat{Z}_x - \hat{Z}_y)^2 - \\ &\quad - 2E (Z_x - Z_y)(\hat{Z}_x - \hat{Z}_y) = \\ &= E(Z_x - Z_y) E(Z_x - Z_y) + C(Z_x - Z_y, Z_x - Z_y) + E(\hat{Z}_x - \hat{Z}_y) E(\hat{Z}_x - \hat{Z}_y) \\ &\quad + C(\hat{Z}_x - \hat{Z}_y, \hat{Z}_x - \hat{Z}_y) - 2E(\hat{Z}_x - \hat{Z}_y) E(Z_x - Z_y) - \\ &\quad - 2C(Z_x - Z_y, \hat{Z}_x - \hat{Z}_y) \end{aligned}$$

where: C = the covariance of variables Z and \hat{Z}

which after a few simplifications leads to

$$\begin{aligned} E (Z_x - Z_y, \hat{Z}_x - \hat{Z}_y)^2 &= C(Z_x - Z_y, Z_x - Z_y) + \\ &\quad C(\hat{Z}_x - \hat{Z}_y, \hat{Z}_x - \hat{Z}_y) - 2C(Z_x - Z_y, \hat{Z}_x - \hat{Z}_y) = \\ &= 2C(Z_x - Z_y, Z_x - Z_y) - 2C(Z_x - Z_y, \hat{Z}_x - \hat{Z}_y) \end{aligned}$$

Making use of the general statistical assumptions given in section (5.3)

we obtain

$$\frac{E \left[(Z_x - Z_y) - (\hat{Z}_x - \hat{Z}_y) \right]^2}{2} = C(0) - C(Z_x - Z_y, \hat{Z}_x - \hat{Z}_y)$$

which leads to the expression of the variogram γ

$$\gamma[(Z_x - Z_y), (\hat{Z}_x - \hat{Z}_y)] = C(0) - C(Z_x - Z_y, \hat{Z}_x - \hat{Z}_y)$$

or

$$\gamma(d) = C(0) - C(d) \tag{B.1}$$

2. Optimization Using Lagrange Multipliers

The problem consists to minimize $E[(z-\hat{z})^2]$ the variance with the constraint $E[z(x,y)] - E[\hat{z}(x,y)] = 0$.

Using the assumptions introduced in section (5.3.1) we obtain

$$E[(z-\hat{z})^2] = C(z,z) + \sum_{\alpha} b_{\alpha} \sum_{\beta} b_{\beta} [C(z_{\alpha}, z_{\beta})] - 2 \sum_{\alpha} b_{\alpha} C(z, z_{\alpha}) \quad (B.2)$$

and

$$E[z] - E[\hat{z}] = \sum_{\ell} a_{\ell} f^{\ell} - \sum_{\alpha} a_{\ell} \left[\sum_{\alpha} b^{\alpha} f_{\alpha}^{\ell} \right] =$$

$$= \sum_{\ell} a_{\ell} \left[f^{\ell} - \sum_{\alpha} b^{\alpha} f_{\alpha}^{\ell} \right] = 0; \quad (B.3)$$

$$\alpha = 1, \dots, n \quad \ell = 1, \dots, k$$

The minimization of the variance will be obtained using the method of Lagrange multipliers as follows.

The Lagrange function being

$$L = C(z,z) - 2 \sum_{\alpha} b_{\alpha} C(z, z_{\alpha}) + \sum_{\alpha, \beta} b^{\alpha} b^{\beta} C(z_{\alpha}, z_{\beta}) -$$

$$- \sum_{\ell} (\mu_{\ell}) \left[f^{\ell} - \sum_{\alpha} b^{\alpha} f_{\alpha}^{\ell} \right]; \quad (B.4)$$

$$\alpha, \beta = 1, \dots, n \quad \ell = 1, \dots, k$$

The conditions to obtain the minimum are

$$\frac{\partial L}{\partial b^{\alpha}} = 0 \quad \text{for all } b \text{ 's} \quad (B.5)$$

$$\frac{\partial L}{\partial \mu_{\ell}} = 0 \quad \text{for all } \mu \text{ 's}$$

The unknowns being b^{μ} 's and μ 's we obtain a linear system of $\alpha+k$ equations.

The differentiation of L with respect to b^α and M_ν gives:

First with respect to b^α .

$$-2 C(z, z_\alpha) + \sum_{\beta} b^\beta C(z_\alpha, z_\beta) + \sum_{\lambda} \mu_\lambda f_\alpha^\lambda = 0 \quad \forall \alpha = 1, n \quad (B.7)$$

Second with respect to μ_λ .

$$-f^\lambda + \sum_{\alpha} b^\alpha f_\alpha^\lambda = 0 \quad \forall \lambda = 1, k \quad (B.8)$$

The system then can be written as

$$\begin{aligned} \sum_{\beta} b^\beta C(z_\alpha, z_\beta) + \sum_{\lambda} \mu_\lambda f_\alpha^\lambda &= 2 C(z_\alpha, z) \\ \sum_{\alpha} b^\alpha f_\alpha^\lambda &= f^\lambda \end{aligned} \quad (B.9)$$

The covariances $c(z_\alpha, z_\beta)$ and $c(z_\alpha, z)$ are obtained from the following relations:

$$C(z_\alpha, z) = -\gamma(Fz_\alpha - Fz) \text{ and } C(z_\alpha, z_\beta) = -\gamma(Fz_\alpha - Fz_\beta)$$

Then the linear system of equations becomes

$$\begin{aligned} \sum_{\beta} b^\beta \gamma(z_\alpha - z_\beta) + \sum_{\lambda} \mu_\lambda f_\alpha^\lambda &= 2 \gamma(z_\alpha - z) \\ \sum_{\beta} b^\beta f^\lambda(z_\beta) &= f^\lambda(z) \end{aligned} \quad (B.10)$$

where the b 's and μ 's are the unknown quantities. Therefore, solving this system the estimator of the variable is defined by:

$$\hat{z}(x, y) = \sum_{\beta} b^\beta z_\beta \quad (B.11)$$

and the variance of the estimate is

$$\sigma_{\hat{z}}^2 = \sum_{\beta} b^\beta \gamma(z_\beta - z) + \sum_{\lambda} \mu_\lambda f^\lambda(z) \quad (B.12)$$

3. Regression analysis estimates versus estimates obtained by the inference correlative model.

The estimation $\hat{Z}(X_0)$ of the examined physical parameter is performed according to the following regression scheme with independent residuals:

$$\hat{Z}(X_0) = \sum_{\beta=1}^m a_{\beta} g_{\beta}(X_0) + \varepsilon(X_0) \quad (\text{B.13})$$

where the coefficients a_{β} are inferred from the set of all known values Z_{β} , $\beta = 1, \dots, m$, $g_{\beta}(X_0)$ are some a priori known functions and $\varepsilon(X_0)$ is an independent residual. The a_{β} 's are determined using the least squares technique.

On the other hand the inference correlative model is based on the assumption of correlated random fields and the estimation is expressed as:

$$\hat{Z}(X_0) = \sum_{\beta=1}^n \lambda_{\beta} Z_{\beta} \quad (\text{B.14})$$

which is a linear combination of the known values Z_{β} . The unknown parameters λ_{β} are determined according to the minimization scheme given in appendix B.2.

To compare the estimation schemes, we compute the deviation $D = D_R - D_E$ and the coefficient of multiple correlation D_E/D_R where

$$D_R = \sum_i (Z_i)^2 - (\sum_i Z_i)^2/n ; \text{ where } Z_i \text{ the real values} \quad (\text{B.15})$$

$$D_E = \sum_i (\hat{Z}_i)^2 - (\sum_i \hat{Z}_i)^2/n ; \text{ where } \hat{Z}_i \text{ the estimated values} \quad (\text{B.16})$$

Appendix C

Computations Related to the Finite Element Uncertainty Analysis

1. Evaluation of the Strain Energy of the Beam Element Considering Geometric Nonlinearity

It is given by the following expression:

$$\pi_s = E \int_V \left[\frac{1}{2} (F_2 + F_3) + F_4 + F_5 + F_6 + \frac{1}{2} \int_V \left[(\epsilon_y^0)^2 + \rho (\epsilon_{xy}^0)^2 \right] dV \right] \quad (C.1)$$

Developing each component of the above expression we obtain

$$\begin{aligned} F_2 &= \int_V \left[(\epsilon_x^L)^2 + \rho (\epsilon_{xy}^L)^2 \right] dV = \int_V (a_1 - y v_{,xx})^2 dV = \\ &= \int_V (a_1^2 + y^2 v_{,xx}^2) dV + \int_V (-2a_1 v_{,xx}) dV \end{aligned}$$

$$\begin{aligned} F_3 &= \int_V \left[(\epsilon_x^N)^2 + (\epsilon_{xy}^N)^2 \right] dV = \int_V \left[\frac{1}{4} (u_{,x}^2 + v_{,x}^2)^2 + \rho u_{,x}^2 v_{,x}^2 \right] dV = \\ &= \int_V \left[\frac{1}{4} u_{,x}^4 + v_{,x}^4 + 2u_{,x}^2 v_{,x}^2 \right] dV + \rho \int_V u_{,x}^2 v_{,x}^2 dV \end{aligned}$$

$$\begin{aligned} F_4 &= \frac{1}{2} \int_V \left[\epsilon_x^0 \epsilon_x^L + \rho \epsilon_{xy}^0 \epsilon_{xy}^L \right] dV = \frac{1}{2} \int_V (\epsilon_x^0 u_{,x}) dV = \\ &= \int_V \epsilon_x^0 (a_1 - y v_{,xx}) dV \end{aligned}$$

$$\begin{aligned} F_5 &= \frac{1}{2} \int_V \left[\epsilon_x^0 \epsilon_x^N + \rho \epsilon_{xy}^0 \epsilon_{xy}^N \right] dV = \frac{1}{2} \int_V \epsilon_x^0 (u_{,x}^2 + v_{,x}^2) dV - \\ &\quad - \frac{\rho}{2} \int_V \epsilon_{xy}^0 u_{,x} v_{,x} dV \end{aligned}$$

$$F_6 = \frac{1}{2} \int_V (\epsilon_x^L \epsilon_x^N + \rho \epsilon_{xy}^L \epsilon_{xy}^N) dV = \frac{1}{2} \int_V u_{,x} (u_{,x}^2 + v_{,x}^2) dV -$$

$$- \frac{1}{2} \int_V \rho \theta u_{,x} v_{,x} dV = \frac{1}{2} \int_V (u_{,x}^3 + u_{,x} v_{,x}^2) dV$$

All these quantities need to be integrated over the volume of the element.

It is to be noticed that:

$$\iiint dz dy = \text{Area} = A$$

$$\iiint y^2 dz dy = \text{Inertia} = I$$

and $\iiint y^n dz dy = \text{for odd } n$

More development of F's expressions are given in the following computations.

$$\frac{1}{2} F_2 = \frac{1}{2} \int_V [a_1^2 + y^2 v_{,xx}^2] dV - \frac{1}{2} \int_V 2a_1 y v_{,xx} dV$$

$$= \frac{1}{2} \left[\int a_1^2 A dx + \int v_{,xx}^2 I dx \right] = \frac{1}{2} A [a_1^2 L + I \int v_{,xx}^2 dx]$$

$$\frac{1}{2} F_3 = \frac{1}{2} \int_V \left[\frac{1}{4} (u_{,x}^4 + v_{,x}^4 + 2u_{,x}^2 v_{,x}^2) dV + \rho \int_V u_{,x}^2 v_{,x}^2 dV \right] =$$

$$= \frac{1}{8} a_1^4 \int dx \int dy dz + \frac{1}{4} a_1^2 \int dx v_{,x}^2 \int y^2 dy dz + \frac{3}{4} a_1^2 \int dx v_{,xx}^2 \int y^2 dy dz$$

$$= \frac{1}{8} a_1^4 A L + \frac{1}{4} A a_1^2 \int v_{,x}^2 dx + \frac{1}{2} \rho A a_1^2 \int v_{,x}^2 dx + \frac{3}{4} a_1^2 I \int v_{,xx}^2 dx$$

$$F_4 = \int_V \epsilon_x^0 (a_1 - y v_{,xx}) dV = \int_V \epsilon_x^0 a_1 dV - \int_V \epsilon_x^c y v_{,xx} dV = \epsilon_x^c a_1 A L$$

$$F_5 = \int_V (\epsilon_x^0 \epsilon_x^N + \rho \epsilon_{xy}^0 \epsilon_{xy}^N) dV = \frac{1}{2} \int_V \epsilon_x^0 (u_{,x}^2 + v_{,x}^2) dV - \rho \int_V \epsilon_{xy}^0 u_{,x} v_{,x} dV$$

$$F_5 = \frac{1}{2} \epsilon_x^0 A a_1^2 \int dx + \epsilon_x^0 I \int v_{,xx}^2 dx + \frac{1}{2} \epsilon_x^0 A \int v_{,x}^2 dx - \\ - \rho \epsilon_{xy}^0 a_1 A \int v_{,x} dx$$

$$F_6 = \frac{1}{2} \int_V (u_{,x}^3 + u_{,x} v_{,x}^2) dV = \frac{1}{2} \int_V (a_1 - y v_{,xx})^3 dV + \\ + \frac{1}{2} \int_V (a_1 - y v_{,xx}) v_{,xx}^2 dV$$

$$= \frac{1}{2} A a_1^3 \int dx - \frac{3}{2} a_1 I \int v_{,xx}^2 dx + \frac{1}{2} A a_1 \int v_{,x}^2 dx$$

The results of these computations are given in Table (6.1) in which the contribution of each type of variable is clearly shown.

2. Evaluation of Matrices $[n_1]$ and $[n_2]$

Differentiating the expressions of ϕ 's with respect to the variable x we obtain:

$$\begin{aligned} \phi_{1,x} &= 0 \\ \phi_{2,x} &= 1 \\ \phi_{3,x} &= \frac{2}{L} x - 1 \\ \phi_{4,x} &= \frac{3}{L^2} x^2 - \frac{3}{L} x + \frac{1}{2} \end{aligned} \tag{C.2}$$

The above expressions as a matter of fact represent the strain (a dimensional quantities). Also

$$\begin{aligned}\phi_{1,xx} &= 0 \\ \phi_{2,xx} &= 0 \\ \phi_{3,xx} &= \frac{2}{L} \\ \phi_{4,xx} &= \frac{6}{L^2} x - \frac{3}{L}\end{aligned}\tag{C.3}$$

Now from the assumptions stated in section 6.3

$$v(x) = \alpha^T \phi(x), \quad v_{,x}(x) = \alpha^T \phi_{,x}(x), \quad v_{,xx}(x) = \alpha^T \phi_{,xx}(x)$$

Therefore:

$$\begin{aligned}v_{,x}^2(x) &= \alpha^T (\phi_{,x}, \phi_{,x}) \alpha \\ v_{,xx}^2(x) &= \alpha^T (\phi_{,xx}, \phi_{,xx}) \alpha\end{aligned}\tag{C.4}$$

and

$$\begin{aligned}\int_x v_{,x}^2 dx &= \alpha^T \left[\int_x (\phi_{,x}^i, \phi_{,x}^j) dx \right] \alpha \\ \int_x v_{,xx}^2 dx &= \alpha^T \left[\int_x (\phi_{,xx}^i, \phi_{,xx}^j) dx \right] \alpha\end{aligned}$$

Then

$$\left[n_1^{(i,j)} \right]_{i,j} = (\phi_{,x}^i, \phi_{,x}^j)_{ij} = \int_x \begin{bmatrix} \phi_x^1 & \phi_x^1 & \phi_x^1 & \phi_x^2 & \dots \\ \phi_x^4 & \phi_x^1 & & & \end{bmatrix} dx$$

or

$$\left[n_1^{(i,j)} \right]_{i,j} = \int_x dx \begin{bmatrix} 0 & 0 & 0 & 0 \\ 0 & 1 & (\frac{2}{L}x-1) & (\frac{3}{L^2}x^2 - \frac{2}{L}x + \frac{1}{2}) \\ 0 & 0 & (\frac{2}{L}x-1)^2 & (\frac{2}{L}x-1)(\frac{3}{L^2}x^2 - \frac{2}{L}x + \frac{1}{2}) \\ 0 & & & (\frac{3}{L^2}x^2 - \frac{2}{L}x + \frac{1}{2})^2 \end{bmatrix}$$

Finally

$$[n_1] = L \begin{bmatrix} 0 & 0 & 0 & 0 \\ 0 & 1 & 0 & 0 \\ 0 & 0 & 1/3 & 0 \\ 0 & 0 & 0 & 1/20 \end{bmatrix} \quad (C.5)$$

In the same way matrix $[n_2]$ is evaluated.

$$\left[n_2^{(i,j)} \right]_{i,j} = \int_x dx \begin{bmatrix} 0 & 0 & 0 & 0 \\ 0 & 0 & 0 & 0 \\ 0 & 0 & (\frac{2}{L})^2 & (\frac{2}{L})(\frac{6}{L^2}x - \frac{3}{L}) \\ 0 & 0 & & (\frac{6}{L^2}x - \frac{3}{L}) \end{bmatrix}$$

and after integration

$$[n_2] = \frac{1}{L} \begin{bmatrix} 0 & 0 & 0 & 0 \\ 0 & 0 & 0 & 0 \\ 4 & 0 & & \\ & & & 3 \end{bmatrix} \quad (C.6)$$

3. Newton Raphson Iterative Procedure

The general form of the equation of equilibrium is given by

$$[NK(u^n)] - \{F\} = 0 \quad (C.7)$$

Expression (C.7) represents a system of nonlinear equations. To apply Newton's iterative procedure we have to guarantee:

- a. The Monotonicity of the nonlinear
- b. The Continuity of the Nonlinear function.

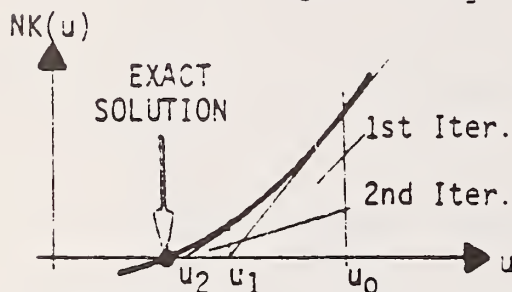
Under the assumption of small strains but large displacements the above conditions are verified.

Then using Taylor's expansion:

$$NK(u^n) = NK(u^{n-1}) + \left[\frac{\partial NK(u^{n-1})}{\partial u} \right] (u^n - u^{n-1}) \quad (C.8)$$

and substituting in Equation (C.7) one obtains:

$$\left[\frac{\partial NK(u^{n-1})}{\partial u} \right] (u^n - u^{n-1}) = F - NK(u^{n-1}) \quad (C.9)$$



This is a linear system of equations and can be solved if $\{u^{n-1}\}$ is a known value. In our case it is given by the initial conditions.

4. Evaluation of First and Second Moments of the Tangent Modulus of Elasticity

The independent random variable to be considered is the Initial Modulus of Elasticity E_i . Therefore the First Moment of E_t is:

$$\bar{E}_t = \frac{1/\bar{E}_i}{\left[\frac{1}{\bar{E}_i} + \frac{R_f \epsilon}{\sigma_1 - \sigma_3} \right]^2}$$

where \bar{E}_i = the mean value of E_i .

The Second Moment is evaluated using an approximation as suggested in section 3.4 by Eq. (3.4). Therefore the variance of E_t is

$$\sigma^2(E_t) = \sigma^2(E_i) \frac{\partial E_t(\bar{E}_i)}{\partial E_i} \quad (C.10)$$

5. Evaluation of the Derivative of the Stiffness Matrix with Respect to the Modulus of Elasticity E and the Poisson Ratio ν

The stiffness matrix of a triangular constant strain element is given by the expression

$$[K] = [B]^T [D] [B] t A \quad (C.11)$$

where $[B]$ = the Influence Matrix

$[D]$ = the Elasticity Matrix

t = the thickness of the element

A = the area

The derivative of $[K]$ with respect to the Modulus of Elasticity is given by

$$\frac{\partial [K]}{\partial E} = [B]^T \frac{\partial [D]}{\partial E} [B] t A \quad (C.12)$$

where

$$\frac{\partial [D]}{\partial E} = \frac{1}{(1+\nu)(1-2\nu)} \begin{bmatrix} 1-\nu & \nu & 0 \\ \nu & 1-\nu & 0 \\ 0 & 0 & \frac{1-2\nu}{2} \end{bmatrix}$$

The derivative of $[K]$ with respect to the Poisson's ratio is given by

$$\frac{\partial [K]}{\partial \nu} = [B]^T \frac{\partial [D]}{\partial \nu} [B] t A \quad (C.13)$$

where $\frac{\partial [D]}{\partial \nu}$ is computed in the following way

$$(1 - \nu - 2\nu^2) [D] = E \begin{bmatrix} 1-\nu & \nu & 0 \\ \nu & 1-\nu & 0 \\ 0 & 0 & \frac{1-2\nu}{2} \end{bmatrix}$$

Taking the derivatives we obtain

$$(-1 - 4\nu) [D] + (1 + \nu)(n - 2\nu) \frac{\partial [D]}{\partial \nu} = E \begin{bmatrix} -1 & 1 & 0 \\ 1 & -1 & 0 \\ 0 & 0 & -1 \end{bmatrix}$$

and finally

$$\frac{\partial [D]}{\partial \nu} = \frac{(1+4\nu)}{(1+\nu)(1-2\nu)} [D] + \frac{E}{(1+\nu)(1-2\nu)} \begin{bmatrix} -1 & 1 & 0 \\ 1 & -1 & 0 \\ 0 & 0 & -1 \end{bmatrix} \quad (C.14)$$

6. Determination of the Equation of Motion

The decomposition of the displacement gives

$$\{d_i(t)\} = \{d_i^B(t)\} + \{d_i^{IN}(t)\}$$

where $\{d_i^B(t)\}$ = the quasistatic displacement due to the displacement of the boundaries

$\{d_i^{IN}(t)\}$ = the inertial contribution to the displacement of the node

Then substituting in the following equation of motion it is obtained

$$[M] \{\ddot{d}\} + [c]\{\dot{d}\} + [K] \{d\} = F = 0$$

where $[M]$ = the mass matrix

$[c]$ = the damping matrix

$[K]$ = the stiffness matrix

$$[M] \{\ddot{d}_i^B + \ddot{d}_i^{IN}\} + [c] \{\dot{d}_i^B + \dot{d}_i^{IN}\} + [K] \{d_i^B + d_i^{IN}\} = 0 \quad (C.15)$$

or $[M] \{\ddot{d}_i^{IN}\} + [c] \{\dot{d}_i^{IN}\} + [K] \{d_i^{IN}\} = -[M] \{\ddot{d}_i^B\} - [c] \{\dot{d}_i^B\}$

If we partition the above matrices into submatrices defined according to the free and constrained nodes as illustrated in Figure C.1 it is obtained (using the following abbreviations).

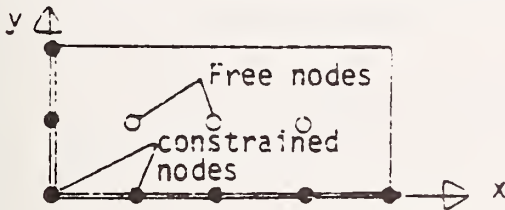


Figure C.1

F = free nodes

C = constrained nodes

B = boundary component

IN = inertial component

$$\begin{bmatrix} m_F & 0 \\ 0 & m_C \end{bmatrix} \begin{Bmatrix} \ddot{d}^{IN} \\ 0 \end{Bmatrix} + \begin{bmatrix} c_{11} & c_{12} \\ c_{21} & c_{22} \end{bmatrix} \begin{Bmatrix} \dot{d}_F^{IN} \\ 0 \end{Bmatrix} + \begin{bmatrix} K_{11} & K_{12} \\ K_{21} & K_{22} \end{bmatrix} \begin{Bmatrix} d_F^{IN} \\ 0 \end{Bmatrix} = \begin{bmatrix} m_F & 0 \\ 0 & m_C \end{bmatrix} \begin{Bmatrix} \ddot{d}_F^B \\ \ddot{d}_C^B \end{Bmatrix} - \begin{bmatrix} c_{11} & c_{12} \\ c_{21} & c_{22} \end{bmatrix} \begin{Bmatrix} \dot{d}_F^B \\ \dot{d}_C^B \end{Bmatrix} \quad (C.16)$$

The equation of motion for the free nodes is then given by:

$$[m_F] \{\ddot{d}_F^{IN}\} + [c_{11}] \{\dot{d}_F^{IN}\} + [K_{11}] \{d_F^{IN}\} = -[m_F] \{\ddot{d}_F^B\}$$

7. Evaluation of the Variance of the Natural Frequencies

Using Equations (6.45) and (6.48) the equations of motion become:

$$\begin{aligned} & m_{oi} \left(1 + \sum_{r=1}^n \alpha_r s_{ir} \right) - \left(Q_{oi} + \sum_{r=1}^n \pi_{ir} \alpha_r \right) \\ & \omega_0^2 + \left(\sum_{r=1}^n \eta_r \alpha_r \right)^2 + 2\omega_0 \left(\sum_{r=1}^n \eta_r \alpha_r \right) + \\ & + [K]_i \left(Q_{oi} + \sum_{r=1}^n \pi_{ir} \alpha_r \right) = 0 \end{aligned} \quad (C.17)$$

Now comparing the terms containing identical powers of the parameter α_r one obtains:

$$-\omega_0^2 m_{oi} Q_{oi} + K_i Q_{oi} = 0 \quad (C.18)$$

$$\{-\omega_0^2 m_{oi} \pi_{ir} + K_i \pi_{ir}\} \sum_r^n \alpha_r = \quad (C.19)$$

$$= \{2\omega_0 \eta_r m_{oi} Q_{oi} + \omega_0^2 m_{oi} Q_{oi} \delta_{ir}\} \sum_r^n \alpha_r$$

or

$$(-\omega_0^2 m_{oi} + K_i) \pi_{ir} = 2\omega_0 \eta_r m_{oi} Q_{oi} + \omega_0^2 m_{oi} Q_{oi} \delta_{ir}$$

Multiplying by the transpose of Q_{oi} it is obtained:

$$(-\omega_0^2 Q_{oi}^T m_{oi} + Q_{oi}^T K_i) \pi_{ir} = 2\omega_0 \eta_r Q_{oi}^T m_{oi} Q_{oi} + \omega_0^2 Q_{oi}^T m_{oi} Q_{oi} \delta_{ir}$$

or

$$\pi_{ir}^T (-\omega_0^2 Q_{oi} m_{oi} + Q_{oi} K_i) = 2\omega_0 \eta_r Q_{oi}^T m_{oi} Q_{oi} + \omega_0^2 Q_{oi}^T m_{oi} Q_{oi} \delta_{ir}$$

Now making use of Eq. (C.18)

$$2\omega_0 \eta_r Q_{oi}^T m_{oi} Q_{oi} + \omega_0^2 Q_{oi}^T m_{oi} Q_{oi} \delta_{ir} = 0 \quad (C.20)$$

Finally for each natural frequency (j) the influence parameter η_r can be computed from (C.20). Thus:

$$(\eta_r)_j = \frac{\omega_{oj} \{Q_o\}_j^T \begin{bmatrix} m_1 \delta_{1r} & \\ & m_n \delta_{nr} \end{bmatrix} \{Q_o\}_j}{2\{Q_o\}_j^T [m_o] \{Q_o\}_j} \quad (C.21)$$

8. Evaluation of the Derivative of Stresses with Respect to the Frequency

The general expression for the stresses is given by Eq. (6.50)

$$\frac{\partial \sigma}{\partial \omega_i} = [D][B] \frac{\partial \{d_F^{IN}\}_i}{\partial \omega_i}$$

for $i = 1, \dots, n$ nodes.

The only term dependent on the frequency is the dynamic displacement $\{d_F^{IN}\}_i$ which is given by Eq. (6.44)

$$\{d_F^{IN}\}_i = [A]_i [B]_i^T \underline{R}_i(t)$$

where: $[A]_i$ = matrix of eigen vectors

$[B]_i^T$ = influence coefficients matrix.

$$\underline{R}_i(t) = \frac{1}{\omega_{di}} \int_0^t \ddot{d}_B(t - \frac{L}{v_B}) e^{-\xi_i \omega_i (t-\tau)} \sin \omega_{di} (t-\tau) d\tau$$

which has the familiar form of Duhamel's integral.

The use of a numerical procedure is suggested by Newmark (63). Following his approach at time $t_j = t_{j-1} + \Delta t$ the loading factor $R_i(t)$ (having the dimension of a displacement) becomes:

$$\begin{aligned} \underline{R}_i(t_j) = & \underline{R}_i(t_{j-1}) + \dot{\underline{R}}_i(t_{j-1})\Delta t + (\frac{1}{2} - \beta) \ddot{\underline{R}}_i(t_{j-1})(\Delta t)^2 + \\ & + \beta \ddot{\underline{R}}_i(t_j)(\Delta t)^2 \end{aligned} \quad (C.22)$$

for $i = 1, \dots, n$ modes.

where: $\beta = \frac{1}{4}$ consistent with a straight-line variation of $\dot{\underline{R}}_i$ in the increment of time Δt ,

and

$$\ddot{\underline{R}}_i(t_j) = -2\varepsilon \omega_i \dot{\underline{R}}_i - \omega_i^2 (\underline{R}_i - \underline{R}_0) - \ddot{\underline{d}}_B(t - \frac{L}{v_B})$$

\underline{R}_0 = static displacement relative to the base.

Therefore:

$$\frac{\partial \underline{R}_i(t_j)}{\partial \underline{R}_i} = \frac{\beta \partial \ddot{\underline{R}}_i(t_j) \Delta t^2}{\partial \omega_i} \quad (C.23)$$

or

$$\frac{\partial \underline{R}_i(t_j)}{\partial \underline{R}_i} = \beta [-2\varepsilon \dot{\underline{R}}_i - 2\omega_i (\underline{R}_i - \underline{R}_0)] \quad (C.24)$$

9. Determination of the Eigenvalue Problem for the Stability Analysis

Substituting Eq. (6.53) in Eq. (6.51) it is obtained:

$$\begin{aligned} \left[\frac{\partial NK(u^n)}{\partial u} \right] \{u^{n+1} - u^n\} &= \{F\} = NK(u^{n-1}) - \frac{\partial NK(u^{n-1})}{\partial u} \{u^n - u^{n-1}\} \\ \left[\frac{\partial NK(u^n)}{\partial u} \right] \{u^{n+1} - u^n\} &= \frac{\partial NK(u^{n-1})}{\partial u} \{-u^n + u^{n-1}\} = \{F\} - NK(u^{n-1}) \\ \left[\frac{\partial NK(u^n)}{\partial u} \right] \{u^{n+1} - u^n\} - \left[\frac{\partial NK(u^{n-1})}{\partial u} \right] \{u^{n+1} - u^n + u^{n-1} - u^{n+1}\} &= \\ &= \{F\} - NK(u^{n-1}) \end{aligned} \quad (C.25)$$

but

$$(u^{n+1} - u^n) + u^{n-1} - u^{n+1} = \lambda(u^{n+1} - u^n)$$

$$\left(\left[\frac{\partial NK(u^n)}{\partial u} \right] - \lambda \left[\frac{\partial NK(u^{n-1})}{\partial u} \right] \right) \{u^{n+1} - u^n\} = \Delta F$$

or

$$\left[\frac{\partial NK(u^n)}{\partial u} \right] - \lambda \left[\frac{\partial NK(u^{n-1})}{\partial u} \right] \Delta u = \Delta F \quad (C.26)$$

Appendix D

Computations related to the Earthquake Generation Model

The equations of motion of the two degrees of freedom system are given (section 7.2). They are:

$$\ddot{x} + 2(\Xi)(\Omega_n)\dot{x} + (\Omega_n^2)x + 2(\xi)(\omega_n) M(\dot{x}-\dot{z}) + \omega_n^2 M(x-z) = -\ddot{y}$$

$$\ddot{z} - 2(\xi)(\omega_n)(\dot{x}-\dot{z}) - \omega_n^2(x-z) = -\ddot{y}$$

or

$$\ddot{x} + (2 \xi \omega_n M + 2 \Xi \Omega_n)\dot{x} + (\Omega_n^2 + \omega_n^2 M)x -$$

$$- (2 \xi \omega_n M)\dot{z} - (\omega_n^2 M)z = -\ddot{y} \quad (D.1)$$

$$- (2 \xi \omega_n)\dot{x} - (\omega_n^2)x + \ddot{z} + (2 \xi \omega_n)\dot{z} + \omega_n^2 z = -\ddot{y} \quad (D.2)$$

Multiplying Eq. (D.2) by M and adding it to Equation (D.1) one obtains:

$$\ddot{x} + (2 \Xi \Omega_n)\dot{x} + \Omega_n^2 x + M \ddot{z} = - (M+1)\ddot{y} \quad (D.3)$$

$$\ddot{z} + (2 \xi \omega_n)\dot{z} + \omega_n^2 z - (2 \xi \omega_n)\dot{x} - (\omega_n^2)x = -\ddot{y} \quad (D.4)$$

By using the Fourier Transform the working space becomes the frequency domain. Then

$$-\omega^2 x + (2 \Xi \Omega_n)(j\omega)x + \Omega_n^2 x - M \omega^2 z = (M+1)\omega^2 y \quad (D.5)$$

$$-\omega^2 z + (2 \xi \omega_n)(j\omega)z + \omega_n^2 z - (2 \xi \omega_n)(j\omega)x - \omega_n^2 x = \omega_n^2 y \quad (D.6)$$

or after a few transformations

$$[\Omega_n^2 + 2(\Xi \Omega_n)(j\omega) - \omega^2]x - M \omega^2 z = (M+1)\omega^2 y \quad (D.7)$$

$$[(\omega_n^2 - \omega^2) + 2j \xi \omega_n \omega]z - [2j \xi \omega_n \omega + \omega_n^2]x = \omega^2 y \quad (D.8)$$

Thus from equations (D.7) and (D.8), x can be evaluated. Indeed:

$$x = \frac{M \omega^2 z + (M+1)\omega^2 y}{\Omega_n^2 + 2(\Xi \Omega_n)(j\omega) - \omega^2} \quad (D.9)$$

Now replacing Equation (D.9) in Equation (D.8) we obtain

$$\begin{aligned} [(\omega_n^2 - \omega^2) + 2j \xi \omega_n \omega]z - \frac{[(2j \xi \omega_n \omega) + \omega_n^2] \cdot M \omega^2 z}{\Omega_n^2 - 2(\Xi \Omega_n)j \omega - \omega^2} - \\ - \frac{[(2j \xi \omega_n \omega) + \omega_n^2](M+1)\omega^2 y}{\Omega_n^2 + 2(\Xi \Omega_n)j \omega - \omega^2} = \omega^2 y \end{aligned} \quad (D.10)$$

Setting: $A = \omega_n^2 - \omega^2$

$B = 2j \xi \omega_n \omega$

$C = 2j \xi \omega_n \omega + \omega_n^2$

$D = \Omega_n^2 + 2(\Xi \Omega_n)(j\omega) - \omega^2$

Equation (D.10) becomes

$$(A+B)z - \frac{C(M \omega^2 z)}{D} - \frac{C(M+1)\omega^2 y}{D} = \omega^2 y \quad (D.11)$$

Then $D(A+B)z - C(M \omega^2 z) = C(M+1)\omega^2 y + (\omega^2(D))y \quad (D.12)$

or $Z[D(A+B) - C M \omega^2] = \omega^2 y[C(M+1) + D]$

Finally $\frac{z}{y} = \frac{\omega^2[D + C(M+1)]}{D(A+B) - C M \omega^2} \quad (D.13)$

Expression which leads to Equation (7.5).

APPENDIX E

COMPUTATIONS RELATED TO THE EVALUATION OF THE ENTROPY OF INFORMATION

The maximization of the entropy E given in equation 8.13 subject to three constraints is handled according to a variational constrained optimization scheme.

The Lagrangian equation is:

$$\begin{aligned}
 L = & \int_{-\infty}^{\infty} p(f) \log_2 p(f) df + \lambda_1 \left[\int_{-\infty}^{\infty} p(f) df - 1 \right] + \\
 & + \lambda_2 \left[\int_{-\infty}^{\infty} p(f) \cdot f \cdot df - \bar{f} \right] + \lambda_3 \left[\int_{-\infty}^{\infty} p(f) \cdot (f - \bar{f})^2 df - \sigma_f^2 \right]
 \end{aligned} \tag{E.1}$$

where $p(f)$ is the unknown probability density function of f , \bar{f} is the known mean value of f , σ_f^2 is the known variance of f and $\lambda_1, \lambda_2, \lambda_3$ are the Lagrange multipliers.

The maximum of L is obtained through Euler's procedure assuming that

$$p(f) = \hat{p}(f) + \epsilon_1 \eta_1(f) \tag{E.2}$$

where ϵ_1 are constants equal to zero for the maximum value of L and η_1 are arbitrary differentiable functions compatible with the constraints.

Euler's equation is then the following:

$$-\frac{\partial}{\partial p} \left[p \log_2 (p) + \lambda_1 p + \lambda_2 p f + \lambda_3 p (f - \bar{f})^2 \right] = 0 \tag{E.3}$$

and finally it becomes

$$p(f) = e^{-[\log_2 e + \lambda_1 + \lambda_2 f + \lambda_3 (f - \bar{f})^2]} \quad (E.4)$$

The normal distribution satisfies this expression and is substituted in the Entropy function

$$E = - \int_{-\infty}^{\infty} p(f) \log_2 (p(f)) df$$

where $p(f) = \frac{1}{\sigma_f \sqrt{2\pi}} e^{-\frac{1}{2} \left(\frac{f - \bar{f}}{\sigma_f}\right)^2}$

After few computations the following Entropy expression is obtained:

$$E = \log_2 (\sigma_f) + \log_2 (\sqrt{2\pi}) + \frac{\log_2(e) \Gamma(1.5)}{\sqrt{\pi}} \quad (E.5)$$

where Γ is the gamma function.

Appendix F

COMPUTER PROGRAMS AND SUBROUTINES IN RELATION WITH THE DIFFERENT COMPUTATIONAL UNITS OF THE STUDY

These programs are exclusively written for a CDC 6500 computer available at the Purdue University computer center. The following listings are provided:

<u>SUBROUTINE LAGR2</u>	(Inference Model Analysis)
<u>PROGRAM MAXACSP</u>	(Earthquake Generation Model)
<u>SUBROUTINES FOURAN, OUT, PRINT, PLT</u>	(To be included in Program PSEQGEN written by J. Ruiz and J. Penzien)
<u>PROGRAM MESHPL</u>	(Checking and Plotting of Finite Elements Meshes)
<u>PROGRAM STFLOW</u>	(Finite Uncertainty Analysis of Underground Steady Flow)
<u>PROGRAM STLINE</u>	(Finite Uncertainty Analysis of the Liner Element)
<u>SUBROUTINES DEIGEN, UNCERT, MOMENTS</u>	(Dynamic Modal Analysis)

All these programs are written in FORTRAN IV source language using hard and soft wire facilities available in the CDC computer system.

This SUBROUTINE defines the Lagrange multipliers and solves the optimization problem at each of the nodes of the given mesh, allowing the determination of the first and second statistical moments of the physical parameter that is to be inferred from a site investigation.

XT, YT = COORDINATES OF THE NODE IN WHICH THE ESTIMATION OF THE STATISTICAL MOMENTS WILL BE PERFORMED

EXPVL = EXPECTED VALUE OF THE PHYSICAL PARAMETER AT THE NODE

VAR = VARIANCE AT THE NODE

NHEIG() = EIGHT GIVEN INFORMATIONS CONCERNING THE PHYSICAL PARAMETERS AROUND THE NODE

```

C      SUBROUTINE LAGR2 (XT,YT,EXPVL,VAR)
C      -----
C      EVALUATION OF THE STOCHASTIC PARAMETERS AND SOLUTION
C      -----
C      NA      = NUMBER OF CONSTRAINS DEFINED AFTER THE CHOOSEN
C              POLYNOME TO APPROXIMATE THE TREND
C
C      NALFA   = NUMBER OF GIVEN POINTS TO PROCEED WITH THE
C              ESTIMATION
C
C      COMMON X(300),Y(300),Z(300),NUM(300),NUMTRI(300,2),NG(300),ND(300)
C      1,NPOINTE(300),NPLA(2),XENT(4),YENT(4),DELTA,NPGIV,XMIN,XMAX,YMIN,Y
C      2MAX,NINTX,NINTY,NADX,NADY,L4,NENT(4,2)
C      COMMON /SEC/ NUMEL(300),NTR(4,8),NHEIG(32),DIST(32),NHEIG1(8),DIST
C      11(8),LHX,KNY,K8,NBEQ
C      COMMON /B3/ NKRIG,NADR
C      DIMENSION STINF(20,20),SECM(20),SOL(20)
C      DIMENSION F(15,6),BSEC(20)
C      DATA NA,NALFA,LEVEL/6,8,1/
C      DATA LSF,LCF/2,2/
C
C      LSF = 1  MODEL WITH MEAN ,   LSF = 2  MODEL WITH FLUCTUATION
C      LCF = 1  MODEL WITH COVAR,   LCF = 2  MODEL WITH VARIOGRAM
C
C      INITIALIZATIONS
C
C      NEQ=NA+NALFA
C      DO 102 IR=1,NEQ
C        DO 101 JC=1,NEQ
C          STINF(IR,JC)=0.
C101    CONTINUE
C102  CONTINUE
C
C      NALFA1=NALFA+1

```



```

C
C      EVALUATE BASES FUNCTIONS
C
      DO 103 IP=1,NALFA
      NPT=NHEIG(IP)
      XA=X(NPT)
      YA=Y(NPT)
      ZA=Z(NPT)
      IF (LEVEL.EQ.5) PRINT , #ZALPHA#,XA,YA,ZA
      F(IP,1)=1.
      F(IP,2)=XA
      F(IP,3)=YA
      F(IP,4)=XA*XA
      F(IP,5)=XA*YA
      F(IP,6)=YA*YA
103  CONTINUE
C
      F(NALFA1,1)=1.
      F(NALFA1,2)=XT
      F(NALFA1,3)=YT
      F(NALFA1,4)=XT*XT
      F(NALFA1,5)=XT*YT
      F(NALFA1,6)=YT*YT
C
C      FORM MATRIX #STINF#
C
      DO 108 IR=1,NA
      DO 107 JC=1,NALFA
      STINF(IR,JC)=F(JC,IR)
      IF (LCF.EQ.2) GO TO 104
      GO TO 105
104      IF (LSF.EQ.2) GO TO 106
105      STINF(JC+6,IR+NALFA)=-F(JC,IR)
      GO TO 107
106      STINF(JC+6,IR+NALFA)=F(JC,IR)
107  CONTINUE
C
      FORM RIGHT SIDE
C
      SECM(IR)=F(NALFA1,IR)
C
      IF (LSF.EQ.2) GO TO 130
      SECM(1) = 0.
C
108  CONTINUE
C
      DO 113 IR=NA+1,NEQ
      DO 110 JC=1,NALFA
      IPT=NHEIG(IR-NA)
      JPT=NHEIG(JC)
      DIS=SQRT((X(IPT)-X(JPT))**2+(Y(IPT)-Y(JPT))**2)
C
      W = 0.
      IF (DIS, EQ. 0.) GO TO 161
      W1 = Z(IPT) - Z(JPT)
      W = ABS(W1) / DIS
C
      IF (LCF.EQ.2) GO TO 109
      STINF(IR,JC)=COVAR(DIS)
      GO TO 110
109      STINF(IR,JC)=VARIOD(DIS)
110  CONTINUE
C
      FORMM RIGHT SIDE
C
      IF (LSF.LT.2) GO TO 112
      DIS=DIST(IR-NA)
      IF (LCF.EQ.2) GO TO 111
      SECM(IR)=COVAR(DIS)
      GO TO 113

```

```

111     SECM(IR)=VARIOG(DIS)
      GO TO 113
112     CONTINUE
C
      SECM(IR)=0.
113     CONTINUE
      DO 114 IS=1,NEQ
114     BSEC(IS)=SECM(IS)
C
***** DEBUG *****
C
      IF (LEVEL.NE.5) GO TO 116
      DO 115 IR=1,NEQ
        PRINT 123, (STINF(IR,J),J=1,NEQ),SECM(IR)
115     CONTINUE
116     CONTINUE
C
      SOLVE SYSTEM **
C
      -----
C
      IC=20
C
      CALL GAUSS (IC,NEQ,STINF,SECM,SOL)
C
      -----
C
      IF (LEVEL.EQ.5) PRINT 124, (SOL(I),I=1,NEQ)
C
      COMPUTE VARIANCE D2(M)
C
      VAR=0.
      V1=0.
      V2=0.
C
      DO 117 IR=1,NA
        F(NALFA1,IR)=ABS(F(NALFA1,IR))
        V1=V1+SOL(NALFA+IR)*F(NALFA1,IR)
117     CONTINUE
      DO 119 IP=1,NALFA
        IF (LCF.EQ.2) GO TO 118
        V2=V2-SOL(IP)*SECM(NA+IP)
        GO TO 119
118     V2=V2+SOL(IP)*SECM(NA+IP)
119     CONTINUE
C
      IF (LSF.EQ.1) V2=0.
      IF (LCF.EQ.1) GO TO 120
      VAR=V1+V2
      GO TO 121
120     DIS=0.
      VAR=COVAR(DIS)+V1+V2
121     CONTINUE
C
      IF (LEVEL.EQ.2) PRINT 125, VAR,XT,YT
C
      ESTIMATE EXPECTED VALUE
C
      EXPVL=0.
      DO 122 IP=1,NALFA
        EXPVL=EXPVL+SOL(IP)*Z(NHEIG(IP))
122     CONTINUE
      IF (LEVEL.EQ.2) PRINT , #EXPECTEDVAL=#,EXPVL
      RETURN
C
123     FORMAT (1X,10(F10.3,2X))
124     FORMAT (1X, 15HSOLUTION VECTOR,/,1X,10(F8.3,2X))
125     FORMAT (1X, 25HESTIMATED VARIANCE D2(M)=,F10.5, 2HAT,2F10.5)
C
      END
      FUNCTION COVAR(R)

```

	COVAR=EXP(-R)		U
	RETURN		U
C	END		U
	FUNCTION VARIOG(R)		U
	IF(R.EQ.0.) R = 1.		V
	VARIOG = ALOG(R)		
	RETURN		V
C	END		V

```

PROGRAM MAXACSP (INPUT,OUTPUT,PLOT)
C
C *****
C
C THIS PROGRAM FINDS THE MAXIMUM ACCELERATION SPECTRA
C OF THE TWO MASSES SYSTEM VIBRATING UNDER ASSUMED
C SEISME .
C A PLOT FOR DIFFERENT VALUES OF THE PHYSICAL
C PARAMETERS IS PROVIDED BY HIDE (PURDUE CENTER)
C
C VERSION DNM377
C
C -----
C
C DIMENSION Z1(110), Z2(110), FR(110), ZR(40)
C DIMENSION Z1M(30,30), Z2M(30,30)
C DIMENSION XAH(110), YAH(110), TL(8), WAH(300,4), DAH(110,110,2)
C
C EQUIVALENCE ( DAH(1,1,1) , Z1M(1,1) ),
C 1 ( DAH(1,1,2), Z2M(1,1) )
C
C -----
C
C REAL MU
C DATA MOD/1/
C
C INITIALIZATION
C
C ND=21
C NN=50
C AL=0.
C ZETA=0.05
C MAXDIM=300
C XMAX=4.
C YMAX=40.
C XLNTH=6.
C YLNTH=3.
C
C DO 107 M1=1,ND
C
C MU=0.
C DO 106 M2=1,ND
C
C FR(M2)=MU
C Z1(1)=0.
C Z2(2)=0.
C
C OM=0.
C DO 104 I=1,NN
C OM=OM+.05
C A1=1.-OM**2
C B1=MU+1.
C AA1=AL**2-OM**2
C AA3=(1./(OM**2))-1.
C ZET1=0.1
C
C IF (MOD.EQ.2) GO TO 101
C
C C1=2.*AA1*B1+4.*(ZETA**2)*(OM**2)*B1
C
C Z1N=AA1**2+B1**2+C1
C
C DD1=(AA1**2)*(AA3**2)+MU**2-2.*AA1*AA3*MU
C D1=(AA1**2/OM**2)+(OM**2)*MU**2-2.*AA1*MU
C DD2=4.*(ZETA**2)*D1
C
C Z1D=DD1+DD2
C GO TO 102
C
C 101 ZZ1=AA1+B1
C ZZ2=4.*OM**2*(ZETA*B1+ZET1*AL)**2
C Z1N=ZZ1**2+ZZ2
C

```



```

C
      ZD1=AA1*AA3-MU-4*ZETA*ZET1*AL
      ZD2=ZETA*AA1*1./OM-ZETA*OM*MU
      ZD3=ZET1*OM*AL*AA3
      ZD4=4*(ZD2+ZD3)**2
      Z1D=ZD1**2+ZD4
C
C
102      Z1(I)=SQRT(Z1N/Z1D)
C
      DIF1=Z1(I)-Z1(I-1)
      IF (DIF1.GT.0.) Z1MAX=Z1(I)
C
      DT=(AL**2/OM**2)-1.
      DDT=ABS(DT)
C
C
      IF (MOD,EG.1) GO TO 103
      DD1=4.*(ZET1**2)*(AL/OM)**2
      DDT=SQRT(DT**2+DD1)
C
C
103      Z2(I)=(MU*Z1(I)+B1)/DDT
C
      DIF2=Z2(I)-Z2(I-1)
      IF (DIF2.GT.0.) Z2MAX=Z2(I)
      IF (DIF1.LT.0.) GO TO 105
C
104      CONTINUE
C
105      CONTINUE
      PRINT , #AL,MU,#,AL,MU
      PRINT 114, (Z1(I),I=1,NN)
      PRINT , #-----#
      PRINT 114, (Z2(I),I=1,NN)
C
      Z1M(M1,M2)=Z1MAX
      Z2M(M1,M2)=Z2MAX
C
      IF (Z1M(M1,M2).GT.YMAX) Z1M(M1,M2)=YMAX
      IF (Z2M(M1,M2).GT.YMAX) Z2M(M1,M2)=YMAX
C
      MU=MU+.2
C
106      CONTINUE
C
      AL=AL+.2
C
107      CONTINUE
C
      =====
C
      AL=0.
C
      DO 109 K=1,ND
      PRINT , #AL#,AL
C
      DO 108 J=1,ND
      PRINT 115, J,FR(J),Z1M(K,J),Z2M(K,J)
      MPD=21-K
      DAK(MPD,J,1)=Z1M(K,J)
      DAK(MPD,J,2)=Z2M(K,J)
C
108      CONTINUE
      AL=AL+.2
109      CONTINUE
C
      READ 116, NPLOT
      IF (NPLOT.EQ.0) GO TO 113
C
      -----

```

```

C      PLOTTING THE COMPUTED VALUES
C      -----
C
DELTAX=XMAX/XLNTH
DELTAY=YMAX/YLNTH
NNG=0
C
CALL PLOTS
C
DO 112 L=1,2
  NNG=0
  READ 117, TL
  YMAH=0.
  XMIN=0.
C
  DO 111 I=1,21
    DO 110 J=1,21
      WAH(J)=FR(J)
110    YAH(J)=DAH(I,J,L)
C
C      -----
C
1    CALL HIDE (XAH,YAH,WAH(1,1),WAH(1,2),WAH(1,3),WAH(1,4),NNG,M
AXDIM,ND,ND,TL,XLNTH,YLNTH,XMIN,DELTAX,YMAH,DELTAY)
C
C      -----
C
111  CONTINUE
    CALL PLOT (14.,-2.,-3)
    NNG=0
112  CONTINUE
    CALL PLOT (0.,0.,999)
113  STOP
C
114  FORMAT (2X,10(F10.3,2X))
115  FORMAT (10X, 3HJ =,I4,2X, 4HMU =,F5.2,2X, 4H Z1=,F10.3,2X, 4HZ
12 =,F10.3)
116  FORMAT (I2)
117  FORMAT (8A10)
C
END

```

Subroutine FOURAN uses subroutine FORT (provided by the computer center) to compute the discrete Fourier transform.

```

C
C      SUBROUTINE FOURAN (AC,NTOT)
C
C      *****
C
C      COMMON /CNTRL/ NEQREC,T,DT,ACMAX,XETA,F0,TI,T0,CE2,NDOUT(6),HED(8)
C      REAL AC(NTOT),TIME(1026),FAC(1026),PIAC(1026)
C      REAL AIC(1024),S(256)
C      COMPLEX AAC(1024),A(1024)
C
C      -----
C
C      N=50
C
C      DO 101 I=1,1000
101 AAC(I)=AC(I)
C      DO 102 I=1001,1024
102 AAC(I)=0.
C
C      DO 103 I=1,1024
103 AIC(I)=AAC(I)
C
C      -----
C
C      CALL FORT (AAC,10,S,1,IER1)
C
C      -----
C
C      DO 104 J=1,1024
104 A(J)=AAC(J)
C
C      DO 105 K=N,1024
105 A(K)=0.
C
C      -----
C
C      CALL FORT (A,10,S,-2,IER3)
C
C      -----
C
C      TN=0.
C      DO 106 I=1,1024
C          TN=TN+DT
C          TIME(I)=TN
C          AC(I)=A(I)
106 CONTINUE
C      PRINT 107, (AC(I),I=1,256)
C
C      RETURN
C
C      107 FORMAT (5(1X,E14.7))
C
C      END
C      SUBROUTINE OUT (ACC,VEL,DISP,NTOT,NEQ)
C
C      PRINT AND PUNCH RECORDS
C
C      COMMON /CNTRL/ NEQREC,T,DT,ACMAX,XETA,F0,TI,T0,CE2,NDOUT(9),HED(4),
100CE2
C      DIMENSION ACC(NTOT),VEL(NTOT),DISP(NTOT)
C      DT5=5.*DT
C      IF (NDOUT(1).NE.0) GO TO 101
C      PRINT 113, HED,NEQ
C      CALL PRIN (ACC,NTOT,DT5)
101 IF (NDOUT(2).NE.0) GO TO 102

```



```

C      CALL PLOT (0.,AAMIN,3)
      CALL PLOT (XL,AAMIN,2)
      CALL PLOT (0.,0.,3)
      CALL AXIS (0.,0.,10HTIME (SEC),-10,XL,0.,0.,DX,0)
C
      IF (NN.EQ.1) GO TO 105
      IF (NN.EQ.2) GO TO 106
      IF (NN.EQ.3) GO TO 107
105 CALL AXIS (0.,0.,24ACCELERATION (PERCENT G),24,YL,90.,AAMINN,DY,-
11)
      GO TO 108
106 CALL AXIS (0.,0.,17HVELOCITY (FT/SEC),17,YL,90.,AAMINN,DY,-1)
      GO TO 108
107 CALL AXIS (0.,0.,17HDISPLACEMENT (FT),17,YL,90.,AAMINN,DY,-1)
108 CALL SYMBOL (0.5,8.5,0.20,32EARTHQUAKE INPUT SPECIFICATIONS:,0.0,
132)
      CALL SYMBOL (1.,8.3,.15,14DURATION (SEC),0.0,14)
      CALL SYMBOL (1.,8.1,.15,20HTIME INCREMENT (SEC),0.0,20)
      CALL SYMBOL (1.,7.9,.15,7HDAMPING,0.,7)
      CALL SYMBOL (1.,7.7,.15,22HNATURAL FREQUENCY (HZ),0.,22)
      CALL SYMBOL (1.,7.5,.15,14HDECAY CONSTANT,0.,14)
      CALL NUMBER (4.,8.3,.15,T,0.0,5HF10.3)
      CALL NUMBER (4.,8.1,.15,DT,0.,5HF10.3)
      CALL NUMBER (4.,7.9,.15,XETA,0.,5HF10.4)
      CALL NUMBER (4.,7.7,.15,F0,0.,5HF10.4)
      CALL NUMBER (4.,7.5,.15,CCCE2,0.,5HF10.4)
      XL=XL+3.
      CALL SYMBOL (0.,9.,0.35,HED,0.0,40)
      CALL PLOT (XL,0.,-3)
      RETURN
C
      END

```



```

C      CALL GRAPH (I,HNOD,0,X,Y)
C
C      DO 105 NCL=1,NELEM
C          READ 132, NL(NCL),NI(NCL),NJ(NCL),NK(NCL)
C          PRINT 132, NL(NCL),NI(NCL),NJ(NCL),NK(NCL)
105 CONTINUE
C
C      MODULUS OF ELASTICITY
C
C      DO 106 I=1,HNOD
C          READ 125, MN,ECC(I)
C          LE(I)=ECC(I)*10.**5
106 CONTINUE
C
C      POISSON'S RATIO
C
C      DO 107 K=1,HNOD
107 READ 125, ML,PSR(K)
C
C      SPECIFIC GRAVITY
C
C      DO 108 L=1,HNOD
C          READ 125, MLL,GANCL)
C          PRINT 126, EE(L),PSR(L),GANCL)
108 CONTINUE
C
C      DO 109 J=1,NELEM
C          NN(J,1)=NI(J)
C          NN(J,2)=NJ(J)
C          NN(J,3)=NK(J)
109 CONTINUE
C
C      IF (NSCALE.EQ.3) GO TO 113
C      IF (NSCALE.LT.2) GO TO 111
C
C      TRANSLATION OF AXIS
C      -----
C
C      DO 110 J=1,HNOD
C          X(J)=X(J)+TFX
C          Y(J)=Y(J)+TFY
110 CONTINUE
C
C      PLOT OF TRIANGULAR MESH
C      -----
C
111 CONTINUE
C      DO 112 I=1,ELEM
C          NEL=I
C          TI=NN(NEL,1)
C          IJ=NN(NEL,2)
C          IK=NN(NEL,3)
C
C          XP(1)=X(TI)
C          XP(2)=X(IJ)
C          XP(3)=X(IK)
C          XP(4)=XP(1)
C
C          YP(1)=Y(TI)
C          YP(2)=Y(IJ)
C          YP(3)=Y(IK)
C          YP(4)=YP(1)
C
C          ZP(5)=0.
C          ZP(5)=YP(5)
C
C          XP(6)=SCF
C          YP(6)=SCF
C
C          PRINT 121, XP,YP
C

```



```

      CALL LTNE (XC,YP,4,1,1,1)
C
C   PREPARE DATA OF THE PHYSICAL PARAMETERS
C
      EC(D)=(CEE(IJ)+EE(IJ)+EE(IK))/3.
C
      PS(D)=(PSR(IJ)+PSR(IJ)+PSR(IK))/3.
C
      GAM(D)=(GAM(IJ)+GAM(IJ)+GAM(IK))/3.
C
      GO TO 112
C
      XC=(X(IJ)+X(IJ)+X(IK))/3.
      YC=(Y(IJ)+Y(IJ)+Y(IK))/3.
      XC=XC/SCF
      YC=YC/SCF
C
      CALL NUMBER (XC,YC,0.1,I,0.,PHIB)
C
112 CONTINUE
C
      GO TO 115
C
      ONE DIMENSIONAL ELEMENT
      -----
C
113 DO 114 I=1,NELEM
C
      II=NN(I,1)
      IK=NN(I,2)
C
      XP(1)=X(II)
      XP(2)=X(IK)
      YP(1)=Y(II)
      YP(2)=Y(IK)
C
      XP(3)=0.
      YP(3)=0.
      XP(4)=SCF
      YP(4)=SCF
C
      CALL LTNE (XP,YP,2,1,1,4)
C
114 CONTINUE
C
      IF (NC.GT.1) GO TO 103
      GO TO 103
C
115 CONTINUE
C
      PUNCH INPUT DATA FOR DYNAMIC + STATIC F.E. PROGRAMS
C
      DO 116 I=1,NELEM
      PUNCH 122, NK(D),NK(D),NK(D),NK(D),EC(D),PS(D),GAM(D)
116 CONTINUE
C
      DO 117 I=1,NELEM
117 PRINT 127, NK(D),NK(D),NK(D),NK(D),EC(D),PS(D),GAM(D)
C
      DO 118 I=1,NMOD
      PUNCH 123, KN(D),X(D),Y(D)
118 CONTINUE
C
      DO 119 I=1,NMOD
119 PRINT 128, KN(D),X(D),Y(D)
      CALL PLOT (0.,0.,999)
C
C
      STOP

```

```
C
120 FORMAT (1H1)
121 FORMAT (1X, 4HXP =, 6F12.3, /CX, 4HYP =, 6F12.3)
122 FORMAT (4I5, 3E12.4)
123 FORMAT (1I5, 2F10.3)
124 FORMAT (3A10)
125 FORMAT (1I2, F10.4)
126 FORMAT (2X, 3E12.4)
127 FORMAT (2X, 4I5, 3E12.4)
128 FORMAT (2X, I5, 2F 10.3)
129 FORMAT (5F10.3)
130 FORMAT (I2, I3, I5)
131 FORMAT (I2, 2F10.3)
132 FORMAT (4I5)
133 FORMAT (3X, I2, 2F10.3)
C
E10)
```

```

PROGRAM STEFLOW (INPUT,OUTPUT)
*****
                                VERSION 04F377

FINITE ELEMENT PROGRAM PERFORMING AN UNCERTAINTY
ANALYSIS OF AN UNDERGROUND STEADY FLOW
COUPLED WITH AN INFERENCE MODEL (PROGRAM INFMOD)

TRIANGULAR ELEMENTS WITH 3 D.F. ARE USED

-----
      XNOD = X-COORDINATE
      YNOD = Y-COORDINATE
      PKX  = PERMEABILITY COEFFICIENT IN X DIRECT.
      PKY  = PERMEABILITY COEFFICIENT IN Y DIRECT.
      HEAD = GIVEN HEAD
-----

REAL XNODE(80), YNODE(80), Q(80), CT(80)
REAL PK(112,2)
REAL AK(80,40), H(80)
REAL AT(80,40), DKXAK(80,40), DKYAK(80,40)
REAL DXQ(80), DYQ(80)
REAL VAR(80), CVAR(80)
INTEGER IB(80), IE(112,3)
COMMON /EQINDEX/ NEQ, NUMEL, NROW, NCOLS
COMMON /REGION/ A, B, C, D, NGRIDX, NGRIDY
DATA A, B, C, D /0., 1., 0., 1./
DATA NUDESQ, NUMF, 0, LEVEL /45, 62, 2/
DATA NROW, NCOL /80, 40/

READ AND PRINT INPUT DATA

-----
101 READ 107, NFLAG
    READ 90, NGRIDX, NGRIDY
    IF (NFLAG.EQ.0) GO TO 106

-----
CALL DATAIN (Q, PK, XNODE, YNODE, IB, IE, NUDESQ, NUMEL, LEVEL)
-----
CALL MESH(XNODE, YNODE, IB, IE, NUMEL, NUDESQ)
-----
CALL BOUNDH (IE, NUMEL)
-----
CALL SECOND (T0)
-----
CALL FORMEQ (AK, Q, IE, IB, XNODE, YNODE, NROW, NCOL, NUMEL,
1          LEVEL, H, AT, DKXAK, DKYAK, DXQ, DYQ, PK )
-----
CALL SECOND (T1)
EXTIME=T1-T0

```

```

C      PRINT 109, TXTIME.
C
C      -----
C
C      CALL EBSOL (AK, P, DKXK, DXQ, DKYK, DYQ, HROHD, HCOLD, CT, VAR, CVAR)
C
C      -----
C
C      CALL SECOND (T2)
C
C      SOLTM=T2-T1
C      TOTAL=T2-T0
C      PRINT 109, SOLTM
C      PRINT 110, TOTAL
C      PRINT 111, NEQ, NRAND, NUMEL, NNODES
C
C      IF (LEVEL.NE.2) GO TO 103
C      PRINT 112
C      DO 102 IF=1, NNODES
C          TRUEV=HEAD(XNODE(IF), YNODE(IF))
C          APRXV=HC(IF)
C          IF (IB(IF).NE.0) APRXV=Q(1B(IF))
C          ABERROR=ABS(TRUEV-APRXV)
C          PRINT 113, IF, TRUEV, APRXV, ABERROR
102 CONTINUE
103 CONTINUE
C
C      ERRMAX=0.
C      DO 104 IF=1, NNODES
C          IF (IB(IF).EQ.0) GO TO 104
C          TRUE=HEAD(XNODE(IF), YNODE(IF))
C          APRXV=Q(1B(IF))
C          ABSERR=ABS(TRUE-APRXV)
C          IF (ABSERR.GT.ERRMAX) ERRMAX=ABSERR
104 CONTINUE
C      PRINT 114, ERRMAX
C
C      -----
C
C      CALL GRAD (XNODE, YNODE, H, NUMEL, TE)
C
C      -----
C
C      PRINT 115
C      NE=J
C      DO 105 IF=1, NNODES
C          IF (IB(IF).EQ.0) GO TO 105
C          PRINT 116, IF, VAR(NE), CVAR(NE)
C
C          NE=NE+1
105 CONTINUE
C      GO TO 101
106 STOP
C
C      107 FORMAT (2I5)
C      108 FORMAT (1X, 25HFORMATION EQUATION TIME =, F10.5)
C      109 FORMAT (1X, 21HQUATION SOLUT. TIME=, F10.5)
C      110 FORMAT (1X, 21HOTAL SOLUTION TIME =, F10.5)
C      111 FORMAT (1X, 14HNUMBER OF EQ =, I5, /, 1X, 14HNUMBER OF ELM =, I5, /, 1X,
C          14HNUMBER OF ELM=, I5, /, 1X, 14HNUMBER OF NOD=, I5)
C      112 FORMAT (1X, 39H NODE   TRUE SOL   APPR SOL   ABS ERROR)
C      113 FORMAT (1X, I5, 3F10.5)
C      114 FORMAT (1X, 24HMAXIMUM ABSOLUTE ERROR =, E10.3)
C      115 FORMAT (1X, 33HNODE - VARIANCE - COEFFICIENT VAR)
C      116 FORMAT (1X, I5, F10.5, F10.5)
C
C      END
C      SUBROUTINE DATIN (Q, PK, XNODE, YNODE, IX, IF, NNODES, NUMEL, LEVEL)
C
C      READS AND/OR PRINTS THE INPUT DATA

```



```

C
C
C      ***** CONSTANTS DEFINITION *****
C
C      REAL XNODE(NNODES), YNODE(NNODES), PK(NUMEL,2), Q(NNODES)
C      INTEGER IE(NUMEL,3), IX(NNODES)
C      COMMON /EINDEX/ NEO,NUMEL,NBAND,NNODES
C
C      READ NODE HIL, BOUND, COND, X-COOR, Y-COOR)
C
C      NEO=0
101  READ 107, NOD, IX1, XNOD, YNOD, HEADY
C      IF (NOD.EQ.0) GO TO 102
C      NNODES=NOD
C      XNODE(NOD)=XNOD
C      YNODE(NOD)=YNOD
C      IX(NOD)=IX1
C      IF (IX1.EQ.1) GO TO 101
C
C      NUMBER THE FREE DEGREES OF FREEDOM
C
C      NEO=NEO+1
C      IX(NOD)=NEO
C      GO TO 101
102  CONTINUE
C
C      READ ELEMENT INCIDENCES
C
103  READ 108, NEL, I1, J1, K1, PKX, PKY
C
C      PKX = 10.** (-PKX)
C      PKY=PKX
C
C      IF (I1.EQ.0) GO TO 104
C      NOD1=NEL
C
C      PK(NEL,1)=PKX
C      PK(NEL,2)=PKY
C      IE(NEL,1)=I1
C      IE(NEL,2)=J1
C      IE(NEL,3)=K1
C      GO TO 103
104  CONTINUE
C
C      OUTPUT INPUT DATA
C
C      IF (LEVEL.NE.2) RETURN
C      PRINT 109
C      DO 105 NOD=1,NNODES
C          PRINT 110, NOD, XNODE(NOD), YNODE(NOD)
105  CONTINUE
C
C      PRINT 111
C      DO 106 NEL=1,NUMEL
C          PRINT 112, NEL, IE(NEL,1), IE(NEL,2), IE(NEL,3), PK(NEL,1), PK(NEL,2)
106  CONTINUE
C      RETURN
C
107  FORMAT (2I5,3F10.0)
108  FORMAT (4I5,2F10.7)
109  FORMAT (1X,33HNODE 1D      X-COOR  Y-COOR  HEADY)
110  FORMAT (1X,I5,2X,I5,2X,F10.5,F10.5)
111  FORMAT (1X,34H ELEMENT I      J      K      KX      KY)
112  FORMAT (1X,4I5,2F10.5)
C
C      END
C      SUBROUTINE RDRDTH (IE,NUMEL)
C
C      COMPUTES MAX NODAL DIFFERENCE AND SEMI-BANDWIDTH
C

```

```

      THD GER TECHNICAL(3)
      COMMON /EQUDEF/ NBO,NUMEL,NBAND,NMODES
C
      MAXDIF=0
      DO 101 NEL=1,NUMEL
      DO 101 J=1,3
      DO 101 K=1,3
         LL=IABS(TE(NEL,J)-TE(NEL,K))
         IF (LL.GT.MAXDIF) MAXDIF=LL
101 CONTINUE
      NBAND=MAXDIF+1
      PRINT *,#BANDWIDTH#,NBAND
      RETURN
C
      END
      SUBROUTINE LINEAR (STIF,DXSTIF,DYSTIF,RS,LEVEL)
C
C     COMPUTES THE ELEMENT STIFFNESS MATRIX
C
      RFA0=STIF(3,3),DYSTIF(3,3),DYSTIF(3,3),RS(3),AJ(P),HC(P),AI(2),AS(2)
1)
      COMMON /PERMRL/ PKX,PKY
      COMMON /ELSPDC/ X1I,Y1I,XJ,J,YJ,J,JKK,YKK
C
      DATA AJ,H,AI,AS/,.2113248654, .7886751346, .5, .5, .1550510257, .6449489
1743, .3764039627, .5124858362/
C
      DEFINE DUMMY VARIABLES
      A1=KKK-XJJ
      A2=X1I-XKK
      A3=XJJ-X1I
C
      B1=YJJ-YKK
      B2=YKK-Y1I
      B3=Y1I-YJJ
C
      COMPUTE AREA
      AREA2=(A3*B2-A2*B3)
C
      COMPUTE DUMMY CONSTANTS
      RAREA=.5/AREA2
      DUMY=AREA2
      A1A1=A1*A1
      A1A2=A1*A2
      A1A3=A1*A3
      A2A2=A2*A2
      A2A3=A2*A3
      A3A3=A3*A3
C
      B1B1=B1*B1
      B1B2=B1*B2
      B1B3=B1*B3
      B2B2=B2*B2
      B2B3=B2*B3
      B3B3=B3*B3
C
      COMPUTE STIFFNESS MATRIX AND ITS FIRST PARTIAL DERIVATIVES
      STIF(1,1)=(PKX*B1B1+PKY*A1A1)*RAREA
      STIF(1,2)=(PKX*B1B2+PKY*A1A2)*RAREA
      STIF(1,3)=(PKX*B1B3+PKY*A1A3)*RAREA
      STIF(2,2)=(PKX*B2B2+PKY*A2A2)*RAREA
      STIF(2,3)=(PKX*B2B3+PKY*A2A3)*RAREA
      STIF(3,3)=(PKX*B3B3+PKY*A3A3)*RAREA
      STIF(2,1)=STIF(1,2)
      STIF(3,1)=STIF(1,3)
      STIF(3,2)=STIF(2,3)
C

```

```

C      COMPUTE DERIVATIVES OF STIFFNESS MATRIX
C
DXSTIF(1,1)=B1B1*PARAEA
DXSTIF(1,2)=B1B2*PARAEA
DXSTIF(1,3)=B1B3*PARAEA
DXSTIF(2,2)=B2B2*PARAEA
DXSTIF(2,3)=B2B3*PARAEA
DXSTIF(3,3)=B3B3*PARAEA
DXSTIF(2,1)=DXSTIF(1,2)
DXSTIF(3,1)=DXSTIF(1,3)
DXSTIF(3,2)=DXSTIF(2,3)
C
DYSTIF(1,1)=A1A1*PARAEA
DYSTIF(1,2)=A1A2*PARAEA
DYSTIF(1,3)=A1A3*PARAEA
DYSTIF(2,2)=A2A2*PARAEA
DYSTIF(2,3)=A2A3*PARAEA
DYSTIF(3,3)=A3A3*PARAEA
DYSTIF(2,1)=DYSTIF(1,2)
DYSTIF(3,1)=DYSTIF(1,3)
DYSTIF(3,2)=DYSTIF(2,3)
C
RS(3)=0.
RS(2)=RS(3)
RS(1)=RS(2)
C
C      COMPUTE RIGHT SIDE
C
DO 102 I=1,2
  DO 101 J=1,2
    RL1=AI(I)
    TEMP=J.-RL1
    RL2=AJ(J)*TEMP
    RL3=TEMP-RL2
    W=AS(I)*H(J)*TEMP
C
C      CHANGE COORDINATE SYSTEM
C
X=XII*RL1+XJJ*RL2+XKK*RL3
Y=YII*RL1+YJJ*RL2+YKK*RL3
C
QVAL=FLFLX(X,Y)
RS(1)=RS(1)+QVAL*RL1*W
RS(2)=RS(2)+QVAL*RL2*W
RS(3)=RS(3)+QVAL*RL3*W
101 CONTINUE
102 CONTINUE
C
DO 103 IR=1,3
  RS(IR)=RS(IR)*DUPY
103 CONTINUE
C
C      *** DEBUG *****
C
IF (LEVEL.NE.5) RETURN
PRINT 107
DO 104 IF=1,3
  PRINT 108, (STIF(IF,JF),JF=1,3),RS(IF)
104 CONTINUE
PRINT 109
DO 105 IF=1,3
  PRINT 108, (DXSTIF(IF,JF),JF=1,3)
105 CONTINUE
PRINT 110
DO 106 IF=1,3
  PRINT 108, (DYSTIF(IF,JF),JF=1,3)
106 CONTINUE
RETURN
C
107 FORMAT (1X,3I1STIFFNESS MATRIX AND RIGHT SIDE)
108 FORMAT (1X,3F10.5,5X,F10.5)

```

```

109 FDMAT (IX, 35)DERIVATIVE OF STIFFNESS MATRIX DKXS)
110 FDMAT (IX, 30)DERIV OF STIFFNESS MATRIX DKYS)
C
C      END
C      FUNCTION FFLX(X,Y)
C
C      FFLX = -2.*EXP(X*Y)
C
C      FFLX=0.
C
C      RETURN
C
C      END
C      SUBROUTINE FORMER (AK,Q,TE,IX,XNODE,YNODE,NROWD,NCOLD,NUMEL,D,LEVEL
1, H, AT, DKXAK, DKYAK, DXQ, DYQ, PK)
C
C      USES DIRECT STIFFNESS PROCEDURE TO ADD THE ELEMENT
C      STIFFNESS MATRICES AND LOADS TO PROPER LOCATIONS
C      IN ASSEMBLAGE STIFFNESS *AK* AND ?FLUX *Q*
C
C      REAL AK(NROWD,NCOLD),Q(NROWD),XNODE(NROWD),YNODE(NROWD),AT(NROWD:H
1COL D),DKXAK(NROWD,NCOLD),DKYAK(NROWD,NCOLD)
C      REAL H(NROWD),DXQ(NROWD),DYQ(NROWD),PK(NUMEL,D,2)
C      INTEGER TE(NUMEL,D,3),IX(NROWD),LM(3)
C      COMMON /ZERNDX/ NEQ,NUMEL,NBAND,NNODES
C      COMMON /PERMPL/ PKX,PKY
C      COMMON /ELSPEC/ XII,YII,XJJ,YJJ,XYK,YKK
C      REAL STIF(3,3),RS(3),DKS(3,3),DYS(3,3)
C
C      INITIALIZE *AK* , *Q*
C
C      DO 102 IR=1,NEQ
C          Q(IR)=0.
C          DO 101 JC=1,NBAND
C              AK(IR,JC)=0.
C              AT(IR,JC)=0.
C              DKXAK(IR,JC)=0.
C              DKYAK(IR,JC)=0.
101      CONTINUE
102      CONTINUE
C
C      COMPUTE BOUNDARY CONDITIONS
C
C      DO 103 IN=1,NNODES
C          H(IN)=0.
C          IF (IX(IN).EQ.0) H(IN)=HEAD(XNODE(IN),YNODE(IN))
103      CONTINUE
C
C      FORM EQUATIONS
C
C      SET CONSTANT COEFFICIENTS
C
C      DO 110 NEL=1,NUMEL
C
C          PKX=PK(NEL,1)
C          PKY=PK(NEL,2)
C
C      COMPUTE ELEMENT STIFFNESS MATRIX AND RIGHT SIDE
C
C      FIND ELEMENT INCIDENCIES
C
C          II=IE(NEL,1)
C          JJ=IE(NEL,2)
C          KK=IE(NEL,3)
C
C      COMPUTE ELEMENT SPECIFICATIONS
C
C          XII=XNODE(II)
C          YII=YNODE(II)

```



```

XJJ=XNODE(JJ)
YJJ=YNODE(JJ)
XKK=XNODE(KK)
YKK=YNODE(KK)
C
C      FIND THE CORRESPONDING DEGREE OF FREEDOM
C
      LM(1)=II
      LM(2)=JJ
      LM(3)=KK
C
C      CALL S/R LINEAR
C
C      -----
C
      CALL LINEAR (SYTE,DYS,DYS,RS,LEVEL)
C
C      -----
C
      DO 106 IF=1,3
C
          NROW=LM(IF)
          IXNROW=IX(NROW)
          IF (IXNROW.EQ.0) GO TO 106
          Q(IXNROW)=Q(IXNROW)+RS(IF)
          ITEMP=1-IXNROW
C
          DO 105 JF=1,3
              NCOL=LM(JF)
              IXNCOL=IX(NCOL)
              IF (IXNCOL.EQ.0) GO TO 104
              IXNCOL=IXNCOL+ITEMP
              IF (IXNCOL.GT.1) GO TO 105
              AK(IXNROW,IXNCOL)=AK(IXNROW,IXNCOL)+STIF(IF,JF)
              GO TO 105
          104      CONTINUE
              Q(IXNROW)=Q(IXNROW)-STIF(IF,JF)*IXNCOL
          105      CONTINUE
          106      CONTINUE
C
          NBAND=MTN0(NC0-NROW)
C
C      ASSEMBLY DEXAK , DKYAK
C
          DO 109 IF=1,3
              NROW=LM(IF)
              IXNROW=IX(NROW)
              IF (IXNROW.EQ.0) GO TO 109
              ITEMP=NBAND-IXNROW
C
              DO 108 JF=1,3
                  NCOL=LM(JF)
                  IXNCOL=IX(NCOL)
                  IF (IXNCOL.EQ.0) GO TO 107
                  IXNCOL=IXNCOL+ITEMP
                  IF (IXNCOL.GT.NBAND) GO TO 108
C
                  DKXAK(IXNROW,IXNCOL)=DKXAK(IXNROW,IXNCOL)+DXS(IF,JF)
                  DKYAK(IXNROW,IXNCOL)=DKYAK(IXNROW,IXNCOL)+DYS(IF,JF)
                  AT(IXNROW,IXNCOL)=AT(IXNROW,IXNCOL)+STIF(IF,JF)
                  GO TO 108
              107      CONTINUE
                  DXQ(IXNROW)=DXQ(IXNROW)+DXS(IF,JF)*IXNCOL
                  DYQ(IXNROW)=DYQ(IXNROW)+DYS(IF,JF)*IXNCOL
          108      CONTINUE
          109      CONTINUE
          110      CONTINUE
C
C      ***** DEBUG *****
C
C

```

```

      IF (LEVEL.NE.4) RETURN
      DO 111 IF=1,NEQ
        PRINT 115, (AK(I,R),JC),JC=1,NBAND),Q(I,R)
111 CONTINUE
C
      PRINT 116
      DO 112 IF=1,NEQ
        PRINT 115, (DKXAK(IF,JF),JF=1,NBAND),DXQ(IF)
112 CONTINUE
C
      PRINT 117
      DO 113 IF=1,NEQ
        PRINT 115, (DKYAK(IF,JF),JF=1,NBAND),DYQ(IF)
113 CONTINUE
C
      DO 114 IF=1,NEQ
        PRINT 115, (AT(I,F),JF),JF=1,NBAND)
114 CONTINUE
C
      RETURN
C
115 FORMAT (1X,10F5.2)
116 FORMAT (1X, 12HMATRIX DKXAK)
117 FORMAT (1X, 13HMATRIX DKYAK )
C
      END
      SUBROUTINE EQSHE, (AK,Q,DKXAK,DXQ,DKYAK,DYQ,NROWD,NCOLD,C,VAR,CVAR)
C
      SOLVES THE SYSTEM OF LINEAR EQUATIONS
C
      REAL XCDV(100),YCDV(100),CDVR(2,2)
      REAL AK(NROWD,NCOLD),Q(NROWD),DKXAK(NROWD,NCOLD),DXQ(NROWD),DKYAK(
1 NROWD,NCOLD),DYQ(NROWD),C(NROWD),VAR(NROWD),CVAR(NROWD)
      COMMON /EQINDEX/ NEQ,NUMEL,NBAND,NNODES
      DATA IPR/4/
C
C
C
C
C
C
C
C
C
C
      SOLVE EQUATIONS
C
      CALL SOLVE (1,AK,Q,NEQ,NBAND,NROWD,NCOLD)
C
      CALL SOLVE (2,AK,Q,NEQ,NBAND,NROWD,NCOLD)
C
      NBAND0=NBAND-1
      CALL VMULQF (DKXAK,NEQ,NBAND0,NROWD,Q,1,NROWD,C,NROWD)
      PRINT 104, (C(I),I=1,NEQ)
      PRINT 104, (Q(I),I=1,NEQ)
C
      DO 101 IF=1,NEQ
        DXQ(IF)=DXQ(IF)+C(IF)
        DYQ(IF)=-DYQ(IF)
101 CONTINUE
      PRINT 104, (DXQ(IF),IF=1,NEQ)
C
      CALL SOLVE (2,AK,DXQ,NEQ,NBAND,NROWD,NCOLD)
C
      PRINT 104, (DXQ(IF),IF=1,NEQ)
C
      CALL VMULQF (DKYAK,NEQ,NBAND0,NROWD,Q,1,NROWD,C,NROWD)
C
      DO 102 IF=1,NEQ
        DYQ(IF)=DYQ(IF)+C(IF)
        DYQ(IF)=-DYQ(IF)
102 CONTINUE
C
      CALL SOLVE (2,AK,DYQ,NEQ,NBAND,NROWD,NCOLD)
C
      PRINT 104, (DYQ(IF),IF=1,NEQ)
C
      COMPUTE VARIANCES AND COEFFICIENT OF VARIATION
C

```

```

DO 103 IA=1,NEQ
  READ 106, XCDV(IA),YCDV(IA)
  PRINT 105, XCDV(IA),YCDV(IA)

  XCDV(IA)=10.**(-XCDV(IA) ) * 10.**(-7)

  XCDV(IA)=XCDV(IA)/IPR

  YCDV(IA)=XCDV(IA)

  CDVR(1,1)=XCDV(IA)
  CDVR(2,2)=YCDV(IA)
  CDVR(1,2)=0.

  VAR(IA)=DXQ(IA)**2*CDVR(1,1)+TYQ(IA)**2*CDVR(2,2)+2.*DXQ(IA)*DY
  Q(IA)*CDVR(1,2)
  CVAR(IA)=SQRT(ABS(VAR(IA)))/Q(IA)
103 CONTINUE

  RETURN

104 FORMAT (1X,10F8.2)
105 FORMAT (2X,2F18.8)
106 FORMAT (2F10.7)

END
FUNCTION HEAD(X,Y)
  HEAD = FUNCTION OF COORDINATE SYSTEM (INF. MODEL)

  HEAD=0.
  IF (X.EQ.0.) HEAD= ABS(Y - 75.) + 14.
  IF (X.EQ.150.) HEAD= ABS(Y - 75.)

  RETURN

END
SUBROUTINE PERM (PKX,PKY)
  PKX=1.
  PKY=1.
  RETURN

END
SUBROUTINE SOLVE (KKK,AK,R,NER,NBAND,NROWD,NCOLD)
  SYMMETRIC BAND EQUATION SOLVER
  MATRIX AK IS STORED IN BAND STORAGE MODE

  REAL AK(NROWD,NCOLD),R(NROWD)
  NRS=NER-1
  NR=NER

  IF (KKK.EQ.2) GO TO 103

  IF (NER.EQ.1) GO TO 107
  DO 102 N=1,NRS
    M=N-1
    NR=MIN0(NBAND,NR-M)
    PIVOT=AK(N,1)
  DO 102 L=2,MR
    CP=AK(N,L)/PIVOT
    I=M+L
    J=0
    DO 101 K=L,MR
      J=J+1
      AK(I,J)=AK(I,J)-CP*AK(N,K)
101 CONTINUE
    AK(N,L)=CP

```

```

102 CONTINUE                                J
GO TO 107                                  J
103 CONTINUE                                J
IF (NEQ.EQ.1) GO TO 106                    J
DO 104 N=1,NRS                              J
M=N-1                                       J
MR=MIN0(NBAND,MR-M)                         J
CP=R(N)                                       J
R(N)=CP/AK(N,1)                              J
DO 104 L=2,MR                               J
L=ML                                         J
R(L)=R(L)-AK(N,L)*CP                        J
104 CONTINUE                                J
C                                           J
C PERFORM BACK SUBSTITUTION                J
C                                           J
R(NR)=R(NR)/AK(NR,1)                        J
C                                           J
DO 105 I=1,NRS                              J
N=NR-I                                       J
M=N-1                                       J
MR=MIN0(NBAND,MR-M)                         J
DO 105 K=2,MR                               J
L=M+K                                       J
R(N)=R(N)-AK(N,K)*R(L)                    J
105 CONTINUE                                J
RETURN                                       J
106 R(NR)=R(NR)/AK(NR,1)                    J
107 RETURN                                   J
C                                           J
END                                          J
SUBROUTINE MESH (XNODE,YNODE,IB,IE,NUMELD,NNODES) K
C                                           K
C GENERATES DATA FOR RECTANGULAR REGIONS K
C                                           K
REAL XNODE(NNODES),YNODE(NNODES)          K
INTEGER IB(NNODES),IE(NUMELD,3)           K
COMMON /EQUIDX/ NEQ,NUMEL,NBAND,NNODES    K
COMMON /REGION/ A,B,C,D,NGRIDX,NGRIDY     K
C                                           K
C NUMBER NODES                              K
C                                           K
NOD=0                                       K
HX=(B-A)/FLOAT(NGRIDX-1)                  K
HY=(D-C)/FLOAT(NGRIDY-1)                  K
DO 102 IX=1,NGRIDX                          K
DO 101 JY=1,NGRIDY                          K
NOD=NOD+1                                   K
XNODE(NOD)=A+FLOAT(IX-1)*HX                K
YNODE(NOD)=C+FLOAT(JY-1)*HY                K
IF (IX.EQ.1.OR. IX.EQ. NGRIDX.OR. JY.EQ.1.OR. JY.EQ. NGRIDY) IB(N K
1 DD)=1                                     K
101 CONTINUE                                K
102 CONTINUE                                K
C                                           K
C NUMBER THE EQUATIONS                      K
C                                           K
NNODES=NOD                                   K
NEQ=0                                       K
C                                           K
DO 104 NOD=1,NNODES                         K
IF (IB(NOD).EQ.1) GO TO 103                 K
NEQ=NEQ+1                                   K
IB(NOD)=NEQ                                 K
GO TO 104                                   K
103 CONTINUE                                K
IB(NOD)=0                                   K
104 CONTINUE                                K
C                                           K
C DETERMINE ELEMENT INCIDENCIES            K
C                                           K

```



```

PROGRAM STLINE (INPUT,OUTPUT)
C
C *****
C FINITE ELEMENT PROGRAM TAKING INTO ACCOUNT THE GEOMETRIC
C NONLINEARITY . UNIDIMENSIONAL ELEMENT MOVING INTO A PLANE
C WITH SIX DEGREES OF FREEDOM . PERFORMS AN UNCERTAINTY ANAL.
C VERSION DNL277
C
C -----
C VARIABLES THAT HAVE TO BE SPECIFIED
C -----
C II = NUMBER OF PROBLEM
C AA(I) = TITLE OF PROBLEM
C -----
C MAXITR = MAX. NUMBER OF ITERATIONS
C ACURCY = NEEDED ACCURACY
C -----
C NNODE = TOTAL NUMBER OF NODES
C NEL = TOTAL NUMBER OF ELEMENTS
C -----
C NODE = NODE NUMBER
C X(NODE) = X COORDINATE
C Y(NODE) = Y COORDINATE
C RL(K,NODE)= LOAD APPLIED IN THE LOCAL COORD.
C ID(K,NODE)= BOUNDARY CONDITION IF 1 DISPL. CONSTRAIN
C -----
C N = ELEMENT NUMBER
C NI = NUMBER OF NODE I
C NJ = NUMBER OF NODE J
C E(N) = MODULUS OF ELASTICITY
C PR(N) = POISSON RATIO
C TH(N) = THICKNESS
C HGT(N) = HEIGHT
C P1(N) = INITIAL LOAD IN X DIRECTION
C P2(N) = INITIAL LOAD IN Y DIRECTION
C -----
C DIMENSION VE(30,10), N(10)
C DIMENSION RL(3,30), ID(3,30)
C DIMENSION S(50,6), SA(50,6), BMASS(30)
C DIMENSION AA(13)
C COMMON /BASIL1/ ST(6,6),BB(6)
C COMMON /BASIL2/ A(50,50),B(50),DD(50)
C COMMON /BASIL3/ R(6,6)
C COMMON /BASIL4/ CDEF(6),D(33)
C COMMON /BASIL5/ AUX(6),DAUX(6,6)
C COMMON /BASIL6/ DELTA(3)
C COMMON /BASIL7/ NI(30),NJ(30),E(30),PR(30),TH(30),HGT(30),P1(30),P
12(30),X(40),Y(40)
C DATA LEVEL/2/
C
C -----
C PRINT 112
C READ 113, II,(AA(I),I=1,13)
C IF (II.EQ.0) GO TO 111
C PRINT 113, II,(AA(I),I=1,13)
C PRINT 114
C PRINT 115
C MBAND=6
C
C READ MAX NO. OF ITERATIONS AND DESIRED ACURCY
C
C READ 116, MAXITR,ACURCY
C
C***** READ TOTAL NO. OF NODES=NNODE,AND ELEMENTS=NEL*****
C
C READ 117, NNODE,NEL
C PRINT 118, NNODE,NEL
C
C DEFINE DIMENSION NDIM OF SYSTEM

```

```

C
      NDIM=3*NMODE
      PRINT 115
C
C*****READ NODE INFORMATION *****
C=====
C
      PRINT 114
      PRINT 119
      PRINT 114
101 READ 120, NODE,X(NODE),Y(NODE),(RL(K,NODE),ID(K,NODE),K=1,3)
      PRINT 121, NODE,X(NODE),Y(NODE),(RL(K,NODE),ID(K,NODE),K=1,3)
      IF (NODE.NE.NMODE) GO TO 101
C
      INITIALIZE DISPLACEMENTS D(I),
      COEFFICIENT MATRIX A(I,J) AND
      RIGHT SIDE MATRIX BB(I,L)
C=====
C
      ICLEAR=0
      DO 103 I=1,NDIM
        D(I)=0.
        DO 102 L=1,MBAND
          SA(I,L)=0.
102   S(I,L)=0.
        DO 103 J=1,NDIM
103   A(I,J)=0.
        DO 104 I=1,NDIM+MBAND
          B(I)=0.
104 CONTINUE
      IF (ICLEAR.EQ.2) GO TO 106
      PRINT 115
C
C***** READ ELEMENT INFORMATION *****
C=====
C
      KOUNT=0
      PRINT 114
      PRINT 122
      PRINT 114
105 READ 123, N,NI(N),NJ(N),E(N),PR(N),TH(N),HGT(N),P1(N),P2(N)
      PRINT 124, N,NI(N),NJ(N),E(N),PR(N),TH(N),HGT(N),P1(N),P2(N)
      IF (N.NE.NEL) GO TO 105
C
      N=1
      NFLAG=0
C
106 CONTINUE
C
C-----
C
      CALL MATRI (N,SL,LEVEL)
C-----
C
      CALL MASS (N,NMODE,NFLAG,SL,BMASS,LEVEL)
C-----
C
      IF (N.EQ.NEL) GO TO 107
      N=N+1
      GO TO 106
107 CONTINUE
C
C***** APPLY LOADS *****
C=====
C
      DO 108 NODE=1,NMODE
        M=3*(NODE-1)
        DO 108 K=1,3
108   B(M+K)=B(M+K)+RL(K,NODE)

```

```

C
C
C      APPLY BOUNDARY CONDITIONS
C      =====
C
C      -----
C
C      CALL BOUND (S,SA,BMASS, ID,NDM,NDIM,MBAND,NMODE,LEVEL,NFLAG,MB)
C
C      -----
C
C      CALL SOLVE (S,NDIM,MBAND)
C
C      -----
C
C      DO 109 K=1,NDIM
109  D(K)=D(K)+DD(K)
      PRINT 114
      PRINT 112
C
C      -----
C
C      CALL PRINTO (M,D,NDIM,KOUNT,ACURCY,MAXITR,NMODE)
C
C      -----
C
C      IF (M.EQ.1) GO TO 110
      N=1
      NFLAG=1
      IF (KOUNT.LT.MAXITR) GO TO 106
110  CONTINUE
C
      NMODE=7
C
C      -----
C
C      CALL BEING (NDM,NMODE,MB,BMASS,SA,VE,W,LEVEL)
C
C      -----
C
C      CALL UNCERT (NDM,VE,SA,BMASS,NMODE,W,LEVEL)
C
C      -----
C
111  STOP
C
112  FORMAT (1H1)
113  FORMAT (I2,13A6)
114  FORMAT (2X,112H=====,/)
115  FORMAT (///)
116  FORMAT (I3,F10.0)
117  FORMAT (2I3)
118  FORMAT (1X, 16HNUMBER OF NODES=,I3,5X, 19HNUMBER OF ELEMENTS=,I3)
119  FORMAT (1X, 4HNODE,2X, 12HX-COORDINATE,2X, 12HY-COORDINATE,2X, 11
      1HHORIZ. LOAD,2X, 7HCONSTR.,2X, 11HVERTC. LOAD,2X, 6HCONSTR,4X,
      26HMENT,4X, 6HCONSTR.)
120  FORMAT (I3,2F10.0,3(F9.0,I1))
121  FORMAT (2X,I3,2F14.5,3(F13.5,5X,I1,3X))
122  FORMAT (1X, 7HELEMENT,2X, 6HNODE 1,2X, 6HNODE 2,2X, 15HMODUL.OF
      1 ELAST.,1X, 13HPOISSON RATIO,4X, 9HTHICKNESS,8X, 5HHIGHT,7X, 11H
      2AXIAL FORCE,4X, 11HSHEAR,FORCE)
123  FORMAT (3I3,1X,E10.0,5F10.0)
124  FORMAT (I4,2I9,5X,E10.0,4X,5F15.5)
C
      END
      SUBROUTINE MATRI (N,SL,LEVEL)
C

```



```

C      *****
C
COMMON /BASIL1/ ST(6,6),BB(6)
COMMON /BASIL2/ A(50,50),B(50),DD(50)
COMMON /BASIL3/ R(6,6)
COMMON /BASIL4/ CDEF(6),D(33)
COMMON /BASIL5/ AUX(6),DAUX(6,6)
COMMON /BASIL6/ DELTA(3)
COMMON /BASIL7/ NI(30),NJ(30),E(30),PR(30),TH(30),HGT(30),P1(30),P
12(30),X(40),Y(40)
C
C
C-----
C*****  COMPUTE USEFUL QUANTITIES OF PRESENT ELEMENT  *****
C=====
C
C-----
C      CALL PARAM (N,SL,C,S,MI,MJ,EA,Q1,Q2,H,XX)
C
C-----
C      CALL TRANSF (SL,C,S)
C
C-----
C      CALL FUDDIS (MI,MJ,SL)
C
C-----
C      DEVELOP AUXILLIARY ARRAYS
C
DO 101 I=1,6
  AUX(I)=0.
DO 101 J=1,6
101 DAUX(I,J)=0.
  KD=0
  W1=EA*(.5+XX)*CDEF(2)
  W2=EA*H*H*(CDEF(2)+1.)/(8.*SL*SL)
C
C-----
C      102 CALL DELT (W1,W2)
C
C-----
C      SUM=0.
DO 103 I=1,3
  EXTRA=DELTA(I)*CDEF(I+3)*CDEF(I+3)
103 SUM=SUM+EXTRA
  IF (KD.EQ.1) GO TO 105
  IF (KD.EQ.2) GO TO 108
  AUX(2)=SUM+Q1*(1.+CDEF(2))-Q2*CDEF(4)+.5*CDEF(2)*(CDEF(2)*(CDEF(2)
1+3.)+2.)*EA
DO 104 J=1,3
104 DAUX(2,J+3)=-2.*DELTA(J)*CDEF(J+3)
  DAUX(2,4)=DAUX(2,4)-Q2
  KD=1
  W1=EA*(.5+XX)
  W2=EA*H*H/(8.*SL*SL)
  GO TO 102
105 DAUX(2,2)=SUM+1.5*EA*CDEF(2)*(CDEF(2)+2.)+EA+Q1
  W1=EA*(.5+XX)*CDEF(2)*CDEF(2)+Q1
  W2=H*H*(EA*(3.*CDEF(2)*(5*CDEF(2)+1.)+1.)+Q1)/(12.*SL*SL)
C
C-----
C      CALL DELT (W1,W2)
C
C-----
DO 106 J=1,3

```

```

      DAUX(J+3,J+3)=DELTA(J)
106  AUX(J+3)=DELTA(J)*COEF(J+3)
      AUX(4)=AUX(4)+Q2*COEF(2)
      DO 107 J=1,3
107  DAUX(J+3,2)=DAUX(2,J+3)
C
C      THE AUXILLIARY QUANTITIES HAVE BEEN DEVELOPED
C
      KD=2
      GO TO 102
C
C      -----
C
108  CALL GLOBAL (SL)
C
C      -----
C
      CALL STIFFN (MI,MJ,LEVEL)
C
C      -----
C
      RETURN
C
      END
      SUBROUTINE PARAM (N,SL,C,S,MI,MJ,EA,Q1,Q2,H,XX)
C
C      *****
C
C      THIS SUBROUTINE COMPUTES SOME USEFUL QUANTITIES
C      THESE PHYSICAL AND GEOMETRIC QUANTITIES ARE FUNCTION
C      OF THE DISPLACEMENTS AT EACH ITERATION
C
C      -----
C
      COMMON /BASIL7/ MI(30),NJ(30),E(30),PR(30),TH(30),HGT(30),P1(30),P
12(30),X(40),Y(40)
      DX=X(NJ(N))-X(NI(N))
      DY=Y(NJ(N))-Y(NI(N))
      SL=SQRT(DX*DX+DY*DY)
      C=DX/SL
      S=DY/SL
      MI=3*(NI(N)-1)
      MJ=3*(NJ(N)-1)
      EA=E(N)*TH(N)*HGT(N)
      H=HGT(N)
      XX=.5/(1.+PR(N))
      Q1=P1(N)
      Q2=P2(N)
      RETURN
C
      END
      SUBROUTINE TRANSF (SL,C,S)
C
C      *****
C
C      THIS SUBROUTINE EVALUATES THE TRANSFORMATION MATRIX WHICH
C      ENABLES US TO PASS FROM THE LOCAL COORDINATES SYSTEM
C      TO THE GLOBAL COORDINATES SYSTEM
C
C      -----
C
      COMMON /BASIL3/ R(6,6)
      DO 101 I=1,6
      DO 101 J=1,6
101  R(I,J)=0.
      R(1,1)=C
      R(1,2)=-C
      R(1,4)=S
      R(1,6)=-2.*S
      R(2,1)=S
      R(2,2)=-S
      R(2,4)=-C
      R(2,6)=2.*C
      R(3,5)=-.5*SL
      R(3,6)=SL

```

```

R(4,2)=C
R(4,3)=-S
R(4,4)=-S
R(4,6)=2.*S
R(5,2)=S
R(5,3)=C
R(5,4)=C
R(5,6)=-2.*C
R(6,5)=.5*SL
R(6,6)=SL
RETURN
C
END
SUBROUTINE DELT (W1,W2)
C
C *****
C AUXILIARY MATRIX USED FOR OPTIMIZING PURPOSES
C TERMS INCLUDES THE PHYSICAL CHARACT. AND THE KNOWN DISPLAC.
C -----
C
COMMON /BASIL6/ DELTA(3)
DELTA(1)=W1
DELTA(2)=W1/3.+4.*W2
DELTA(3)=.05*W1+3.*W2
RETURN
C
END
SUBROUTINE FUCDIS (MI,MJ,SL)
C
C *****
C THIS SUBROUTINE COMPUTES COEFF. FUNGTION OF KNOWN DISPLAC.
C -----
C
COMMON /BASIL3/ R(6,6)
COMMON /BASIL4/ CDEF(6),D(33)
DO 104 I=1,6
  CDEF(I)=0.
  DO 103 J=1,6
    IF (J.LT.4) GO TO 101
    K=MJ+J-3
    GO TO 102
101  K=MI+J
102  TERM=R(J,I)*D(K)/SL
103  CDEF(I)=CDEF(I)+TERM
104 CONTINUE
RETURN
C
END
SUBROUTINE GLOBAL (SL)
C
C *****
C COMPUTATION OF STIFFNESS MATRIX FUNCTION OF DISPLACEMENTS
C IN GLOBAL SYSTEM OF COORDINATES
C -----
C
COMMON /BASIL1/ ST(6,6),BB(6)
COMMON /BASIL3/ R(6,6)
COMMON /BASIL5/ AUX(6),DAUX(6,6)
DO 101 I=1,6
  BB(I)=0.
  DO 101 J=1,6
101  ST(I,J)=0.
  DO 103 M=1,6
  DO 103 L=1,6
  DO 103 I=1,6
    SUM=0.
    DO 102 J=1,6
102  SUM=SUM+DAUX(I,J)*R(L,J)/SL
103  ST(M,L)=ST(M,L)+R(M,I)*SUM
  DO 104 I=1,6
  DO 104 J=1,6

```

```

104 BB(I)=BB(I)+R(I,J)*AUX(J)
RETURN
C
END
SUBROUTINE STIFFN (MI,MJ,LEVEL)
C
C *****
C STIFFNESS MATRIX AND SECOND MEMBER
C -----
C
COMMON /BASIL1/ ST(6,6),BB(6)
COMMON /BASIL2/ A(50,50),B(50),DD(50)
C
DO 101 I=1,3
  B(MI+I)=B(MI+I)-BB(I)
  B(MJ+I)=B(MJ+I)-BB(3+I)
DO 101 J=1,3
  A(MI+I,MI+J)=A(MI+I,MI+J)+ST(I,J)
  A(MI+I,MJ+J)=A(MI+I,MJ+J)+ST(I,3+J)
  A(MJ+I,MI+J)=A(MJ+I,MI+J)+ST(3+I,J)
101 A(MJ+I,MJ+J)=A(MJ+I,MJ+J)+ST(3+I,3+J)
C
C *****DEBUG*****
C
IF (LEVEL.NE.2) RETURN
C
DO 102 I=MI,MI+6
  PRINT 103, (A(I,J),J=MI,MI+6)
102 CONTINUE
C
RETURN
C
103 FORMAT (5X,6(F10.3,2X))
C
END
SUBROUTINE SOLVE (S,NDIM,MBAND)
C
C *****
C THIS SUBROUTINE SOLVE THE LINEAR SYSTEM OF EQUATIONS
C USING THE GAUSS-SEIDEL ELIMINATION PROCEDURE
C -----
C
DIMENSION S(50,6)
COMMON /BASIL2/ A(50,50),B(50),DD(50)
C
FORWARD REDUCTION OF MATRIX ( GAUSS ELIMINATION )
C =====
C
DO 103 N=1,NDIM
  DO 102 L=2,MBAND
    IF (S(N,L).EQ.0.) GO TO 102
    I=N+L-1
    C=S(N,L)/S(N,1)
    J=0
    DO 101 K=L,MBAND
      J=J+1
101 S(I,J)=S(I,J)-C*S(N,K)
      S(N,L)=C
102 CONTINUE
103 CONTINUE
C
FORWARD REDUCTION OF CONSTANT
C =====
C
DO 105 N=1,NDIM
  DO 104 L=2,MBAND
    IF (S(N,L).EQ.0.) GO TO 104
    I=N+L-1
    B(I)=B(I)-S(N,L)*B(N)
    IF (S(N,1).EQ.1.) B(N)=0.

```



```

104 CONTINUE
105 B(N)=B(N)/S(N,1)
C
C SOLVE FOR UNKNOWN BY BACK SUBSTITUTION
C =====
C
DO 107 M=2,NDIM
  N=NDIM+1-M
  DO 106 L=2,MBAND
    IF (S(N,L).EQ.0.) GO TO 106
    K=N+L-1
    B(N)=B(N)-S(N,L)*B(K)
106 CONTINUE
107 CONTINUE
DO 108 N=1,NDIM
  DD(N)=B(N)
108 CONTINUE
RETURN
C
END
SUBROUTINE PRINTO (M,D,NDIM,KOUNT,ACURCY,MAXITR,NNODE)
C
C *****
C THIS SUBROUTINE PRINT THE RESULTS OF THE PROGRAM
C -----
C
DIMENSION D(50)
COMMON /BASIL2/ A(50,50),B(50),DD(50)
IF (KOUNT.EQ.0) GO TO 102
IF (KOUNT.EQ.1) GO TO 101
PRINT 110, KOUNT
PRINT 111
GO TO 103
101 PRINT 112
PRINT 111
GO TO 103
102 PRINT 113
PRINT 111
103 PRINT 114
PRINT 111
DO 104 NODE=1,NNODE
  K=3*(NODE-1)
  PRINT 115, D(K+1)
  PRINT 116, NODE,D(K+2)
  PRINT 118, D(K+3)
  PRINT 117
104 CONTINUE
IF (KOUNT.EQ.0) GO TO 107
K=0
105 K=K+1
ZZ=DD(K)
IF (ABS(ZZ).GT.ACURCY) GO TO 106
IF (K.NE.NDIM) GO TO 105
M=1
PRINT 111
PRINT 119
PRINT 111
RETURN
106 IF (KOUNT.EQ.MAXITR) GO TO 109
KOUNT=KOUNT+1
DO 108 I=1,NDIM
  B(I)=0.
DO 108 J=1,NDIM
108 A(I,J)=0.
N=1
RETURN
109 PRINT 120, MAXITR
RETURN
C
110 FORMAT (30X, 19HDISPLACEMENTS AFTER,I4,1X, 10HITERATIONS)
111 FORMAT (30X, 38H-----,/)

```

```

112 FORMAT (30X, 35HDISPLACEMENTS AFTER FIRST ITERATION)
113 FORMAT (30X, 21HINITIAL DISPLACEMENTS)
114 FORMAT (30X, 21HNODE DISPLACEMENTS)
115 FORMAT (29X, 1H+,6X, 10HHORIZONTAL,=,F15.5, 7H +)
116 FORMAT (29X, 1H+,1X,13,2X, 10HVERTICAL,=,F15.5, 7H +)
117 FORMAT (/)
118 FORMAT (29X, 1H+,6X, 10HROTATION,=,F15.5, 7H +)
119 FORMAT (30X, 34H CONVERGENCE HAS BEEN OBTAINED,/)
120 FORMAT (1X, 31HMETHOD FAILED TO CONVERGE AFTER,14,1X, 10HITERATION
1S)
C
C END
C SUBROUTINE MASS (N,NMODE,NFLAG,SL,BMASS,LEVEL)
C
C *****
C
C COMMON /BASIL7/ NI(30),NJ(30),E(30),PR(30),TH(30),HGT(30),P1(30),P
12(30),X(40),Y(40)
C DIMENSION BMASS(30)
C
C IF (NFLAG.EQ.1) RETURN
C NN=NMODE*2
C
C II=(NI(N)-1)*2
C JJ=(NJ(N)-1)*2
C
C A=TH(N)*HGT(N)
C GAM=10.
C V=A*SL
C SM=V*GAM
C
C DO 101 I=1,2
C
C BMASS(II+I)=BMASS(II+I)+SM/2.
C BMASS(JJ+I)=BMASS(JJ+I)+SM/2.
101 CONTINUE
C
C *****DEBUG*****
C
C IF (LEVEL.NE.2) RETURN
C PRINT 102
C PRINT 103, (BMASS(I),I=1,NN)
C
C RETURN
C
102 FORMAT (5X, 13H MASS VECTOR,/)
103 FORMAT (5X, 8(F10.3,2X))
C
C END
C SUBROUTINE BEING (NN,NMODE,MM,BMASS,AST,W,LEVEL)
C
C *****
C
C DIMENSION BMASS(30), Z(30,10), AST(30,10), W(30), VE(30,10)
C
C *****DEBUG*****
C
C IF (LEVEL.NE.2) GO TO 102
C PRINT 113, (BMASS(I),I=1,NN)
C
C DO 101 I=1,NN
C PRINT 113, (AST(I,J),J=1,MM)
101 CONTINUE
C
102 CONTINUE
C
C DO 103 I=1,NN
C DO 103 J=MM+1,NMODE
103 AST(I,J)=0.

```

```

C
DO 105 I=1,NN
  X=BMASS(I)
  IF (X.GT.0.) GO TO 104
  PRINT 114, I
  IF=1
  GO TO 106
104  BMASS(I)=1./SQRT(X)
105  CONTINUE
106  IF (IF.EQ.1) STOP
C
DO 107 I=1,NN
  L=I-1
  MR=MIN0(MM,NN-I+1)
  DO 107 J=1,MR
    K=L+J
107  AST(I,J)=AST(I,J)*BMASS(I)*BMASS(K)
C
C   MATRIX IN SYMMETRIC MODE
C
MM=NMODE
DO 108 J=1,MM
  N1=0
  DO 108 I=MM-J+1,NN
    Z(I,J)=AST(I+1,MM-J+1)
    N1=N1+1
108  CONTINUE
C
C   ****DEBUG****
C
IF (LEVEL.ME.2) GO TO 110
DO 109 I=1,NN
  PRINT 113, (Z(I,J),J=1,MM)
109  CONTINUE
110  CONTINUE
C
IND=2
NM=30
C
C   -----
C
CALL RSBEIG (NM,NN,NMODE,Z,IND,W,VE)
C
C   -----
C
DO 111 I=1,NN
  X=BMASS(I)
  NEV=MM
  BMASS(I)=1./X**2
  DO 111 J=1,NEV
    VE(I,J)=VE(I,J)*X
111  CONTINUE
C
DO 112 I=1,NMODE
  W(I)=SQRT(W(I))
  PRINT 115, I,W(I)
  PRINT 116
C
  N2=NN/2
  DO 112 J=1,N2
    KK=2*J-1
    PRINT 117, J+1,VE(KK,I),VE(KK+1,I)
112  CONTINUE
C
RETURN
C
113  FORMAT (5X,8(F10.3,2X))
114  FORMAT (5X, 9HZERO MASS,15)
115  FORMAT (//5X, 20HTHE FREQ. OF MODE ,2X,I2, 6H IS =,F10.4//)
116  FORMAT (5X, 32H+ NMODE + X-EIGEN + Y-EIGEN ,//)
117  FORMAT (114,2E15.5)

```

```

C                                     L
C   END                               M
C   SUBROUTINE BOUND (S, SA, BMASS, ID, NDM, NDIM, MBAND, NNODE, LEVEL, NFLAG, M M
1B) M
C                                     M
C   ***** M
C   COMMON /BASIL2/ A(50,50), B(50), DD(50) M
C                                     M
C   DIMENSION S(50,6), SA(30,4), BMASS(30) M
C   DIMENSION ID(3,30) M
C                                     M
C   DO 102 NODE=1,NNODE M
C   DO 102 K=1,3 M
C     IF (ID(K,NODE).EQ.0) GO TO 102 M
C     JJ=3*(NODE-1)+K M
C     DO 101 J=1,NDIM M
C       A(J, JJ)=0. M
101   A(JJ, J)=0. M
C       A(JJ, JJ)=1. M
C       B(JJ)=0. M
102 CONTINUE M
C                                     M
C   DO 103 I=1,NDIM M
C   DO 103 L=1,MBAND M
C     S(I, L)=A(I, L+I-1) M
C                                     M
103 CONTINUE M
C                                     M
C   ND=NNODE*2 M
C   MB=4 M
C   NB=0 M
C                                     M
C   NF=0 M
C                                     M
C   DO 105 I=1,ND,2 M
C     NFB=0 M
C     DO 104 J=1,MB,2 M
C                                     M
C       II=I+NF M
C       JJ=J+NFB M
C                                     M
C       SA(I, J)=S(II, JJ) M
C       SA(I, J+1)=S(II, JJ+1) M
C                                     M
C       SA(I+1, J)=S(II+1, JJ) M
C       SA(I+1, J+1)=S(II+1, JJ+2) M
C                                     M
C       NFB=NFB+1 M
104   CONTINUE M
C       NF=NF+1 M
C                                     M
105 CONTINUE M
C                                     M
C   ****DEBUG**** M
C                                     M
C   IF (LEVEL.NE.2) GO TO 107 M
C   DO 106 I=1,ND M
C     PRINT 114, (SA(I, J), J=1, MB) M
106 CONTINUE M
107 CONTINUE M
C                                     M
C   DO 110 I=1,ND M
C     IB=I-MB M
C     DO 108 J=1,MB M
C                                     M
C       IF (SA(I, J).EQ.1.) GO TO 109 M
C       SINT=SA(I, J) M
C       SA(IB, J)=SINT M

```



```

C          IF (NFLAG.EQ.1) GO TO 108
          BMS=BMASS(I)
          BMASS(IB)=BMS
C
108      CONTINUE
          GO TO 110
109      NB=NB+1
C
110 CONTINUE
C          NDM=IB-1
C
C          *****DEBUG*****
C
          IF (LEVEL.NE.2) GO TO 113
          DO 111 I=1,NDIM
            PRINT 114, (S(I,J),J=1,MRAND)
111 CONTINUE
          PRINT 114, (B(I),I=1,NDIM)
C
          DO 112 I=1,NDM
            PRINT 114, (SA(I,J),J=1,MB)
112 CONTINUE
C
          PRINT 114, (BMASS(I),I=1,NDM)
C
113 CONTINUE
C
          RETURN
C
114 FORMAT (SX,6(F10.3,2X))
C
          END
          SUBROUTINE UNCERT (ND,VE,AST,BMASS,NMODE,W,LEVEL)
C
C          *****DEBUG*****
C
          DIMENSION FR1(30,10), FR2(30,10)
          DIMENSION VE(30,10), W(10), BMASS(30), NUM1(30), DEN(10)
          DIMENSION AST(30,10), NUM2(30)
C
          DO 102 I=1,NMODE
            VECT=0.
            DO 102 K=1,ND
C
              DO 101 J=1,ND
                VECT=VECT+(VE(K,J,I)**2)*BMASS(J)
101 CONTINUE
              DEN(I)=2.*W(I)*VECT
              NUM1(K)=(W(I)**2)*VE(K,I)**2*BMASS(K)
              NUM2(K)=VE(K,I)**2*AST(K,1)
C
              FR1(K,I)=NUM1(K)/DEN(I)
              FR2(K,I)=NUM2(K)/DEN(I)
C
102 CONTINUE
C
C          *****DEBUG*****
C
          IF (LEVEL.NE.2) GO TO 105
          DO 103 K=1,ND
103 PRINT 106, (FR1(K,I),I=1,NMODE)
C
          DO 104 K=1,ND
104 PRINT 106, (FR2(K,I),I=1,NMODE)
C
          PRINT 106, (NUM1(I),I=1,NMODE)
          PRINT 106, (NUM2(I),I=1,NMODE)
          PRINT 106, (DEN(I),I=1,NMODE)

```

```

C
C 105 CONTINUE
C
C -----
C CALL MOMENTS (ND,NMODE,W,FR1,FR2,LEVEL)
C -----
C
C RETURN
C
C 106 FORMAT (5X,8(E15.5,2X))
C
C END
C SUBROUTINE MOMENTS (ND,NMODE,W,FR1,FR2,LEVEL)
C
C *****
C
C DIMENSION FR1(30,10), FR2(30,10), W(10), EXP(10), VAR(10)
C DIMENSION CFV(10), SG1(30), SG2(30), EX1(30), EX2(30)
C
C DO 101 I=1,ND
C   SG1(I)=.05
C   SG2(I)=0.04
C   EX1(I)=.02
C   EX2(I)=.02
C 101 CONTINUE
C
C DO 104 I=1,NMODE
C   SUM1=0.
C   SUM2=0.
C
C   DO 102 J=1,ND
C     SUM1=(FR1(J,I)*EX1(J)+FR2(J,I)*EX2(J))+SUM1
C     SUM2=(FR1(J,I)**2*SG1(J)+FR2(J,I)**2*SG2(J))+SUM2
C 102 CONTINUE
C
C   ****DEBUG****
C
C   IF (LEVEL.NE.2) GO TO 103
C   PRINT *, #SUM1,SUM2#,SUM1,SUM2
C
C 103 CONTINUE
C
C   EXP(I)=W(I)+SUM1
C   VAR(I)=SUM2
C   CFV(I)=SQRT(VAR(I))/EXP(I)
C 104 CONTINUE
C
C PRINT 106
C DO 105 I=1,NMODE
C   PRINT 107, I,EXP(I),VAR(I),CFV(I)
C 105 CONTINUE
C
C RETURN
C
C 106 FORMAT (///5X, 8H*NMODE *, 38HEXPECT. * VARIANCE * COEF. OF VA
C 1R *,//)
C 107 FORMAT (5X,I3,2X,3(E15.5,2X))
C
C END

```

This program evaluates the first thirty frequencies and the associate modes of vibration, using subroutine RSBEIG which combines BANDR, TQLRAT and TQL2 obtained from Argonne National Laboratory as part of the EISPACK subroutine package.

The input parameters are the stiffness matrix [A] (given in Band form), the mass matrix [SMASS] and the nodes at the boundaries.

These matrices can be computed by any of the existing finite element codes, using plane strain or stress triangular elements.

```

PROGRAM DEIGEN ( INPUT, OUTPUT, PUNCH )
C *****
C
C   DIMENSION      EV(31), NEBC(200),  NPB(15),
1 SMASS(200), A(160,160)
C   DIMENSION  W(160)
C   DIMENSION  Z(160,40)
C   DIMENSION  U(160,10)
C
C   DATA LEVEL /2/
C
C   INITIALIZE
C
C   NUMBC = 7
C   NBAND = 40
C   NN = NBAND
C   NEV = 10
C   NH = 160
C
C
C   DO 210 K = 1, NUMBC
C     READ 1005, NPB(K)
C     PRINT 1005, NPB(K)
210  CONTINUE
C
C   NBC = 2 * NUMBC
C   DO 223 I = 1, NUMBC
C     II = 2 * I - 1
C     NEBC(II) = 2 * NPB(I) - 1
223  NEBC(II+1) = NEBC(II) + 1
C
1005  FORMAT (I5)
C
C   DO 300 I = 1, NH
C     READ 20, (A(I,J), J= 1, NBAND )
300  CONTINUE
C     READ 20, (SMASS(I), I=1, NH)
20   FORMAT (5E15.6)
C
C
C   IFLAG = 0
C
C   PRINT 11, (SMASS(I), I=1, NH)
C

```

```

C      REDUCE CLASSICAL EIGENVALUE PROBLEM      A*X = E*X
C
C      TRACE = 0.
C      DO 120 I = 1,NN
C      TRACE = TRACE + ABS( A(I,1) )
C      X = SMASS(I)
C      IF (X. GT. 0. ) GO TO 110
C      PRINT 12, I
120  FORMAT ( 2X, * ONEG. OR ZERO MASS EQUATION*,15)
C      IFLAG = 1
C      GO TO 120
110  SMASS(I) = 1. / SQRT (X)
120  CONTINUE
C      IF (IFLAG. NE. 0 ) STOP
C      DO 130 I = 1,NN
C      L = I - 1
C      MR = MIN0 (MM, NN -I +1 )
C      DO 130 J = 1, MR
C      K = L + J
130  A(I,J) = A(I,J) * SMASS(I) * SMASS(K)
C
C      IMPOSE BOUNDARY CONDITIONS ON A
C
C      IF ( NBC. LE. 0 ) GO TO 100
C      DO 140 N = 1,NBC
C      I = NEBC(N)
C      A(I,1) = 100. * TRACE
C      DO 140 J = 2,MM
C      A(I,J) = 0.
C      L = I - J + 1
C      IF ( L. LE. 0 ) GO TO 140
C      A(L,J) = 0.
140  CONTINUE
C
C      ***** DEBUG *****
C      IF ( LEVEL. EQ. 1 ) GO TO 200
C
C      DO 9 I = 1, NN
C      PRINT 11, ( A(I,J) , J = 1,MM )
C      CONTINUE
9
C      MATRIX IN SYMETRIC MODE
C
C      DO 1 J = 1, MM
C      N1 = NBC
C      DO 1 I = MM- J+1, NN - NBC
C      Z( I, J ) = A ( 1 + N1, MM-J+1 )
C      N1 = N1 + 1
1  CONTINUE
C
C
C      ***** DEBUG *****
C      IF ( LEVEL. EQ. 1 ) GO TO 201
C
C      DO 10 I = 1,NN
C      PRINT 11, ( Z(I,J) , J = 1,MM )
11  FORMAT ( 2X,10(F10.3,2X) )
10  CONTINUE
201 CONTINUE
C
C      IND = 2
C      NM = 150
C
C
C      -----
C      CALL RSBEIG ( MM, NN, MM,Z,IND,W,A )
C      -----
C
C      PRINT, #IND=#, IND
C
C      DO 202 I = 1, NN
202 PRINT, #W = #, W(I)
C
C

```



```

C
DO 918 I = 1, NN
918 PRINT 11, (A(I, J), J = 1, NN)
C
DO 919 J = 1, NEV
EV(J) = W(J + NBC)
C
EV(J) = SORT(EV(J))
PUNCH 2014, J, EV(J)
2014 FORMAT(1I5,1F10.3)
PRINT 2014, J, EV(J)
C
919 CONTINUE
C
C
DO 920 I = 1, NN
C
C
X = SMASS(I)
SMASS(I) = 1. / X**2
DO 920 J = 1, NEV
C
920 U(I, J) = A(I, J+NBC) * X
C
DO 263 N = 1, NEV
DO 263 M = 1, 80
KK = 2 * M - 1
263 PUNCH 2015, K, U(KK, N), U(KK+1, N)
2015 FORMAT (1I12, 2E15.6)
C
DO 1001 I = 1, NN
1001 PRINT 11, (A(I, J), J = 1, NEV)
100 STOP
END

```

Subroutine UNCERT performs an uncertainty analysis related to the previously computed eigenvalues and corresponding eigenvectors U.

The procedure is based on a perturbation scheme.

ST () = STIFFNESS MATRIX

SMASS () = VECTOR OF LUMPED MASSES

```

C      SUBROUTINE UNCERT ( U )
C      *****
C
C      COMMON / BAS4/ NUMNP, NUMEL, NUMBC, NMODE
C      COMMON / BAS/  NN, NEV, NBC, EV(31), NEBC(200),
1     SMASS(200),          B(200), EX1(200), SN(200), NUM1(200),
2     ST(170,45)
C      COMMON / BAS5/ NN, PSP, ITR, NBAND
C
C      DIMENSION DEN(15), FR1(100,30), U(100,15)
C      DATA LEVEL/1/
C
C      EQUIVALENCE (ST,FR1)
C
C      DO 1 I = 1, NEV
C      VECT = 0.
C      DO 1 K = 1+NBC, NN
C
C      DO 2 J = 1+NBC, NN
C      VECT = VECT + ( U(J,I)**2 ) * SMASS(J)
2     CONTINUE
C
C      DEN(I) = 2. * EV(I) * VECT
C      NUM1(K) = ( EV(I)**2 ) * U(K,I)**2 * SMASS(K)
C
C      IF ( DEN(I). EQ. 0. ) GO TO 1
C
C      FR1(K,I) = NUM1(K) / DEN(I)
1     CONTINUE
C
C      ****DEBUG****
C
C      IF(LEVEL. NE. 2 ) GO TO 10
C
C      DO 4 K = 1, NN
4     PRINT 5, (FR1(K,I), I = 1, NEV )
5     FORMAT ( 5X, 8(E12.4, 2X) )
C
C      PRINT 5, (NUM1(I), I = 1, NEV )
C      PRINT 5, (DEN(I), I=1, NEV)
10    CONTINUE
C
C      -----
C      CALL MOMENTS ( FR1, NN )
C      -----
C
C      RETURN
C      END

```

Subroutine MOMENTS is called from subroutine UNCERT and computes the second statistical moment and the coefficient of variation of the provided eigenvalues.

EXP () = EXPECTED VALUE OF THE EIGENVALUE

VAR () = VARIANCE OF THE EIGENVALUE

```

SUBROUTINE MOMENTS (FR1, NN )
C
C
C *****
COMMON / BAS/ MM, NEV, NBC, EV(31), NEBC(200),
1 SMASS(200), B(200), EX1(200), SH(200), NUM1(200)
2 , ST(170,45)
C
C DIMENSION FR1(100,30),EXP(15),VAR(15),CFV(15)
C
C DO 1 I = 1+NBC, NN
  SH(I) = 0.05
  EX1(I) = .02
1 CONTINUE
C
C DO 2 I = 1, NEV
  SUM1 = 0.
  SUM2 = 0.
C
C DO 3 J = 1+NBC, NN
  SUM1 = ( FR1(J,I)* EX1(J) ) + SUM1
  SUM2 = ( FR1(J,I)**2 * SH(J) ) + SUM2
C
3 CONTINUE
C
  EXP(I) = EV(I) + SUM1
  VAR(I) = SUM2
  CFV(I) = SQRT( VAR(I) ) / EXP(I)
2 CONTINUE
C
4 PRINT 4
  FORMAT (5X, # *MODE*          EXPECT      VARIANCE      COEF. VAR#)
C
  DO 5 I = 1, NEV
    PRINT 6, I, EXP(I), VAR(I), CFV(I)
    FORMAT ( 5X, I3, 2X, 3(E15.5, 2X) )
6 CONTINUE
5
C
RETURN
END

```

TE 662

.A3

no. FHWA-RD-

~~78-159~~

BORROWE



FEDERALLY COORDINATED PROGRAM OF HIGHWAY RESEARCH AND DEVELOPMENT (FCP)

The Offices of Research and Development of the Federal Highway Administration are responsible for a broad program of research with resources including its own staff, contract programs, and a Federal-Aid program which is conducted by or through the State highway departments and which also finances the National Cooperative Highway Research Program managed by the Transportation Research Board. The Federally Coordinated Program of Highway Research and Development (FCP) is a carefully selected group of projects aimed at urgent, national problems, which concentrates these resources on these problems to obtain timely solutions. Virtually all of the available funds and staff resources are a part of the FCP, together with as much of the Federal-aid research funds of the States and the NCHRP resources as the States agree to devote to these projects.*

FCP Category Descriptions

1. Improved Highway Design and Operation for Safety

Safety R&D addresses problems connected with the responsibilities of the Federal Highway Administration under the Highway Safety Act and includes investigation of appropriate design standards, roadside hardware, signing, and physical and scientific data for the formulation of improved safety regulations.

2. Reduction of Traffic Congestion and Improved Operational Efficiency

Traffic R&D is concerned with increasing the operational efficiency of existing highways by advancing technology, by improving designs for existing as well as new facilities, and by keeping the demand-capacity relationship in better balance through traffic management techniques such as bus and carpool preferential treatment, motorist information, and rerouting of traffic.

3. Environmental Considerations in Highway Design, Location, Construction, and Operation

Environmental R&D is directed toward identifying and evaluating highway elements which affect the quality of the human environment. The ultimate goals are reduction of adverse highway and traffic impacts, and protection and enhancement of the environment.

4. Improved Materials Utilization and Durability

Materials R&D is concerned with expanding the knowledge of materials properties and technology to fully utilize available naturally occurring materials, to develop extender or substitute materials for materials in short supply, and to devise procedures for converting industrial and other wastes into useful highway products. These activities are all directed toward the common goals of lowering the cost of highway construction and extending the period of maintenance-free operation.

5. Improved Design to Reduce Costs, Extend Life Expectancy, and Insure Structural Safety

Structural R&D is concerned with furthering the latest technological advances in structural designs, fabrication processes, and construction techniques, to provide safe, efficient highways at reasonable cost.

6. Prototype Development and Implementation of Research

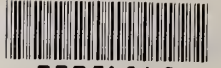
This category is concerned with developing and transferring research and technology into practice, or, as it has been commonly identified, "technology transfer."

7. Improved Technology for Highway Maintenance

Maintenance R&D objectives include the development and application of new technology to improve management, to augment the utilization of resources, and to increase operational efficiency and safety in the maintenance of highway facilities.

* The complete 7-volume official statement of the FCP is available from the National Technical Information Service (NTIS), Springfield, Virginia 22161 (Order No. PB 242057, price \$45 postpaid). Single copies of the introductory volume are obtainable without charge from Program Analysis (HRD-2), Offices of Research and Development, Federal Highway Administration, Washington, D.C. 20590.

DOT LIBRARY



00056148

